UNIVERSIDAD COMPLUTENSE DE MADRID
FACULTAD DE CIENCIAS BIOLÓGICAS
Departamento de Bioquímica y Biología Molecular I

TESIS DOCTORAL

Nuevas oxidorreductasas GMC de basidiomicetos ligninolíticos: screening genómico, mecanismo catalítico y potencial biotecnológico

New Gmc oxidoreductases from ligninolytic basydiomycetes: genomic screening, catalytic mechanisms and biotechnological potential

MEMORIA PARA OPTAR AL GRADO DE DOCTOR

PRESENTADA POR

Juan Rogelio Carro Aramburu

Directores

Ángel T. Martínez Ferrer
Patricia Ferreira Neila

Madrid, 2018

© Juan Rogelio Carro Aramburu, 2017

UNIVERSIDAD
COMPLUTENSE
MADRID

Facultad de Ciencias Biológicas
Departamento de Bioquímica y Biología Molecular I
UNIVERSIDAD COMPLUTENSE DE MADRID

NUEVAS OXIDORREDUCTASAS GMC DE BASIDIOMICETOS LIGNINOLÍTICOS: SCREENING GENÓMICO, MECANISMO CATALÍTICO Y POTENCIAL BIOTECNOLÓGICO

NEW GMC OXIDOREDUCTASES FROM LIGNINOLYTIC BASIDIOMYCETES: GENOMIC SCREENING, CATALYTIC MECHANISM AND BIOTECHNOLOGICAL POTENTIAL

DOCTORAL THESIS
Juan Rogelio Carro Aramburu

Supervisors:
Ángel Tomás Martínez Ferrer **Patricia Ferreira Neila**
2017

NEW GMC OXIDOREDUCTASES FROM LIGNINOLYTIC BASIDIOMYCETES: GENOMIC SCREENING, CATALYTIC MECHANISM AND BIOTECHNOLOGICAL POTENTIAL

Thesis submitted by

Juan Rogelio Carro Aramburu

for the fulfilment of the requirements for the degree of doctor (Ph.D.) in the Universidad Complutense de Madrid

Supervisors:

Dr. Ángel T. Martínez Ferrer
Profesor de Investigación
Centro de Investigaciones Biológicas
CSIC

Dra. Patricia Ferreira Neila
Profesora Contratada Doctora
Universidad de Zaragoza

Madrid, 2017

This is the whole of the story and we might
have left it at that had there not been
profit and pleasure in the telling

V. Nabokov

Laughter in the Dark

Acknowledgements

This work has been carried out in the Centro de Investigaciones Biológicas belonging to the CSIC in Madrid, in different periods at the Departamento de Bioquímica y Biología Molecular y Celular of the Universidad de Zaragoza and during a three-month stay at the Georgia State University, in USA. My thesis has been financed by a Formación de Profesorado Universitario (FPU) fellowship and an Estancias Breves fellowship, both from the Spanish Ministry for Education, Culture and Sports. My teaching training was carried out at the Departamento de Bioquímica y Biología Molecular I of the Universidad Complutense de Madrid. Moreover, the work has been supported by different projects: PEROXICATS (KBBE-2010-4-265397), INDOX (KBBE-2013-7-613549), EnzOx2 (H2020-BBI-PPP-2015-720297), HIPOP (BIO2011-26694) and NOESIS (BIO2014-56388-R).

More than five years have gone by since I first set foot in CIB back in January 2012 to embark on this challenge and I've met wonderful people during this time. I'd like to express my most heartfelt gratitude to all those who have accompanied me these years:

Querría agradecer a Ángel el haberme dado la oportunidad de unirme a su laboratorio. He aprendido muchísimo durante estos años y no habría podido ser sin su dirección y ayuda. Gracias también por las correcciones a deshora y por el tiempo que me ha dedicado.

Gracias a Patricia por haberme acogido en Zaragoza y haberme enseñado tanto sobre cinéticas. Está claro que sin su dirección y su ayuda esta tesis no tendría nada que ver con cómo es. Gracias también por las largas horas de corrección y de sueño que te he robado.

Gracias a Mili por haberme recibido con los brazos abiertos en su grupo y haber hecho que me sintiese como en casa todas las veces que he ido a Zaragoza.

I'd like to thank Dr. Giovanni Gadda for giving me the opportunity to go to Atlanta, where I learnt a lot and met fantastic people. It was a great experience. Thank you for the time you spent helping and designing the experiments and discussing the results with me.

Gracias a Marta Martínez por haberme enseñado cómo se cristaliza una proteína. También por todo el tiempo empleado en hacer figuras y resolver la estructura de la AAO en complejo.

Asimismo, me gustaría agradecer a todo mi grupo del CIB por lo bien que me he sentido durante estos cinco años. Hemos sido casi como una familia, a pesar del continuo recambio de gente. Gracias a María Jesús por toda la ayuda y los consejos a lo largo de estos años. Gracias a Ali por siempre tener una sonrisa y buena disposición, y por las cañas a las que nos invitas por cualquier motivo. A Susana por los buenos momentos compartidos, por la fiesta del congreso que no dejó indiferente a nadie. A Javi por la ayuda y el entretenimiento que nos proporcionas. A Marta por ayudarme con todo y las charlas que me ayudan a desconectar de la tesis. Agradezco a Aitor el haberme enseñado gran parte de las cosas que sé y que han hecho posible esta tesis, por la paciencia y la ayuda cuando estabas en las mismas difíciles circunstancias que yo ahora. Ana, gracias por la ayuda durante estos años, por las risas y por los viajazos que nos hemos pegado. A Andrés, por ser el gaditano con menos salero y más mala leche que se ha visto. A Bea, por tantos años de ayuda y de risas, dentro y fuera del CIB. A Cris, por ser tan así que me hace reír mucho con sus crueldades. Gracias a Davi porque nunca he encontrado a nadie con quien los chistes a dos voces salgan tan mal, hemos pasado grandes momentos juntos. Gracias a David por la compañía y las risas que nos hemos pegado. A Elena por la ayuda, los consejos en el labo y la UPO. A Felipe por ser como es, ya tú sabes, y por las risas que nos provocas. Gracias a Fran por estar siempre tan dispuesto a ayudar y con una gran sonrisa en la boca. A Isa P. por la amabilidad, la ayuda y ser la cordura del labo en tantas ocasiones. A Isa V. por darme a conocer nuevos tratamientos para un vientre plano y por haber desarrollado conmigo un nuevo lenguaje cerdil. Gracias a Iván por ser un gran liante y un gran compañero de piso, además de por tu fe ciega durante años en mis capacidades matutinas. A Jesús por su arte con el Photoshop y lo majo que has sido siempre. A Jorge por haberme quitado tantas horas de sueño, por las cañitas y lo demás que no recuerdo. Gracias a Juan por la amabilidad y la tranquilidad que infunde. A Laura por haber hecho, y seguir haciendo, los chistes más insultantes sobre mi persona que se hayan hecho. No hay rencor, esas cosas se diriman en los tribunales. A Lola por haber sido mi compañera de mesa tantos años, por el entretenimiento, las galletas y las birrillas en su piscina. A Manolito, por haber ido a la par conmigo en todos los pasos para llegar a esta tesis y por ese salero del sur (de Galicia) que tanta gracia me hace. A María, por las charlas, la ayuda y el desahogo que nos proporcionamos. A Mario, tan majete y tan responsable, por haber traído juventud al laboratorio. A Mariu, por todos los momentos compartidos, las risas y los masajes de la casa rural. Neumara, obrigado por enseñarnos cómo se baila la samba y hacernos reír todos los días. A Rosa por todo el tiempo que compartimos, las risas nocturnas para pillar el bicimadrid y por apreciar tanto mis yogures. A Sonia por haberme mostrado ese Madrid nocturno que aún desconocía y ser una lianta de las importantes. Gracias a Vero por haber sido tan encantadora, colaboradora y dulce durante estos años. Si me dejo a alguien perdonadme, que somos unos cuantos y cada hoja imprimida se paga cara.

Me gustaría también dar las gracias a toda la gente del laboratorio de Zaragoza, que siempre me han hecho sentir como en casa: Ana Sánchez, Isaías, Raquel, María Sebastián, Silvia, Ernesto, María Conde, Sandra, Juanjo… Ha sido genial compartir tiempo con vosotros, un desahogo frente a las malas rachas del stopped flow.

I’d like to thank all the people at Dr. Gadda’s lab, who made me feel at home even if I was so far away. I had a great time with you. Gracias a Chris por haberme entretenido tantas veces en Atlanta, por haberme llevado a tomar cervezas y margaritas, porque poder hablar en tu idioma es un alivio. I thank Dan Su for all his help inside and outside the lab during my months there. Thanks, Daniel, for all the hours you spent teaching me how to use the stopped flow and all the time we spent talking about a thousand different things. Gracias a Elías por haberme llevado a tomar cervezas, por haber hecho que lo pasase tan bien. Thank you, Jakob, for all your help and laughs.

Grazas a Raquel por tódolos anos baixo o mesmo teito ou fóra del. Grazas por entreterme calquera día da semana, facer que non colla po e non deixar que me deite cedo. Tamén por suxeitarme pola noitiña cando me dá o sono e aturarme cos problemas. Non podería ter atopado a ninguén tan coma min.

Gracias a mi familia. A mi madre por aguantarme y preocuparse por mí. A mi padre por ser tan atento y preocupado aunque yo sea un toxo. A Pilar por todos estos años, la ayuda y los consejos. A mis hermanos, Antonio y Jaime, por hacerme reír y portarse tan bien conmigo.

Abbreviations

AAO, aryl-alcohol oxidase
A_{D}, Arrhenius pre-exponential factor for D
ADP, adenosine diphosphate
AH, Arrhenius pre-exponential factor for H
AH/AD, isotope effect on Arrhenius pre-exponential factors
${}^{\mathrm{app}}k_{\mathrm{ox}}$, apparent second-order rate constant for oxidation
BSTFA, bis(trimethylsilyl)trifluoroacetamide
CDH, cellobiose dehydrogenase
CHD, choline dehydrogenase
CHO, cholesterol oxidase
D, deuterium
DFF, 2,5-diformylfuran
${}^{\mathrm{D}}({}^{\mathrm{app}}k_{\mathrm{ox}})_{\mathrm{D2O}}$, substrate deuteration KIE on ${}^{\mathrm{app}}k_{\mathrm{ox}}$ in deuterated solvent
${}^{\mathrm{D}}({}^{\mathrm{app}}k_{\mathrm{ox}})_{\mathrm{H2O}}$, substrate deuteration KIE on ${}^{\mathrm{app}}k_{\mathrm{ox}}$
${}^{\mathrm{D,D2O}}({}^{\mathrm{app}}k_{\mathrm{ox}})$, multiple deuteration KIE on ${}^{\mathrm{app}}k_{\mathrm{ox}}$
${}^{\mathrm{D2O}}({}^{\mathrm{app}}k_{\mathrm{ox}})_{\mathrm{D}}$, solvent deuteration KIE on ${}^{\mathrm{app}}k_{\mathrm{ox}}$ in deuterated substrate
${}^{\mathrm{D2O}}({}^{\mathrm{app}}k_{\mathrm{ox}})_{\mathrm{H}}$, solvent deuteration KIE on ${}^{\mathrm{app}}k_{\mathrm{ox}}$
${}^{\mathrm{D}}k_{\mathrm{cat}}$, deuterium isotope effect on k_{cat}
${}^{\mathrm{D}}K_{\mathrm{d}}$, deuterium isotope effect on K_{d}
${}^{\mathrm{D}}(k_{\mathrm{cat}}/K_{\mathrm{m}})$, deuterium isotope effect on $k_{\mathrm{cat}}/K_{\mathrm{m}}$
${}^{\mathrm{D}}k_{\mathrm{red}}$, deuterium isotope effect on k_{red}
${}^{\mathrm{D2}}k_{\mathrm{redD}}$ dideuteration effect on ${}^{\mathrm{D}}k_{\mathrm{red}}$
DT, deuteride transfer
E_{a}, energy of activation
E_{aD}, energy of activation for DT
E_{aH}, energy of activation for HT
FAD, flavin adenine dinucleotide
FDCA, 2,5-furandicarboxylic acid
FFCA, 5-formylfurancarboxylic acid
GC-MS, gas chromatography coupled to mass spectrometry
GLX, glyoxal oxidase
GMC, glucose-methanol-choline (superfamily of enzymes)
GOX, glucose oxidase
HMF, 5-hydroxymethylfurfural

HMFCA, 5-hydroxymethylfurancarboxylic acid

HRP, horseradish peroxidase

HT, hydride transfer

JGI, Joint Genome Institute

k_{cat}, catalytic constant

k_{cat}/K_m, catalytic efficiency

K_d, dissociation constant

k_{dis}, dissociation rate constant

k_{for}, formation rate constant

KIE, kinetic isotope effect

K_m, Michaelis constant

$K_{m(al)}$, Michaelis constant for the alcohol substrate

$K_{m(ox)}$, Michaelis constant for O_2

k_{obs}, observed rate constant

k_{rev}, reverse constant

k_{red}, reductive rate constant

LiP, lignin peroxidase

MMF, 5-methoxymethylfurfural

MMFA, 5-methoxymethylfurancarboxylic acid

MnP, manganese peroxidase

MOX, methanol oxidase

P2O, pyranose 2-oxidase

PBT, poly(buthylene-terephthalate)

PDA, photodiode array

PDH, pyranose dehydrogenase

PEF, poly(ethylene-2,5-furandicarboxylate)

PET, poly(ethylene-terephthalate)

pL, pH or PD

PPT, poly(propylene-terephthalate)

TMSi, trimethylsilyl

TOF, turnover frequency

TON, turnover number

TTN, total turnover number

UPO, unspecific peroxigenase

VP, versatile peroxidase

Table of Contents

List of Figures xi

List of Tables xix

Abstract xxiii

Resumen xxv

1. Introduction 1

1.1. Introduction to the glucose-methanol-choline (GMC) superfamily of enzymes. 3

1.2. Introduction to AAO 4

1.3. GMC and lignocellulose decay 6

1.3.1. The AAO family and ligninolytic fungi 9

1.3.2. White-rot decay 11

1.3.3. Brown-rot decay 12

1.4. AAO catalytic mechanism in detail 13

1.4.1. Involvement of quantum-mechanical tunneling in AAO catalysis 14

1.4.2. Reduction of O_2 by AAO and related oxidases 16

1.5. Biotechnological applications of GMC oxidoreductases 18

1.5.1. Paper pulp industry: Biopulping and biobleaching 18

1.5.1. Flavour synthesis 18

1.5.2. Deracemization of chiral secondary alcohols 20

1.5.3. Oxidation of furfurals 21

1.6. Summary 23

Structure and Objectives 25

2. Materials and Methods 27

2.1. Reagents 29

2.2. Genome screening and evolutionary studies 29

2.2.1. Genome sequencing 29

2.2.2. Genome screening for GMC gene families in Polyporales 29

2.2.3. Sequence analysis 30

2.2.4. GMC evolutionary history 31

2.2.5. Reconciliation analyses 31

2.3. AAO purification and mutagenesis 31

2.3.1. Enzyme production and purification 31

2.3.2. Site-directed mutagenesis 32

2.3.3. Estimation of the molar extinction coefficient of AAO 33

2.4. Kinetic and affinity studies 34

2.4.1. Stopped-flow measurements 34

2.4.2. Steady-state kinetics 37

2.4.3. Estimation of the rate constants for AAO-*p*-anisic acid complex formation and dissociation. 38

2.4.4. Studies on the temperature dependence of AAO catalysis. 38

2.4.5. Spectral characterization of the AAO-p-anisic acid complex. 39

2.5. Crystallization of wild-type AAO in complex with *p*-anisic acid 39

2.6. Reactions and enzymatic cascades of AAO with furfurals 41
2.6.1. Reactions 41

HMF and derivatives reactions 41
2.6.2. GC-MS analyses 41
2.6.3. Measurements of AAO and UPO residual activities after incubation with furfurals 42

2.7. NMR studies 42

3. GMC genes in 10 Polyporales genomes: A survey of genes encoding H_2O_2-producing GMC oxidoreductases 43

3.1. Results 45
3.1.1. GMC gene families in ten Polyporales genomes 45
3.1.2. Structural modeling of GMC oxidoreductases from Polyporales genomes 46
3.1.3. Evolutionary history of GMC oxidoreductases in the Polyporales genomes 49
3.1.4. GMC gene duplication and loss during diversification of Polyporales 51

3.2. Discussion 53
3.2.1. Aryl-alcohol oxidase 53
3.2.2. Glucose oxidase 54
3.2.3. Pyranose 2-oxidase 54
3.2.4. Methanol oxidase 55
3.2.5. Pyranose and cellobiose dehydrogenases 55
3.2.6. GMC oxidoreductases in Polyporales: final evolutionary/ecological remarks 56

4. An active site Phe contributes to product release in AAO catalysis 59

4.1. Results 62
4.1.1. Spectral properties and steady-state kinetics of AAO and its Phe397-mutated variants 62
4.1.2. Redox state during turnover 64
4.1.3. Rapid kinetics of the two AAO half reactions 66
4.1.4. Studies on AAO:*p*-anisic acid complex formation and dissociation 69

4.2. Discussion 72
4.2.1. Conservation of active-site Phe397 within the AAO family 72
4.2.2. Phe397 is critical for substrate diffusion to the active site 73
4.2.3. Phe397 also plays a role in AAO reoxidation 74
4.2.4. Phe397 involvement in product release 75

5. Protein motions promote hydride tunneling in AAO catalysis 77

5.1. Results 79
5.1.1. Crystallographic structure of WT AAO in complex with *p*-anisic acid 79
5.1.2. Temperature dependence of KIEs on WT AAO catalysis 81
5.1.3. Temperature dependence of the hydride transfer reaction of AAO Y92 variants 85

5.2. Discussion 89
5.2.1. Involvement of tunneling in HT transfer for WT and Y92 AAO variants 89
5.2.2. Role of protein motions in HT and DT 90
5.2.3. Substitution of an active-site residue alters HT and DT 91
5.2.4. AAO structure fosters HT 93

6. Non-concerted hydrogen and proton transfers from AAO to dioxygen 95
6.1. Results 97
6.1.1. Preparing reduced AAO 97
6.1.2. Reoxidation of AAO 97
6.1.3. Solvent isotope and pL-related effects 99
6.1.4. Substrate isotope effects 101
6.1.5. Individual and multiple isotope effects at pL 8 101
6.1.6. Presence of intermediate species 103
6.1.7. Wash-out of the hydrogen bound to flavin N5 103
6.2. Discussion 105
6.2.1. The AAO catalytic cycle 105
6.2.2. H transfer limits the reoxidation reaction in AAO 106
6.2.3. Isotope effects (at high pL) reveal non-concerted H and H^+ transfers 107
7. 5-Hydroxymethylfurfural conversion by fungal aryl-alcohol oxidase and unspecific peroxygenase 109
7.1. Results 111
7.1.1. AAO oxidation of HMF and its partially-oxidized derivatives 111
7.1.2. AAO kinetic parameters for HMF and its partially-oxidized derivatives 113
7.1.3. Oxidation of FFCA's aldehyde group by H_2O_2 114
7.1.4. Fungal peroxygenase for HMF conversion 114
7.1.5. Complete HMF conversion by an AAO-UPO reaction cascade 115
7.1.6. NMR analysis of carbonyl hydration in HMF-derived furanaldehydes 117
7.2. Discussion 119
7.2.1. Substrate specificity of a fungal model flavooxidase (AAO) 119
7.2.2. HMF and DFF: Two new AAO substrates 119
7.2.3. Oxidase/peroxygenase cascade for HMF conversion into FDCA 121
8. Discussion 123
8.1. Wealth of GMC genes and their biotechnological potential 126
8.2. Elucidation of the catalytic mechanisms to obtain better biocatalysts. 128
8.3. Reoxidation of wild-type AAO and mutated variants 129
8.4. Rate-limiting steps in AAO catalysis 129
8.5. New AAO substrates 130
Conclusions 131
Annexes 135
Bibliography 141

List of Figures

Figure 1.1. Lignin structure showing its syringyl (S), guaiacyl (G) and *p*-hydroxyphenyl (H) phenylpropanoid with different inter-unit linkages. 7

Figure 1.2. Scheme of the natural role of AAO in decay of plant cell-wall producing H_2O_2 for: i) activation of lignin-degrading peroxidases; and ii) formation of cellulose-depolymerising hydroxyl radical (also causing lignin oxidation). 10

Figure 1.3. Substrate migration studies revealed several positions of substrate and AAO active-site residues. Taken from Hernández-Ortega et al. (2011). 14

Figure 1.4. Proposed *P. eryngii* AAO catalytic cycle. 15

Figure 1.5. Catalytic efficiencies of *P. eryngii* and *B. adusta* AAOs in bioconversion of some flavours and aromas. **A.** Oxidation of vanillyl alcohol into vanillin. **B.** Oxidation of benzyl alcohol into benzaldehyde. **C.** Oxidation of *p*-methoxybenzyl alcohol into *p*-methoxybenzaldehyde. 19

Figure 1.6. Chiral HPLC chromatograms showing the deracemization of 1-(*p*-methoxyphenyl)-ethanol by *P. eryngii* AAO. **A.** Chromatogram of the untreated racemate. **B.** Chromatogram after 24-h reaction with AAO, where only the peak of the (*R*) isomer is detected (the peak of the *p*-methoxyacetophenone, formed from oxidation of the (*S*) isomer, eluted in a different region of the chromatogram). .. 21

Figure 1.7. Oxidative pathways from HMF (**1**) to FDCA (**5**). FFCA (**4**) formation can take place through two alternative intermediate compounds: DFF (**2**) or HMFCA (**3**). 22

Figure 1.9. Scheme depicting the physiological role of AAO in lignocellulose degradation and its potential applications in the cellulose and other chemical sectors. 23

Figure 3.1. Ribbon models for the molecular structures of representative members of the five GMC oxidoreductase families found in 10 Polyporales genomes (flavin and heme cofactors as yellow and red sticks, respectively). **A.** AAO of *B. adusta* (JGI protein ID 245059) indicating the position of 4 β-sheets, individual β-strands, and 19 α-helices. **B.** MOX (monomer) of *F. pinicola* (JGI protein ID 156775). **C.** GOX (monomer) of *P. chrysosporium* (JGI protein ID 131961). **D.** CDH of *G. subvermispora* (JGI protein ID 84792) (flavin domain in the left and heme domain in the right. **E.** P2O (monomer) of *B. adusta* (JGI protein ID 34622). The molecular models were built using crystal structures of related proteins as templates.. 47

Figure 3.2. Detail of active-site residues in the molecular models for the five Polyporales GMCs shown in **Figure 3.1**. **A.** *B. adusta* AAO. **B.** *F. pinicola* MOX. **C.** *P. chrysosporium* GOX. **D.** *G. subvermispora* CDH. **E.** *B. adusta* P2O. Residue numbering corresponds to the putative mature proteins. FAD and the selected residues are shown in sticks in CPK yellow and grey colors respectively. The Asn390-Thr402 loop of AAO is shown in orange. 48

Figure 3.3. Maximum likelihood tree of the 95 GMC sequences from 10 Polyporales genomes (different color labels), prepared with RaxML (with gaps treated as deletions). The AAO, MOX, P2O and CDH clusters (and the *a* and *b* subclusters mentioned in the text) are shown, together with a few GOX sequences related to AAOs. Numbers at nodes indicate bootstrap values. Those sequences modeled in **Figures 3.1** and **3.2** are indicated by arrows. See **Table 3.1** for abbreviations of the fungal species. 50

Figure 3.4. Estimated range of GMC gene copies at the ancestral nodes (and extant species) of the represented phylogeny of Polyporales taken from Binder et al. (2013) after reconciliation with the gene phylogeny (**Figure 3.3**) using Notung. Branches and numbers after gene expansion and contraction are in blue and red color, respectively. For reconciliation of the individual GMC families, see **Figure 3.5**. 51

Figure 3.5. Estimated range of individual AAO (**A**), MOX (**B**), GOX (**C**), CDH (**D**) and P2O (**E**) gene copies, and total GMC from sum of family gene numbers (**F**), at the ancestral nodes of the represented phylogeny of Polyporales taken from Binder et al. (2013) after reconciliation with the gene phylogeny. Branches and numbers after gene expansion and contraction are in blue and red color, respectively. 52

Figure 4.1. Characteristic loop and aromatic residues delimiting the FAD access in AAO. **A.** Channel opening in AAO surface. **B.** Semitransparent surface showing aromatic residues (Tyr92, Phe397 and Phe501) and loop (green) limiting the access to FAD and catalytic histidine (His502), with one product (*p*-anisic acid) molecule at the active site. From AAO:anisic acid structure (Carro et al. 2017). ..61

Figure 4.2. Spectra of the WT (solid line), F397Y (dotted line), F397A (short dash line), F397W (dash-dot line) and F397L (long dash line) AAO variants recorded between 300 and 600 nm in 50 mM sodium phosphate pH 6.0.......... 62

Figure 4.3. Linearized Hanes-Woolf plots of the bi-substrate kinetics of **A.** F397Y. **B.** F397A. **C.** F397W. **D.** F397L AAO variants measured by varying the concentrations of *p*-methoxybenzyl alcohol and O_2 in 50 mM sodium phosphate pH 6.0 at 12°C. Vertical solid line represents x = 0. Filled circles, 0.06 mM O_2; open circles, 0.16 mM O_2; filled triangles, 0.34 mM O_2; open triangles, 0.71 mM O_2; and filled squares, 1.60 mM O_2. 63

Figure 4.4. Redox state during turnover of native AAO and its Phe397-mutated variants. Wild-type (*green*), F397W (*orange*), F397L (*blue*), F397A (*black*) and F397Y (*red*) AAO variants (~10 μM) were mixed with an excess of *p*-methoxybenzyl alcohol in 50 mM sodium phosphate (pH 6) at 25°C under aerobic conditions. Lines show the time course of absorbance changes at the maxima of the flavin band I (between 459 and 463 nm, depending on the variant).....64

Figure 4.5. Spectral changes of F397 AAO mutated variants recorded between 300 and 700 nm under air-saturated atmosphere in 50 mM sodium phosphate pH 6.0 at 25°C with excess of *p*-methoxybenzyl alcohol. **A.** F397Y at 0.001, 0.05, 0.1, 0.2, 0.5, 1, 5, 10, 50, 100, 200 s. **B.** F397W at 0.001, 0.05, 2, 5, 10, 20, 200, 1000 s. **C.** F397A at 0.001, 0.005, 0.01, 0.05, 0.1, 0.2, 0.5, 1, 200 and 500 s. **D.** F397L at 0.001, 0.005, 0.05, 0.1, 0.2,0.5, 1, 2, 50, 100 and 500 s.....65

Figure 4.6. Time course of the reduction of Phe397-mutated variants of AAO with 37 µM of *p*-methoxybenzyl alcohol. **A.** F397Y spectra measured after 0.001, 0.005, 0.01, 0.015, 0.02, 0.025, 0.03, 0.04, 0.05 and 0.1 s. **B.** F397W spectra recorded at 0.001, 0.01, 0.02, 0.03, 0.05, 0.07, 0.1, 0.13, 0.15, 0.2 and 0.5 s. **C.** F397A reduction spectra at 0.001, 0.01, 0.02, 0.03, 0.04, 0.05, 0.06, 0.08, 0.1, 0.15 and 0.3. **D.** F397L spectra after 0.001, 0.01, 0.02, 0.03, 0.05, 0.07, 0.1, 0.13, 0.15, 0.2 and 0.4. Dashed lines correspond to the oxidized enzymes. Data were globally fitted to a single-step model described from initial species A to final species B (shown in insets). Estimated k_{obs} is represented in each panel.....66

Figure 4.7. Time course of the oxidation of Phe397-mutated variants of AAO. **A.** F397Y oxidation spectra with 26 µM O_2 measured at 0.002, 0.01, 0.02, 0.03, 0.05, 0.1, 0.15, 0.2, 0.3, 0.5, 1 and 3 s. **B.** F397W oxidized with 60 µM O_2 recorded at 0.002, 0.003, 0.005, 0.1, 0.15, 0.2, 0.025, 0.03, 0.04, 0.05 and 0.5 s. **C.** F397A after mixing with 26 µM O_2 at 0.002, 0.01, 0.05, 0.1, 0.15, 0.5, 1, 1.5, 2, 3, 4 and 5 s. **D.** F397L oxidized with 26 µM O_2 recorded at 0.003, 0.006, 0.009, 0.012, 0.015, 0.025, 0.03, 0.5, 0.7, 1, 2 and 3 s. Dashed lines correspond to the reduced enzymes. Insets show the traces at the maximum of flavin band I superimposed with their fits in red. Residuals of each fit displayed at the bottom of the insets. The estimated k_{obs} for each phase is also represented.....68

Figure 4.8. LigPlot+ diagram showing the interactions among the active-site residues and the FAD cofactor with the ligand, *p*-anisic acid, in the crystallographic structure of the complex. Green dashed lines represent H bonds between donor and acceptor atoms accompanied by their bonding distances. Red lines in semicircles represent hydrophobic interactions among the represented residues and the different atoms of *p*-anisic acid (Laskowski and Swindells 2011).....69

Figure 4.9. Spectral changes upon titration of wild-type and Phe397 AAO variants with increasing concentrations of *p*-anisic acid. Unbound spectra of each of the variants were subtracted to the spectra of the titrated enzyme to obtain the data represented. **A**, Native AAO, and **B-D**, F397Y, F397W and F397A variants, respectively.....70

Figure 4.10. Spectral changes upon formation of the AAO-*p*-anisic acid complex. **A.** Native AAO, mixed with 0.5 mM of the ligand at 0.003, 0.01, 0.02, 0.03, 0.04, 0.05, 0.065, 0.085, 0.1, 0.13, 0.15, 0.2 and 0.4 s.**B.** F397Y AAO, mixed with 0.65 mM of *p*-anisic acid measured after 0.005, 0.05, 0.1, 0.2, 0.3, 0.4, 0.5, 0.6, 0.7, 0.8, 0.9, 1, 2, 3 and 4 s, and **C.** F397W AAO mixed with *p*-anisic acid 1 mM recorded at 0.005, 0.02, 0.04, 0.05, 0.07, 0.1, 0.2, 0.4, 0.5, 0.7, 1, 2 and 5 s. Insets show disappearance of initial species A and formation of final species B. The rate constant obtained from the global fitting of the spectral changes is shown. **D.** Fits of the obtained $k_{obs}$for each variant and ligand concentration to **equation 6**: y_0 and slope represent the rate constants for dissociation (k_{dis}) and formation (k_{for}) of the AAO-*p*-anisic acid complexes, respectively, for native AAO (filled circles), and its F397Y (open circles) and F397W (inverted triangles) variants. 71

Figure 4.11. Sequence logo for 70 putative AAO sequences from various basidiomycetes corresponding to positions 390–403 of mature *P. eryngii* AAO generated using WebLogo (Crooks et al. 2004). Sequences were taken either from genomes available at the Joint Genome Institute (www.jgi.doe.gov) or from GenBank; the numbers of sequences are indicated in the parentheses: *Bjerkandera adusta* (11), *Dichomitus squalens* (9), *Fomitiporia mediterranea* (1), *Fomitopsis pinicola* (1), *Ganoderma* sp. (7), *Gelatoporia subvermispora* (4), *Gloeophyllum trabeum* (2), *Laccaria bicolor* (1), *Phanerochaete chrysosporium* (3), *Phlebia brevispora* (3), *P. eryngii* (1), *Pleurotus pulmonarius* (1), *Punctularia strigosozonata* (6), *Rhodonia placenta* (2), *Stereum hirsutum* (15) and *Trametes versicolor* (3). Numbering represents the position in the *P. eryngii* mature AAO sequence and the heights of each symbol in the same column indicate the relative frequency of each amino acid at that very position. 73

Figure 5.1. Reductive half-reaction of AAO. Hydrogen in position pro-*R* of the α-carbon is abstracted as a hydride by the N5 locus of FAD concomitantly to the abstraction of the hydroxyl proton by His502. This results in the formation of $FADH_2$, an aldehyde and the protonation of His502. 79

Figure 5.2. A. Cartoon superposition of the crystallographic structures of AAO:*p*-anisic acid complex (orange) and apo AAO (pdb 3FIM) (blue). **B.** Detail of the active site superimposed in AAO:*p*-anisic acid complex and in apoAAO. The H-bounds between the O carboxylic atoms of the *p*-anisic acid and the N atoms of the isoalloxazine ring and His 546 and 502 residues are drawn in black lines and distances in Å. FAD, *p*-anisic acid and residues are drawn as CPK colored sticks with Cα in wheat (complex) and blue (apoAAO). 80

Figure 5.3. Temperature dependences of steady-state kinetic parameters for WT AAO. **A.** Arrhenius plots of k_{cat} with [α-$^1H_2$]-*p*-methoxybenzyl alcohol (filled circles) and [α-$^2H_2$]-*p*-methoxybenzyl alcohol (open circles). **B.** Temperature dependence of the KIE of k_{cat} ($^Dk_{cat}$) with [α-$^2H_2$]-*p*-methoxybenzyl alcohol. **C.** Arrhenius plots of k_{cat}/K_m with [α-$^1H_2$]-*p*-methoxybenzyl alcohol (filled triangles) and [α-$^2H_2$]-*p*-methoxybenzyl alcohol (open triangles). **D.** Temperature dependence of the KIE of catalytic efficiency $^D(k_{cat}/K_m)$,. Vertical bars represent standard deviations. 81

Figure 5.4. Temperature dependences of HT reaction for WT AAO **A.** Arrhenius plots of k_{red} with α-protiated *p*-methoxybenzyl alcohol (filled circles), (*R*)-[α-^{2}H]-*p*-methoxybenzyl alcohol (open circles) and [α-$^2H_2$]-*p*-methoxybenzyl alcohol (open inverted triangles). **B.** Temperature dependence of the KIE of k_{red} ($^Dk_{\text{red}}$) with (*R*)-[α-^{2}H]-*p*-methoxybenzyl alcohol (open circles) and [α-$^2H_2$]-*p*-methoxybenzyl alcohol (filled circles). Vertical bars represent standard deviations. 84

Figure 5.5. Reduction spectra of Y92 AAO variants with [α-$^2H_2$]-*p*-methoxybenzyl alcohol at 12°C. **A.** WT AAO with 31 µM of substrate at times: 0.004, 0.015, 0.02, 0.03, 0.05, 0.07, 0.1, 0.13, 0.15, 0.2 and 0.3 s. **B.** Y92F with 37 µM of substrate after: 0.001, 0.01, 0.02, 0.03, 0.05, 0.07, 0.1 0.13 and 0.15 s. **C.** Y92L with 37µM of substrate at times: 0.001, 0.02, 0.03, 0.05, 0.07, 0.1 0.15, 0.2, 0.3, 0.4, 0.6 and 0.8. **D.** Y92W with 312 µM of substrate after: 0.16, 0.5, 1, 3, 5, 7, 10, 15, 20, 30 and 60 s. Dashed lines represent the unbound enzyme spectra. Insets show initial and final species determined after global fitting of the reduction spectra. 86

Figure 5.6. Temperature dependences of of HT reaction for AAO Y92 variants: **A.** Arrhenius plots for the reduction of Y92F with α-protiated *p*-methoxybenzyl alcohol (filled triangles) and [α-$^2H_2$]-*p*-methoxybenzyl alcohol (open triangles). **B.** Arrhenius plots for the reduction of Y92L with α-protiated *p*-methoxybenzyl alcohol (filled squares) and [α-$^2H_2$]-*p*-methoxybenzyl alcohol (open squares). C. Arrhenius plots for the reduction of Y92W with α-protiated *p*-methoxybenzyl alcohol (filled diamonds) and [α-$^2H_2$]-*p*-methoxybenzyl alcohol (open diamonds). **D.** Temperature dependence of $^Dk_{\text{red}}$ for Y92F (filled inverted triangles), Y92L (open triangles) and Y92W (filled squares). Vertical bars represent standard deviations. 87

Figure 6.1. Time-resolved absorbance spectroscopy of the reoxidation of reduced AAO, which was premixed with *p*-methoxybenzyl alcohol (1:1 concentration) allowed to age for 1 s, at varying O_2 concentrations. Traces at 463 nm show the biphasic behavior of the reaction (first and second phase separation is shown by a vertical dashed line). Fits to exponential equations are shown. Inset shows spectra of the initial (reduced, black) and final (oxidized, red) flavin species. 98

Figure 6.2. Plots of the O_2 dependency of the k_{obs} of the two phases of the reoxidation. **A.** k_{obs1} *vs* O_2 concentration showing its linear dependency. **B.** k_{obs2} *vs* O_2 concentration showing its independency. Values are shown as means and vertical lines are standard deviations. Average of the mean values in **B** is 17 ± 0.1 s^{-1}. 99

Figure 6.3. pH (filled circles) and pD (open triangles) contributions to solvent effects on $^{\text{app}}k_{\text{ox}}$. Values shown are means and vertical lines indicate standard deviations. Average of the log $^{\text{app}}k_{\text{ox}}$mean values in both H_2O and D_2O is 5.8 ± 0.1. 100

Figure 6.4. Spectra of wild-type AAO in sodium phosphate 25 mM pH 8.0 (solid line) and sodium acetate 100 mM pH 5.0 (dotted line). Differences in the shoulder around 500 nm and the ratio band I/band II are shown. 101

Figure 6.5. Traces showing the reoxidation of AAO (7°C, pH 8.0 and 5.0) at different wavelengths characteristic of possible intermediates in the reaction. **A.** Reaction in 25 mM sodium phosphate, pH 8.0. **B.** Reaction in 100 mM sodium acetate, pH 5.0. Insets show the spectra of the reduced and oxidized species of the enzyme with arrows indicating the direction of the spectral changes. Lack of transient species points out the absence of any detectable intermediates. Fits to exponential equations are shown under the spectral evolution changes. 104

Figure 6.6. Plot of the values of k_{obs1} as a function of the time of incubation after reduction of the enzyme using [α-$^2H_2$]-*p*-methoxybenzyl alcohol in aqueous buffer, which was fitted to an exponential function yielding $y = 58 + 29 \times (1 - e^{-0.003 \times t})$ ($R^2 = 0.99$). There is an evident tendency towards the increase of the values, indicating the gradual loss of the deuterated tag on flavin N5 by exchange with the solvent. Means and standard deviations. 105

Figure 7.1. Pathway for 5-hydroxymethylfurfural (HMF) conversion into 2,5-furandicarboxylic acid (FDCA), *via* 2,5-formylfurancarboxylic acid (FFCA), including 2,5-diformylfuran (DFF) or 2,5–hydroxymethyl furancarboxylic acid (HMFCA) intermediates. 111

Figure 7.2. HMF and DFF transformation by *P. eryngii* AAO. (**A**, **B**) HMF and DFF (3 mM), respectively, treatment (5 mL) with AAO (5 µM, corresponding to 54 U measured with veratryl alcohol) yielding 90-98% FFCA after 4 h, which was then slowly oxidized to FDCA (6-10% after 24 h). The AAO residual activity is also shown in **A**. 112

Figure 7.3. FFCA transformation by *A. aegerita* UPO. FFCA (3 mM, 5 mL reaction) was slowly oxidized by UPO (20 U measured with veratryl alcohol) and H_2O_2 (4 mM) to FDCA (~90% after 120 h). The UPO residual activity is also shown, as well as the comparison with the blank reactions (controls without enzyme). 115

Figure 7.4. HMF transformation by P. eryngii AAO plus A. aegerita UPO (successive addition). After 4 h treatment of HMF with AAO almost all HMF was converted into FFCA, and UPO was added to complete the HMF transformation into FDCA. 116

Figure 7.5. ^1H-NMR spectra (5.6-10.0 ppm) of HMF (A), DFF (B) and FFCA (C) in DMSO-d_6. 118

Figure 7.6. ^1H-NMR analyses revealing different hydration degrees. The ^1H-NMR spectra (5.8-10.2 ppm) of 10 mM HMF (A), DFF (B) and FFCA (C) in ^2H_2O show the H_1 to H_4 signals in the aldehyde and *gem*-diol (asterisks) forms, enabling calculation of their hydration degrees. 118

Figure 7.7. Scheme for enzymatic conversion of HMF into FDCA in a cofactor-free reaction cascade involving *P. eryngii* AAO and *A. aegerita* UPO. 1, HMF; 2, DFF; 3, FFCA; 4, FDCA. Symbols by numbers indicate hydrated, *gem*-diol forms of the carbonyl groups. Percentages on the reactions indicate the abundance of each of the species at equilibrium. 122

List of Tables

Table 1.1. Comparison of the catalytic efficiencies of *P. eryngii* and *B. adusta* AAO oxidising representative alcohol and aldehyde substrates..............................5

Table 1.2. Inventory of peroxidase and GMC (AAO, aryl-alcohol oxidase; CDH, cellobiose dehydrogenase; MOX, methanol oxidase and P2O, pyranose 2-oxidase) genes in eleven white-rot Agaricomycotina (AD, *Auricularia delicata*; PST, *Punctularia strigosozonata*; FM, *Fomitiporia mediterranea*; DS, *Dichomitus squalens*; TV, *Trametes versicolor*; SH, *Stereum hirsutum*; BA, *Bjerkandera adusta*; PB, *Phlebia brevispora*; PC, *Phanerochaete chrysosporium*; GS, *Ganoderma* sp. in the *Ganoderma lucidum* complex and CS, *Ceriporiopsis subvermispora*) genomes...12

Table 1.3. Inventory of peroxidase and GMC genes (see **Table 1.2** for enzyme abbreviations) in six brown-rot Agaricomycotina (CP, *Coniophora puteana*; GT, *Gloeophyllum trabeum*; FP, *Fomitopsis pinicola*; WC, *Wolfiporia cocos*; DSP, *Dacryopinax* sp. and RP, *Rhodonia placenta*) genomes......................................13

Table 2.1. Cycles of the mutagenic PCR programme..33

Table 2.2. Data collection and refinement statistics for *AAO:*p*-anisic acid* complex..40

Table 3.1. Inventory of 95 genes from six GMC families in the genomes of 10 Polyporales species (BJE AD*, B. adusta*; PHL BR, *P. brevispora*; PHA CH*, P. chrysosporium*; DIC SQ, *D. squalens*; GAN SP, *Ganoderma* sp.; TRA VE, *T. versicolor*; GEL SU, *G. subvermispora*; FOM PI, *F. pinicola*; RHO PL, *R. placenta*; and WOL CO*, W. cocos*) from four different clades, producing white-rot and brown-rot decay of wood. Four allelic variants are excluded from the inventory (**Annex 1**)..46

Table 4.1. Kinetic parameters for steady-state reaction of native AAO and its Phe397 variants in the oxidation of *p*-methoxybenzyl alcohol.............................63

Table 4.2. Transient-state kinetic parameters for the reductive half-reaction of native AAO and its Phe397 variants...67

Table 4.3. Transient-state kinetic parameters for the oxidative half-reaction of native AAO and its Phe397 variants...67

Table 4.4. Dissociation constant (K_d), and rate constants of formation (k_{for}) and dissociation (k_{dis}) of *p*-anisic acid complexes by native AAO and its Phe397 variants...72

Table 5.1. Estimated k_{cat}, K_m and k_{cat}/K_m constants (value ± S.D.) for the steady-state kinetics of wild-type AAO with α-protiated and α-dideuterated *p*-methoxybenzyl alcohols..82

Table 5.2. Thermodynamic parameters from the temperature dependence of the turn-over and hydride transfer reaction in WT AAO oxidation of α-protiated and α-deuterated *p*-methoxybenzyl alcohols....82

Table 5.3. KIEs determined from the temperature dependence of the steady-state in WT AAO....83

Table 5.4. Reduction rate (k_{red}) and dissociation (K_d) constants (value ± S.D.) for wild-type AAO with α-protiated and α-deuterated *p*-methoxybenzyl alcohols....83

Table 5.5. KIEs determined from the temperature dependence of hydride transfer reaction (k_{red}) in WT AAO....84

Table 5.6. Estimated KIEs on K_d for wild-type AAO and Y92F, Y92L and Y92W....85

Table 5.7. Thermodynamic parameters from the temperature dependence of the hydride transfer reaction (k_{red}) in Y92 AAO variants oxidation of α-protiated and (*R*)-[α-^{2}H]-*p*methoxybenzyl alcohols....88

Table 5.8. Reduction rate (k_{red}) and dissociation (K_d) constants (value ± S.D.) for Y92F AAO with α-protiated and [α-$^2H_2$]-*p*-methoxybenzyl alcohol....88

Table 5.9. Reduction rate (k_{red}) and dissociation (K_d) constants (value ± S.D.) for Y92L AAO with α-protiated and [α-$^2H_2$]-*p*-methoxybenzyl alcohol....88

Table 5.10. Reduction rate (k_{red}) and dissociation (K_d) constants (value ± S.D.) for Y92W AAO with α-protiated and [α-$^2H_2$]-*p*-methoxybenzyl alcohol....89

Table 5.11. Estimated KIEs on K_d for wild-type AAO and Y92F, Y92L and Y92W....89

Table 5.13. Secondary KIE on the reduction (k_{red}) of wild-type AAO with α-deuterated *p*-methoxybenzyl alcohols....90

Table 6.1. Reduction times of AAO mixed protiated or dideuterated alcohol substrates **(1:1, *c:c*)** at 12 °C in H_2O or D_2O calculated by following the reaction spectrophotometrically in a stopped-flow apparatus....97

Table 6.2. Substrate and solvent KIE at different pL values for the reoxidation of AAO at 12°C....99

Table 6.3. Kinetic parameters for the reoxidation of AAO with protiated (H) and deuterated (D) *p*-methoxybenzyl alcohol in protiated and deuterated solvents at different pLs and 12°C....102

Table 6.4. KIE on the second-order rate constant for flavin oxidation at pL 8.0....102

Table 7.1. Kinetic parameters for HMF, DFF, FFCA and HMFCA oxidation by AAO (estimated from H_2O_2 formed)....113

Table 7.2. Molar percentages (from 5-mL reactions) after 24-h treatment of HMF (3 mM) with AAO alone (5 µM, corresponding to 54 U measured with veratryl alcohol), UPO alone (0.65 µM, corresponding to 20 U measured with veratryl alcohol), and with AAO (5 µM, 54 U) and UPO (0.65 µM, 20 U) added simultaneously (sim) or successively (suc); as well as after 24-h treatment of DFF (3 mM) with AAO (5 µM, 54 U), and FFCA (3 mM) with 6 and 200 mM H_2O_2.......117

Abstract

The glucose-methanol-choline oxidase/dehydrogenase (GMC) superfamily of enzymes is composed of FAD-containing, phylogenetically-related proteins that share a common fold subdivided into two different domains: the FAD-binding and substrate-binding ones. Some fungal oxidoreductases belonging to the superfamily play a role as auxiliary enzymes in the lignocellulose-degrading process. Most of them are extracellular oxidoreductases that produce the H_2O_2 required: (i) by high redox potential peroxidases to act on lignin; or (ii) to trigger Fenton reactions, which give rise to radical oxygen species that attack lignocellulose.

Investigation of the genomes of 10 selected Polyporales fungi, the only microorganisms able to completely mineralize lignin, shed light on the involvement of 5 families of GMC oxidoreductases in the lignocellulose decay. These were glucose oxidases (GOX), cellobiose dehydrogenases (CDH), pyranose 2-oxidases (P2O), methanol oxidases (MOX) and aryl-alcohol oxidases (AAO). Phylogenetic studies carried out suggest that they share a common ancestor whose diversification took place at a more ancestral stage of fungal evolution, which is characterized by a low number of these GMC genes. AAO and MOX proved to be the most abundant GMC oxidoreductases present in the selected genomes. The number of genes encoding for these enzymes varies from one genome to another according to the ecophysiology of the fungi. In fact, brown-rot fungi, which do not mineralize lignin but alter its structure to gain access to carbohydrates, lost most of their lignin-degrading enzymes and GMC repertoire, except MOX. These fungi cause the demethoxylation of lignin that releases methanol and relies on the reactivity of radical oxygen species stemming from H_2O_2. These findings point out the co-evolution of these fungal GMC enzymes with the lignin-degrading peroxidases.

AAO from the basidiomycete *Pleurotus eryngii* was selected as a model representative of the GMC superfamily to be studied from a mechanistic point of view. It is an enzyme that catalyzes (i) the oxidative dehydrogenation of benzylic alcohols into their corresponding aldehydes and (ii) the reduction of O_2 to H_2O_2, in two separate half-reactions. The reductive one consists in the abstractions of the pro-*R* hydrogen as a hydride from the α-carbon of the alcohol substrate by the FAD cofactor and of the proton from the hydroxyl group by the catalytic H502 residue. During the reoxidative half-reaction, these particles are eventually transferred to O_2, thereby reducing it to H_2O_2.

The role of the residue Phe397 in AAO catalysis was studied by comparing the steady and transient-state kinetics of the wild-type enzyme with those of mutated variants for this position. Results suggested that, opposite to wild-type enzyme in which the reduction acts as the limiting step of the overall catalysis, in some variants neither of the half reactions was rate limiting. Affinity studies, as well as the rate constants estimated for the formation and dissociation of the enzyme-product complex using a product analog suggested the involvement of residue Phe397 in the product release from the active site. Furthermore, substitution of Phe397 with non-aromatic residues resulted in a decrease in the oxidation constants.

The temperature dependence of AAO catalysis was studied with the aim of elucidating the involvement of the mechano-quantical effect known as hydrogen tunneling in the hydride transfer taking place during the reductive half-reaction of the enzyme. Data drawn from steady-state and rapid kinetics with protiated and deuterated substrates indicate that the tunneling effect is actually involved in the said transfer. Moreover, comparison of kinetic data for wild-type AAO and mutated variants of residue Tyr92 suggests that the transfer depends on thermally-activated protein motions that enable the enzyme to transfer the particle from an already pre-formed, highly organized, enzyme-substrate configuration. These results are also reinforced by the crystallographic structure resolved for the AAO:*p*-anisic acid complex, an inhibitor of the enzyme.

The mechanisms lying behind the reoxidation of the enzyme and concomitant production of H_2O_2 had not been extensively characterized. Therefore, they were studied by rapid kinetics using solvent and substrate kinetic isotope effects. These investigations revealed that, after the initial and obligate electron transfer to overcome the spin inversion barrier, the enzyme transfers one hydrogen atom from FAD and one proton from a solvent exchangeable site in two separate kinetic steps, which are, thus, non-concerted. The solvent isotope effect that revealed this feature was negligible at acidic pHs and appeared as a consequence of the combination of the lower proton availability at basic pHs and the use of a deuterated solvent that slowed down the reaction.

Finally, the potential biotechnological application of GMC oxidases was also assessed for the production of 2,5-furandicarboxylic acid (FDCA), which can be polymerized with ethylene glycol to produce renewable bioplastics. AAO from *P. eryngii* demonstrated to be capable of catalyzing the oxidation of precursors of FDCA that are derived from the dehydration of fructose present in plant biomass: 5-hydroxymethylfurfural (HMF) and its partially oxidized derivatives. In spite of its activity on HMF and some partially oxidized derivatives, AAO alone was not able to convert any of them into FDCA. Such inability was solved by the combined action of unspecific peroxygenase (UPO) from the fungus *Agrocybe aegerita*, which was able to overcome the AAO limitations at expenses of the H_2O_2 generated by it. The synergistic activity of these two enzymes allowed the creation of an enzymatic cascade for the production of FDCA from HMF. AAO and UPO converted 90% of initial HMF into FDCA with the only net consumption of atmospheric O_2.

Resumen

La superfamilia de enzymas glucosa-metanol-colina (GMC) oxidasas/deshidrogenasas se compone de proteínas que contienen FAD filogenéticamente relacionadas entre sí que comparten un plegamiento común que se subdivide en dos dominios diferentes: el de unión a FAD y el de unión a sustrato. Algunas oxidorreductasas fúngicas que pertenecen a esta superfamilia desempeñan la función de enzimas auxiliares en el proceso de degradación de la lignocelulosa. La mayor parte de ellas son oxidorreductasas extracelulares que producen el H_2O_2 requerido: (i) por las peroxidasas de alto potencial redox para actuar sobre la lignina; o (ii) para desencadenar las reaciones de Fenton, que dan lugar a especies radicales de oxígeno que atacan a la lignocelulosa.

El estudio de los genomas de 10 hongos seleccionados del orden Poliporales, los únicos organismos capaces de mineralizar totalmente la lignina, arrojó luz sobre la participación de 5 familias de oxidorreductasas GMC en la descomposición de la lignocelulosa. Estas fueron las glucosa oxidasas (GOX), celobiosa deshidrogenasas (CDH), piranosa 2-oxidasas (P2O), metanol oxidasas (MOX) y aril-alcohol oxidasas (AAO). Los estudios filogenéticos sugieren que estas enzimas comparten un ancestro común cuya diversificación tuvo lugar en una etapa más temprana de la evolución fúngica, que se caracterizó por el escaso número de estos genes GMC. Las AAO y las MOX resultaron ser las oxidorreductasas GMC más abundantes en los genomas seleccionados. El número de genes que codifican para estas proteínas varía ampliamente de un genoma a otro de acuerdo con las características ecofisiológicas de cada hongo. De hecho, los hongos de podredumbre parda, que no mineralizan la lignina, sino que alteran su estructura con el fin de acceder a los carbohidratos embebidos en esta, perdieron la mayor parte del repertorio de enzimas GMC, con excepción de las MOX. Estos hongos causan la demetoxilación de la lignina, que libera metanol y depende de la reactividad de las especies radicales de oxígeno que se originan del H_2O_2. Estos hallazgos indican la coevolución de la enzimas GMC fúngicas con las peroxidasas degradadoras de la lignina.

La AAO del basidiomiceto *Pleurotus eryngii* fue seleccionada como modelo representativo de la familia para ser estudiada desde el punto de vista mecanístico. Se trata de una enzima que cataliza: (i) la deshidrogenación oxidativa de alcoholes aromáticos produciendo los correspondientes aldehídos y (ii) la reducción de O_2 a H_2O_2 en dos semirreacciones separadas. La semirreacción de reducción consiste en las abstracciones del hidrógeno en posición pro-*R* del carbono α del substrato alcohol en forma de hidruro por el FAD y la del protón del grupo hidroxilo por la His502 catalítica. Durante la semirreacción de oxidación estas partículas son finalmente transferidas al O_2 reduciéndolo.

El papel que el residuo Phe397 desempeña en la catálisis de la AAO se estudió mediante la comparación de las cinéticas tanto de estado estacionario como transitorio entre la enzima salvaje y variantes mutadas para este residuo. Los resultados sugieren que la Phe397 está involucrada en ayudar al sustrato a entrar y acomodarse en el centro activo, así como en la salida del producto aldehído. Además, los estudios de afinidad llevados a cabo, así como las constantes cinéticas estimadas para la formación y disociación del complejo enzima-producto empleando un análogo del mismo, avalan esta hipótesis.

La dependencia de la temperatura de la catálisis de AAO se estudió con el objetivo de dilucidar la participación del efecto mecano-cuántico conocido como *tunneling* de hidrógeno en la transferencia del hidruro durante la semirreacción de reducción de la enzima. Los datos obtenidos de las cinéticas en estado estacionario así como de las cinéticas rápidas con sustratos protiados y deuterados indican que el efecto túnel está involucrado en la mencionada transferencia. Además, la comparación de los datos cinéticos de la AAO salvaje con los de variantes mutadas del residuo Tyr92 sugieren que la transferencia depende de los movimientos proteicos activados térmicamente que permiten a la enzima transferir la partícula desde una configuración altamente organizada que se forma antes de la catálisis. Estos resultados se ven reforzados por la resolución de la estructura cristalográfica AAO:ácido *p*-anísico, un inhibidor de la enzima.

Los mecanismos que subyacen a la reoxidación de la enzima y la producción de H_2O_2 no se habían caracterizado en detalle. Por ello, estos procesos se estudiaron mediante cinéticas rápidas empleando efectos isotópicos de sustrato y solvente. Esta investigación reveló que, tras la transferencia obligada inicial de un electrón para superar la barrera de inversión de spin, la enzima transfiere al O_2 un átomo de hidrógeno desde el FAD y un protón desde un lugar de intercambio con solvente en dos procesos químicos independientes, que son, por tanto, no concertados. El efecto cinético isotópico de solvente que desveló esto es despreciable a pH ácidos y se hizo evidente como consecuencia de la combinación de la baja disponibilidad de protones a pH básicos y el uso de solvente deuterado, que ralentiza la reacción.

Finalmente, la aplicación biotecnológica potencial de oxidasas GMC se evaluó para la producción de ácido 2,5-furandicarboxílico (FDCA), que puede ser polimerizado con etilenglicol con el fin de obtener bioplásticos. La AAO de *P. eryngii* demostró ser capaz de catalizar la oxidación de precursores del FDCA que provienen de la deshidratación de la fructosa presente en la biomasa vegetal: 5-hidroximetilfurfural (HMF) y derivados parcialmente oxidados. A pesar de su actividad sobre HMF y algunos de sus derivados parcialmente oxidados, la AAO por sí sola no fue capaz de producir FDCA. Esto fue solventado por la acción combinada de una peroxigenasa inespecífica (UPO) del hongo *Agrocybe aegerita*, que fue capaz de catalizar las reacciones necesarias a expensas del H_2O_2 generado por AAO. La acción sinérgica de estas dos enzimas permitió el establecimiento de una cascada enzimática para la producción del FDCA desde HMF. AAO y UPO

convirtieron un 90% del HMF inicial en FDCA con el único consumo neto de O_2 atmosférico.

1

Introduction

1.1. Introduction to the glucose-methanol-choline (GMC) superfamily of enzymes.

The glucose-methanol-choline (GMC) oxidoreductase/dehydrogenase superfamily of proteins was first described in 1992 by Cavener (1992) taking into account the similarities among the sequences of several enzymes: glucose dehydrogenase (GLD) from *Drosophila melanogaster*, methanol oxidases (MOX) from *Hansenula polymorpha* and *Pichia pastoris*, glucose oxidase (GOX) from *Aspergillus niger* and choline dehydrogenase (CHD) from *Escherichia coli*.

Since its first description, many enzymes have been assigned to this superfamily owing to their sequences' common features. In particular, all of them share 5 regions, which are: the ADP-binding motif, the flavin attachment loop, the substrate-binding domain, the FAD-covering lid and the extended FAD-binding domain (Kiess et al. 1998). Such sequence similarities translate into very similar 3D structures, as revealed by the crystallographic data available of enzymes belonging to the superfamily (Mattevi 1998). They all share a *p*-hydroxybenzoate hydroxylase (PHBH)-like fold (Wierenga et al. 1983) and, thus, possess the same secondary structures constituting the different domains.

In general terms, these enzymes can be subdivided in two different substructures: the FAD-binding and the substrate-binding domains (Hallberg et al. 2002). Analysis of the sequences reveals that the FAD-binding domain shows a higher degree of conservation than the substrate-binding one. Such differences in the structure where the substrates bind open up a huge variability of different specificities for these enzymes. At first, given the great versatility of the isoalloxazine ring of FAD for the catalysis of redox reactions, the superfamily was thought to be composed of only oxidoreductases. However, another new class of enzymes has been discovered, hydroxynitrile lyase, in which FAD is regarded as an evolutionary remnant that is not involved in the actual catalysis of the enzyme (Dreveny et al. 2001).

Representatives of this superfamily can be traced from prokaryotes to eukaryotes and their phylogeny has been more extensively studied in insects (Iida et al. 2007; Sun et al. 2012) and fungi (Zámocký et al. 2004; Ferreira et al. 2015a). Given the high similarities they share, among which the presence of the FAD as a prosthetic group in noticeable, it has been proposed that they have evolved in different lines from a common ancestor. Therefore, phylogenetic studies have revealed that the superfamily can be subdivided into 5 different clades (Zámocký et al. 2004):

i) Alcohol oxidases and dehydrogenases, glucose oxidases and dehydrogenases, sorbose dehydrogenases and choline dehydrogenases, which is the most populated group in which the identities of sequence is higher amongst proteins.

ii) Hydroxynitrile lyases, which, as explained above, have evolved differently and FAD is supposed to have lost its catalytic function, so that they do not catalyze redox reactions.

iii) Cholesterol oxidases

iv) Cellobiose dehydrogenases, which underwent a gene fusion and bear two separate domains: one that binds FAD and another that harbors a heme.

v) Some eubacterial and archaeal dehydrogenases.

This work focuses on enzymes that catalyze the oxidation of alcohols, which is one of the most important reactions catalyzed by the members of the superfamily. This reaction takes place by the deprotonation of the hydroxyl moiety thanks to the action of a catalytic His that acts as a base (Wongnate and Chaiyen 2013). Therefore, this His is conserved among all the representatives of the superfamily, along with another residue, which can be another His or an Asn, around 40 residues apart (Dreveny et al. 2001). The catalysis of aryl-alcohol oxidase (AAO) from *Pleurotus eryngii* as a model representative of the superfamily is detailed below.

1.2. Introduction to AAO

Aryl-alcohol oxidase (AAO) is a fungal enzyme secreted from the mycelium of different fungi, including basidiomycetes involved in the degradation of lignocellulose.

AAO activity was reported during the 1960s in cultures of the lignicolous fungus *Trametes versicolor* by Farmer et al. (1960), although this enzyme was not further characterized. It was during the late 1980s and early 1990s that AAO was isolated from several Agaricales species, such as *Pleurotus sajor-caju* (Bourbonnais and Paice 1988), *Pleurotus eryngii* (Guillén et al. 1990b) and *Pleurotus ostreatus* (Sannia et al. 1991), and identified as the source of the H_2O_2 (Guillén et al. 1994) and aromatic aldehydes found in cultures of the above fungi (Gutiérrez et al. 1994; Guillén and Evans 1994). During subsequent years, its involvement in the ligninolytic process was demonstrated. AAO is responsible along with other GMC oxidoreductases and copper-radical oxidases for production of the H_2O_2 that, as described below, is required by: i) the activity of ligninolytic peroxidases; and ii) the formation of oxygen radicals that exert oxidative and depolymerising activities on polysaccharides and also on lignin.

Some AAOs have been exhaustively characterized, being those of *P. eryngii* (Guillén et al. 1992b; Ferreira et al. 2005) and *Bjerkandera adusta* (de Jong et al. 1994; Romero et al. 2009) two remarkable examples. Its substrate specificity showed to be broad, probably due to its extracellular and ligninolytic nature, since it proved to use secondary fungal metabolites, *p*-methoxybenzyl alcohol and other benzylic alcohols, as substrates. In fact, it is currently known that it can oxidise both phenolic and non-phenolic aryl-alcohols, together with other polyunsaturated (aliphatic) primary alcohols, to their corresponding aldehydes, as well as aromatic secondary alcohols, albeit with much lower efficiency (**Table 1.1**). Moreover, the presence of low amounts of acids attributed to its activity in some fungal cultures (and *in vitro* reactions) paved the way for the demonstration of its activity on aryl aldehydes (Ferreira et al. 2010).

Table 1.1. Comparison of the catalytic efficiencies of *P. eryngii* and *B. adusta* AAO oxidising representative alcohol and aldehyde substrates

		k_{cat}/K_m ($s^{-1} \cdot mM^{-1}$)	
		P. eryngii	*B. adusta*
Benzyl alcohol	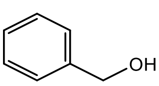	47 ± 9	18 ± 1
p-Fluorobenzyl alcohol	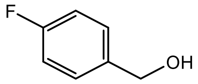	59 ± 6	22 ± 2
m-Fluorobenzyl alcohol	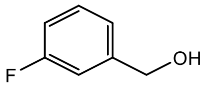	13 ± 1	47 ± 2
p-Chlorobenzyl alcohol	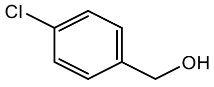	398 ± 32	361 ± 15
m-Chlorobenzyl alcohol	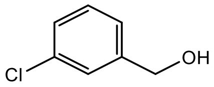	203 ± 4	1050 ± 30
p-Methoxybenzyl alcohol	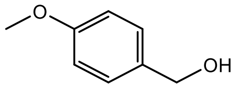	5230 ± 620	646 ± 45
m-Methoxybenzyl alcohol	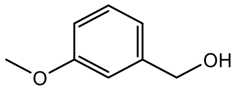	65 ± 24	349 ± 8
Veratryl alcohol	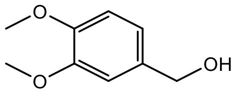	210 ± 5	22 ± 1
Isovanillyl alcohol	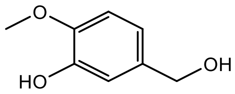	152 ± 5	51 ± 1
Vanillyl alcohol	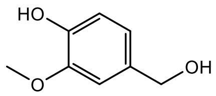	0	31 ± 1
3-Chloro-*p*-methoxybenzyl alcohol	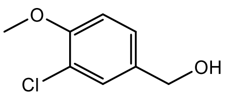	4090 ± 200	1480 ± 110
2-4-Hexadien-1-ol	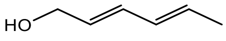	1270 ± 60	186 ± 7
Cinnamyl alcohol	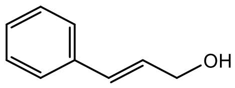	78 ± 11	305 ± 11
Coniferyl alcohol	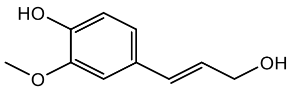	0	5 ± 0.2

m-Chlorobenzaldehyde	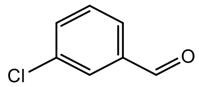	0.64 ± 0.05	1 ± 0.09
3-Chloro-*p*-methoxy-benzaldehyde	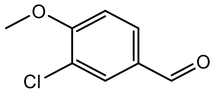	0.085 ± 0.006	0.050 ± 0.002
m-Fluorobenzaldehyde	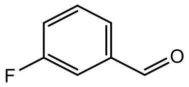	0.40 ± 0.02	0.05 ± 0.005
p-Nitrobenzaldehyde	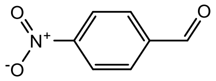	0.31 ± 0.006	0.010 ± 0.001
5-Hydroxymethyl-2-furfural	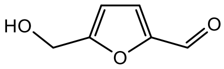	0.21 ± 0.02	n.d.[1]
2,5-Diformylfuran	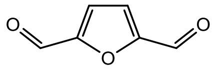	0.150 ± 0.008	n.d.[1]

[1] n.d., not determined

This plethora of substrates of AAO (**Table 1.1**), among which several reduced species derived from lignin decay products are noticeable, makes it a promising biocatalyst. The lignocellulosic materials are the main renewable resource on Earth because they are widespread and abundant (forests cover 27% of world's area) and, thus, they are cheap and can be easily stored. As a consequence, the conversion of these materials into biofuels in biorefineries is of great interest. However, not only biofuels, that is heat and power, are important, but other by-products obtained during the biorefinery processes are also being carefully examined aiming at using them for the production of valorised chemicals (Bozell and Petersen 2010). AAO is a candidate for the enzymatic delignification of plant biomass (in synergy with other oxidoreductases) and for the production of aromatic aldehydes and acids that can originate from this renewable resource.

1.3. GMC and lignocellulose decay

Lignocellulosic biomass (in wood and nonwoody vascular plants) accounts for the 20% of the total carbon fixed by land photosynthesis, and is constituted of three main polymers: cellulose, hemicellulose and lignin (Higuchi 1997). Both cellulose and lignin are the two most abundant polymers on Earth. Lignin is located in the middle lamellae, where it attains its highest concentration, and the secondary wall of vascular plants, together with the above polysaccharides. Its main functions are conferring rigidity to the plants, waterproofing vessels, and providing protection against desiccation, pathogens and irradiation (Gellerstedt and Henriksson 2008). Since lignin is very recalcitrant, it constitutes the main sink of carbon in land ecosystems and, as a consequence, its degradation is a key step to complete the carbon cycle. In fact, before it started to be biodegraded and mineralised, at the end of the Carboniferous period (~300 million year ago), the carbon that the plants fixed accumulated and therefore gave rise to the coal deposits we currently use as source of fossil fuels (Floudas et al. 2012).

The only organisms capable of degrading wood are some saprotrophic agaricomycetes, feeding on the simple sugars produced when cellulose and hemicelluloses are hydrolysed. However, to accomplish this task, fungi must overcome a very recalcitrant barrier: lignin. Lignin is an amorphous polymer including a variety of bonds established among the phenylpropanoid units that form its structure (**Figure 1.1**). Although these fungi do not use lignin as a nutrient, they have to remove or modify lignin to gain access to carbohydrates. The development of an extracellular system capable of altering the structure of lignin was, thus, a great achievement in evolutionary and ecological terms, since the polymer is mineralised and the carbon "sequestered" in it may go back to the atmosphere as CO_2. It is generally accepted that the first lignin-degrading organism must have been a basidiomycete (Floudas et al. 2012), which developed some strategies to act on the recalcitrant lignin polymer oxidising its subunits, causing bond breakages, and releasing the carbohydrates embedded within its matrix.

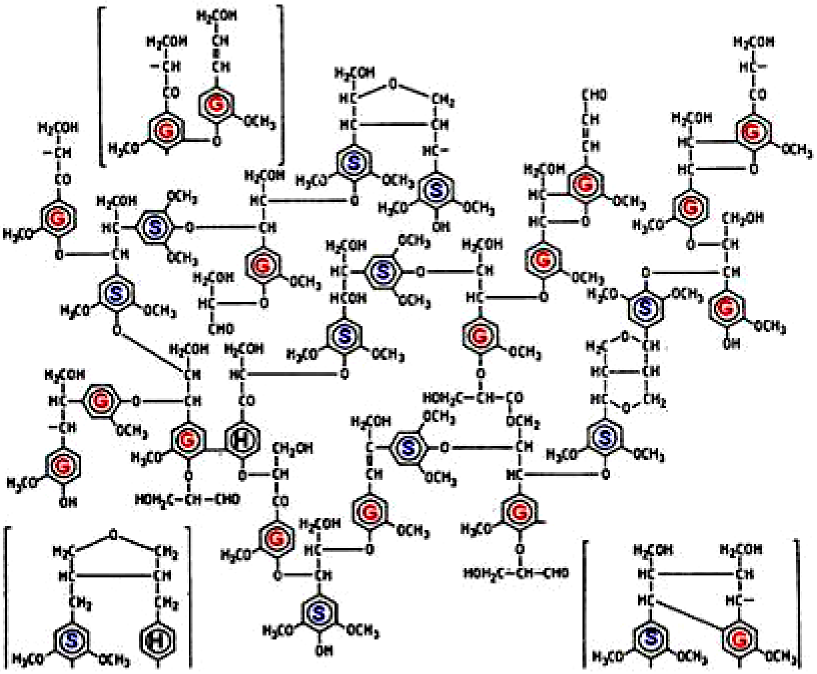

Figure 1.1. Lignin structure showing its syringyl (S), guaiacyl (G) and *p*-hydroxyphenyl (H) phenylpropanoid with different inter-unit linkages.

The role of H_2O_2 in lignocellulose decay was studied as it proved to be produced simultaneously with the ligninolytic system. It was seen that the addition of catalase, an enzyme that degrades H_2O_2, to cultures of the white-rot fungus *Phanerochaete chrysosporium* diminished its lignin-degrading ability (Faison and Kirk 1983). Two families of oxidoreductases include oxidases being able to produce this strong oxidant: copper-radical oxidases and GMC oxidoreductases.

The copper-radical oxidases are proteins that have one copper ion and a protein radical involved in catalysis, such as extracellular glyoxal oxidase (Kersten and

Kirk 1987) and the related enzymes recently identified from sequenced genomes (Kersten and Cullen 2014), among others. On the contrary, as exposed above, GMC oxidoreductases are a superfamily of enzymes that share common structural patterns, including the FAD cofactor and a histidine catalytic base, although they differ in their substrate ranges. Extracellular enzymes of this superfamily involved in the lignocellulose-degradation process are cellobiose dehydrogenase (Ayers et al. 1978; Bao et al. 1993), pyranose 2-oxidase (Daniel et al. 1994), aryl-alcohol oxidase (Guillén et al. 1990b) and methanol oxidase (Nishida and Eriksson 1987). The latter enzyme lacks a signal peptide to transport the protein to the extracellular space, but its presence out of the hyphae has been revealed, and it is supposed to be secreted by alternative secretion pathways not known yet (Daniel et al. 2007). Glucose oxidase (Eriksson et al. 1986) is an intracellular enzyme, so its role in lignocellulose degradation is controversial, since a transport system for the H_2O_2 formed would be required in order that it could carry out functions in the extracellular medium.

The study of genomes of ligninolytic fungi is, thus, important to identify the enzymes that carry out the lignin degradation. In this way, the first basidiomycete genome to be sequenced was that of *Phanerochaete chrysosporium* (= *Phanerodontia chrysosporium*) (Martinez et al. 2004) due to the interest in this white-rot fungus of the order Polyporales as a model lignin-degrading organism (Kersten and Cullen 2007). Wood attack by white-rot fungi is based on their ability to degrade the recalcitrant polymer of lignin in a process that was defined as an enzymatic "combustion" (Kirk and Farrell 1987) and combines extracellular oxidases and peroxidases (Kersten and Cullen 2007; Ruiz-Dueñas and Martínez 2009). With a few exceptions corresponding to poor wood rotters (e.g., species of Jaapiales and Cantharellales), the presence of lignin peroxidase (LiP[3], EC 1.11.1.14), manganese peroxidase (MnP, EC 1.11.1.13) or versatile peroxidase (VP, EC 1.11.1.16) genes is a constant characteristic of all typical white-rot fungi based on comparative genome analysis (Floudas et al. 2012; Ruiz-Dueñas et al. 2013). The diversity, distribution and evolutionary relationships of ligninolytic peroxidases in the order Polyporales has been recently studied (Ruiz-Dueñas et al. 2013).

Brown-rot fungi have developed an alternative strategy, based on Fenton chemistry, to overcome the lignin barrier (Baldrian and Valaskova 2008). H_2O_2 reduction by ferrous iron yields hydroxyl free radical, which is able to access, oxidize and depolymerize wood cellulose with a more or less limited modification of lignin (Kirk 1975; Martínez et al. 2011; Yelle et al. 2011). In 2009, the genome of *Rhodonia placenta* (syn.: *Postia placenta*) was sequenced as the model brown-rot fungus to increase our understanding of this type of wood decay (Martinez et al. 2009).

1.3.1. The AAO family and ligninolytic fungi

AAO activity has been reported in different fungi including *T. versicolor* (Farmer et al. 1960), *Fusarium solani* (Iwahara et al. 1980), *Rigidoporus microporus* (Waldner et al. 1988), *Pleurotus* species (Bourbonnais and Paice 1988; Sannia et al. 1991; Guillén et al. 1992b), *B. adusta* (Kimura et al. 1990; Muheim et al. 1990b; Romero et al. 2009; 2010a) and *Botrytis cinerea* (Goetghebeur et al. 1993); and the corresponding genes have been identified in many basidiomycete genomes (Floudas et al. 2012; Hernández-Ortega et al. 2012a; Ruiz-Dueñas et al. 2013), as described below. Further evidence of the simultaneous expression of AAO along with enzymes typically expressed under ligninolytic condition such as lignin peroxidase (LiP) in *B. adusta* (Muheim et al. 1990a) and manganese-oxidizing peroxidases in *Pleurotus* cultures (Camarero et al. 1996), supported the involvement of this oxidase in the degradation of lignin. Moreover, the enzyme was located in the hyphal sheath (which is formed by secreted fungal polysaccharide) during lignocellulose degradation (Barrasa et al. 1998), as it had been previously reported for ligninolytic peroxidases and laccases (Gallagher et al. 1989; Green III et al. 1992).

The activity of AAO is supported by both non-phenolic and phenolic aryl alcohols that can derive from fungal metabolism (Gutiérrez et al. 1994; de Jong et al. 1994) and from lignin degradation (Kirk and Farrell 1987; Shimada and Higuchi 1991) and are substrates for the enzyme in cooperation with related dehydrogenases. It was seen that H_2O_2 is produced when adding aromatic alcohols, as well as the corresponding aldehydes and acids, to the mycelium of *P. eryngii* (Guillén et al. 1994). Thus, it was postulated that the redox cycling of these compounds results in a continuous supply of H_2O_2. The product of the reaction with AAO (aldehyde or acid) needs to be reduced in order to be re-used by the enzyme. Therefore, it is hypothesised that the oxidised species is transported to the intracellular space, where aryl-alcohol or aryl-aldehyde dehydrogenases, both NADPH-dependent enzymes, convert it into alcohol again (de Jong et al. 1994; Guillén and Evans 1994). Supply of reduced NADPH must be supported by the high carbon availability for a fungus under ligninolytic conditions (**Figure 1.2**).

P. eryngii AAO's preferential substrate is *p*-methoxybenzyl alcohol (**Table 1.1**), which is a secondary metabolite detected in fungal cultures grown both in glucose and lignin media (Gutiérrez et al. 1994). It is known that aromatic alcohols, aldehydes and acids are derived from the shikimic acid pathway of fungal secondary metabolism (Turner and Aldridge 1983). It was seen that the oxidised product, *p*-methoxybenzaldehyde (also known as *p*-anisaldehyde), was much more abundant in the *Pleurotus* cultures than its alcoholic counterpart (Gutiérrez et al. 1994). High levels of related compounds, such as 3-chloro-*p*-anisaldehyde, were also found to be abundant in *B. adusta* cultures (de Jong et al. 1992) and agree with catalytic efficiencies toward the corresponding alcohol for *B. adusta* AAO, for which seems to be the preferential substrate **(Table 1.1)**. These chlorinated derivatives are also minor extracellular metabolites in *P. eryngii* and *P. ostreatus* (Gutiérrez et al. 1994; Okamoto et al. 2002).

These findings further supported the hypothesis postulating that AAO was acting in the extracellular space involved in the said redox-cycling process for H_2O_2 production.

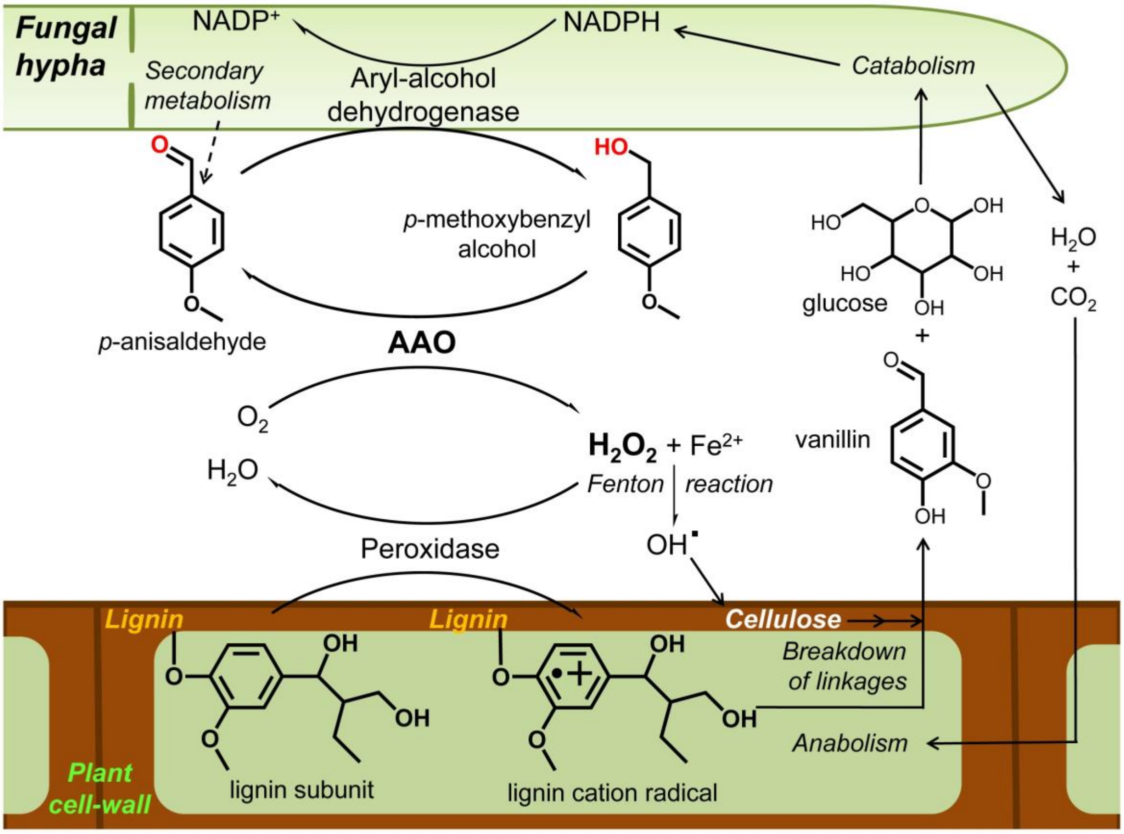
Fungal hypha
NADP+
NADPH
Secondary metabolism
Aryl-alcohol dehydrogenase
Catabolism
p-methoxybenzyl alcohol
p-anisaldehyde
glucose
AAO
O2
H2O
H2O2 + Fe2+
Fenton reaction
OH•
vanillin
H2O + CO2
Peroxidase
Lignin
Lignin
Cellulose
Breakdown of linkages
Anabolism
Plant cell-wall
lignin subunit
lignin cation radical

Figure 1.2. Scheme of the natural role of AAO in decay of plant cell-wall producing H_2O_2 for: i) activation of lignin-degrading peroxidases; and ii) formation of cellulose-depolymerising hydroxyl radical (also causing lignin oxidation).

As mentioned above, based on macroscopic and chemical composition features, the wood-degrading processes were split into two different types involving different decay mechanisms. Some fungi leave a whitish residue, and thus were named white-rot fungi, while others produce a brown residue and were called brown-rot fungi (Zabel and Morrell 1992; Schwarze et al. 2000; Martínez et al. 2005). Owing to genomic and enzymatic studies, it is now thought that AAO could act as an auxiliary enzyme in both processes due to its H_2O_2-producing activity and presence in the sequenced genomes of Agaricomycotina responsible for the two types of wood-decay processes.

1.3.2. White-rot decay

White-rot fungi developed an enzymatic machinery to degrade lignin and, hence, be able to use cellulose and hemicellulose as a source of carbon and energy. The main enzymes involved are metalloproteins including LiP, manganese peroxidase (MnP) and versatile (VP), as well as laccases (Ruiz-Dueñas and Martínez 2009). Ligninolytic peroxidases are heme proteins that use H_2O_2 as the electron-accepting substrate to oxidise the lignin units. In contrast, laccases have copper as a cofactor, use O_2 as electron aceptor, and are thought to often act through small intermediate compounds, redox mediators, which in turn oxidise lignin. Since most enzymes cannot penetrate the intricate and compact structure of sound wood, small chemical oxidisers, activated oxygen species (as hydroxyl radical), metal cations (as Mn^{3+} produced by MnP and VP) and aromatic radicals (formed by different oxidoreductases) are probably responsible for the first stages of lignin decay (Evans et al. 1994). In white-rot decay there is a need of a continuous H_2O_2 flow in the extracellular environment in order that peroxidases be able to act on lignin. Moreover, hydroxyl radical can be produced through Fenton reaction between Fe^{2+} and H_2O_2, and participate in oxidative modification of cellulose (as described below for brown-rot decay) and also of lignin (**Figure 1.2**) (Forney et al. 1982; Bes et al. 1983; Gómez-Toribio et al. 2009).

White-rot fungi can be classified into two groups according to their gross degradation patterns. Some of them degrade lignin and cellulose simultaneously as it is the case for *P. chrysosporium*, one of the most studied lignin-degrading organisms. Instead, others, such as *Ceriporiopsis subvermispora*, degrade lignin before cellulose (Otjen and Blanchette 1986). The main differences between the sequenced genomes of these two fungi appear to be related to (i) the peroxidase repertoire, and (ii) the genes involved in lipid metabolism (Fernández-Fueyo et al. 2012). The latter is related to the fact that free radicals from unsaturated lipids are supposed to play a role in lignin attack too (Bao et al. 1994). Selective white-rot fungi are the most interesting for industrial applications in which carbohydrates are the raw material, since they release cellulose from the lignin matrix without significantly consuming it.

The analysis of genomes of white-rot fungi in which AAO appeared to be produced, along with peroxidases, further confirmed its involvement in the white-rot process as an auxiliary enzyme producing H_2O_2. For instance, Floudas et al. (2012) analysed 24 basidiomycete genomes to search for enzymes involved in the degradation of lignin. On the one hand, all white-rot genomes studied possessed AAO genes with the only exception of *Auricularia delicata*. On the other hand, AAO appears to be the most common H_2O_2-producing GMC, since methanol oxidase genes are not as abundant, glucose oxidase genes are absent, and pyranose 2-oxidase genes are only found in two of the genomes (**Table 1.2**).

Table 1.2. Inventory of peroxidase and GMC (AAO, aryl-alcohol oxidase; CDH, cellobiose dehydrogenase; MOX, methanol oxidase and P2O, pyranose 2-oxidase) genes in eleven white-rot Agaricomycotina (AD, *Auricularia delicata*; PST, *Punctularia strigosozonata*; FM, *Fomitiporia mediterranea*; DS, *Dichomitus squalens*; TV, *Trametes versicolor*; SH, *Stereum hirsutum*; BA, *Bjerkandera adusta*; PB, *Phlebia brevispora*; PC, *Phanerochaete chrysosporium*; GS, *Ganoderma* sp. in the *Ganoderma lucidum* complex and CS, *Ceriporiopsis subvermispora*) genomes

		AD	PST	FM	DS	TV	SH	BA	PB	PC	GS	CS
Peroxidases		21	21	33	21	39	11	34	16	18	14	25
GMCs:	AAO	0	4	2	9	3	14	11	3	3	9	4
	CDH	1	1	1	1	1	1	1	1	1	1	1
	MOX	3	3	2	4	4	7	5	6	3	4	1
	P2O	2	0	0	0	2	0	1	1	1	0	0

From Floudas et al. (2012) and Ruiz-Dueñas et al. (2013)

1.3.3. Brown-rot decay

The brown-rot decay is based on a non-enzymatic attack on wood that leads to lignin modification, instead of degradation/mineralisation, and cellulose depolymerisation. On having no longer the machinery for degrading lignocellulose (**Table 1.3**), brown-rot fungi are the only organisms known to be able to nearly completely remove all polysaccharides from wood without causing substantial lignin degradation (Arantes et al. 2012). Nevertheless, it has been demonstrated that they do alter lignin in order to gain access to the carbohydrates leaving it partially modified but still polymeric and with a recognisable chemical structure (Martínez et al. 2011). Genomic studies have proved that these fungi stem from the white-rot lineage, and that they have lost most of the energy-consuming apparatus their white-rot ancestors used to have, which means that peroxidases are absent or residual in their genomes (only one generic peroxidase gene in some species) (Ruiz-Dueñas et al. 2013). They have originated independently in several lineages and have representatives in five basidiomycete orders (Floudas et al. 2012).

The initial oxidative step alters the plant cell-wall structure in order to make it more accessible to enzymes involved in subsequent decay (Goodell et al. 1997). Reactive oxygen species, such as hydroxyl radical, generated by Fenton chemistry, play a key role in this oxidative process (**Figure 1.2**) (Halliwell 1965; Baldrian and Valaskova 2008). Fenton chemistry is based on reactions among H_2O_2 and Fe^{2+} ions giving rise to hydroxyl free radical. This is a radical-chain mechanism where Fe^{2+} is generated from Fe^{3+} in a cycle that involves fungal enzymes. The hydroxyl radical is the most powerful (non-specific) oxidant in biological systems but it has an extremely short half-life (10^{-9} s) and, as a consequence, Fenton reactions need occur immediately adjacent to the site of oxidative action within the plant cell-wall because of spatial diffusion limitations (Arantes et al. 2012).

Table 1.3. Inventory of peroxidase and GMC genes (see **Table 1.2** for enzyme abbreviations) in six brown-rot Agaricomycotina (CP, *Coniophora puteana*; GT, *Gloeophyllum trabeum*; FP, *Fomitopsis pinicola*; WC, *Wolfiporia cocos*; DSP, *Dacryopinax* sp. and RP, *Rhodonia placenta*) genomes

		CP	GT	FP	WC	DSP	RP
Peroxidases		0	0	1	1	0	1
GMCs:	AAO	0	2	1	0	0	2
	CDH	1	1	0	0	0	0
	MOX	2	1	4	4	1	4
	P2O	0	0	0	0	0	0

From Floudas et al. (2012) and Ferreira el al. (2015a)

Since one of the most remarkable chemical alterations that brown-rot decay cause to lignin is demethoxylation (Yelle et al. 2008; Niemenmaa et al. 2008), which ultimately gives rise to methanol, methanol oxidase is thought to be the most important H_2O_2-producing enzyme in brown-rot decay. Nevertheless, genomic studies have shown that brown-rot fungi have AAO too (Martinez et al. 2009), suggesting that the latter oxidase might play a role in Fenton chemistry. Floudas et al. (2012) analysed seven brown-rot fungal genomes and found AAO genes in several of them, although they were not as abundant as those of methanol oxidases (**Table 1.3**).

1.4. AAO catalytic mechanism in detail

AAO catalyzes the two-electron oxidation of aromatic alcohols bearing an α-carbon hydroxyl group (Ferreira et al. 2005) concomitantly with the reduction of O_2 to H_2O_2 in two separate half reactions. Furthermore, AAO activity on some aliphatic polyunsaturated and secondary aromatic alcohols (Hernández-Ortega et al. 2012b), as well as on *geminal* diols that originate from the hydration of aldehyde has also been demonstrated (Ferreira et al. 2010).

Diffusion of the alcohol substrate into the active site of the enzyme is limited by the presence of three residues —Tyr92, Phe397 and Phe501— that form a hydrophobic bottleneck shielding the cavity from the outer environment. Computational studies of the migration of the alcohol into the active site by PELE (Borrelli et al. 2005) showed that the substrate adopts a configuration such that its α-carbon is situated near the flavin ring and the chains of residues H502 and H546 (**Figure 1.3**) (Hernández-Ortega et al. 2011a).

The mechanism and the active site residues involved in both half reactions have been deeply characterized by a combination of experimental and computational studies. Isotope labeling showed that alcohol oxidation takes place by concerted asynchronous proton transfer from alcohol hydroxyl to His502, and hydride transfer from α-carbon position to flavin N5. Two conserved active site histidines, His502 and His546, are involved as catalytic base and substrate hydrogen bonding, respectively, as confirmed by mutational research (**Figure 1.4A**). The above hydride transfer is stereoselective (pro-(*R*) hydrogen is transferred) as direct consequence of AAO active site architecture and concerted mechanism, since when the alcohol hydroxyl is oriented to His502 (proton abstraction) only the pro-(*R*) hydrogen can be transferred to flavin N5 (hydride transfer). This half reaction gives rise to the protonated H502, the aldehyde and the hydroquinone form of the FAD cofactor (**Figure 1.4B**)

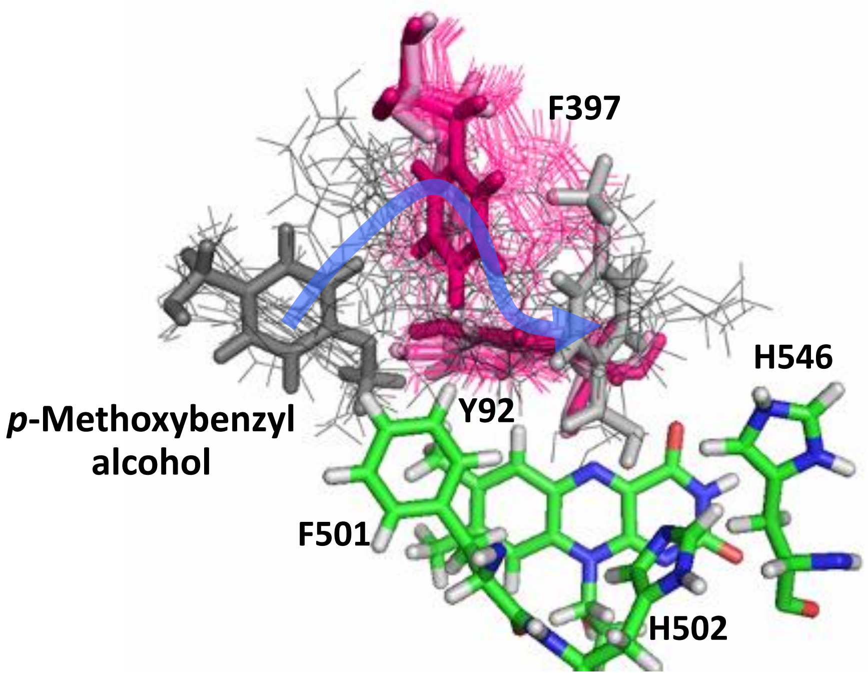

Figure 1.3. Substrate migration studies revealed several positions of substrate and AAO active-site residues. Taken from Hernández-Ortega et al. (2011).

During the oxidative half-reaction, O_2 positioning in front of flavin C4a-N5 locus is facilitated by Phe501, as shown by mutagenesis studies (Hernández-Ortega et al. 2011b). QM/MM calculations concluded that O_2 is first one-electron reduced by FADH2 yielding superoxide anion radical (**Figure 1.4C**). This process is activated by His502 charged state, which additionally provides a proton that reduces the singlet/triplet energy gap. The reaction is followed by second proton transfer from $FADH^-$ concomitant with spin inversion (and second electron transfer) without formation of a flavin-hydroperoxide intermediate. The first transfer is very fast but the second one seems to be rate limiting, as shown by isotope labeling (**Figure 1.4D**). The reoxidative half reaction produces reoxidized flavin and the H_2O_2. Release of the products permits the enzyme go back to the initial state.

1.4.1. Involvement of quantum-mechanical tunneling in AAO catalysis

There exist enzymes displaying hydrogen transfer mechanisms, either as a hydrogen atom (H), proton (H^+) or hydride (H^-), for which the postulated theories on enzymatic reactions did not suit. This has encouraged the development of new models able to explain such different behaviors.

Transition state theory (TST) was first used to explain the reactions catalyzed by enzymes, including hydrogen and electron transfer reactions (Kraut 1988). This theory describes the reaction coordinate as a potential energy surface with a single free energy minimum (the reactant well) and a single maximum (the activated transition state complex) required to go to product.

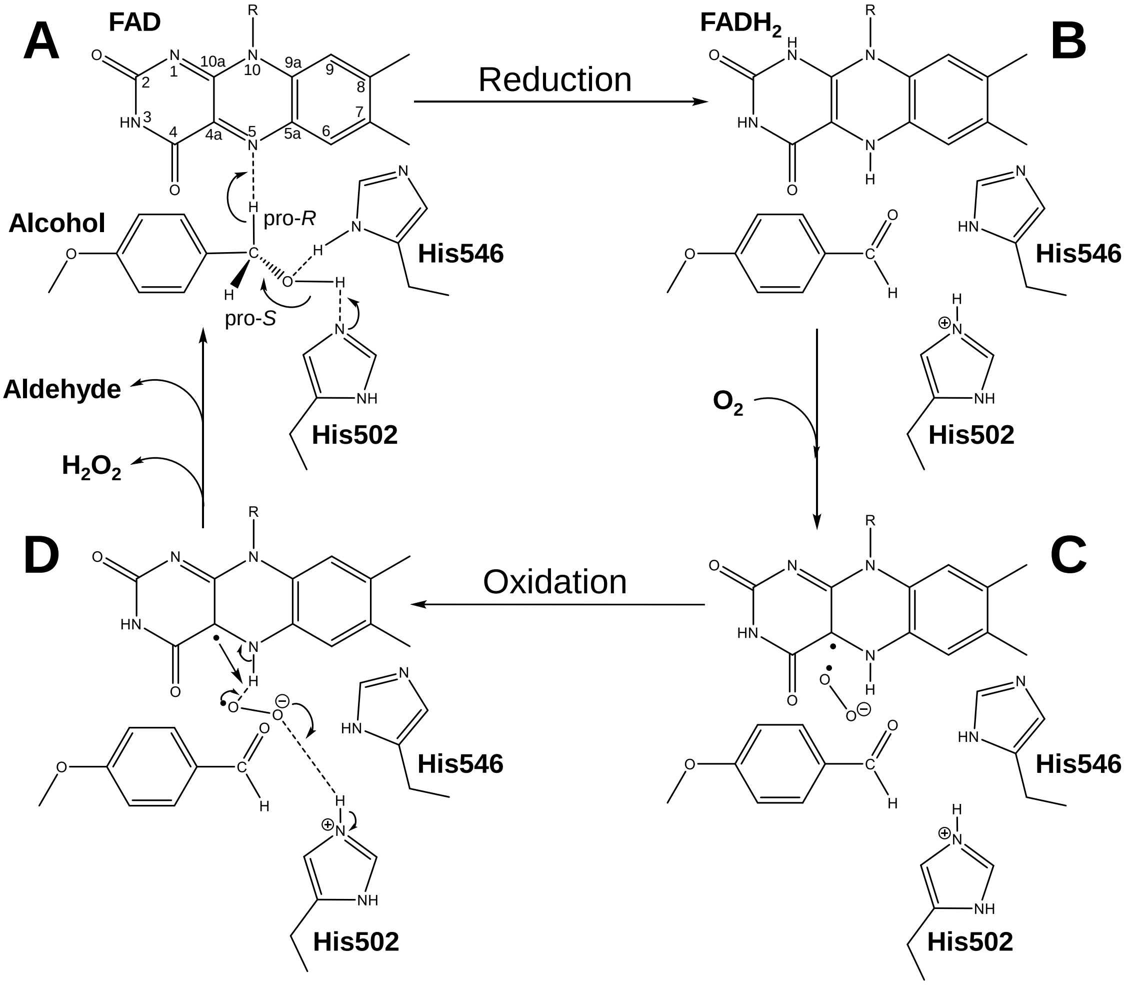

Figure 1.4. Proposed *P. eryngii* AAO catalytic cycle.

The study of the transfer reaction for different hydrogen isotopes soon revealed changes in the energy of activation (E_a) values, so that it became necessary to incorporate quantized approaches of quantum physics (Melander and Saunders 1987). This semiclassical model postulated that the observed kinetic isotope effects (KIE) for C-H cleavage were the consequence of the differences in zero point energies for the isotopes of hydrogen (protium H, deuterium ^{2}H and tritium ^{3}H) and predicted KIE, that is, the ratio of a given rate measured with a protiated substrate and the one estimated with deuterated substrate, over 7, as long as tunneling occurs in an isotope-dependent manner. Therefore, some corrections were introduced in the theory, first including tunneling as having some involvement in the processes (Bell 1980). Hence, the enzymes were thought to catalyze hydrogen transfer through a mixture of semiclassical and quantum-mechanical contributions. These models considered KIE and activation energy (E_a) to measure the magnitude of semiclassical and quantum-mechanical contributions, respectively (Kohen and Klinman 1999; Nagel and Klinman 2009). Nevertheless, extensive investigation on the transfer processes of soybean lipoxygenase (Knapp et al. 2002) and alcohol dehydrogenase (Kohen et al. 1999a) led to the discovery of huge nearly temperature-independent KIEs that could not be explained by these tunneling corrections of TST.

Consequently, hydrogen transfer is nowadays regarded as a fully quantum-mechanical process governed by a hierarchy of enzyme motions (Knapp et al. 2002; Knapp and Klinman 2002a; Nagel and Klinman 2009). Those include “passive” dynamics that pre-organize the active site in a way that create an appropriate ground-state structure for catalysis and “active” dynamics, also known as gating, that help sample donor-acceptor distances (DAD) between substrate and enzyme to produce a tunneling-ready conformation that permits the transfer (Klinman and Kohen 2013). Such DAD samplings help bring the reacting atoms together so that their wave function overlap and, thus, particle can be transferred across the barrier width, which is the basic premise of tunneling. Therefore, these protein motions have gained momentum because of its involvement in catalysis and, especially, tunneling in hydrogen transfer (Fan and Gadda 2005; Allemann et al. 2006; Singh et al. 2015; Klinman 2015; Luk et al. 2015).

Breakage of a C–H bond followed by H transference is a key biochemical process in which many enzymes rely for their catalysis (Basran et al. 2006), Amongst them, aryl-alcohol oxidase (AAO) from the fungus *Pleurotus eryngii*.

1.4.2. Reduction of O_2 by AAO and related oxidases

Reduction of O_2 by flavoenzymes is a fascinating yet intriguing process in nature. It is an impaired reaction due to the intrinsic characteristics of the O_2 and flavin molecules. Although the reactivity is favored by the differences in redox potential among the oxygen species and the flavin hydroquinone (Sawyer 1988), given the difference in the spin ground state of both molecules (O_2 is in triplet state and the cofactor in singlet state) the reaction is said to be impeded by the law of spin conservation (Malmstrom 1982). However, flavooxidases have overcome this restriction by single one-electron transfers in a stepwise manner (Mattevi 2006). Flavin cofactors play a central role in the whole process as they act receiving the two electrons from organic substrates during the reductive half-reaction and donating them eventually to O_2. Together with cofactors, also the architecture of active site is important for the redox process. In fact, flavooxidases are said to speed up reactions with O_2 by at least hundred-fold in comparison with free flavins aided by the presence of a positive charge near flavin C4a, and the whole flavin environment (Gadda 2012).

Oxidases and monooxygenases are supposed to initiate the reoxidation reaction by transferring a first electron from the reduced flavin to O_2, thereby giving rise to a caged radical pair formed by the neutral semiquinone and the superoxide cation radical. The radical pair is very unstable and immediately decays following different pathways (Massey 1994). In spite of such instability and the velocity of its disappearance, one intermediate with similar features to those of a flavosemiquinone was detected during the reoxidative half-reaction of the human liver glycolate oxidase (Pennati and Gadda 2011). The first electron transfer seems to be a bottleneck for the whole reaction, as demonstrated for glucose oxidase (Roth and Klinman 2003). Therefore, stabilization of the transition state to form the caged radical pair is crucial in these enzymes to attain the magnitude of acceleration of this first electron transfer (Klinman 2007; Gadda 2012).

Typically, oxidases are not supposed to stabilize any adduct after the second electron transfer and the decay of this radical pair; whereas monooxygenases normally stabilize C4a-peroxyflavin intermediates that can, in turn, either donate an O atom to their substrates or receive a proton and eliminate H_2O_2 rapidly. As a consequence, the C4a-peroxyflavin has been considered a possible transient intermediate in oxidases and experiments were conducted to detect it. Glucose oxidase from *Aspergillus niger* was subjected to pulse radiolysis experiments that suggested the presence of this C4a intermediate, but it was not detected spectroscopically (Ghisla and Massey 1989). However, pyranose 2-oxidase (P2O) proved to stabilize this C4a-peroxyflavin adduct before releasing H_2O_2, being the first oxidase to be found to stabilize it (Sucharitakul et al. 2008; 2011).

The reduction of O_2 to H_2O_2 requires also two protons to be transferred along with the two above-mentioned electrons (Massey 1994). At least one of these protons is supposed to come from the flavin N5 (as a H atom), which has previously abstracted it from the organic substrate thereby oxidizing it; whereas the other one is supposed to originate from the solvent or a solvent exchangeable site. Elucidation of the provenance, transfer mechanism and relative timing of these particles employing deuterated substrates and solvents is a key step to gain insight into the reduction of O_2. Several examples of these studies have enlightened our knowledge on flavoenzymes' oxidation, such as those on choline oxidase (Gannavaram and Gadda 2013), glucose oxidase (Bright and Gibson 1967; Roth et al. 2004) or P2O.

To the best of our knowledge, no other electron acceptor has been found for this AAO from *P. eryngii* so far, opposite to what has been seen for other GMC oxidoreductases as glucose oxidase (Leskovac et al. 2005) and the recently-described quinone-dependent aryl-alcohol dehydrogenases (Mathieu et al. 2016).

1.5. Biotechnological applications of GMC oxidoreductases

1.5.1. Paper pulp industry: Biopulping and biobleaching

One of the main steps of pulp and paper industry is the treatment of wood chips to separate cellulosic fibres (the actual raw material used) from the lignin forming the middle lamella, a process called pulping. The concern about environment and energy wasting has stimulated studies on the use of microorganisms to accomplish this task. The resulting biopulping process is thought to be energetically and environmentally more favourable than chemical and/or mechanical treatments (Blanchette et al. 1992; Rasmussen et al. 2010).

The biopulping process starts with the colonization of wood xylem and parenchyma by the fungi. After hyphae have grown on the substrate, the fungus will start producing its ligninolytic enzymatic system in order to degrade the middle lamellae and separate fibres (Breen and Singleton 1999). Since the loss of cellulose is undesirable, the organisms of choice are white-rot fungi showing preference for lignin degradation rather than cellulose degradation, whose task is to make cellulosic fibres accessible for the papermaking process (Scott and Swaney 1998). Several selective ligninolytic fungi, such as *C. subvermispora* and *P. eryngii*, together with the model white-rot fungus *P. chrysosporium*, and brown-rot fungi such as *Postia placenta*, among others, have been investigated for biopulping of wood and annual plants (Akhtar et al. 1997; Camarero et al. 1998; Ferraz et al. 2008; Vicentim et al. 2009; Masarin et al. 2009; Giles et al. 2014). AAO is supposed to act as an auxiliary enzyme providing H_2O_2 in these processes, as it is the case of natural degradation of lignin.

Pulp bleaching, which is the removal of chromophores in order to obtain white paper pulp, is another process in which AAO has shown to contribute. In a study in which two flax pulps were treated with fungal enzymes –laccases, peroxidases and feruroyl esterases– the ability of AAO from *Pleurotus pulmonarius* CBS 507.85, which is a natural hyperproducer of the enzyme, to aid in this process was tested (Sigoillot et al. 2005). The results showed that the presence of AAO along with laccase improved the bleaching process probably due to the ability of AAO to prevent the repolymerisation of the phenoxy radicals released by laccases by using them as electron acceptors (as an alternative for O_2). In a similar way, AAO can be combined with ligninolytic peroxidases, in the presence of a substrate enabling it to release the H_2O_2 required by the former enzymes.

1.5.1. Flavour synthesis

White-rot fungi are among the most versatile flavour and aroma producers in nature (Lapadatescu et al. 2000; Fraatz and Zorn 2011). These compounds are mainly of aromatic nature and synthesised through biotransformations by plant, enzymatic or microbial processes (Serra et al. 2005). Since there exists demand for naturally produced compounds, the biotechnological production of flavours and aromas attracts much attention (Krings and Berger 1998) due to the great economic importance this industry has.

One of the most important flavours is vanillin. It is naturally produced by orchids of the *Vanilla* genus, but this source represents only the 1% of the commercial vanilla flavour. As a consequence, several methods of obtaining vanillin have been developed (Priefert et al. 2001) that use bioconversion of lignin and phenylpropanoids, such as eugenol (Overhage et al. 2003). The ability of *B. adusta* AAO to oxidise vanillyl alcohol reported by Romero et al. (2009), could be exploited in the biotechnological production of this flavour. It has been suggested that AAO may be used to avoid formation of vanillyl alcohol as a by-product diminishing the yield of vanillin formation (**Figure 1.5A**), by the fungi of the genus *Pycnoporus* (Lomascolo et al. 2011).

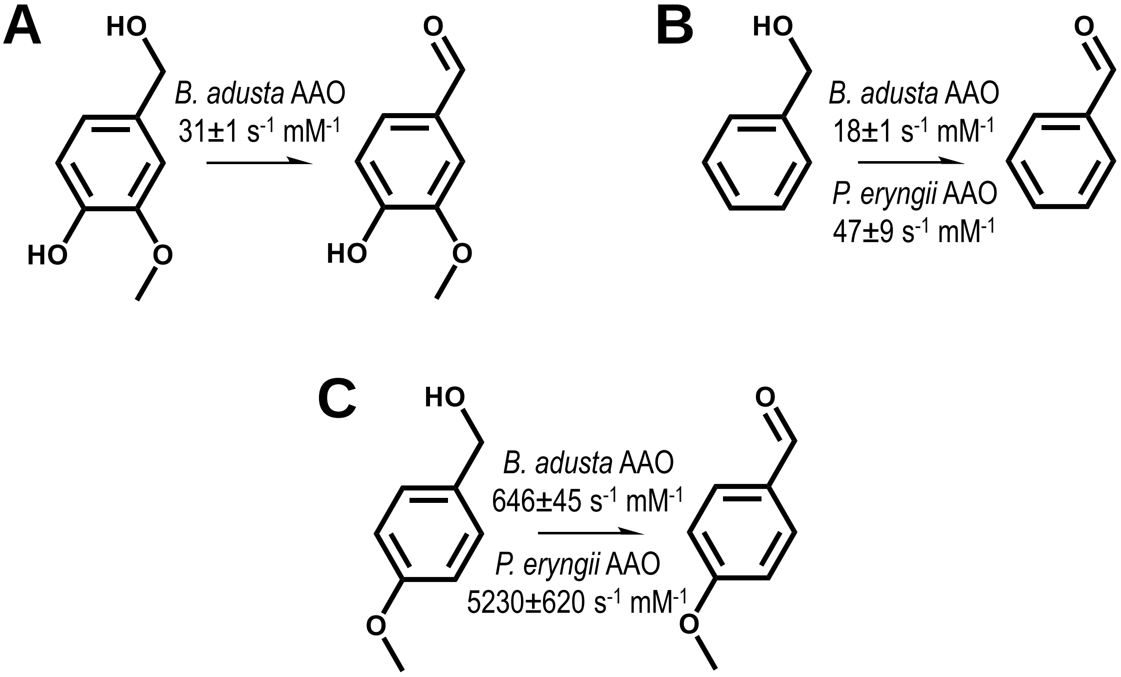

Figure 1.5. Catalytic efficiencies of *P. eryngii* and *B. adusta* AAOs in bioconversion of some flavours and aromas. **A.** Oxidation of vanillyl alcohol into vanillin. **B.** Oxidation of benzyl alcohol into benzaldehyde. **C.** Oxidation of *p*-methoxybenzyl alcohol into *p*-methoxybenzaldehyde.

Another very remarkable commercial aromatic compound is benzaldehyde. Some research has been carried out using the fungus *B. adusta* for the production of this chemical from *L*-phenylalanine (Lapadatescu and Bonnarme 1999; Lapadatescu et al. 2000). In this reaction of *L*-phenylalanine for flavour production, aryl-alcohols are the main products obtained, as reported for *B. adusta* (Lapadatescu et al. 2000) and *P. chrysosporium* (Jensen et al. 1994). Consequently, the application of AAO to such biotransformations could result in the obtention of higher levels of aromatic aldehydes, since their alcohol counterparts are substrates of the enzyme **(Figure 1.5B)**. Finally, using AAO plus an unspecific peroxygenase (UPO) from the fungus *Agrocybe aegerita* (Ullrich et al. 2004), an oxidoreductase cascade can be used for toluene conversion into benzaldehyde, with the second enzyme using the peroxide generated by AAO.

Another flavour that AAO produces as a consequence of its auxiliary role in lignin degradation is *p*-anisaldehyde (4-methoxybenzaldehyde) (**Figure 1.5C**). It was shown that the corresponding alcohol is the physiological and preferential substrate of the *P. eryngii* enzyme (Guillén et al. 1992b; Ferreira et al. 2005) and that AAO and mycelium-associated aromatic dehydrogenases establish a concerted anisaldehyde redox cycle to produce H_2O_2 continuously as described above (Figure 1). Therefore, AAO can be used for biotransformations aiming at the production of vanillin, benzaldehyde, anisaldehyde and other aromas.

1.5.2. Deracemization of chiral secondary alcohols

Many of the drugs and potential drug candidates possess chiral centres and most of them need to be commercialized as enantiomers rather than racemates given that enantiomers often carry out different activities within biological systems (Carey et al. 2006). Therefore, chiral intermediates for pharmaceuticals are synthesised through enantioselective asymmetric reactions (Patel 2013). As an alternative, deracemization of chiral mixtures is used by the pharmaceutical industry to obtain pure enantiomers. Among chiral compounds, some secondary alcohols are used as chiral intermediates and analytical reagents, and the development of synthesis procedures for the production of enantiomerically-enriched alcohols has gained importance in the pharmaceutical industry.

Biological systems are generally chiral and, as a consequence, many enzymes are regio- and enantioselective. These properties are regarded to be a consequence of the active sites' architecture and the enzyme's mechanism. Therefore, many microorganisms and enzymes offer attractive alternatives for easy production (asymmetrical synthesis of deracemization) of enantiomeric compounds of interest in the fine chemicals and pharmaceutical sectors (Matsuda et al. 2009; de Albuquerque et al. 2015). As explained above, the AAO catalytic mechanism consists in a hydride abstraction from the benzylic position of the alcohol by the oxidized flavin, in a reaction aided by an active-site histidine acting as a catalytic base to form the alkoxide intermediate (Hernández-Ortega et al. 2012a). Due to active site architecture, and the simultaneous nature of the hydride and proton abstractions, hydride transfer by AAO is stereoselective (only takes place from the pro-*R* position) as shown using the two α-monodeuterated enantiomers of *p*-methoxybenzyl alcohol (Hernández-Ortega et al. 2012b). Taking advantage from this information, Hernández-Ortega *et al.* (2012b) assayed the transformation of racemic secondary alcohols using *P. eryngii* AAO. They saw that the enzyme was able to oxidise the racemic 1-(*p*-methoxyphenyl)-ethanol, although it showed an apparent efficiency orders of magnitude smaller than the one for *p*-

methoxybenzyl alcohol. AAO enantioselectivity toward the (*S*) isomer was shown using chiral HPLC, which allows for the isolation of (R) isomer from chiral mixtures (**Figure 1.6**). Moreover, the AAO enantioselectivity toward another secondary alcohol 1-(*p*-fluorophenyl)-ethanol was estimated as a S/R ratio of 21, in reactions using the individual enantiomers.

Therefore, it is plausible that AAO could be used for the isolation of isomers from racemates taking advantage from its kinetic behaviour. However, AAO activity on secondary alcohols is low, due to some hindrances among such substrates and the residues forming the active site (Fernández et al. 2009). A mutated variant (F501A), in which the side chain of a bulky aromatic residue was removed to make room in the cavity, was created with the purpose of facilitating oxidation of secondary alcohols. The removal of this side chain resulted in a stereoselectivity *S*/*R* ratio on 1-(*p*-fluorophenyl)-ethanol three-fold higher than that of the wild-type enzyme. Hence, improved variants by directed evolution, as it has been done with galactose oxidase for these purposes (Escalettes and Turner 2008), or further site-directed mutagenesis would result in better deracemization reactions.

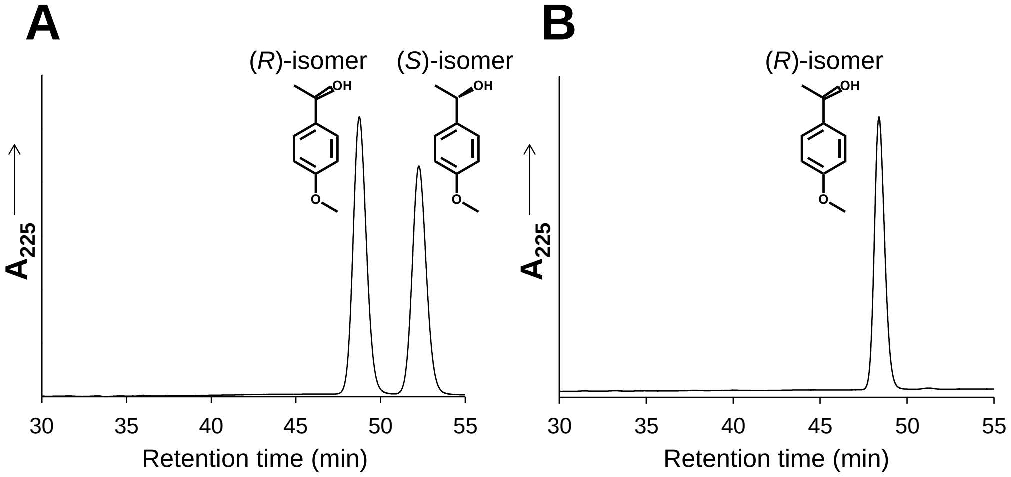

Figure 1.6. Chiral HPLC chromatograms showing the deracemization of 1-(*p*-methoxyphenyl)-ethanol by *P. eryngii* AAO. **A.** Chromatogram of the untreated racemate. **B.** Chromatogram after 24-h reaction with AAO, where only the peak of the (*R*) isomer is detected (the peak of the *p*-methoxyacetophenone, formed from oxidation of the (*S*) isomer, eluted in a different region of the chromatogram).

1.5.3. Oxidation of furfurals

Over the last years, the use of renewable carbon sources instead of the classical fossil sources has come up as a necessity due to the expected decrease of crude oil reserves, as well as to reduce the sharp increase in the associated greenhouse effect emissions (Gallezot 2012). Within such a paradigm, lignocellulosic biomass is expected to substitute for fossil sources thanks to its interesting properties, which make it unique among other carbon resources. Some valuable chemicals that can be obtained from lignocelluloses are the furaldehydes. These are primarily furfural and 5-hydroxymethylfurfural (HMF). Furfural comes from pentoses present in the hemicelluloses, whereas HMF is formed from hexoses, which are present both in cellulose and hemicelluloses. HMF is synthesized by dehydration of monosaccharides, generally fructose (Antal et al. 1990), but direct conversion of glucose is also possible (Zhao et al. 2007). After optimized hydrolysis, disaccharides and polysaccharides would be the starting materials for these renewable building blocks (Rosatella et al. 2011).

The presence of two functional groups in HMF, combined with its furan aromatic ring, makes it an appealing starting material for various chemical applications. Serious attention has been paid to its oxidation and reduction, because they provide convenient synthetic pathways for the production of chemical building blocks for the polymer industry. One of these important building blocks is 2,5-furandicarboxylic acid (FDCA), which originates from the oxidation of HMF. Its importance resides in the ability to copolymerize with diols, producing poly(ethylene-2,5-furandicarboxylate) (PEF) among other polyesters. These polymers are thought to be able to substitute for polyesters based on terephthalic acid such as poly(ethylene-terephthalate), poly(propylene-terephthalate) or poly(butylene-terephthalate), which are biologically not degradable, and the precursors of which are fossil resources. Notably, PEF exhibits good mechanical and barrier properties (Papageorgiou et al. 2014) and has the double advantage of being renewable and biodegradable

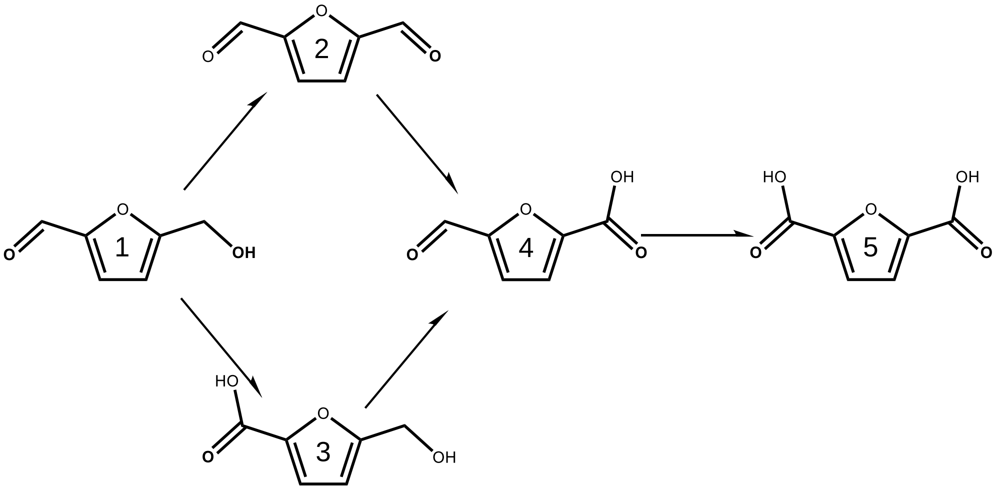

Figure 1.7. Oxidative pathways from HMF (**1**) to FDCA (**5**). FFCA (**4**) formation can take place through two alternative intermediate compounds: DFF (**2**) or HMFCA (**3**).

The oxidative pathway leading from HMF to FDCA takes place *via* 2,5-formylfurancarboxylic acid (FFCA) and includes two alternative intermediates: 2,5-diformylfuran (DFF) and 2,5-hydroxymethylfuran-carboxylic acid (HMFCA) (**Figure 1.7**). FFCA and other of these partially-oxidized compounds are also of interest as intermediates for the preparation of surfactants, biofuels, resins and other compounds (Moreau et al. 2004).

Several processes involving enzymes and organisms have been reported aiming at the obtention of FDCA from HMF (van Deurzen et al. 1997; Koopman et al. 2010;

Hanke 2012; Dijkman and Fraaije 2014; Dijkman et al. 2014; Carro et al. 2015; Dijkman et al. 2015). Regarding the use of AAO with this purpose, Hanke et al. (2012) screened for available AAOs capable of oxidising HMF with variable results. With the same purpose, Carro et al. (2015) analysed the ability of *P. eryngii* AAO to oxidise HMF.

These findings paved the way to implement AAO together with the peroxygenase to obtain a valorised by-product originated from lignocellulosic biomass. Furthermore, they widened the spectrum of aromatic substrates of the enzyme, which is now thought to range from benzylic carbocycles to heterocycles, as HMF and DFF.

1.6. Summary

The finite character of fossil fuels their make it necessary to find new resources, preferentially renewable ones, which allow for the substitution of the classical resources. In this way, lignocellulosics are a remarkable material due to their ubiquitous and renewable character. Furthermore, the concern about the environment impels us to search for new catalytic procedures that take advantage from natural processes, instead of the chemical environmentally polluting and energy-wasting ones. Hence, the use of organisms or enzymes to carry out catalytic industrial processes is gaining importance.

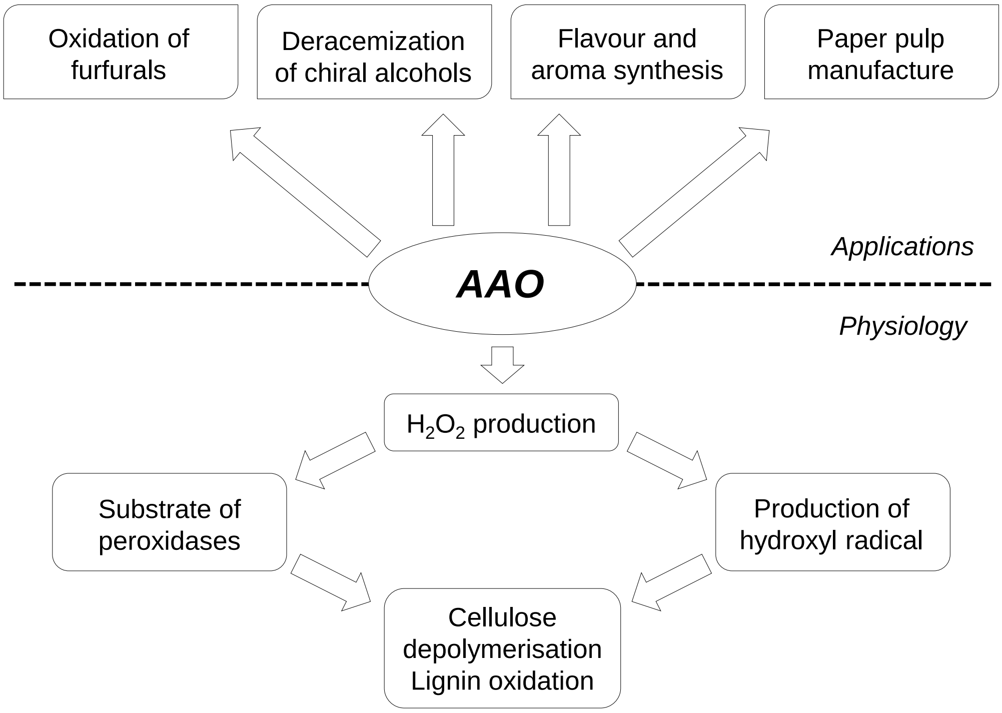
Oxidation of furfurals
Deracemization of chiral alcohols
Flavour and aroma synthesis
Paper pulp manufacture
Applications
AAO
Physiology
H_2O_2 production
Substrate of peroxidases
Production of hydroxyl radical
Cellulose depolymerisation Lignin oxidation

Figure 1.8. Scheme depicting the physiological role of AAO in lignocellulose degradation and its potential applications in the cellulose and other chemical sectors.

AAO, like all GMC oxidoreductases involved in lignocellulose decay, is a very promiscuous enzyme. It catalyses the oxidation of a great deal of polyunsaturated alcohols (and hydrated aldehydes). Its applicability on some industrial processes showed to be promising as a biocatalyst in several conversions. AAO, because of its involvement in the lignocellulose decay process, has potential to be applied to lignocellulose biorefineries. AAO has so far shown its potential applications in paper pulp manufacture and bioconversion of lignocellulose-derived compounds, synthesis of flavours, and deracemization of chiral alcohols (**Figure 1.9**) In spite of the fact that the use of GMC enzymes (among which AAO) for these purposes is not yet sufficiently developed, much progress has been done the recent years in this field as one can infer from the huge amount of publications available on enzymatic biocatalysis.

This chapter has been partially redrafted after the book chapter: Fungal aryl-alcohol oxidase in lignocellulose degradation and bioconversion. Microbial enzymes in Bioconversions of Biomass. Carro J, Serrano A, Ferreira P, Martínez AT. Springer, Berlin, Germany, pp 301–322.

Structure and Objectives

This Thesis has been structured into different sections. One general Introduction dealing with aspects of the GMC superfamily of oxidoreductases with special emphasis on AAO, its catalytic mechanism and biotechnological applications, as a model representative of the superfamily, is presented. Afterwards, the Materials and Methods employed throughout the Thesis are detailed. Then, six different chapters in which results and discussion of the various topics studied in this Thesis are presented. Finally, a general Discussion that brings together and relates the results described in each of the chapters has been added in order to sum up the main results of this work, followed by a section that briefly summarizes the main conclusions of the Thesis.

The objectives of the present work were three:

i) The investigation of the genomes of basidiomycetes in search for genes encoding for GMC oxidoreductases and the study of their phylogenetic relationships, evolution history, as well as their relation with physioecological aspects of the different fungi.

ii) The investigation of the mechanistics of AAO from the basidiomycete *Pleurotus eryngii* as a model representative of the GMC superfamily of enzymes, focusing on the reoxidative half-reaction, the temperature dependence of its reductive half-reaction and the elucidation of the role of active-site Phe397.

iii) The application of GMC oxidases in a biotechnological process: the production of 2,5-furandicarboxylic acid, a building block that gives rise to renewable and biodegradable bioplastics, from precursors derived from plant biomass.

2

Materials and Methods

2.1. Reagents

Glucose oxidase type VII from *Aspergillus niger*, glucose, *p*-methoxybenzyl alcohol, *p*-anisic acid, HMF (=5-hydroxymethylfurfural), HMFCA (=5-hydroxymethylfurancarboxylic acid), DFF (=2,5-diformylfuran), FDCA (=2,5-furandicarboxylic acid), *t*-butyl-methyl-ether, D_2O and BSTFA (=bis(trimethylsilyl)trifluoroacetamide) were purchased from Sigma-Aldrich. FFCA (=5-formylfurancarboxylic acid) was from TCI America. Deuterium oxide 99.9% isotopic purity was bought from Cambridge Isotope Co. AmplexRed® and HRP (=horseradish peroxidase) were purchased from Invitrogen. [α-$^2H_2$]-*p*-methoxybenzyl alcohol and (*R*)-[α-^2H]-*p*-methoxybenzyl alcohol were synthesized at the Instituto de Ciencia de Materiales de Aragón.

2.2. Genome screening and evolutionary studies

2.2.1. Genome sequencing

The genomic sequences of *B. adusta* (HHB-12826-SP), *P. brevispora* (HHB-7030-SS6) and *Ganoderma* sp. (10597-SS1) were obtained at the Joint Genome Institute (JGI), as part of the Saprotrophic Agaricomycotina Project coordinated by D.S. Hibbett (Clark University, USA). The genomes were produced as described by Binder et al. (2013) and the gene prediction is available for searching through http://genome.jgi-psf.org/Bjead1_1, http://genome.jgi-psf.org/Gansp1 and http://genome.jgi-psf.org/Phlbr1, respectively.

2.2.2. Genome screening for GMC gene families in Polyporales

The above genomes, plus those of *Dichomitus squalens*, *Fomitopsis pinicola*, *Gelatoporia subvermispora* (syn.: *Ceriporiopsis subvermispora*), *P. chrysosporium*, *R. placenta*, *Trametes versicolor* and *Wolfiporia cocos* (= *Wolfiporia extensa*) available at the JGI MycoCosm portal (http://genome.jgi-psf.org/programs/fungi) (Grigoriev et al. 2012), were screened for genes of the AAO, MOX, GOX, CDH, P2O and PDH families in the GMC superfamily. Among the above genomes, those from the Antrodia clade (*F. pinicola*, *R. placenta* and *W. cocos*) correspond to wood decay by brown-rot species, while the other species (*B. adusta*, *D. squalens*, *Ganoderma* sp., *G. subvermispora*, *P. chrysosporium*, *P. brevispora* and *T. versicolor*) cause white-rot decay of wood.

The screening for each of the GMC families was performed by blasting an entire set of filtered model proteins for each of the genomes with the following (GenBank) reference sequences: i) AAO from *Pleurotus eryngii* (AAC72747); ii) MOX from *Gloeophyllum trabeum, Pichia methanolica* and *Candida boidinii* (ABI14440, AF141329 and Q00922); iii) GOXs from *Talaromyces flavus*, *Penicillium expasum*, *Penicillium amagasakiense*, *Aspergillus niger* and

Botryotinia fuckeliana (AAB09442, ABN79922, AAD01493, AAF59929 and CAD88590); iv) CDHs from *P. chrysosporium, G. subvermispora*, *Coniophora puteana, Pycnoporus cinnabarinus* (syn.: *Trametes cinnabarina*) and *T. versicolor* (CAA61359, ACF60617.1, BAD32781 AAC32197and AAC50004); v) P2Os from *T. versicolor*, *Peniophora* sp., *P. chrysosporium*, *Lyophyllum shimeji* and *G. trabeum* (BAA11119, AAO13382, AAS93628, BAD12079 and ACJ54278); and vi) PDHs from *Leucoagaricus meleagris* (syn.: *Agaricus meleagris*), *Agaricus xanthodermus* and *Agaricus bisporus* (AAW82997, AAW92123 and AAW92124).

2.2.3. Sequence analysis

The genomic sequences with the highest similarities with the reference sequences for the different GMC families were, firstly, examined for the automatically annotated introns, searching for consensus 5' - 3' and lariat sequences (Ballance 1986), as well as for the annotation of N- and C-termini. The presence or absence of secretion signal peptides predicted by the JGI automatic annotation pipeline was manually revised to detect possible mistakes (e.g. in neighbor introns) that could result in inaccurate predictions, followed by inspection of the eventually revised sequences using the Signal P 4.0 server (www.cbs.dtu.dk/services/SignalP-4.0) (Petersen et al. 2011). Moreover, other servers as TargetP 1.1 (Emanuelsson et al. 2000), Wolf psort (Horton et al. 2007) and TMHMM 2.0 were used to confirm the secreted nature of proteins as well as to predict their putative subcellular locations. Predictions were confirmed by multiple alignment with MUSCLE (Edgar 2004) and by the comparison with reference sequences. Multiple alignments were also used for analysis of motifs conserved in GMC proteins (the ADP-binding domain and, at least, one of the two characteristic Prosite PS00623 and PS00624 sequences) (Cavener 1992). The sequences that lacked these GMC conserved motifs were discarded.

Finally, molecular models of 94 out of the 95 GMC sequences (JGI references in **Annex 1**) could be generated at the Swiss-Model server (www.swissmodel.expasy.org), which selected the most adequate templates (Bordoli et al. 2009). For AAO, MOX, GOX, CDH and P2O sequences, the crystallographic structures of *P. eryngii* AAO (PDB 3FIM), *Arthrobacter globiformis* choline oxidase (PDB 3LJP, note that no MOX crystal structure is available), *A. niger* GOX (PDB 1CF3), *P. chrysosporium* CDH (PDB 1KDG) and *Aspergillus oryzae* P2O (PDB 1TTO) were used as templates, respectively. Strictly conserved histidine and histidine/asparagine residues at the active site (Hernández-Ortega et al. 2012c) (Wongnate et al. 2014) were searched for in all the models, and species lacking these residues were discarded.

2.2.4. GMC evolutionary history

The evolutionary history of the (95) GMC sequences obtained was estimated with RaxML v.7.7.1 (Stamatakis et al. 2008) from the multiple alignment obtained with MEGA5 (Tamura et al. 2011). For evolutionary tree construction, a maximal likelihood with clustering method was used, with the WAG model of amino acid substitutions, and the gaps treated as deletions (a 100 iteration bootstrap was performed). Identity degrees between all the above sequences were obtained after pairwise alignment with ClustalW2.

2.2.5. Reconciliation analyses

The histories of gene duplication and losses for total GMCs (and the individual families) were inferred using Notung 2.6 (Durand et al. 2006). The gene tree was used as input and combined with a Polyporales phylogenetic tree (Binder et al. 2013) from TreeBase (www.treebase.org, tree ID Tr67497). The estimated numbers of gene duplications and deletions on each branch were used to hypothesize the number of sequences at the ancestral nodes. Two different threshold levels (30% and 90%) were used to assess the significance of the predictions obtained.

2.3. AAO purification and mutagenesis

2.3.1. Enzyme production and purification

Recombinant AAO from *Pleurotus eryngii* was obtained by expressing the mature AAO cDNA (GenBank AF064069) in *Escherichia coli* W3110 strain. Pre-cultures were grown in LB media for 16 h at 180 rpm and 37ºC in the presence of ampicillin (1 μg · mL^{-1}).

After this time, flasks containing 900 mL of TB medium were inoculated with 30 mL of the pre-culture, along with the addition of 100 mL of a solution containing 170 mM KH_2PO_4 and 720 mM of K_2HPO_4 and ampicillin. Cultures were grown at 37ºC and 220 rpm until they attained an optical density of 1 measured at 500 nm, when expression was triggered by the addition of 1 mM IPTG. 4 hours after induction cells were pelleted by centrifugation at 8000 rpm for 5 min.

Cells were resuspended in lysis solution containing Tris HCl 50 mM pH 8.0, EDTA 10 mM and DTT 5 mM. Then, lysozyme was added at a final concentration of 2 mg/mL and was put in ice for 30 min, after which time DNase was added and left to act for other 30 min. Afterwards, cells were sonicated and centrifuged for 30 min at 12500 rpm. Supernatant was discarded and the inclusion bodies obtained were dissolved in wash solution (20 mM Tris HCl pH 8.0, EDTA 1 mM and DTT 5 mM) with the use of a homogeneizer and once again centrifuged at 12500 rpm for 30 min. The washing process was repeated twice.

The washed inclusion bodies were dissolved in unfolding solution, which contained 20 mM Tris HCl pH 8.0, EDTA 2 mM, DTT 5 mM and urea 8 M, with the use of a tissue homogeneizer. The protein solution in urea was centrifuged for 30 min at 12500 rpm.

The protein concentration was estimated by the method described by Bradford and, then, the inclusion bodies were *in vitro* refolded. The refolding solution is composed of 20 mM Tris HCl pH 9.0, L-glutathione oxidized 2.5 mM, 40% glycerol, DTT 1 mM, urea 600 mM and FAD 0.02 mM. Protein was added to the said solution at a final concentration between 100–200 µg/mL and refolding took place at 4◦C in the shade for 5 days.

After this time the enzyme was concentrated by tangential filtration using cassettes of 10 µM of pore (Millipore). Enzyme was then centrifuged for 15–20 h at 13500 rpm to remove glycerol and dialyzed against 50 mM sodium phosphate pH 6.0. Enzyme was then further concentrated using amicon® filters of 10 µm of pore (Millipore).

The enzyme was eventually purified by anion exchange chromatography in an FPLC apparatus (GE Healthcare) in a Resource Q column 6 mL (GE Healthcare). The column was equilibrated with 50 mM sodium phosphate pH 6.0 (solution A), into which 5 mL of the protein solution were injected. The solution employed to elute the protein was the same described above supplemented with NaCl 1 M (solution B). Two column volumes of solution A were employed to inject the protein and let it bind the column. Then, 1 column volume of solution B was passed through the column in order to elute the purified protein, which was manually collected and whose activity was determined with *p*-methoxybenzyl alcohol. The chromatographic process was monitored at 465 and 280 nm with a UV-visible detector. AAO was then aliquoted and conserved at -80ºC.

The above-described procedure was employed for the production and purification of wild-type AAO as well as its mutated variants.

2.3.2. Site-directed mutagenesis

AAO mutated variants were produced by site-directed mutagenesis using the QuickChange® kit (Stratagene) based on PCR reactions run with oligonucleotides bearing mismatches. These primers were specifically designed for each variant according to the desired mutation. All of them were designed obeying the following rules: i) they were 25-40 bases long, ii) their melting temperatures were equal or higher than 78ºC, iii) the mismatches were placed in the middle of the oligonucleotide, iv) their cytosine/guanine content was equal or higher than 40% and v) their extremes must be composed of either cytosine or guanine. The 5'-primers employed were the following (along with their reverse complementary counterparts):

Y92F: 5’-GGGTCTAGCTCTGTTCACT***T***CATGGTCATGATGCG-3’
Y92L: 5’-GGGTCTAGCTCTGTTCAC***CT***CATGGTCATGATGCG-3’
Y92W: 5’-GGGTCTAGCTCTGTTCACT***GG***ATGGTCATGATGCG-3’
F397Y: 5’-CTTTTCCAACCAATGGT***A***CCACCAGCTATCCCTCG-3’
F397W: 5’-CTTTTCCAACCAATGGT***GG***CACCCAGCTATCCCTCG-3’
F397A: 5’-CTTTTCCAACCAATGG***GC***CCACCCAGCTATCCCTCG-3’
F397L: 5’-CTTTTCCAACCAATGGTT***G***CACCCAGCTATCCCTCGC3’

These primers were employed in PCR reactions to introduce the mutation at the desired location. The DNA polymerase employed was *Pfu* (Roche) and the template DNA was the pFLAG1 vector harboring the WT AAO gene. **Table 2.1** shows the PCR programme used.

The products of the PCR reaction were subjected to enzymatic digestion with the restriction enzyme DpnI (Roche), which shows specificity towards methylated and hemimethylated DNA, hence destroying the parental, non-mutated DNA. PCR products were sequenced at Secugen to prove the success of the site-directed mutagenesis.

Table 2.1. Cycles of the mutagenic PCR programme

Part	Cycles	Temperature	Time
1	1	95ºC	60 s
2	18	95ºC	50 s
		60ºC	50 s
		68ºC	480 s
3	1	68ºC	420 s

The vectors containing the mutated AAO genes were transformed into *E. coli* DH5α strain for propagation. Competent cells were transformed by incubation with 10 μL of vector in ice for 30 min, followed by a temperature shock at 42ºC for 1.5 min. Then, cells were added 800 μL of antibiotic-free LB medium and grown for 1 h at 37ºC under shaking. After this time, they were inoculated on LB-agar plates containing ampicillin and colonies grown for 20 h.

Isolated colonies were inoculated into liquid LB medium and grown overnight under shaking to purify propagated plasmid using the High Pure Plasmid Isolation Kit (Roche). Vectors were then transformed into the expression host above-mentioned following the protocol described for transformation.

2.3.3. Estimation of the molar extinction coefficient of AAO

In order to carry out kinetic studies proteins must be properly quantified. AAO is normally quantified spectroscopically thanks to the estimation of its molar extinction coefficient (ε) at the maximum of the flavin band I (around 460 nm).

Molar extinction coefficients are estimated by heat denaturation of the enzyme and quantification of the released FAD cofactor, whose extinction coefficient is known to be 11300 $M^{-1}{\cdot}cm^{-1}$ at 450 nm. Comparison of the absorbance of the maximum of flavin band I of the protein prior to being denatured at 100 °C for 5 min with the absorbance of FAD at 450 nm allows the estimation.

2.4. Kinetic and affinity studies

2.4.1. Stopped-flow measurements

Enzyme monitored turnover

Experiments were performed using a stopped-flow spectrophotometer from Applied Photophysics Ltd., model SX17.MV.

Enzyme-monitored turnover experiments were carried out by mixing AAO (~10 µM, final concentration) with exceedingly saturating *p*-methoxybenzyl alcohol concentrations (at least 10-fold the Km for each of the variants), under air-saturated conditions at 25°C. Spectral evolution of the enzymes during redox turnover was recorded between 350–700 nm with a photodiode array (PDA) detector.

Studies on the reductive half-reaction

Reduction rate constants were determined using a stopped-flow spectrophotometer from Applied Photophysics Ltd., model SX17.MV, under anaerobic conditions. Solutions, buffers, substrates and proteins (WT AAO and mutated variants above-mentioned) were poured into glass tonometers and subsequently subjected to 20–25 cycles of evacuation and Ar flushing connected to an anaerobic train. Glucose (10 mM final concentration) and glucose oxidase (10 U·mL-1) were added after some vacuum-Ar cycles to all solutions, except for the sodium dithionite, in order to ensure anaerobiosis.

The stopped-flow equipment was made anaerobic by flushing a solution of sodium dithionite so that it scavenged all traces of oxygen. Sodium dithionite was then removed by rinsing the apparatus with anaerobic 50 mM sodium phosphate buffer pH 6.0. Reactions were followed with the photodiode array (PDA) detector and baseline was made with anaerobic 50 mM sodium phosphate buffer pH 6.0. Kinetics were measured by mixing ~20 µM of AAO with increasing concentrations of [α-$^{1}H_2$]-*p*-methoxybenzyl, [α-$^{2}H_2$]-p-methoxybenzyl and (*R*)-[α-^{2}H]-p-methoxybenzyl alcohols using the single-mixing mode of the equipment at several temperatures. Temperature was maintained constant with a thermostated water bath and enzyme and substrate were equilibrated for 10 min so that they attained the desired temperature prior to measuring kinetics.

Observed rate constants (k_{obs}) were estimated by global fitting the reduction spectra of the enzyme to a one-species model using the ProKineticist software from Applied Photophysics. Reduction rate constants were estimated by nonlinear fitting of the observed rate constants at different substrate concentrations to either **Equation 1** or **Equation 2**:

$$k_{\mathrm{obs}} = \frac{k_{\mathrm{red}} A}{K_{\mathrm{d}} + A}$$

$$k_{\mathrm{obs}} = \frac{k_{\mathrm{red}} A}{K_{\mathrm{d}} + A} + k_{\mathrm{rev}}$$

where k_{obs} is the observed rate for flavin reduction at a given substrate concentration, k_{red} and k_{rev} are the limiting rate for hydride transfer (HT) from the substrate to flavin N5 and its reverse reaction, respectively, at saturating substrate concentration; K_{d} stands for the dissociation constant of the enzyme-substrate complex.

Single-mixing reoxidation studies

The reoxidative half-reaction was investigated by mixing reduced AAO with increasing O_2 concentrations obtained by bubbling O_2/N_2 mixtures into 50 mM sodium phosphate buffer pH 6.0 from tanks for 15 min.

Procedures were as explained above for the reductive half-reaction, except for that, in this case, AAO and glucose were put into a tonometer bearing a side-arm, where *p*-methoxybenzyl alcohol (1.3-fold the concentration of AAO) was poured along with glucose oxidase. After the required vacuum-Ar cycles, enzyme and substrate were mixed before being mounted onto the stopped-flow equipment. In the single-mixing mode, reduced enzyme and substrate are mixed at equal proportions in the mixing chamber.

Reactions were measured with both the PDA and the monochromator detectors at 12°C. k_{obs} were obtained by either global fitting of the spectra or fitting the monochromator traces to exponential equations describing two-step and three-step processes. Fitting averaged k_{obs} to **Equation 3** allowed the estimation of the apparent second-order rate constant for reoxidation (${}^{\mathrm{app}}k_{\mathrm{ox}}$):

$$k_{\mathrm{obs}} = {}^{\mathrm{app}}k_{\mathrm{ox}} \cdot [O_2] + k_{\mathrm{rev}}$$

Double-mixing reoxidation studies

Reactions were conducted in either 50 mM sodium phosphate, pH 6.0, 30 mM sodium phosphate, pH 7.0, 25 mM sodium phosphate, pH 8.0 or 100 mM sodium acetate, pH 5.0 (concentrations were chosen so that ionic strength of the buffers would be similar to that of 50 mM sodium phosphate, pH 6.0, the optimal pH for the enzyme) (Ferreira et al. 2005), at 12 °C, unless otherwise stated. The measurements were performed using a TgK Scientific Model SF-61DX stopped-flow spectrophotometer. In the double-mixing mode, enzyme and one substrate are mixed together at equal proportions in a so-called ageing loop and, after the ageing time, they are pushed by buffer into the optical cell (pathlength 1 cm), where they mix with the second substrate at equal proportions. Then, the enzyme and the first substrate are diluted four times, whereas the second substrate —O_2 in this case— is only diluted by one half.

The stopped-flow apparatus is made anaerobic by flushing O_2-free buffer (50 mM sodium phosphate, pH 6.0) containing glucose 2 mM and glucose oxidase 5 μM through the system. The buffer was made anaerobic by O_2-free argon bubbling for at least 15 min. Glucose and glucose oxidase reacted overnight inside the equipment, and were then rinsed out by flushing anaerobic buffer prior to the measurements. Reactions were investigated using the monochromator mode, following absorbance at a given wavelength. The observed rate constants (k_{obs}) were calculated by fitting the obtained traces using exponential fits with the software Kinetic Studio (TgK Scientific).

The enzyme was made fresh prior to being used by gel filtration through PD-10 desalting columns (General Electric), followed by centrifugation to remove denatured enzyme. The desalting columns were equilibrated by passing the desired buffer through it prior to being used, and the enzyme was eluted using the same buffer (prepared in H_2O or D_2O, or containing glycerol). D_2O buffers were prepared by dissolving the salts in deuterium oxide and pD was adjusted with sodium deuteroxide (99.5% isotopic purity) using a pHmeter (pD = pH reading + 0.41). Viscosity effect experiments were performed in 50 mM sodium phosphate buffer, pH 6.0, with 7.4% (*v:v*) glycerol to mimic the viscosity of deuterium oxide at 12°C ($1.6x10^{-3}$ $N{\cdot}s{\cdot}m^{-2}$).(Cheng 2008) To study the reaction of the reduced enzyme with O_2, the enzyme was put in a tonometer connected to an anaerobic train, where it was subjected to 20–25 cycles of gas removal by applying vacuum, followed by O_2-free argon flushing. Besides, glucose oxidase was added to the enzyme at a final concentration of 0.05 μM and glucose 1 mM was poured into a side arm connected to the tonometer. After the cycles glucose was mixed with the glucose oxidase.

Buffers and *p*-methoxybenzyl alcohol were made anaerobic by O_2-free argon bubbling for 15 min into air-tight glass syringes and glucose (1 mM) and glucose oxidase (0.05 μM) were added. Buffers containing O_2 at desired concentrations were prepared by bubbling different O_2/N_2 mixtures for 15 min. Different percentages of O_2 were attained using an O_2/N_2 blender connected to pure and certified O_2 and N_2 tanks. Actual O_2 concentrations were measured at 25°C using a computer-interfaced Oxy-32 O_2-monitoring system (Hansatech Instruments, Inc) just prior to the use of the buffers. Once mounted onto the apparatus, all solutions containing enzyme, buffers and substrates were equilibrated for 10 min so they could attain the temperature of the system (12°C unless otherwise stated) and possible traces of O_2 were scavenged.

However, single-mixing mode was used to calculate the time the enzyme and the substrate had to age together when mixed at equal concentrations so that the enzyme got completely reduced. Such reactions were followed at 463 nm with deuterated and protiated substrates, both in H_2O and D_2O buffers. This experiment allowed avoiding the enzyme's turnover when mixed with O_2 in the double-mixing experiments. The monochromator was the detector used throughout the experiments due to its shorter dead time compared to that of the photo-diode-array (PDA), too slow to record the reoxidative reactions of AAO. All measurements were made by triplicate.

Rate constants were obtained by nonlinear fitting of the k_{obs} at various O_2 concentrations to **Equation 3**.

2.4.2. Steady-state kinetics

Direct measurements of AAO activity

Steady-state kinetics were measured for AAO by following spectrophotometrically the oxidation of *p*-methoxybenzyl alcohol into *p*-anisaldehyde at 285 nm (ε_{285} = 16950 $M^{-1}\cdot cm^{-1}$).

Bi-substrate kinetics were obtained by varying both the alcohol substrate and O_2 concentrations in 50 mM sodium phosphate buffer pH 6.0 at the desired temperatures.

Reactions were performed in screw-cap cuvettes in which buffer was equilibrated using different O_2/N_2 mixtures that were bubbled for 15 min in a thermostated water bath set at the desired temperatures. O_2 solubility in water strongly depends on temperature and, thus, actual O_2 concentrations were calculated for each O_2/N_2 mixtures and temperatures.

Reactions were triggered by the addition of the alcohol substrate and AAO (final concentrations between 5 and 3 nM) with syringes into the cuvette at a final volume of 1 mL. Initial rates were calculated as the change in absorbance divided by time from the linear phase of the oxidation of the alcohol to its aldehyde. Kinetic constants were obtained by fitting the observed rate constants to **Equation 4** or **Equation 5**, describing ternary mechanism or ping-pong mechanisms, respectively:

$$\frac{\mathrm{v}}{\mathrm{e}} = \frac{k_{\mathrm{cat}} AB}{K_{\mathrm{m(ox)}} A + K_{\mathrm{m(al)}} B + K_{\mathrm{d}} B + AB}$$

$$\frac{\mathrm{v}}{\mathrm{e}} = \frac{k_{\mathrm{cat}} AB}{K_{\mathrm{m(ox)}} A + K_{\mathrm{m(al)}} B + AB}$$

where ν stands for the initial velocity, e is the enzyme concentration, k_{cat} is the maximal turnover number, A the alcohol concentration, B the O_2 concentration, and $K_{m(ox)}$ and $K_{m(al)}$ are the Michaelis-Menten constants for O_2 and alcohol, respectively.

Indirect measurements of AAO activity

Some AAO substrates do not allow the direct spectrophotometric measurement of the product of their reaction with AAO. Therefore, steady-state kinetic parameters for AAO oxidation of HMF, MMF, DFF, HMFCA and FFCA were calculated by monitoring AAO-catalyzed production of H_2O_2 upon reacting with the substrates at several concentrations (0.125 – 32 mM) using a HRP-coupled assay, at 25 °C in air-saturated 50 mM sodium phosphate, pH 6.

The reactions were initiated by adding the enzyme (0.11 µM) with an adder-mixer. In the presence of the H_2O_2 generated by AAO, HRP (6 U/ml) oxidized AmplexRed® (60 µM) in a 1:1 stoichiometry forming resorufin (ε_{563} 52,000 $M^{-1} \cdot cm^{-1}$). Kinetic parameters were obtained by fitting the data to the Michaelis-Menten equation using SigmaPlot software.

2.4.3. Estimation of the rate constants for AAO-*p*-anisic acid complex formation and dissociation.

Studies on the formation of the AAO-*p*-anisic acid complex were performed by analyzing spectral changes upon mixing enzyme (~20 µM) with increasing concentrations of the ligand (within the range 0.04–2 mM) at 12 °C. Formation of the complex was followed with the PDA detector between 300–700 nm.

Data were globally fitted to an equation describing a one-step process. The obtained k_{obs} linearly depended on the ligand's concentration and were, thus, fitted to **equation 6**:

$$k_{\text{obs}} = k_{\text{for}} \cdot [L] + k_{\text{dis}}$$

in which k_{for} stands for the second-order rate constant for the complex formation; [L] represents the ligand concentration, and k_{dis} is the rate constant for the complex dissociation.

2.4.4. Studies on the temperature dependence of AAO catalysis.

Temperature dependence of the calculated rate constants (k_{cat}, k_{cat}/K_m or k_{red}) was estimated by fitting to the Arrhenius equation (**Equation 7**). This allowed the estimation of the corresponding Arrhenius pre-exponential prefactors for protium and deuterium isotope (A_H and A_D respectively) and its corresponding activation energy values (E_{aH} and E_{aD}). KIEs (i.e., the ratios of the rate with protium to the rates with deuterium) were determined using **Equation 8**. Combination of **Equations 7** and **8** led to the graphic representation of the temperature dependence of the KIE.

$$k = A \times e^{\frac{E_a}{RT}}$$

$$\mathrm{KIE} = \frac{k_{\mathrm{H}}}{k_{\mathrm{D}}}$$

2.4.5. Spectral characterization of the AAO-p-anisic acid complex.

The affinity of the five AAO variants for *p*-anisic acid was assessed by titration of the enzyme with increasing amounts of the ligand in 50 mM sodium phosphate pH 6.0 at 12°C. Spectral changes were recorded using a spectrophotometer and their magnitude upon complex formation was fitted to **equation 9**, which accounts for a 1:1 stoichiometry, as a function of *p*-anisic acid concentration:

$$\Delta\mathrm{A} = \frac{\Delta\varepsilon \cdot (\mathrm{E} + \mathrm{L} + K_{\mathrm{d}}) - \Delta\varepsilon\sqrt{(\mathrm{E} + \mathrm{L} + K_{\mathrm{d}})^2 - 4\mathrm{EL}}}{2}$$

in which ΔA accounts for the observed change in absorbance, Δε represents the maximal absorption difference in each of the spectra, K_d is the dissociation constant, and E and L, the enzyme and *p*-anisic acid concentrations.

2.5. Crystallization of wild-type AAO in complex with *p*-anisic acid

AAO was crystallized in complex with its inhibitor *p*-anisic acid. Crystallization was achieved from a protein solution at 6 mg·mL^{-1} mixed with *p*-anisic acid (1.35 mM), both in 150 mMNaCl and 100 mM NaK_2PO_4 pH 7.0. Then, 0.5 uL of this mixture was added to 0.5 uL of mother liquor consisted of 0.1 M sodium acetate, pH 4.5 and 1.0 M di-ammonium hydrogen phosphate. Crystals were cryoprotected with reservoir solution containing 20% of glycerol solution. Diffraction data sets were collected on the I24 beamline at the Diamond Synchrotron (Oxfordshire, UK) at 100 K using a wavelength of 0.96862 Å. Data were processed, scaled and reduced with XDS (Kabsch 2010) and SCALA (Kabsch 1988) from the CCP4 package (Collaborative Computational Project, Number 4, 1994). MOLREP (Vagin and Teplyakov 1997) from CCP4 was used to solve all the structures with the native *AAO* structure (PDB code: 3FIM) as search model. Refinements were performed automatically by REFMAC 5 (Murshudov et al. 1997) from CCP4 and manually by COOT (Emsley et al. 2010). PROCHECK (Laskowski et al. 1993) and MOLPROBITY (Chen et al. 2010) were used to assess and validate final structures.

Crystal belonged to the $P6_422$ hexagonal space group with one AAO: *p*-anisic acid complex molecule in the asymmetric unit and diffracted up to 2.30 Å. Residues lacking electron density were not included in the final models. Statistics for data collection and refinement are shown in **Table 2.2**.

The PISA server (Krissinel and Henrick 2007) was used to infer macromolecular assemblies from crystal structures, as well as to study their interfaces.

Table 2.2. Data collection and refinement statistics for *AAO:*p*-anisic acid* complex

Crystal data	**AAO:*p*-anisic acid complex**
Spacegroup	$P6_422$
UnitCellParameters (Å)	a = b = 179.33, c = 160.18 α = β = 90°, γ = 120°
Data Collection	
Temperature (K)	100
Beamline	ID24 DLS
Wavelength (Å)	0.96862
Resolution (Å)	43.99 - 2.30 (2.42 -2.30)
Total reflections	2710007 (392719)
Uniquereflections	67615 (9716)
Mean I/σ(I)	28.1 (6.2)
Completeness (%)	100 (100)
Redundancy	40.1 (40.4)
R_{merge}[a]	0.133 (0.806)
Data Refinement	
Resolutionrange (Å)	42.3 -2.30
Protein non-hydrogenatoms	4299
Ligand non-hydrogenatoms	94
Solvent non-hydrogenatoms	280
R_{work}(%)	17.43
R_{free}[b] (%)	19.50
r.m.s.d. bond length, (Å)	0.012
r.m.s.d. bond angles, (°)	1.661
Average B-factor, (Å^2)	32.93

Values in parentheses correspond to the highest resolution shell

[a] $R_{merge} = \Sigma|I - I_{av}| / \Sigma I$, where the summation is over symmetry-equivalent reflection

[b] R calculated for 7% of data excluded from the refinement

This work was carried out in collaboration with Dr. Marta Martínez Júlvez from the University of Zaragoza.

2.6. Reactions and enzymatic cascades of AAO with furfurals

2.6.1. Reactions

HMF and derivatives reactions

The time-course of 24-h conversions of HMF and by AAO was followed (samples were taken after 2, 4, 8 and 24 h) at 25 ºC, in 5 mL of sodium phosphate (pH 6) containing 5 µM enzyme (corresponding to 54 units measured with veratryl alcohol) and 3 mM substrate. Similar reactions were performed with the partially-oxidized HMF derivatives DFF, HMFCA and FFCA.

UPO reactions in 5 mL on the same substrates (3 mM) were followed for up to 120 h using 0.65 µM enzyme (corresponding to 20 U measured with veratryl alcohol) in 50 mM phosphate (pH 7) and 10 mM H_2O_2.

The effect of UPO on the HMF conversion by AAO was evaluated by simultaneous (from the beginning of the reaction on) or successive (after 4-h of reaction with AAO) addition of 0.65 µM UPO to the reaction solutions under the conditions described above in 50 mM sodium phosphate (pH 7).

In addition to the above 24-h reactions, the time courses of initial transformation of HMF (32 mM) by AAO (0.3 µM, 3.4 U) and UPO (86 nM, 2.6 U) were followed (after 30, 60 and 180 s) using 50 mM sodium phosphate of pH 6 and pH 7, respectively.

2.6.2. GC-MS analyses

Samples were taken from the one-pot reactions after different times in order to analyze the products present. 250 µL of the reaction mixtures were harvested and reactions were stopped by the addition of HCl to pH 2–3. Low pH values cause protonation of the organic acids and permit their subsequent liquid-liquid extraction. The latter was carried out by mixing the reaction mixtures with an excess of *t*-butyl-methyl-ether three times, followed by desiccation with $NaSO_4$ to remove water traces. Then, *t*-butyl-methyl-ether was evaporated using a rotary evaporator at room temperature and samples were derivatized with 50 µL of BSTFA for 15 min at 25°C (Teixidó et al. 2006).

Products of the reactions were separated and identified by gas chromatography-mass spectrometry in a gas chromatograph equipped with an HP-5MS column (Agilent, Santa Clara, CA, USA; 30 m 9 0.25 mm internal diameter; 0.25 µm film thickness) coupled to a quadrupole mass detector. The oven program started at 110 °C for 2 min, increasing at 20 $°C·min^{-1}$ until 310 °C. Helium was used as the carrier gas at a flow rate of 1.2 mL min^{-1}. Response factors were obtained by fitting the responses of various concentrations of these standard compounds (after its liquid-liquid extraction and derivatization) as a function of concentration to a linear equation. These response factors were used to estimate the molar percentage of each of the compounds in the reactions.

2.6.3. Measurements of AAO and UPO residual activities after incubation with furfurals

Residual activities of AAO and UPO were measured after different times of incubation with HMF and its partially-oxidized derivatives.

In the case of AAO, activity was determined by following spectrophotometrically the production of *p*-anisaldehyde at 285 nm ($\Delta\varepsilon_{285}$ = 16950 $M^{-1} \cdot cm^{-1}$) with 5 nM AAO and 200 µM *p*-methoxybenzyl alcohol at a final volume of 1 mL, at 25°C.

Regarding UPO, its residual activity was measured as the veratraldehyde production at 310 nm (ε_{310} = 9300 $M^{-1} \cdot cm^{-1}$) with 5 nm of enzyme and 10 mM of veratryl alcohol at a final volume of 1 mL, at 25°C. Experimental points of residual activity were fitted to equations describing their activity decay as a function of time. This allowed the estimation of the enzyme's half-life as well as their total turnover number.

2.7. NMR studies

The hydration rates of aldehyde solutions (~10 mM) (HMF, DFF and FFCA) in 50 mM sodium phosphate, pH 6; and 50 mM sodium borate-acetate-phosphate, pH 3 and pH 9, prepared with 99.9% isotopic purity ^2H_2O were estimated by ^{1}H-NMR using a Bruker Avance 600 MHz instrument. The internal reference for chemical shifts was the signal from residual water proton (δ_H 4.9 ppm). The signal of the $\underline{H}$-C-$(OH)_2$ proton in the *gem*-diol form was integrated and referred to that of the $\underline{H}$-C=O proton of the aldehyde species for the hydration degree estimation. Spectra in DMSO-d_6 (isotopic purity ≥ 99.8 %) were run as a reference, showing only the non-hydrated species.

3

GMC genes in 10 Polyporales genomes: A survey of genes encoding H_2O_2-producing GMC oxidoreductases

Three representative Polyporales —*Bjerkandera adusta, Ganoderma* sp. (*G. lucidum* complex) and *Phlebia brevispora*— were recently sequenced (Hibbett et al. 2013) and their different GMC gene families are analyzed in this chapter. *Bjerkandera adusta* is a strong lignin degrader, which produces AAO (Muheim et al. 1990b) together with ligninolytic peroxidases (Kimura et al. 1991; Heinfling et al. 1998). Some species of *Ganoderma* cause extensive wood delignification (González et al. 1986; Martínez et al. 1995; Martínez et al. 2011) and little is known about GMC production by these fungi (Peláez et al. 1995; Ralph et al. 1996). Finally, *P. brevispora* was investigated for wood biopulping due to selective lignin removal (Akhtar et al. 1993; Fonseca et al. 2014). Moreover, seven additional sequenced Polyporales genomes were screened and included in the present comparative analysis of GMC-encoding genes. The present chapter is part of a wider genomic project covering other gene families (Ruiz-Dueñas et al. 2013; Hori et al. 2013; Mgbeahuruike et al. 2013; Syed et al. 2013; Kovalchuk et al. 2013) as an example of genome-enabled mycology to gain insight into the biology and evolution of fungi (Hibbett et al. 2013).

3.1. Results

3.1.1. GMC gene families in ten Polyporales genomes

A total of 41 GMC genes —21 AAO, 15 MOX, 3 CDH and 2 P2O genes (**Table 3.1**)— were identified in the recently sequenced genomes of *B. adusta*, *Ganoderma* sp. and *P. brevispora*. Family classification was completed by inspection of the enzyme molecular models described below for characteristic flavin environment and catalytic residues (Gadda 2008; Hernández-Ortega et al. 2012a; Wongnate and Chaiyen 2013; Romero and Gadda 2014). The genome of *B. adusta* has the highest number of GMC genes (a total of 18), while similar numbers (11-12 genes) were found in the two other genomes (**Table 3.1**). No GOX or PDH genes were found in any case and P2O genes were also absent from the *Ganoderma* sp. genome. AAO genes are the most abundant GMC genes in *B. adusta* and *Ganoderma* sp. (11 and 7, respectively) while MOX genes are the most abundant in *P. brevispora* (6 genes). None of the 41 GMC genes identified in the three genomes had been previously cloned and deposited in databases. Annotated genomes from seven more species of Polyporales were included for a wider comparison. The resulting ten genomes include representatives of the Phlebioid (*B. adusta, P. brevispora* and *P. chrysosporium*), core Polyporoid (*D. squalens, Ganoderma* sp. and *T. versicolor*) Gelatoporia (*G. subvermispora*) and Antrodia (*F. pinicola, R. placenta* and *W. cocos*) clades (Binder et al. 2005).

The number of genes of the different GMC families in each of the genomes is shown in **Table 3.1**, up to a total of 95 (their JGI protein ID references are in **Annex 1**, which also indicates the existence of alleles and recognized signal peptides. MOX genes are equally present in the white-rot and brown-rot genomes (average 4.0-4.4 genes/genome) while those of AAOs are nearly 6-fold more abundant in the genomes of white-rot (average 5.7 genes/genome) than brown-rot (average 1.0 gene/genome) species. Moreover, CDH genes were present in all the white-rot genomes (1 copy per genome), but absent from the brown-rot genomes. Finally, also P2O genes were absent from the brown-rot genomes and no PDH genes were found in any of the genomes.

Table 3.1. Inventory of 95 genes from six GMC families in the genomes of 10 Polyporales species (BJE AD*,* *B. adusta*; PHL BR, *P. brevispora*; PHA CH*,* *P. chrysosporium*; DIC SQ, *D. squalens*; GAN SP, *Ganoderma* sp.; TRA VE, *T. versicolor*; GEL SU, *G. subvermispora*; FOM PI, *F. pinicola*; RHO PL, *R. placenta*; and WOL CO*,* *W. cocos*) from four different clades, producing white-rot and brown-rot decay of wood. Four allelic variants are excluded from the inventory (**Annex 1**)

Clade	Phlebioid			Core polyporoid			Gelatoporia	Antrodia		
	BJE AD	PHL BR	PHA CH	DIC SQ	GAN SP	TRA VE	GEL SU	FOM PI	RHO PL	WOL CO
AAO	11	3	3	8	7	3	4	1	2	0
MOX	5	6	3	4	4	4	1	4	4	4
GOX	0	0	1	0	0	0	0	0	2	0
CDH	1	1	1	1	1	1	1	0	0	0
P2O	1	1	1	0	0	1	0	0	0	0
PDH	0	0	0	0	0	0	0	0	0	0
All GMC	18	11	9	13	12	9	6	5	8	4
Ecol.	---------------------- White-rot -------------------------- Brown-rot ------									

3.1.2. Structural modeling of GMC oxidoreductases from Polyporales genomes

Most of the predicted GMC sequences (94 of 95) were modeled using related crystal structures as templates. Five representative structures are shown in **Figure 3.1** corresponding to *B. adusta* AAO (A), *F. pinicola* MOX (B), *R. placenta* GOX (C), *G. subvermispora* CDH (D) and *B. adusta* P2O (E) mature proteins. All these GMCs show a common folding with the lower domain harboring the FAD cofactor. Specific features are present in AAO, which possesses a loop partially covering the entrance to the active site (**Figure 3.2A**, in orange); and CDH, which has a heme domain connected by an unstructured linker (**Figure 3.1D**). Interestingly, AAOs and CDHs are known as monomeric proteins, while GOXs, P2Os and MOXs form oligomers (Romero and Gadda 2014). One large β-sheet is present in both the FAD-binding (sheet A) and the substrate-binding (sheet C) domains, the former being accompanied by two small sheets (B and D) and the latter by only one (sheet E) (**Figure 3.1A**). Similar numbers of α-helices exist in the FAD-binding and the substrate-binding

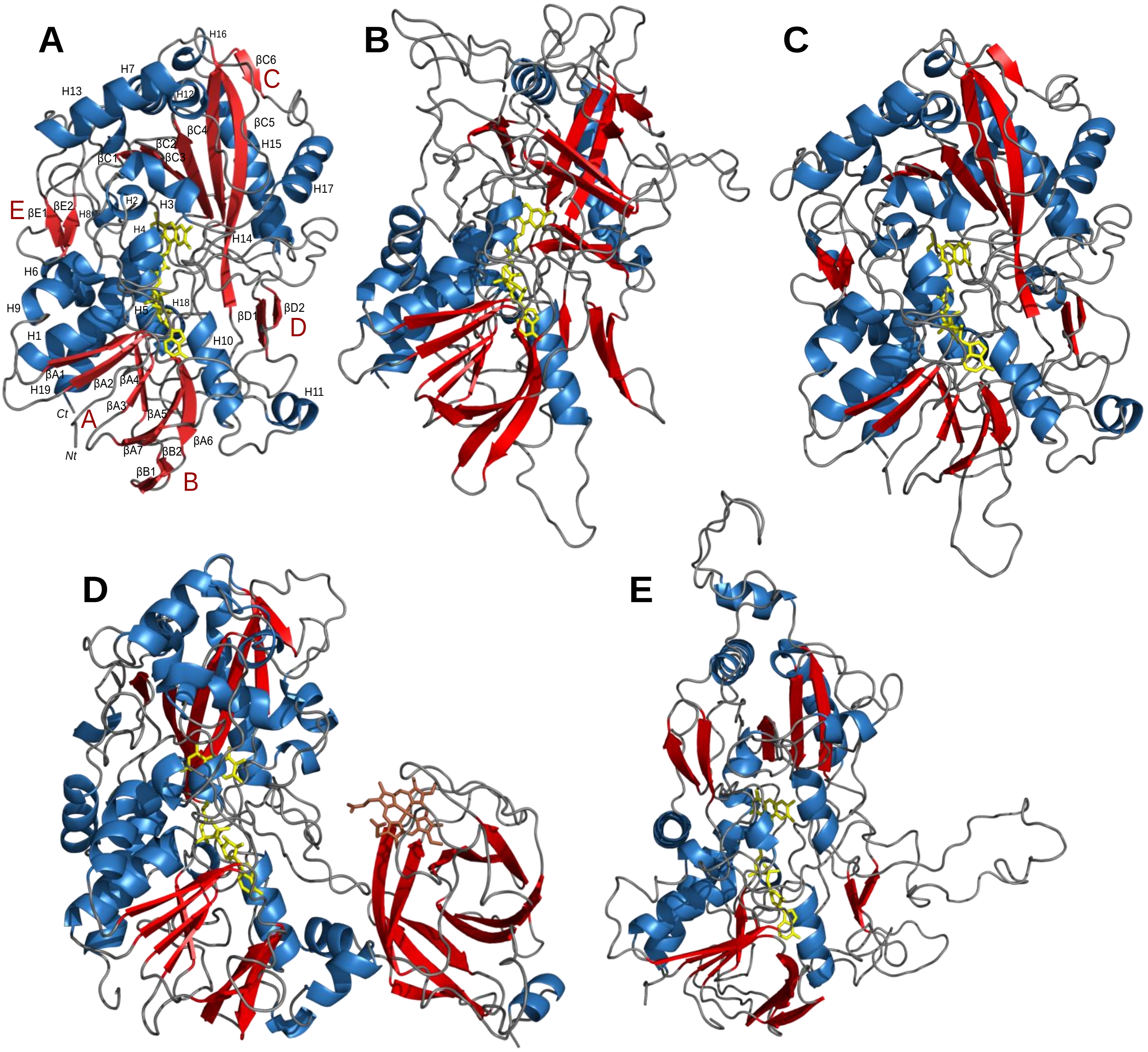
A
B
C
D
E
H16
βC6
C
H7
H13
H12
βC5
βC4
H15
βC2
βC3
βC1
H17
E
βE1
βE2
H8
H2
H3
H4
H14
H6
H18
βD2
H9
H5
βD1
D
H1
H10
βA1
H19
βA2
βA4
H11
βA3
Ct
A
βA5
βA6
Nt
βA7
βB2
βB1
B

Figure 3.1. Ribbon models for the molecular structures of representative members of the five GMC oxidoreductase families found in 10 Polyporales genomes (flavin and heme cofactors as yellow and red sticks, respectively). **A.** AAO of *B. adusta* (JGI protein ID 245059) indicating the position of 4 β-sheets, individual β-strands, and 19 α-helices. **B.** MOX (monomer) of *F. pinicola* (JGI protein ID 156775). **C.** GOX (monomer) of *P. chrysosporium* (JGI protein ID 131961). **D.** CDH of *G. subvermispora* (JGI protein ID 84792) (flavin domain in the left and heme domain in the right. **E.** P2O (monomer) of *B. adusta* (JGI protein ID 34622). The molecular models were built using crystal structures of related proteins as templates.

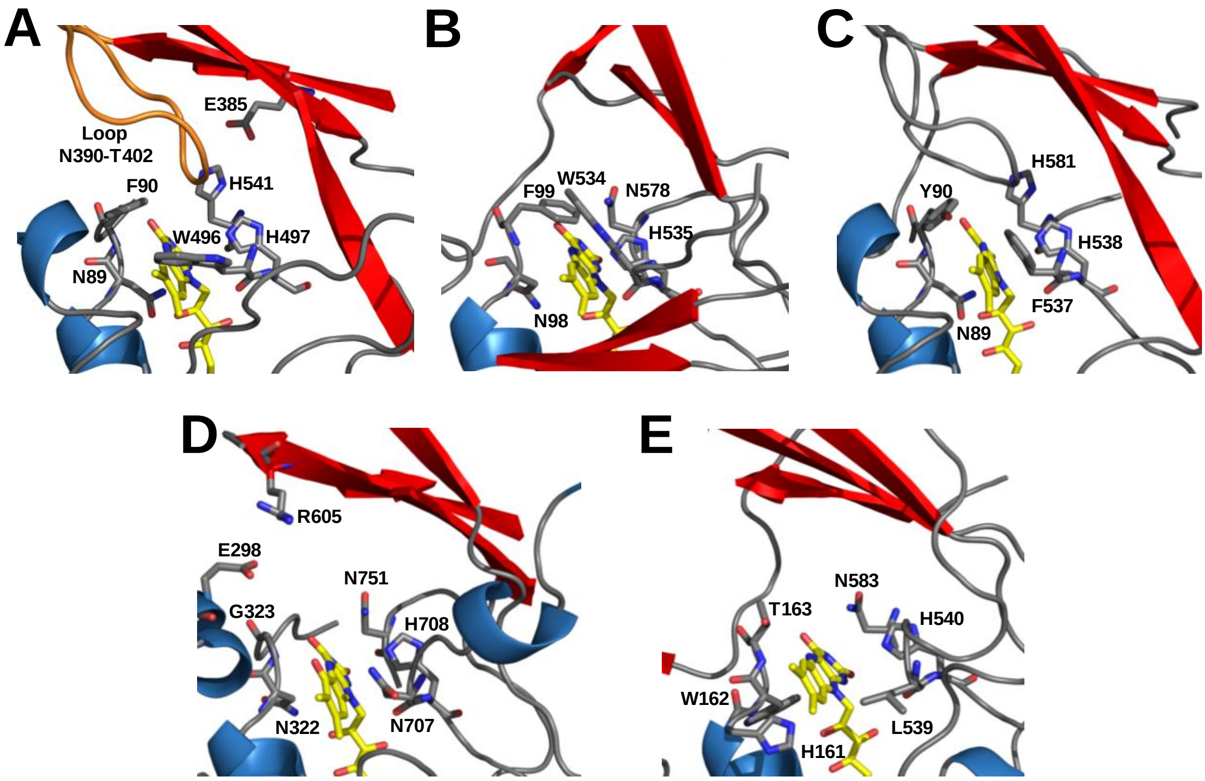

Figure 3.2. Detail of active-site residues in the molecular models for the five Polyporales GMCs shown in **Figure 3.1**. **A.** *B. adusta* AAO. **B.** *F. pinicola* MOX. **C.** *P. chrysosporium* GOX. **D.** *G. subvermispora* CDH. **E.** *B. adusta* P2O. Residue numbering corresponds to the putative mature proteins. FAD and the selected residues are shown in sticks in CPK yellow and grey colors respectively. The Asn390-Thr402 loop of AAO is shown in orange.

domains (9-10 in AAO), some of them (e.g. AAO helices 1, 4 and 10) conserved in most GMCs. All the predicted models present the ADP-binding *βαβ* motif near their N-termini (**Annex 2A**) and the GMC signatures 1 and 2 (Prosite PS00623 and PS00624, respectively; **Annexes 2B** and **2C**), with the only exception of P2O that lacks signature 1. The FAD flavin ring enters the GMC upper domain, where several residues form a substrate-binding site at the *re*-side of the isoalloxazine ring (**Figure 3.2**). They include a histidine strictly conserved in the superfamily, corresponding to *B. adusta* AAO His497 (**Figure 3.2A**), *F. pinicola* MOX His535 (**Figure 3.2B**), *P. chrysosporium* GOX His538 (**Figure 3.2C**), *G. subvermispora* CDH His688 (**Figure 3.2D**) and *B. adusta* P2O His540 (**Figure 3.2E**).

A second conserved histidine in AAO and GOX (His541 and His581 in **Figure 3.2A** and **C**, respectively), is replaced by an asparagine in MOX, CDH and P2O proteins (Asn 578, Asn731 and Asn583 in **Figure 3.2B**, **D** and **E**, respectively). An aromatic residue often precedes the fully conserved histidine, being a tryptophan in AAO (Trp496) and MOX (Trp534) and a phenylalanine in GOX (Phe537), while a leucine (Leu539) and an asparagine (Asn687) occupy this position in the P2Os and CDHs, respectively (**Figure 3.2**). At the opposite (*si*) side of the isoalloxazine ring, another aromatic residue, which points towards the active site, is conserved, being a phenylalanine in AAO (Phe90) and a tyrosine in MOX (Tyr99) and GOX (Tyr90) (**Figure 3.2A-C**).

An asparagine preceding the latter position is conserved in all the Polyporales GMCs (Asn89, Asn98, Asn89 and Asn322 in Figure 2 AAO, GOX, MOX and CDH, respectively) with the exception of P2Os. This asparagine residue, also conserved in other GMCs, is involved in flavin bent conformation (Kiess et al. 1998).

3.1.3. Evolutionary history of GMC oxidoreductases in the Polyporales genomes

The evolutionary history of the 95 GMCs identified in the ten Polyporales genomes (five allelic variants excluded) was inferred by comparing their predicted amino-acid sequences (mature proteins). It is worth noting that all the sequences from each of the GMC families cluster together in the maximal likelihood tree (**Figure 3.3**). The two main groups correspond to the 39 MOXs and the 42 AAOs (100% and 79% bootstrap, respectively), with the only 3 GOXs distantly associated to the AAOs. Interestingly, ten of the eleven *B. adusta* AAOs are included in a thirteen-member subgroup (*a*, 100% bootstrap), suggesting recent duplication. In contrast, MOXs include a subgroup (*b*, 100% bootstrap) of ten sequences, each from one of the genomes. These ten sequences share an insertion and a slightly longer C-terminus involved in oligomerization and/or secretion of the enzymes through a unique secretory pathway (Danneel et al. 1994), suggesting a common origin of these genes. At the basal nodes the well supported (100% bootstrap) P2O (4 sequences) and CDH (7 sequences) families appear unrelated between them and with the rest of the GMCs. The distant position of the latter families and the relatedness between AAOs, GOXs and MOXs, agree with the pairwise identity values across and within gene families. In fact, the average pairwise (inter-family) identity between P2O and CDH sequences is 8% and, among them and the rest of the families, range between 11% and 14%. These values are significantly lower than those between AAO and MOX (25% inter-family average), GOX and MOX (24% inter-family average) and AAO and GOX sequences (31% inter-family average). On the other hand, the pairwise (intra-family) identities within the CDH and P2O families are higher, 73 and 51%, respectively; whereas AAOs, GOXs and MOXs show values of 46, 30 and 57%, respectively. In fact, the average pairwise (inter-family) identity between P2O and CDH sequences is 8% and, among them and the rest of the families, range between 11% and 14%. These values are significantly lower than those between AAO and MOX (25% inter-family average), GOX and MOX (24% inter-family average) and AAO and GOX sequences (31% inter-family average). On the other hand, the pairwise (intra-family) identities within the CDH and P2O families are higher, 73 and 51%, respectively; whereas AAOs, GOXs and MOXs show values of 46, 30 and 57%, respectively.

Figure 3.3. Maximum likelihood tree of the 95 GMC sequences from 10 Polyporales genomes (different color labels), prepared with RaxML (with gaps treated as deletions). The AAO, MOX, P2O and CDH clusters (and the *a* and *b* subclusters mentioned in the text) are shown, together with a few GOX sequences related to AAOs. Numbers at nodes indicate bootstrap values. Those sequences modeled in **Figures 3.1** and **3.2** are indicated by arrows. See **Table 3.1** for abbreviations of the fungal species.

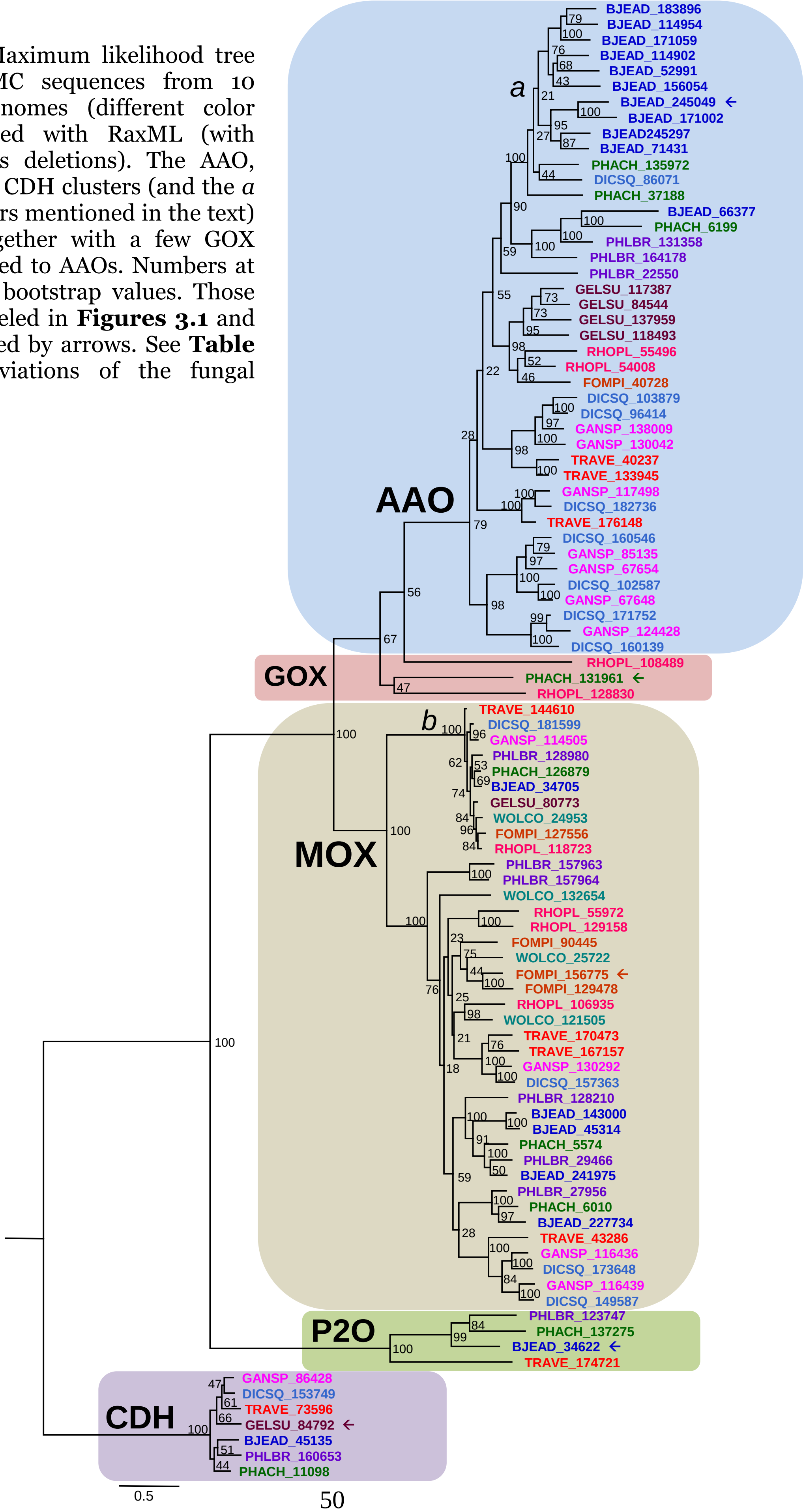
AAO
a
BJEAD_183896
BJEAD_114954
BJEAD_171059
BJEAD_114902
BJEAD_52991
BJEAD_156054
BJEAD_245049 ←
BJEAD_171002
BJEAD245297
BJEAD_71431
PHACH_135972
DICSQ_86071
PHACH_37188
BJEAD_66377
PHACH_6199
PHLBR_131358
PHLBR_164178
PHLBR_22550
GELSU_117387
GELSU_84544
GELSU_137959
GELSU_118493
RHOPL_55496
RHOPL_54008
FOMPI_40728
DICSQ_103879
DICSQ_96414
GANSP_138009
GANSP_130042
TRAVE_40237
TRAVE_133945
GANSP_117498
DICSQ_182736
TRAVE_176148
DICSQ_160546
GANSP_85135
GANSP_67654
DICSQ_102587
GANSP_67648
DICSQ_171752
GANSP_124428
DICSQ_160139
GOX
RHOPL_108489
PHACH_131961 ←
RHOPL_128830
MOX
b
TRAVE_144610
DICSQ_181599
GANSP_114505
PHLBR_128980
PHACH_126879
BJEAD_34705
GELSU_80773
WOLCO_24953
FOMPI_127556
RHOPL_118723
PHLBR_157963
PHLBR_157964
WOLCO_132654
RHOPL_55972
RHOPL_129158
FOMPI_90445
WOLCO_25722
FOMPI_156775 ←
FOMPI_129478
RHOPL_106935
WOLCO_121505
TRAVE_170473
TRAVE_167157
GANSP_130292
DICSQ_157363
PHLBR_128210
BJEAD_143000
BJEAD_45314
PHACH_5574
PHLBR_29466
BJEAD_241975
PHLBR_27956
PHACH_6010
BJEAD_227734
TRAVE_43286
GANSP_116436
DICSQ_173648
GANSP_116439
DICSQ_149587
P2O
PHLBR_123747
PHACH_137275
BJEAD_34622 ←
TRAVE_174721
CDH
GANSP_86428
DICSQ_153749
TRAVE_73596
GELSU_84792 ←
BJEAD_45135
PHLBR_160653
PHACH_11098
0.5

3.1.4. GMC gene duplication and loss during diversification of Polyporales

The expansion or reduction in the number of GMC genes upon evolution of Polyporales was investigated by reconciliation of the evolutionary tree of the 95 GMC genes (**Figure 3.3**) and the phylogenetic tree of the 10 species of Polyporales (from TreeBase) using Notung. The results obtained (using two different threshold levels) suggest that the ancestors of Polyporales had a high number of GMC genes, more than found in any of the extant species or the predicted intermediate ancestors (**Figure 3.4**). Therefore, during GMC evolution 14 contraction events and two expansions (from nodes *d* to node *g* and from node *e* to node *h*) were predicted. A similar tendency was observed for each of the individual GMC families (**Figure 3.5A-E**) with a total of 39 contraction events and 7 expansions.

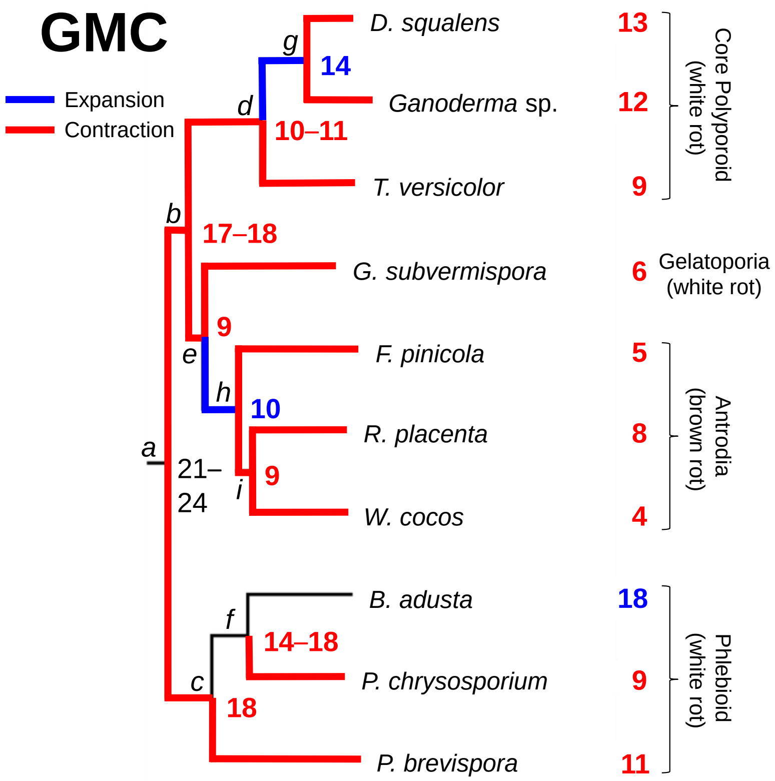
GMC
Expansion
Contraction
g
14
d
10–11
b
17–18
9
e
h
10
a
21–24
i
9
f
14–18
c
18
D. squalens
Ganoderma sp.
T. versicolor
G. subvermispora
F. pinicola
R. placenta
W. cocos
B. adusta
P. chrysosporium
P. brevispora
13
12
9
6
5
8
4
18
9
11
Core Polyporoid (white rot)
Gelatoporia (white rot)
Antrodia (brown rot)
Phlebioid (white rot)

Figure 3.4. Estimated range of GMC gene copies at the ancestral nodes (and extant species) of the represented phylogeny of Polyporales taken from Binder et al. (2013) after reconciliation with the gene phylogeny (**Figure 3.3**) using Notung. Branches and numbers after gene expansion and contraction are in blue and red color, respectively. For reconciliation of the individual GMC families, see **Figure 3.5**.

In this case, expansions resulted in higher AAO (in node *g* and in *B. adusta*; **Figure 3.5A**), GOX (in *R. placenta*; **Figure 3.5C**) and P2O (in node *c*; **Figure 3.5E**) gene numbers (often after previous contractions) than predicted for the initial Polyporales ancestor. The stronger contraction of GMC gene numbers was evident in the Antrodia clade, resulting in only 4-5 genes in *W. cocos* and *F. pinicola* and the largest expansion was observed in *B. adusta* (Phlebioid clade) with 18 GMC genes, including 11 AAOs (**Figure 3.4**). Interestingly, most of the

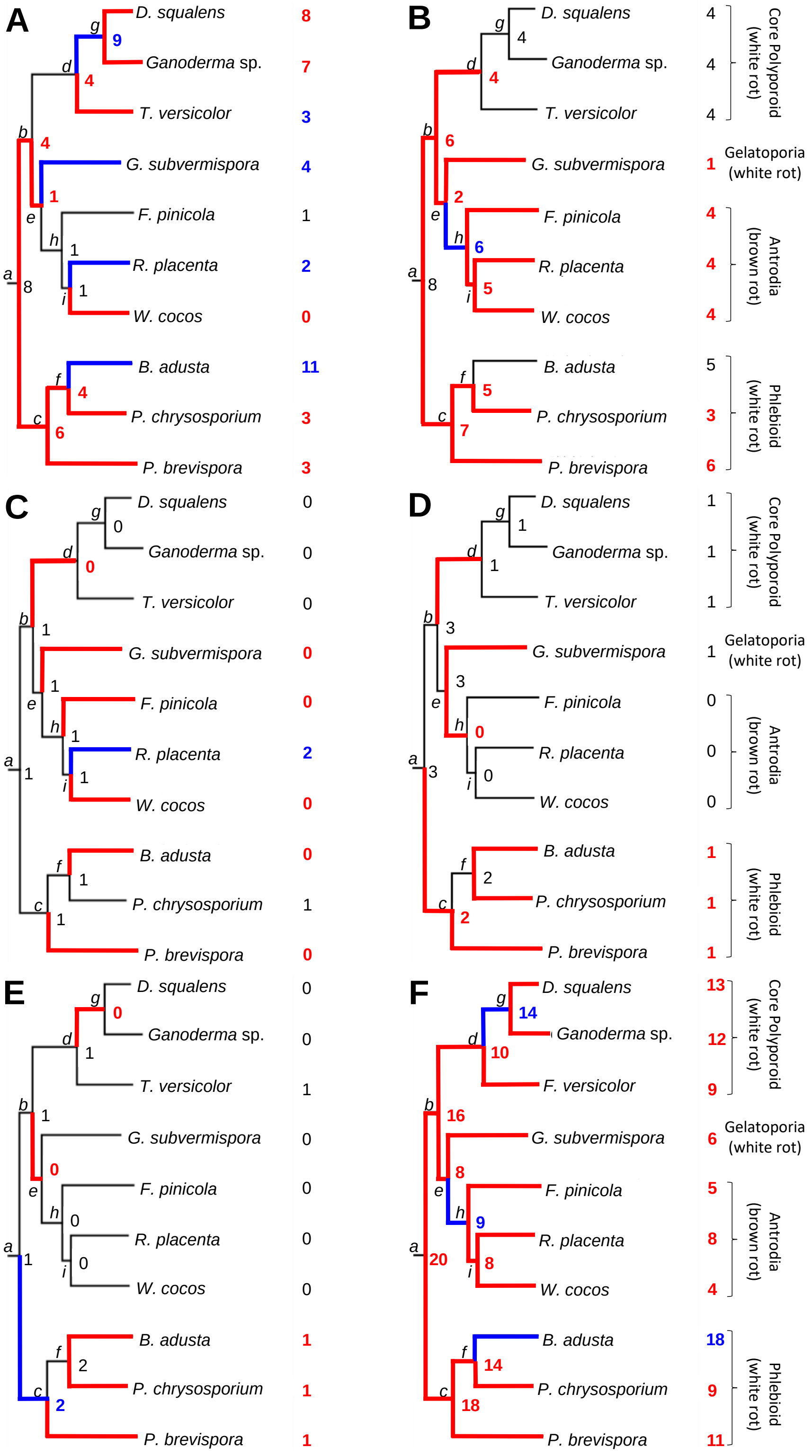
A
D. squalens 8
g 9
Ganoderma sp. 7
d 4
T. versicolor 3
b 4
G. subvermispora 4
1
e
F. pinicola 1
h 1
R. placenta 2
a 8
i 1
W. cocos 0
B. adusta 11
f 4
P. chrysosporium 3
c 6
P. brevispora 3
B
D. squalens 4
g 4
Ganoderma sp. 4
d 4
T. versicolor 4
Core Polyporoid (white rot)
b 6
G. subvermispora 1
Gelatoporia (white rot)
2
e
F. pinicola 4
h 6
R. placenta 4
a 8
i 5
W. cocos 4
Antrodia (brown rot)
B. adusta 5
f 5
P. chrysosporium 3
c 7
P. brevispora 6
Phlebioid (white rot)
C
D. squalens 0
g 0
Ganoderma sp. 0
d 0
T. versicolor 0
b 1
G. subvermispora 0
1
e
F. pinicola 0
h 1
R. placenta 2
a 1
i 1
W. cocos 0
B. adusta 0
f 1
P. chrysosporium 1
c 1
P. brevispora 0
D
D. squalens 1
g 1
Ganoderma sp. 1
d 1
T. versicolor 1
Core Polyporoid (white rot)
b 3
G. subvermispora 1
Gelatoporia (white rot)
3
e
F. pinicola 0
h 0
R. placenta 0
a 3
i 0
W. cocos 0
Antrodia (brown rot)
B. adusta 1
f 2
P. chrysosporium 1
c 2
P. brevispora 1
Phlebioid (white rot)
E
D. squalens 0
g 0
Ganoderma sp. 0
d 1
T. versicolor 1
b 1
G. subvermispora 0
0
e
F. pinicola 0
h 0
R. placenta 0
a 1
i 0
W. cocos 0
B. adusta 1
f 2
P. chrysosporium 1
c 2
P. brevispora 1
F
D. squalens 13
g 14
Ganoderma sp. 12
d 10
F. versicolor 9
Core Polyporoid (white rot)
b 16
G. subvermispora 6
Gelatoporia (white rot)
8
e
F. pinicola 5
h 9
R. placenta 8
a 20
i 8
W. cocos 4
Antrodia (brown rot)
B. adusta 18
f 14
P. chrysosporium 9
c 18
P. brevispora 11
Phlebioid (white rot)

Figure 3.5. Estimated range of individual AAO (**A**), MOX (**B**), GOX (**C**), CDH (**D**) and P2O (**E**) gene copies, and total GMC from sum of family gene numbers (**F**), at the ancestral nodes of the represented phylogeny of Polyporales taken from Binder et al. (2013) after reconciliation with the gene phylogeny. Branches and numbers after gene expansion and contraction are in blue and red color, respectively.

remaining GMC genes in the Antrodia clade correspond to the MOX family (4/5 in *F. pinicola*, 4/8 in *R. placenta* and 4/4 in *W. cocos*).

3.2. Discussion

The global reaction in initial wood decay by white-rot and brown-rot basidiomycetes is iron-catalyzed oxidation of lignin or polysaccharides, respectively, by H_2O_2 generated by oxidases (from the GMC and/or the copper-protein radical superfamilies). In white-rot decay, this reaction is catalyzed by Fe^{3+} in the heme cofactor of ligninolytic peroxidases, while in brown-rot decay free Fe^{2+} reduces H_2O_2 forming the highly-reactive hydroxyl radical (Martínez et al. 2005; Kersten and Cullen 2007; Baldrian and Valaskova 2008). The information available on the presence and relevance of GMC families in the different Polyporales species is discussed below.

3.2.1. Aryl-alcohol oxidase

AAO was first isolated from *Pleurotus* species (Agaricales) (Bourbonnais and Paice 1988; Guillén et al. 1990a; Sannia et al. 1991; Guillén et al. 1992a), where it generates H_2O_2 by redox-cycling of anisaldehyde (Guillén and Evans 1994), an extracellular fungal metabolite (Gutiérrez et al. 1994). Subsequent studies focused on the *Pleurotus eryngii* enzyme, which was cloned and sequenced (Varela et al. 1999), heterologously expressed (Varela et al. 2001; Ruiz-Dueñas et al. 2006), crystallized (Fernández et al. 2009) and its reaction mechanisms investigated by a variety of techniques (Ferreira et al. 2005; 2006; 2009; 2010; Hernández-Ortega et al. 2011a; 2011b; 2012b; 2012c; 2015b). Then, a Polyporales AAO was isolated from *B. adusta* (Muheim et al. 1990b). Although the above enzymes are known as secreted proteins (Hernández-Ortega et al. 2012a), recognized signal peptides are missing from four of the 42 sequences from the ten Polyporales genomes, including one sequence from *B. adusta* and two from *D. squalens* and *P. chrysosporium*. The latter is in agreement with the description of an intracellular AAO in this fungus (Asada et al. 1995).

AAO activity has been detected in cultures of a few other Polyporales species (Peláez et al. 1995), although a Southern blot (using a *P. eryngii* probe) did not detect the corresponding gene in many of these (Varela et al. 2000) suggesting gene variability among different fungi. AAO activity in *B. adusta* (Romero et al. 2010b), a sequence corresponds to BJEAD_171002 from the JGI genome, has been largely characterized showing higher activity on *p*-hydroxy and chlorinated benzyl alcohols than *Pleurotus* AAO (Romero et al. 2009). *p*-Hydroxybenzyl alcohols are the typical substrates of vanillyl alcohol oxidase, a flavoenzyme from a different superfamily (Leferink et al. 2008), but they are not efficiently oxidized by *Pleurotus* AAO, whose best substrates are *p*-methoxylated benzyl alcohols (Guillén et al. 1992b; Ferreira et al. 2005). Therefore, the best characterized Polyporales AAO shows catalytic properties intermediate between Agaricales AAO and vanillyl-alcohol oxidase. The higher activity of *B. adusta* AAO on chlorinated benzyl alcohols, which was already noticed by de Jong et al. (1994), is related to the ability of this species to synthesize 3-chloro-*p*-methoxybenzaldehyde (de Jong et al. 1992; de Jong and Field 1997). Redox cycling of this and related chlorinated compounds provides a continuous source of H_2O_2 to *B. adusta* peroxidases (de Jong et al. 1994), similar to the *Pleurotus* anisaldehyde redox cycling. Chloroaromatics could also help wood colonization due to their antibiotic properties.

3.2.2. Glucose oxidase

In contrast to AAO, which has been rarely reported in ascomycetes (Goetghebeur et al. 1992), GOX has been largely studied in *A. niger* (Frederick et al. 1990) and other ascomycetous fungi, but rarely in basidiomycetes (Danneel et al. 1993). This is the protein with the largest sequence identity with AAO, as shown in the gene tree, both sharing the general folding and active-site residues (Hecht et al. 1993; Wohlfahrt et al. 1999; Witt et al. 2000).

GOX is widely used in biosensors and other biotechnological applications (Bankar et al. 2009) but its involvement in lignocellulose degradation was discarded, since the best known representatives are confirmed intracellular enzymes. However, two of the only three GOX sequences identified in the Polyporales genomes include a typical signal peptide, suggesting participation in the extracellular attack on lignocellulose.

3.2.3. Pyranose 2-oxidase

P2O, which differs from GOX in glucose oxidation at the C2 (instead of the C1) position, is known as a secreted enzyme (Daniel et al. 1994) involved in lignocellulose degradation (Nyanhongo et al. 2007). This oxidoreductase was first investigated in *P. chrysosporium* (Artolozaga et al. 1997) and these studies suggested that P2O rather than GOX is secreted during wood decay (Volc et al. 1996). However, none of the four genes found in the Polyporales genomes has a recognized signal peptide, in agreement with the sequence obtained by de Koker et al. (2004) for the cloned P2O gene from *P. chrysosporium*. Therefore, if secreted, this would be by an alternative mechanism, as suggested for MOX (see below).

P2O is produced by other Polyporales, including *Trametes multicolor* (= *Trametes ochracea*) (Leitner et al. 2001) and most recent P2O research focuses on this enzyme, whose reaction mechanisms have been elucidated in a variety of crystallographic, spectroscopic, directed mutagenesis, isotope labeling and kinetic studies (Hallberg et al. 2004; Sucharitakul et al. 2008; Prongjit et al. 2009; Pitsawong et al. 2010; Wongnate et al. 2011; Sucharitakul et al. 2011; Wongnate et al. 2014).

3.2.4. Methanol oxidase

MOX is mostly known as a peroxysomal enzyme in methylotrophic ascomycetous yeasts, such as *Pichia pastoris* or *C. boidinii* (Ozimek et al. 2005). The first basidiomycete MOX was purified and characterized from *P. chrysosporium* (Nishida and Eriksson 1987) and it is also known from *Phlebiopsis gigantea* (Danneel et al. 1994). MOX was proposed as the main oxidase in brown-rot decay based on biochemical characterization and expression analyses in *Gloeophyllum trabeum* (Daniel et al. 2007). The corresponding gene is present in the genome of *R. placenta* (Martinez et al. 2009), and was overexpressed in wood-containing cultures of this brown-rot fungus and also in those of the white-rot *P. chrysosporium* (Vanden Wymelenberg et al. 2010).

The MOX gene of *G. trabeum* and other basidiomycetes does not include a recognized signal peptide. However, the extracellular location of MOX has been demonstrated and operation of an alternative secretion mechanism was proposed (Daniel et al. 2007). The rationale for MOX involvement in brown-rot decay is that demethoxylation, resulting in methanol release, was reported first by Kirk (1975) and confirmed by 2D-NMR analyses (Martínez et al. 2011) as the main lignin modification in brown-rot decay.

3.2.5. Pyranose and cellobiose dehydrogenases

PDH and CDH use electron acceptors different from O_2 and, therefore, do not contribute to H_2O_2 supply. However, they oxidize plant carbohydrates and participate in electron transfer to other lignocellulose-degrading oxidoreductases.

PDH catalyzes the same oxidations of P2O but uses quinones as electron acceptors, being an enzyme of interest in biotechnology (Peterbauer and Volc 2010). The first PDH was isolated from *Agaricus bisporus* (Volc et al. 1997) and also found in related species (Kujawa et al. 2007; Kittl et al. 2008) including *L. meleagris* where it was thoroughly investigated (Tan et al. 2013; Krondorfer et al. 2014a; 2014b). Screening for PDH revealed its exclusive presence in the above and other litter-degrading Agaricales (Volc et al. 2001), an observation that is consistent with its absence from all the (wood-rotting) Polyporales genomes analyzed.

CDH includes both flavin and heme domains, the former being able to oxidize cellobiose to cellobiolactone by transferring the electrons to Fe^{3+} *via* the heme domain (Henriksson et al. 2000; Zámocký et al. 2006). CDH was first described in *P. chrysosporium* (whose conidial state was referred as *Sporotrichum pulverulentum* in some of these studies) (Ayers et al. 1978; Bao et al. 1993). The ancestral fusion between the two CDH domains and the subsequent evolution in different fungi has been discussed (Zámocký et al. 2004). One CDH gene was present in the genomes of the 7 white-rot Polyporales analyzed and absent from the three brown-rot Polyporales genomes, in agreement with a recent review

(Hori et al. 2013), in which CDH was found only in white-rot genomes. However, this GMC seems to be present in other brown-rot fungi, as revealed by its early description in *C. puteana* (order Boletales) (Schmidhalter and Canevascini 1993) and its detection in the genomes of brown-rot fungi from other Agaricomycotina orders (Floudas et al. 2012).

Its ability to generate hydroxyl radical by simultaneous Fe^{3+} and O_2 reduction has been suggested (Kremer and Wood 1992), but O_2 reduction by CDH is inefficient and only takes place in the absence of Fe^{3+}. However, recent studies showed that CDH increases the cellulolysis yield and contributes to the action of lytic polysaccharide monooxygenase (Langston et al. 2011).

CDH from *P. chrysosporium* experiences proteolytic cleavage in cultures releasing the flavin domain (Wood and Wood 1992), which was described as a different enzyme, cellobiose-quinone oxidoreductase (Westermark and Eriksson 1974). However, the physiological significance of such cleavage and the role of cellobiose-quinone oxidoreductase under natural conditions is unknown (Raices et al. 2002).

3.2.6. GMC oxidoreductases in Polyporales: final evolutionary/ecological remarks

The total number of GMC genes cloned to date from species of the order Polyporales is fewer than 10: from P. chrysosporium, P. cinnabarinus, Pycnoporus sanguineus (syn.: Trametes sanguinea), T. ochracea and T. versicolor (Leitner et al. 1998; Raices et al. 1995; Dumonceaux et al. 1998; Moukha et al. 1999; Vecerek et al. 2004; de Koker et al. 2004; Sulej et al. 2013). However, the present survey of GMC genes from a broader sampling including ten Polyporales genomes (from different clades and lifestyles) reveals nearly one hundred GMC genes representing five of the six best-known families (no PDH genes present).

The GMC superfamily is thought to have evolved from an old common ancestor, which very likely exhibited broad substrate specificity and poor kinetic parameters and gave rise to more specialized and efficient enzymes as evolution proceeded (Cavener 1992). The present study suggests that this diversification took place at a more ancestral stage of fungal evolution, with predominant gene loss among members of the Polyporales. This resulted in two main GMC types (groups) corresponding to AAO and MOX, with an average of ~4 gene copies per genome, and three small groups corresponding to P2O, CDH and GOX (neighbor to the AAO group) with 0-1 copies per genome, in agreement with previous studies (Zámocký et al. 2004; Kittl et al. 2008).

While ligninolytic peroxidases (from the LiP, MnP and VP families) were absent from the brown-rot fungal genomes but present in all the white-rot fungal genomes (Ruiz-Dueñas et al. 2013), H_2O_2-producing GMCs were present in genomes of both white-rot and brown-rot species. Floudas et al. (2012) showed that the first wood-rotting fungus appeared by incorporation of secreted high redox-potential (ligninolytic) peroxidase genes in the genome of an ancestral basidiomycete. This was most likely accompanied by the evolution of several extracellular H_2O_2-producing oxidases, some of them with different evolutionary origin. These included copper-radical oxidases and several families of GMCs derived from related enzymes involved in intracellular metabolism.

White-rot decay was likely the ancestral lifestyle in wood decay basidiomycetes (Floudas et al. 2012; Ruiz-Dueñas et al. 2013) and brown-rot evolved several times among Polyporales, and other Agaricomycotina orders. The white-rot to brown-rot transition in Polyporales included loss of the ligninolytic peroxidase genes, which are not required since lignin remained polymeric in brown-rotted wood. However, extracellular H_2O_2, used as peroxidase-activating substrate in white-rot decay, also plays an important role in brown-rot decay as the precursor of the hydroxyl radical formed by Fenton reaction. Therefore, it seems that the same H_2O_2-generating oxidases present in white-rot fungi remained in the derived brown-rot species. During the subsequent evolution, some differences in the frequency of the individual GMC families appeared. In this way, MOX genes are the most abundant GMC genes in the brown-rot Polyporales, while AAO genes are the most abundant in the white-rot species (up to eleven copies in *B. adusta*). Finally, the number of CDH genes predicted in the ancestor of Polyporales diminished, but all the white-rot species maintain one CDH gene, which contributes to polysaccharide degradation by these fungi. However, CDH genes disappeared in brown-rot fungi, where Fenton chemistry is the main mechanism for polysaccharide attack.

The results described in this chapter have been drawn from the publication: Ferreira P, Carro J, Serrano A, Martínez AT. A survey of genes encoding H_2O_2-producing GMC oxidoreductases in 10 Polyporales genomes. Mycologia 107:1105–1119, 2015.

4

An active site Phe contributes to product release in AAO catalysis

The catalytic pocket of AAO from *Pleurotus eryngii* is shielded from the outer environment by a triad of aromatic residues —Y92, F501 and Phe397— that form a hydrophobic bottleneck and constitute a barrier for the access to the active site (**Figure 4.1**) (Fernández et al. 2009). This is one striking difference opposed to the structure of other related enzymes from the same superfamily. The roles of Y92 and F501 have been unveiled and are involved in i) establishing aromatic stacking interactions that guide the alcohol substrate to a catalytically competent configuration (Ferreira et al. 2015b) and ii) in compressing the active site to promote the reactivity with O_2 (Hernández-Ortega et al. 2011b), respectively. However, the role of F397 in AAO catalysis had not been previously studied.

This phenylalanine residue is located in a loop unique to the AAO family, which partially covers the access to the active site (Ferreira et al. 2015a). It is supposed to act as an additional barrier that prevents the free diffusion of molecules in and out of the catalytic pocket. AAO, in contrast to the majority of related GMC flavoproteins, is a monomeric enzyme. Polymeric enzymes rely on the correct positioning of the adjacent monomers to cover the entrances to their active sites. This is probably the reason why AAOs have developed the 390–402 loop in which the phenylalanine studied is located. Computational studies of substrate migration into the active site suggested that Phe397 was displaced as it swung along with the alcohol substrate helping it enter the catalytic pocket (Hernández-Ortega et al. 2011a) (www.youtube.com/watch?v=CqSDn5OmagI).

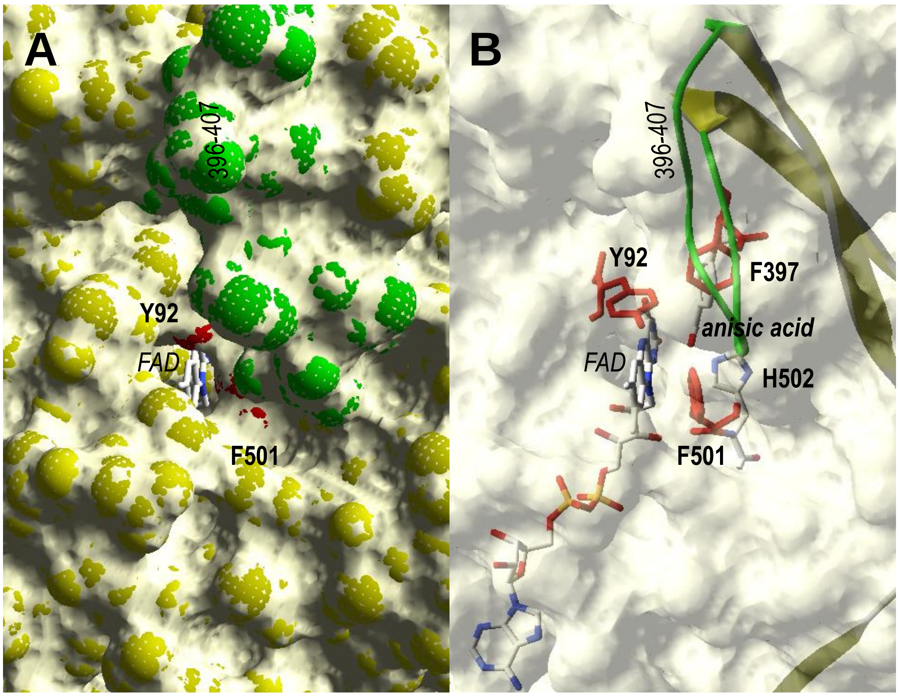

Figure 4.1. Characteristic loop and aromatic residues delimiting the FAD access in AAO. **A.** Channel opening in AAO surface. **B.** Semitransparent surface showing aromatic residues (Tyr92, Phe397 and Phe501) and loop (green) limiting the access to FAD and catalytic histidine (His502), with one product (*p*-anisic acid) molecule at the active site. From AAO:anisic acid structure (Carro et al. 2017).

In this chapter, steady-state and transient-state kinetic studies on wild-type AAO and several mutated variants have been performed to elucidate the role of Phe397 in AAO catalysis.

4.1. Results

4.1.1. Spectral properties and steady-state kinetics of AAO and its Phe397-mutated variants

The four AAO Phe397 variants, analogously to the native enzyme, were purified as oxidized monomeric holoproteins. The UV-visible spectra of all variants showed the typical bands I and II of the Flavin and the absorbance ratios between A280 nm/A band I around 10–11, showing that FAD cofactor was in oxidized state and correctly incorporated into the variants. Maxima of flavin bands I and II showed some slight shifts upon mutation. F397Y showed a maximum at 463 nm, as native AAO, whereas F397L and F397W had their maxima at 462 nm and F397A at 459 nm, for band I. Regarding band II, F397L, F397W and F397A showed their maxima at 385 nm, while F397Y showed it at 387, as the native enzyme (**Figure 4.2**). However, all the variants displayed similar band I/band II absorbance ratios, and shoulder around 500 nm, indicating similar folding aroun cofactor.

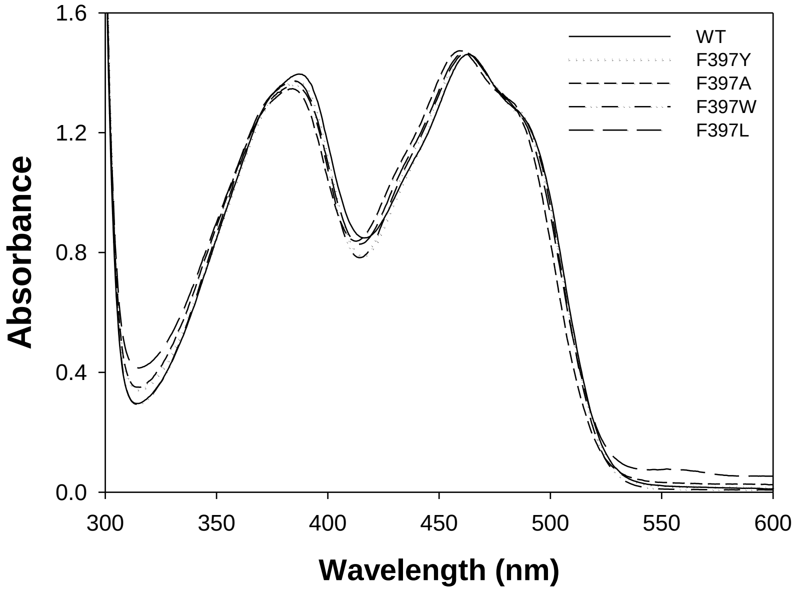

Figure 4.2. Spectra of the WT (solid line), F397Y (dotted line), F397A (short dash line), F397W (dash-dot line) and F397L (long dash line) AAO variants recorded between 300 and 600 nm in 50 mM sodium phosphate pH 6.0.

Steady-state kinetics revealed remarkable differences among native AAO and its Phe397-mutated variants (**Table 4.1**). Measurements were carried out using *p*-methoxybenzyl alcohol, the physiological substrate of AAO (Ferreira et al. 2005). In all four cases, the kinetics best fitted **equation 5** describing a ping-pong mechanism, as revealed by the Hanes-Woolf plots of its bi-substrate kinetics (**Figure 4.3**), in which all lines intersect at x = 0.

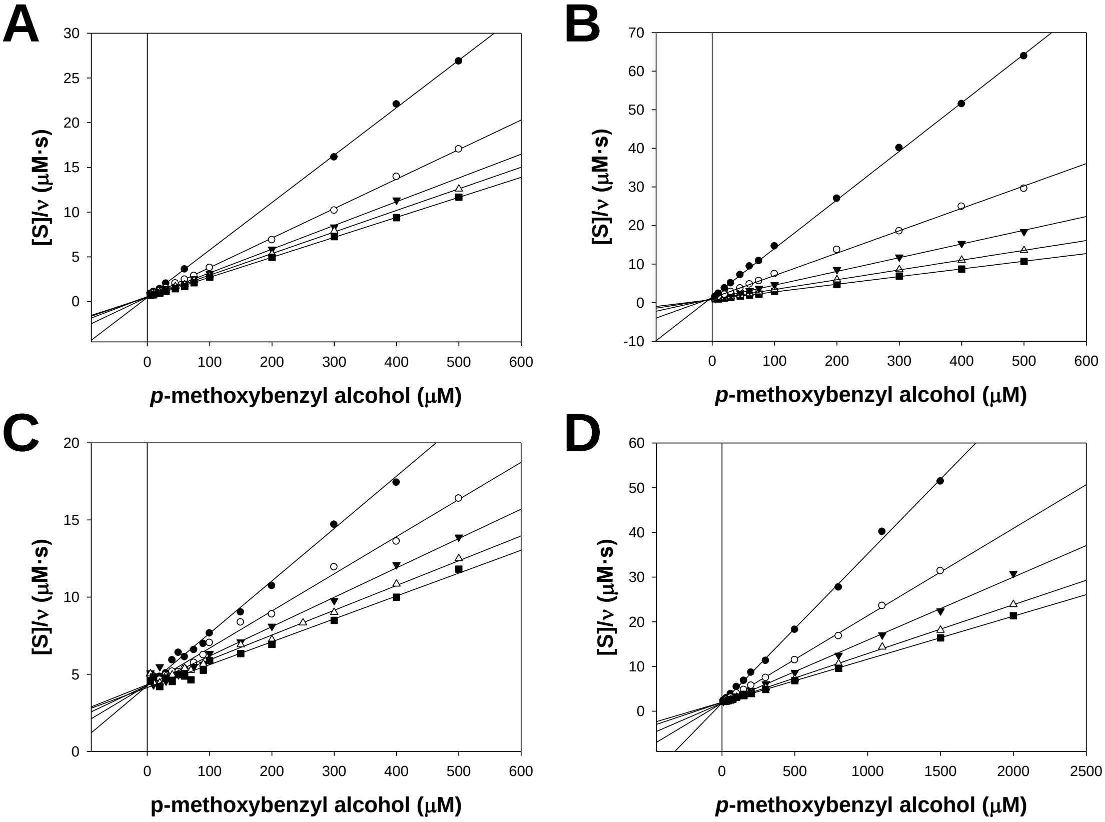

Figure 4.3. Linearized Hanes-Woolf plots of the bi-substrate kinetics of **A.** F397Y. **B.** F397A. **C.** F397W. **D.** F397L AAO variants measured by varying the concentrations of *p*-methoxybenzyl alcohol and O_2 in 50 mM sodium phosphate pH 6.0 at 12°C. Vertical solid line represents x = 0. Filled circles, 0.06 mM O_2; open circles, 0.16 mM O_2; filled triangles, 0.34 mM O_2; open triangles, 0.71 mM O_2; and filled squares, 1.60 mM O_2.

The F397Y variant displays a three-fold lower k_{cat} than that of the native enzyme, whereas their $K_{m(al)}$ values are exactly the same. Consequently, $k_{cat}/K_{m(al)}$ shows a three-fold lower value than that of native AAO. Its behavior towards O_2 is also altered, since $K_{m(ox)}$ is almost four-fold lower than that of the native enzyme (**Table 4.1**).

Table 4.1. Kinetic parameters for steady-state reaction of native AAO and its Phe397 variants in the oxidation of *p*-methoxybenzyl alcohol

	k_{cat} (s^{-1})	$K_{m(Al)}$ (μM)	$k_{cat}/K_{m(Al)}$ ($s^{-1}\cdot mM^{-1}$)	$K_{m(Ox)}$ (μM)	$k_{cat}/K_{m(Ox)}$ ($s^{-1}\cdot mM^{-1}$)
AAO[1]	129 ± 5	25 ± 3	5160 ± 650	348 ± 36	371 ± 41
F397Y	48 ± 1	25 ± 1	1920 ± 65	94 ± 4	512 ± 20
F397W	68 ± 1	280 ± 8	240 ± 5	90 ± 4	718 ± 10
F397A	66 ± 1	54 ± 1	1224 ± 32	500 ± 10	133 ± 3
F397L	115 ± 1	226 ± 4	506 ± 10	190 ± 4	610 ± 13

Measured in 50 mM sodium phosphate (pH 6.0) at 12°C. [1] From Ferreira et al. (2015b)

Concerning variant F397W, its k_{cat} is half of that of the native enzyme and its $K_{m(al)}$ is inflated by ten-fold due to the presence of the bulky tryptophan. Therefore, $k_{cat}/K_{m(al)}$ is almost 20-fold smaller than that of the native enzyme. Its reactivity with O_2 shows also some differences with regard to the native enzyme, since it has a low $K_{m(ox)}$ as well as a higher $k_{cat}/K_{m(ox)}$. In fact it seems to be the most efficient of all the variants (native AAO comprised) at reacting with O_2 (**Table 4.1**).

Variant F397A has a very similar k_{cat} to F397W, half of that of native AAO. Its $K_{m(al)}$ is slightly higher than that of native AAO or F397Y, but $k_{cat}/K_{m(al)}$ is lower than native AAO. It is the variant presenting a highest $K_{m(ox)}$ and, thus, lowest $k_{cat}/K_{m(ox)}$ (**Table 4.1**).

Replacement of phenylalanine with leucine in the F397L variant showed that, although the resulting k_{cat} had no difference with the native enzyme, the $K_{m(al)}$ is high, similar to that of variant F397W, and thus the catalytic efficiency for alcohol oxidation ($k_{cat}/K_{m(al)}$) is low. However, the resulting $K_{m(ox)}$ was lower than that of native AAO and, as a consequence, its catalytic efficiency reducing O_2 ($k_{cat}/K_{m(ox)}$) is higher, and similar to those for the F397Y and F397W variants (**Table 4.1**).

4.1.2. Redox state during turnover

To investigate the redox state of the cofactor during turnover, the F397 variants were mixed in the stopped-flow instrument with equal volumes of an exceedingly saturating concentration of *p*-anisyl alcohol in aerobic conditions. This allows the reaction to proceed and to attain the turnover, a lag phase characterized by a plateau in the absorbance of flavin band I, until this eventually drops to the reduced state.

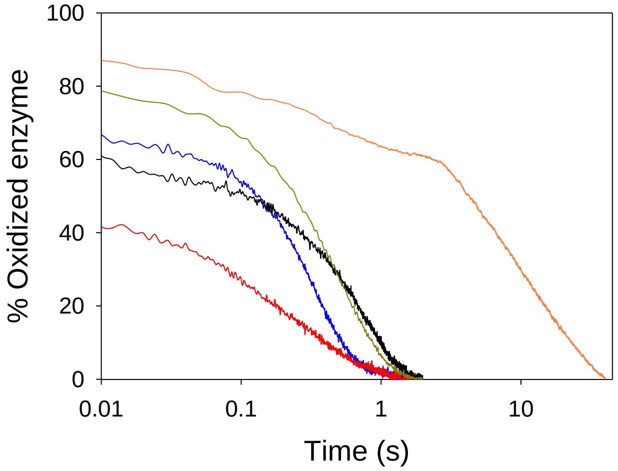

Figure 4.4. Redox state during turnover of native AAO and its Phe397-mutated variants. Wild-type (*green*), F397W (*orange*), F397L (*blue*), F397A (*black*) and F397Y (*red*) AAO variants (~10 µM) were mixed with an excess of *p*-methoxybenzyl alcohol in 50 mM sodium phosphate (pH 6) at 25°C under aerobic conditions. Lines show the time course of absorbance changes at the maxima of the flavin band I (between 459 and 463 nm, depending on the variant).

The absorbance decrease from the initial mixing, until attaining the steady-state turnover indicates the percentage of the oxidized enzyme that remains as such during turnover. On the one hand, for native AAO and the majority of the variants —F397W, F397A and F397L— the most abundant species during turnover is the oxidized enzyme (**Figure 4.4**). This indicates that, for the native protein and these variants, the reduction of FAD is slower than the oxidation by oxygen. Nevertheless, all these variants show decreased percentages of oxidized enzyme in comparison to native AAO, whose percentage is around 80%. F397L, F397A and F397W display around 60% of oxidized enzyme in turnover. In contrast, variant F397Y shows around 40% oxidized enzyme at the steady-state turnover, suggesting that the reductive half-reaction predominates over its oxidative counterpart.

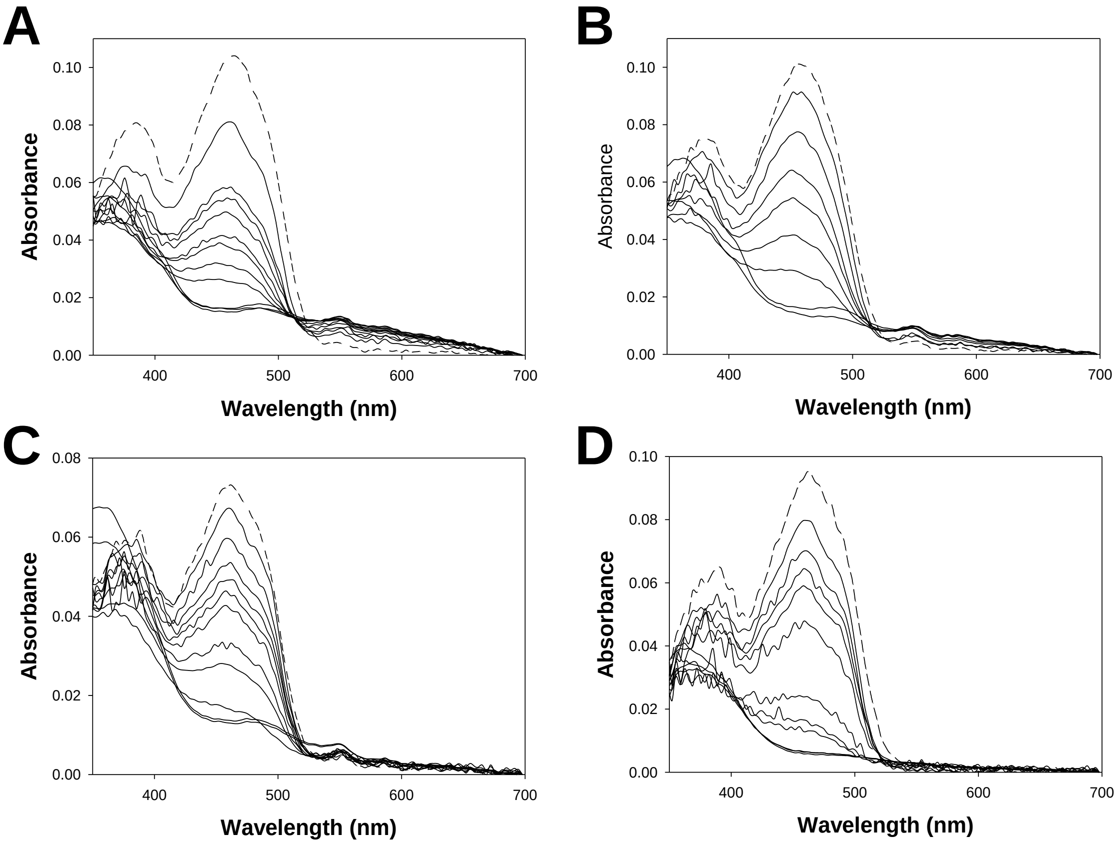

Figure 4.5. Spectral changes of F397 AAO mutated variants recorded between 300 and 700 nm under air-saturated atmosphere in 50 mM sodium phosphate pH 6.0 at 25ºC with excess of *p*-methoxybenzyl alcohol. **A.** F397Y at 0.001, 0.05, 0.1, 0.2, 0.5, 1, 5, 10, 50, 100, 200 s. **B.** F397W at 0.001, 0.05, 2, 5, 10, 20, 200, 1000 s. **C.** F397A at 0.001, 0.005, 0.01, 0.05, 0.1, 0.2, 0.5, 1, 200 and 500 s. **D.** F397L at 0.001, 0.005, 0.05, 0.1, 0.2,0.5, 1, 2, 50, 100 and 500 s.

On the other hand, substitution of the phenylalanine with other aromatic residues, tyrosine or tryptophan, results in formation of charge-transfer complex between the reduced enzyme and the aldehyde product, also found for native AAO (not shown), which is characterized by an increase in absorbance within the range 520–650 nm with time (**Figure 4.5A** and **4.5B**, respectively). However, the replacement by a non-aromatic residue —that is, alanine or leucine— impairs the formation of this complex (**Figure 4.5C** and **4.5D**, respectively).

4.1.3. Rapid kinetics of the two AAO half reactions

In the light of the above results, the reductive and oxidative half reactions of the variants were analyzed to obtain their kinetic parameters, and unveil the rate-limiting step of the variants' catalytic cycles.

The reductive half-reaction of the F397 variants was studied using the stopped flow spectrophotomer under anaerobic conditions. The spectra obtained for all variants indicated two-electron reduction of the Flavin, in agreement with the previously reported hydride transfer reaction for the native protein. Global analyses of the spectral evolution for all variants were fitted to a one-step model (A→B) (**Figure 4.6**). The k_{obs} values obtained at different substrate concentrations exhibited a hyperbolic dependence that allowed k_{red} and K_d determination upon fitting to **Equation 1** or **2**. The insignificant k_{rev} values determined indicated an essentially irreversible reduction of the flavin for all variants.

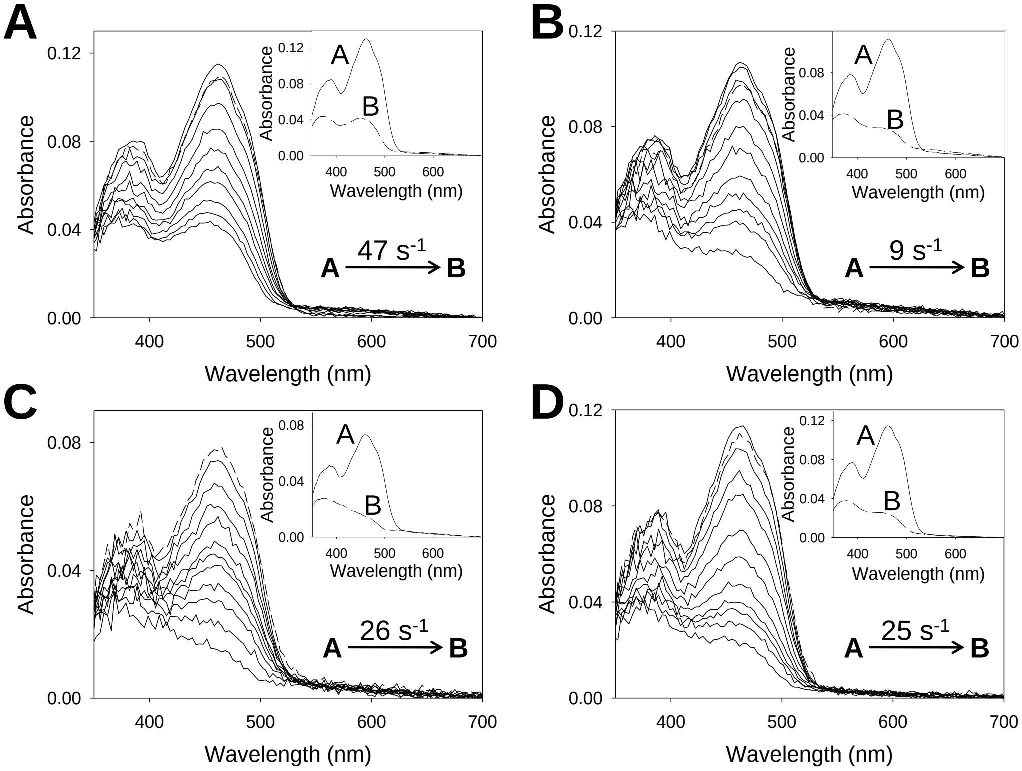

Figure 4.6. Time course of the reduction of Phe397-mutated variants of AAO with 37 µM of *p*-methoxybenzyl alcohol. **A.** F397Y spectra measured after 0.001, 0.005, 0.01, 0.015, 0.02, 0.025, 0.03, 0.04, 0.05 and 0.1 s. **B.** F397W spectra recorded at 0.001, 0.01, 0.02, 0.03, 0.05, 0.07, 0.1, 0.13, 0.15, 0.2 and 0.5 s. **C.** F397A reduction spectra at 0.001, 0.01, 0.02, 0.03, 0.04, 0.05, 0.06, 0.08, 0.1, 0.15 and 0.3. **D.** F397L spectra after 0.001, 0.01, 0.02, 0.03, 0.05, 0.07, 0.1, 0.13, 0.15, 0.2 and 0.4. Dashed lines correspond to the oxidized enzymes. Data were globally fitted to a single-step model described from initial species A to final species B (shown in insets). Estimated k_{obs} is represented in each panel.

For native AAO (spectral changes not shown) and F397A and F397L variants, k_{cat} and k_{red} were of the same range (**Tables 4.2** and **4.3**) indicating that the reductive half reaction is the rate-limiting in AAO catalysis. Nevertheless, variants F397Y and F397W showed k_{red} slightly higher than the native AAO, and were 3-fold and 2-fold faster than their k_{cat} values suggesting that the reductive half-reaction is not the limiting step in the reaction catalyzed by these variants. For all variants, K_d values were similar to the $K_{m(al)}$ estimated under steady-state conditions. In this way, F397W showed the highest K_d, followed by F397L and then by F397A, F397Y and native AAO (**Table 4.3**).

Table 4.2. Transient-state kinetic parameters for the reductive half-reaction of native AAO and its Phe397 variants

	k_{red} (s^{-1})	K_d (μM)	$^{app}k_{red}$ ($s^{-1}·mM^{-1}$)
AAO	115 ± 3	31 ± 2	3710 ± 258
F397Y	150 ± 3	41 ± 3	3660 ± 277
F397W	124 ± 3	292 ± 17	425 ± 10
F397A	69 ± 1	61 ± 2	1130 ± 40
F397L	87 ± 1	180 ± 7	483 ± 20

Measured using stopped-flow rapid spectrophotometry in 50 mM sodium phosphate (pH 6.0) at 12°C under anaerobic conditions.

The oxidative half-reactions of these variants were also investigated by stopped-flow spectrophotometry by following the absorbance increase in both bands I and II of the flavin (**Figure 4.7**). For the four Phe397-mutated variants (and native AAO), it fitted equations describing a process composed of more than one step (with k_1 and k_2 values in **Table 4.3**).

Table 4.3. Transient-state kinetic parameters for the oxidative half-reaction of native AAO and its Phe397 variants

	k_{ox1} (s^{-1})	K_{d1} (μM)	$^{app}k_{ox1}$ ($s^{-1}·mM^{-1}$)	k_{ox2} (s^{-1})	$^{app}k_{ox2}$ ($s^{-1}·mM^{-1}$)
AAO	-	-	770 ± 40	17 ± 1[1]	0
F397Y	-	-	770 ± 70	nd[2]	nd[2]
F397W	125.5 ± 11.3[3]	156 ± 27[3]	801 ± 156[4]	nd[2]	nd[2]
F397A	-	-	78 ± 4	-	9.8 ± 0.1[5]
F397L	-	-	340 ± 10	-	11 ± 1[5]

Measured using stopped-flow rapid spectrophotometry in 50 mM sodium phosphate (pH 6.0) at 12°C under anaerobic conditions. [1] k_{ox2} is constant and independent of O_2 concentration. [2] nd, not determined (too high variability). [3] The F397W constants for the first phase show a hyperbolic dependence on O_2 concentration (in contrast to all other variants). [4] k_{ox1}/K_{d1} ratio.[5] The F397A and F397L second phase (~25% of total amplitude) constants depend linearly on O_2 concentration.

The spectral evolution for the reoxidation of F397Y and F397W variants fitted an equation describing a two-step model (A→B→C). The first step (A→B) was faster than the second one and accounts for ~90% of the amplitude of the reaction. In contrast to what observed for the native AAO and other variants, the $k_{obsA\rightarrow B}$ values for F397W hyperbolic dependence on O_2 concentrations, describing an essentially irreversible process involved in enzyme:oxygen complex formation followed by flavin reoxidation. The obtained k_{ox} is similar to k_{red}, indicating that the rates for the reductive and the reoxidative half-reactions are almost balanced, in agreement with its redox state during turn-over (Tables 2 and 3). K_d value is in the same range than $K_{m(ox)}$, leading to k_{ox}/K_d ratio that agrees with the catalytic efficiency value determined by steady-state assays (**Tables 4.1** and **4.3**). For F397Y variant, these $k_{obsA\rightarrow B}$ were linearly dependent on oxygen concentration, allowing the determination of an $^{app}k_{ox}$ second order rate constant identical to that reported for native enzyme (**Table 4.3**). The second process for both variants (B→C) account for less than 10%, and were concentration independent and too slow to be relevant for catalysis.

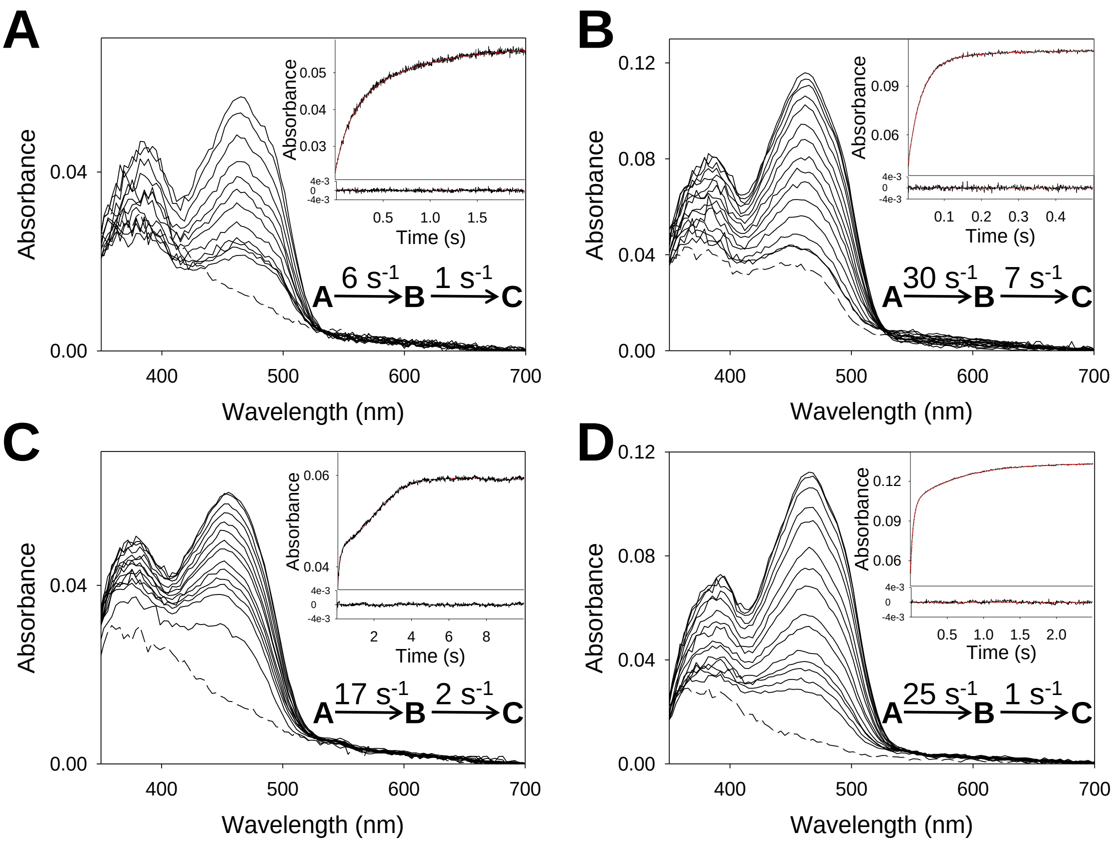

Figure 4.7. Time course of the oxidation of Phe397-mutated variants of AAO. **A.** F397Y oxidation spectra with 26 µM O_2 measured at 0.002, 0.01, 0.02, 0.03, 0.05, 0.1, 0.15, 0.2, 0.3, 0.5, 1 and 3 s. **B.** F397W oxidized with 60 µM O_2 recorded at 0.002, 0.003, 0.005, 0.1, 0.15, 0.2, 0.025, 0.03, 0.04, 0.05 and 0.5 s. **C.** F397A after mixing with 26 µM O_2 at 0.002, 0.01, 0.05, 0.1, 0.15, 0.5, 1, 1.5, 2, 3, 4 and 5 s. **D.** F397L oxidized with 26 µM O_2 recorded at 0.003, 0.006, 0.009, 0.012, 0.015, 0.025, 0.03, 0.5, 0.7, 1, 2 and 3 s. Dashed lines correspond to the reduced enzymes. Insets show the traces at the maximum of flavin band I superimposed with their fits in red. Residuals of each fit displayed at the bottom of the insets. The estimated k_{obs} for each phase is also represented.

F397A and F397L showed more complex oxidation patterns, their spectral evolution best fitted a three-step model (A→B→C→D). The third phase was too small to be determined, but the other two, two $k_{obsA\rightarrow B}$ and $k_{obsB\rightarrow C}$ values could be determined and showed a linear dependence on O_2 concentration that allow the estimation of their corresponding $^{app}k_{ox1}$ and $^{app}k_{ox2}$ second-order rate constants

(**Table 4.3**). Values of ${}^{app}k_{ox2}$ proved to be one order of magnitude smaller than ${}^{app}k_{ox1}$ for both variants. Moreover, the ${}^{app}k_{ox1}$ values for F397L and F397A were half and one order of magnitude slower that for native AAO, respectively.

Even though the oxidations suggest that different chemical steps are taking place in the oxidation AAO, analysis of the different spectra did not reveal any intermediates (**Figure 4.7**).

4.1.4. Studies on AAO:*p*-anisic acid complex formation and dissociation

The differences observed between k_{cat} and k_{red} (or either k_{cat}/K_m and ${}^{app}k_{ox}$) values for both F397Y and F397W encouraged the investigation of the affinity of AAO and *p*-anisic acid (as a substrate/product analog) to figure out which process was limiting the rate of the reaction. Release of the aldehyde product was a likely candidate, rather than H_2O_2, which is a smaller molecule that was not expected to encounter a barrier to exit the active site because of the presence of a bulky amino-acid.

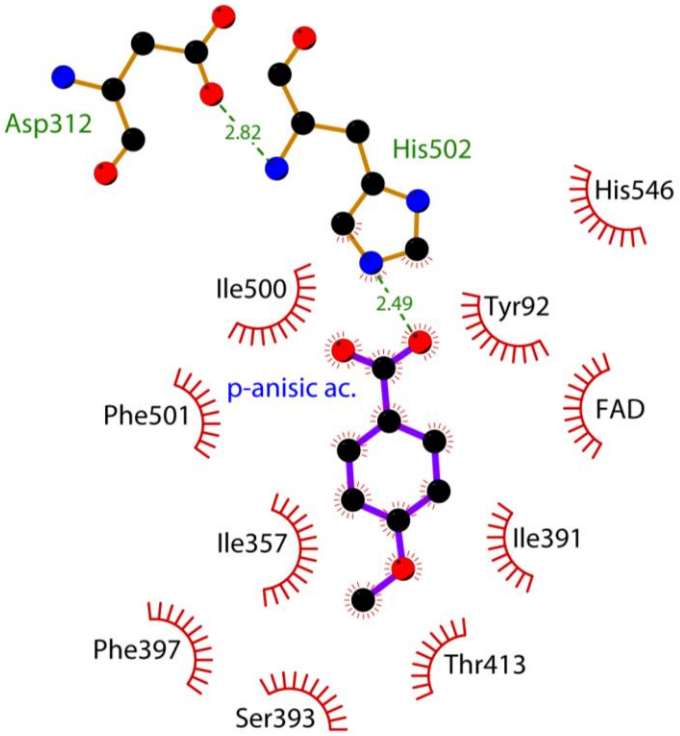

Figure 4.8. LigPlot+ diagram showing the interactions among the active-site residues and the FAD cofactor with the ligand, *p*-anisic acid, in the crystallographic structure of the complex. Green dashed lines represent H bonds between donor and acceptor atoms accompanied by their bonding distances. Red lines in semicircles represent hydrophobic interactions among the represented residues and the different atoms of *p*-anisic acid (Laskowski and Swindells 2011).

The reasons for choosing *p*-anisic acid instead of *p*-anisaldehyde were two: **i)** AAO has activity on the *gem*-diol hydrated forms of aldehydes, which coexist in aqueous solutions (Ferreira et al. 2010); and **ii)** the formation of the enzyme-aldehyde complex was too fast to be recorded with the stopped flow equipment. Affinity constants for the acid were expected to be high as this molecule is known for acting as a competitive inhibitor of AAO (Ferreira et al. 2009), stabilized at the enzyme's active site through a H bond with His502, as revealed by crystallographic data (**Figure 4.8**).

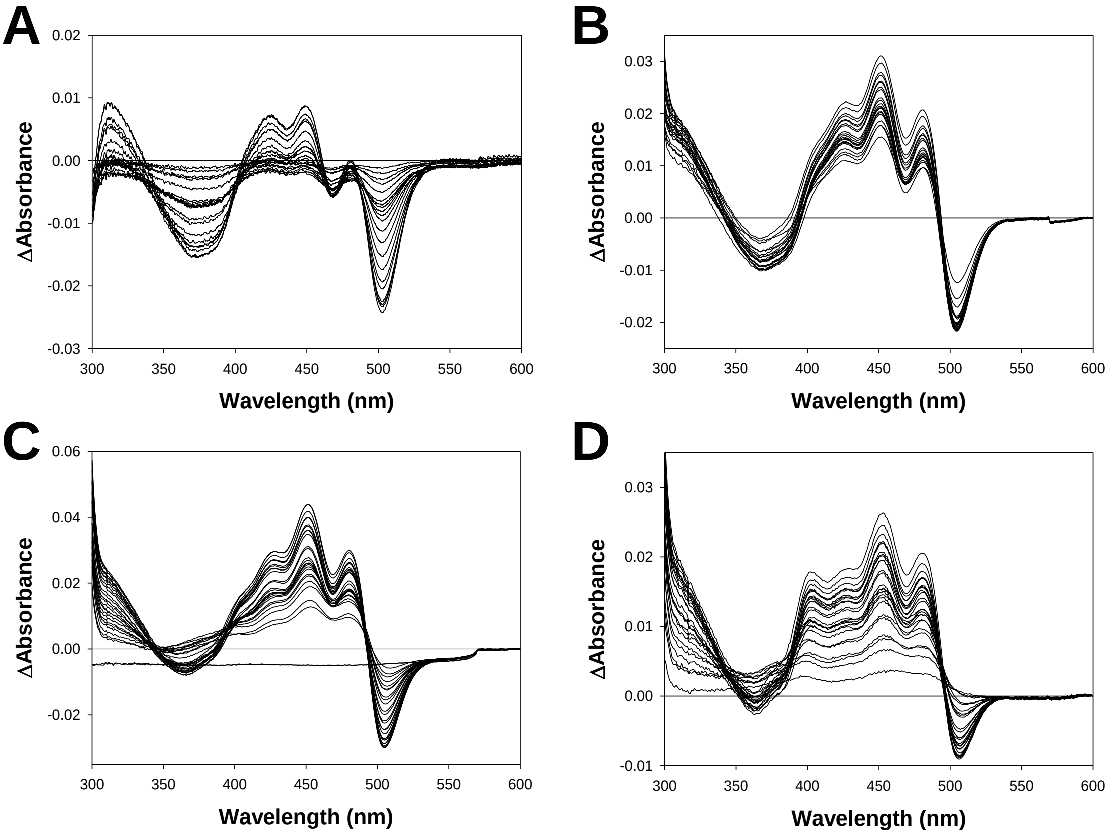

Figure 4.9. Spectral changes upon titration of wild-type and Phe397 AAO variants with increasing concentrations of *p*-anisic acid. Unbound spectra of each of the variants were subtracted to the spectra of the titrated enzyme to obtain the data represented. **A**, Native AAO, and **B-D**, F397Y, F397W and F397A variants, respectively.

The *p*-anisic acid dissociation constants (K_d), obtained from spectral changes during AAO titration with increasing concentrations of *p*-anisic acid (**Figure 4.9**), proved to be very high for both F397L and F397A variants (**Table 4.4**). In fact, the K_d of the former variant could not be estimated since saturation, as shown by the AAO spectral changes upon the acid's titration, could not be attained. Therefore, the F397L K_d is supposed to lie well within the millimolar range. F397A had the highest among the estimated K_d, while F397Y showed the smallest one, which means that it is the variant that more tightly binds *p*-anisic acid.

The rate constants for the formation (k_{for}) and the dissociation (k_{dis}) of the complex between *p*-anisic acid and AAO variants were also investigated by studying the velocity of the spectral changes of the enzyme upon binding of the ligand in a stopped-flow spectrophotometer (**Figure 4.10**).

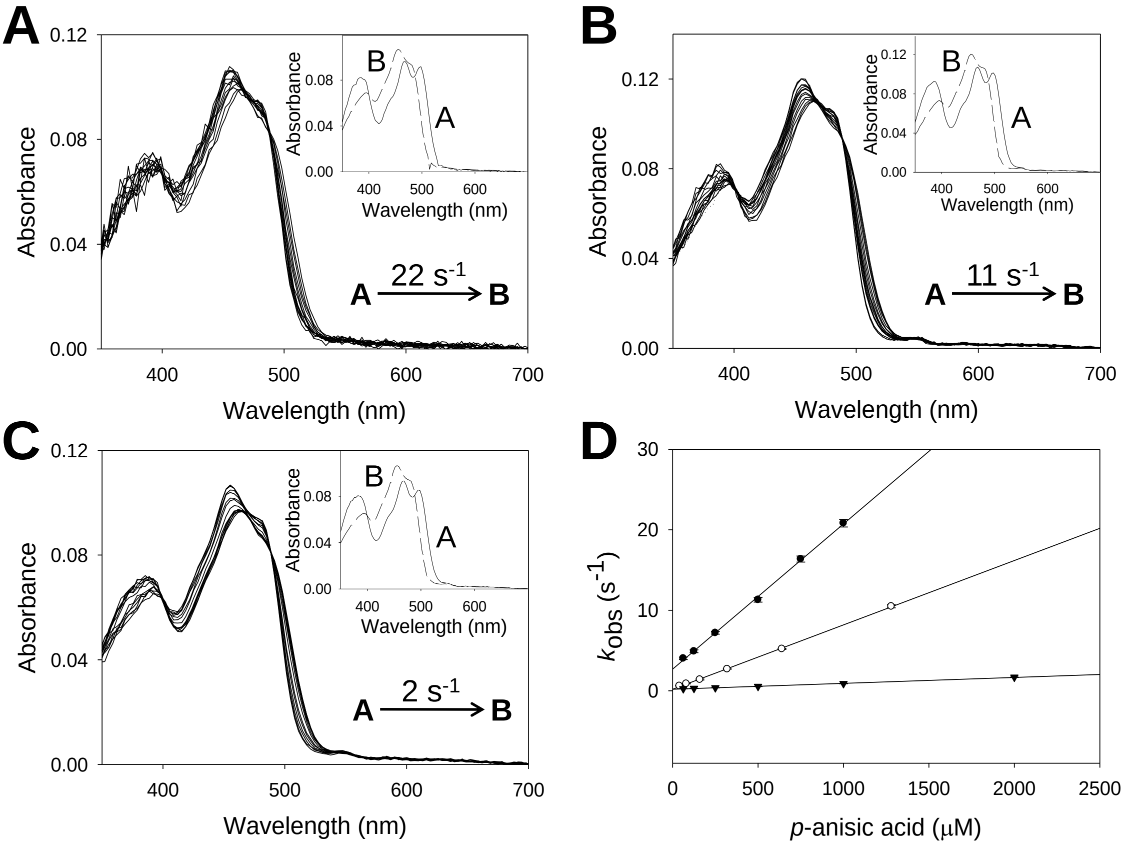

Figure 4.10. Spectral changes upon formation of the AAO-*p*-anisic acid complex. **A.** Native AAO, mixed with 0.5 mM of the ligand at 0.003, 0.01, 0.02, 0.03, 0.04, 0.05, 0.065, 0.085, 0.1, 0.13, 0.15, 0.2 and 0.4 s.**B.** F397Y AAO, mixed with 0.65 mM of *p*-anisic acid measured after 0.005, 0.05, 0.1, 0.2, 0.3, 0.4, 0.5, 0.6, 0.7, 0.8, 0.9, 1, 2, 3 and 4 s, and **C.** F397W AAO mixed with *p*-anisic acid 1 mM recorded at 0.005, 0.02, 0.04, 0.05, 0.07, 0.1, 0.2, 0.4, 0.5, 0.7, 1, 2 and 5 s. Insets show disappearance of initial species A and formation of final species B. The rate constant obtained from the global fitting of the spectral changes is shown. **D.** Fits of the obtained $k_{obs}$for each variant and ligand concentration to **equation 6**: y_0 and slope represent the rate constants for dissociation (k_{dis}) and formation (k_{for}) of the AAO-*p*-anisic acid complexes, respectively, for native AAO (filled circles), and its F397Y (open circles) and F397W (inverted triangles) variants.

The high velocity of complex formation by the F397L and F397A variants impeded estimation of these parameters at 12°C, and even 6°C. Therefore, only the rate constants for native AAO, F397Y and F397W could be estimated. The F397Y k_{for} was two-fold lower than that for the native enzyme, whereas the one for F397W was two orders of magnitude lower. Differences in k_{dis} values were also observed between the native enzyme and the above two variants, since the latter were not significantly different among them, but their k_{dis} values were at least 10-fold slower than that of the native AAO (**Table 4.4**).

Table 4.4. Dissociation constant (K_d), and rate constants of formation (k_{for}) and dissociation (k_{dis}) of *p*-anisic acid complexes by native AAO and its Phe397 variants

	K_d(µM)	k_{for} ($s^{-1}\cdot mM^{-1}$)	k_{dis}(s^{-1})
AAO	170 ± 5	18.0 ± 0.3	2.69 ± 0.17
F397Y	25 ± 2	7.7 ± 0.1	0.24 ± 0.04
F397W	155 ± 9	0.70 ± 0.01	0.19 ± 0.01
F397A	660 ± 40	nd[2]	nd[2]
F397L	nd[1]	nd[2]	nd[2]

Data were measured in 50 mM sodium phosphate (pH 6.0) at 12°C. [1]nd, not determined (due to solubility limitations). [2]nd, not determined (too fast complex formation)

4.2. Discussion

4.2.1. Conservation of active-site Phe397 within the AAO family

Phe397 is located within a loop unique to the AAO family. This loop is placed in a location that is prone to harboring insertions and deletions amongst the members of the GMC superfamily, so analogous structures can be found in other GMCs (Hallberg et al. 2002). Among them, choline oxidase (Quaye et al. 2008; Xin et al. 2009) and cholesterol oxidase (Vrielink et al. 1991; Vrielink and Ghisla 2009) are notable examples, whose insertions seemed to be even longer than that of AAO. However, other GMC proteins lack this feature, like glucose oxidase or pyranose 2-oxidase (Hecht et al. 1993; Hallberg et al. 2004; Ferreira et al. 2015a). Representatives of the GMC superfamily are usually multimeric enzymes, and their monomers group together in a way such that the entrances to their active sites, which tend to be wider than in AAO's, are partially covered by the monomer placed next to it. Given their monomeric nature, AAOs, cholesterol oxidases and cellobiose dehydrogenases have developed such structures to control de diffusion of molecules into buried active sites.

The said insertion spans the residues 390 to 402 in *P. eryngii* AAO and is supposed to enclose the active-site cavity from the outer environment (Fernández et al. 2009) as well as to oscillate as a mechanism of gating for the substrate into its binding pocket, as revealed by computational studies (Hernández-Ortega et al. 2011a), similar to what has been reported for phenylalanine residues in P450 enzymes (Borrelli et al. 2005; Fishelovitch et al. 2009).

Due to its central location within the loop, Phe397 forms, along with F501, Y92, and the side chains of other nonpolar residues, a highly hydrophobic bottleneck that acts as a barrier for the entrance of the substrate into the catalytic cavity (Fernández et al. 2009) (**Figure 4.1**). Tyr92 establishes aromatic stacking interactions with the substrates and helps them accommodate in a catalytically relevant position inside the pocket (Ferreira et al. 2015b). F501, in its turn, modulates the O_2 reactivity with the FAD cofactor by helping the molecule attain a proper distance to both flavin C4a and His502 (Hernández-Ortega et al. 2011b).

Several residues forming the loop are highly conserved during the superfamily evolution, revealing its important role for the enzyme. Furthermore, the phenylalanine in position analogous to 397 in *P. eryngii* AAO is conserved within the family of AAO-like proteins. Analysis of 70 sequences of putative AAO from basidiomycetes, mostly from the Polyporales order (**Figure 4.11**), showed that phenylalanine was the residue present in, at least, 50% of them. The other aromatic amino-acids, tyrosine and tryptophan, were also found in some of the sequences, so up to 60% of all these putative AAOs possessed an aromatic residue in that position. Other amino-acids that turned out to appear in the same place were aliphatic—isoleucine, leucine or valine— and even polar, like proline, making up the other 40% of the residues in this position. In any case, all the residues present instead of this phenylalanine possess a relatively bulky side chain that would permit some interaction with the substrates, so that the accessibility to the active site would be controlled instead of permitting a free diffusion of molecules from the environment to the active site.

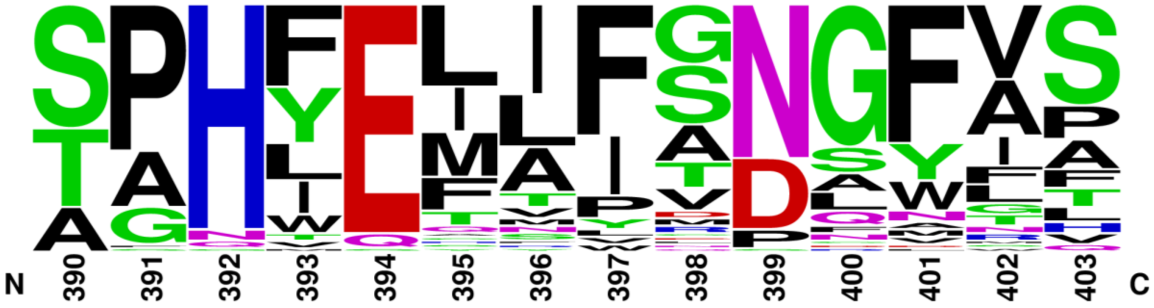

Figure 4.11. Sequence logo for 70 putative AAO sequences from various basidiomycetes corresponding to positions 390–403 of mature *P. eryngii* AAO generated using WebLogo (Crooks et al. 2004). Sequences were taken either from genomes available at the Joint Genome Institute (www.jgi.doe.gov) or from GenBank; the numbers of sequences are indicated in the parentheses: *Bjerkandera adusta* (11), *Dichomitus squalens* (9), *Fomitiporia mediterranea* (1), *Fomitopsis pinicola* (1), *Ganoderma* sp. (7), *Gelatoporia subvermispora* (4), *Gloeophyllum trabeum* (2), *Laccaria bicolor* (1), *Phanerochaete chrysosporium* (3), *Phlebia brevispora* (3), *P. eryngii* (1), *Pleurotus pulmonarius* (1), *Punctularia strigosozonata* (6), *Rhodonia placenta* (2), *Stereum hirsutum* (15) and *Trametes versicolor* (3). Numbering represents the position in the *P. eryngii* mature AAO sequence and the heights of each symbol in the same column indicate the relative frequency of each amino acid at that very position.

4.2.2. Phe397 is critical for substrate diffusion to the active site

The residue Phe397 seems to play an important role in helping the substrate to enter the cavity and attain a catalytically relevant position inside the active site, as it had been suggested in a previous study (Hernández-Ortega et al. 2011a). Evidence for this assumption comes from the fact that the replacement of Phe397 provokes a steep decrease in the $k_{cat}/K_{m(al)}$ values for all the variants herein investigated. This effect is most noticeable in F397W, which shows the highest K_m and, thus, the lowest $k_{cat}/K_{m(al)}$ value, probably due to the bulkiness of the residue, which hinders the entrance of the substrate. However, once the substrate is into the active site, the reduction of the F397W variant takes place as in native AAO, as shown by the k_{red}.

The above effect is similar to that observed when Phe501 was replaced with tryptophan in AAO (Hernández-Ortega et al. 2011b). Nevertheless, it is noticeable that in the case of F397Y, the drop of the catalytic efficiency (for alcohol oxidation) is due to the small k_{cat} that the variant shows, and the K_m for *p*-methoxybenzyl alcohol, as well as the K_d, remain almost invariable upon mutation. This is indicative of the role that aromaticity plays in helping the alcohol substrate to attain a relevant position with respect to the catalytic residues and the FAD cofactor (the k_{red} was even increased after the F397Y and F397W mutations). Similar effects were also seen when Tyr92 was mutated by phenylalanine or even leucine, which could establish the T-shaped stacking interactions with the substrate (Ferreira et al. 2015b). Mutation of phenylalanine with leucine, which is a residue of the same length as phenylalanine, but that lacks aromaticity, proved not to affect the reductive half-reaction measured as k_{red}. However, as in the case of tryptophan, the $K_{m(al)}$ was very increased and, thus, entrance and achieving a relevant position in the active site must be impaired as well.

Removal of the side chain in F397A provokes a decrease in both k_{cat} and k_{red} concomitantly to an increase in $K_{m(al)}$. Diffusion of the substrate into the active site, given it K_d values, must not be impaired, but the proper positioning to attain a catalytically relevant state is hindered. This causes the K_m increase as well as the k_{red} decrease, which is what is limiting the overall catalysis.

4.2.3. Phe397 also plays a role in AAO reoxidation

The substitution of phenylalanine by other aromatic and non-aromatic residues also points towards the involvement of Phe397 in the oxidation of the enzyme's cofactor. In fact, the oxidation of the F397A and F397L variants is slowed down as shown by the small rate estimated constants, in particular, those for the second phase. However, they do not seem to limit the whole catalytic cycle, as k_{cat} and k_{red} values are similar, or even higher when a leucine (or other bulky) side-chain is introduced.

As recently reported, oxidation of AAO takes place through two different kinetic steps in which a H atom and a H^+ are transferred from the FAD moiety to O_2, thereby reducing it. Nevertheless, according to spectroscopic data, these processes cannot be separated, although this could be the case for these two variants. Most probably, each phase accounts for one of these processes that could be uncoupled in these variants. Other GMC enzymes as pyranose 2-oxidase display biphasic oxidations that account for different processes (Sucharitakul et al. 2008; 2011).

The F397Y and F397W variants show high oxidation rates (${}^{app}k_{ox1}$) that are not limiting the catalysis. Therefore, the involvement of the product release step in slowing down the catalytic cycle is likely. Surprisingly, the F397W variant showed saturation upon increase in O_2 concentration, which had not been seen for any other AAO variant so far. High affinity for O_2 might be responsible for this behavior, since compression of the active site has previously been suggested as playing a role in increasing the enzyme's reactivity with O_2 due to the limitation of the diffusion of the molecule in the active site (Hernández-Ortega et al. 2011b). These changes, however, preclude a proper entrance of the alcohol substrate in the active site, so they are not beneficial for the catalysis of the enzyme. The same applies for variants F397L and F397Y, whose side chains seem to improve the reactivity of the enzyme with O_2, given their lower *K*m and higher $k_{cat}/K_{m(ox)}$.

4.2.4. Phe397 involvement in product release

The differences among the k_{cat} and k_{red} values for the F397Y and F397Wvariants suggest that, in contrast to the case of native AAO, whose catalytic cycle is limited by the reductive half reaction (Ferreira et al. 2009), the rate-limiting process of the whole catalysis by these mutated variants must be a different step. Estimation of the ${}^{app}k_{ox}$ for these variants, reinforced by the values of $k_{cat}/K_{m(ox)}$, which are equal or even higher than those calculated for native AAO, ruled out that the reaction with O_2 or its diffusion to the active site could be involved in limiting the catalysis.

In the case of F397Y, the K_d values 6-26 fold lower than found for the native AAO and the other variants suggest that the affinity of this variant for *p*-anisic acid was high. Somehow, the enzyme is retaining this product analog inside the active site without letting it to out. The estimation of k_{dis}, that is, the rate constant for the dissociation of the enzyme-*p*-anisic acid complex, gave additional insight on the mechanism. Since this velocity was 10-fold lower than that of native AAO, it can be indicative of a slower product (*p*-anisaldehyde) release from the active site of the enzyme. The same can be applied to the variant F397W, which shows also a slower k_{dis} than native AAO.

The product release is, therefore, impaired in these two Phe397-mutated variants, thereby limiting the whole catalytic cycle. It is likely that the reaction with O_2 is also precluded by the presence of the aldehyde molecule in the active site. In fact, linearized plots of the steady-state kinetics rule out the ternary complex formation for these variants. Furthermore, the redox state during turnover for F397Y and F397W shows that the percentage of oxidized enzyme is lower than for the native enzyme. Such results point towards the inability of the enzyme to be oxidized in presence of the aldehyde product in the active-site pocket. Other flavoenzymes with catalytic cycles limited or partially limited by the product release have been reported, as it is the case for D-amino acid oxidase (Setoyama et al. 2002), cyclohexanone monooxygenase (Sheng et al. 2001) or nitroalkane oxidase (Valley et al. 2010). The case of amadoriase I is also relevant, since its catalysis is partially limited by the product release, although the oxidation of the enzyme takes place through an ordered ternary complex with the enzyme, product and the O_2 (Wu et al. 2001).

5

Protein motions promote hydride tunneling in AAO catalysis

In the present chapter, KIEs employing different isotopically-substituted substrates, both in steady-state and rapid kinetics, have been used to assess the temperature dependence of the hydride transfer (HT) (**Figure 5.1)** and, thus, the mechanistics lying behind this process. Furthermore, disruption of the AAO's active site by site-directed mutagenesis of a residue, Y92, involved in the stacking-stabilization of the substrate in the active site (Ferreira et al. 2015b), has been used to unveil the role that the structure of substrate binding pocket plays in promoting the HT. These studies are complemented with crystallographic data that shed light on the catalytically relevant position of the substrate into the active site and the distances over which the H^- must be transferred.

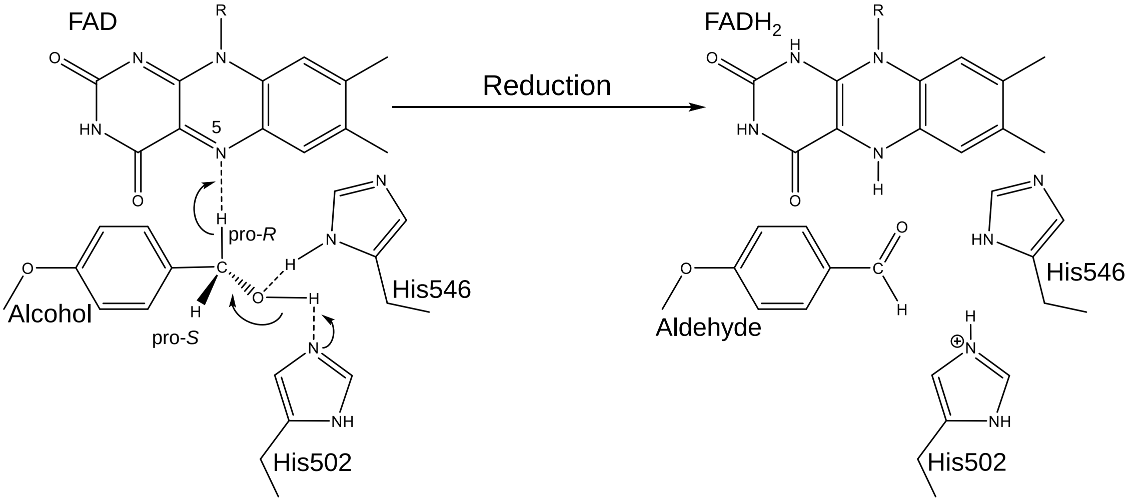

Figure 5.1. Reductive half-reaction of AAO. Hydrogen in position pro-*R* of the α-carbon is abstracted as a hydride by the N5 locus of FAD concomitantly to the abstraction of the hydroxyl proton by His502. This results in the formation of $FADH_2$, an aldehyde and the protonation of His502.

5.1. Results

5.1.1. Crystallographic structure of WT AAO in complex with *p*-anisic acid

The crystallographic structure of AAO in complex with *p*-anisic acid was resolved at a resolution of 2.3 Å. The structural model of *p*-anisic acid:AAO complex comprises residues 2-566, 1 FAD, 1 *p*-anisic acid, 5 glycerols and 280 water molecules. Structural superposition of the complex with the apoAAO shows a r.m.s.d value of 0.21 Å (superimposing 565 Cα atoms) (**Figure 5.2A**) concluding that their overall structures are pretty similar.

p-Anisic acid is a competitive inhibitor of AAO that binds tightly to AAO's active site, showing a K_i of 0.25 mM (at pH 8.0)(Ferreira et al. 2005) and a K_d of 94 ± 3 μM(Ferreira et al. 2010). It is also the product of the reaction of AAO with the hydrated *gem*-diol form of the *p*-anisaldehyde, which coexists in aqueous solution with the pure aldehyde form of the compound(Ferreira et al. 2010).

The crystal structure shows the *p*-anisic acid tightly bound through three H bonds between its O caboxilic atoms and NE2 atom of the catalytic His502, which acts as a base during AAO reductive half reaction, ND1 atom of His 546 and N5 atom of FAD isoalloxazine ring (**Figure 5.2B**). Several other residues located at the active site, F397 and Y92, and the FAD itself establish hydrophobic interactions with atoms of the ligand molecule (**Figure 5.2B**). The distances from *O* carboxilic atoms of the acid to the Nε of His502 and the flavin N5 are of 2.55 and 2.99 Å, respectively (**Fig 5.2B**). The flavin N5 locus receives the H⁻ from the corresponding *pro*-R position of the alcohol substrate. However, since it is the acid, instead of the alcohol acting as a ligand in the active site, it must be taken into account that the H is displaced due to the presence of the carbonyl group.

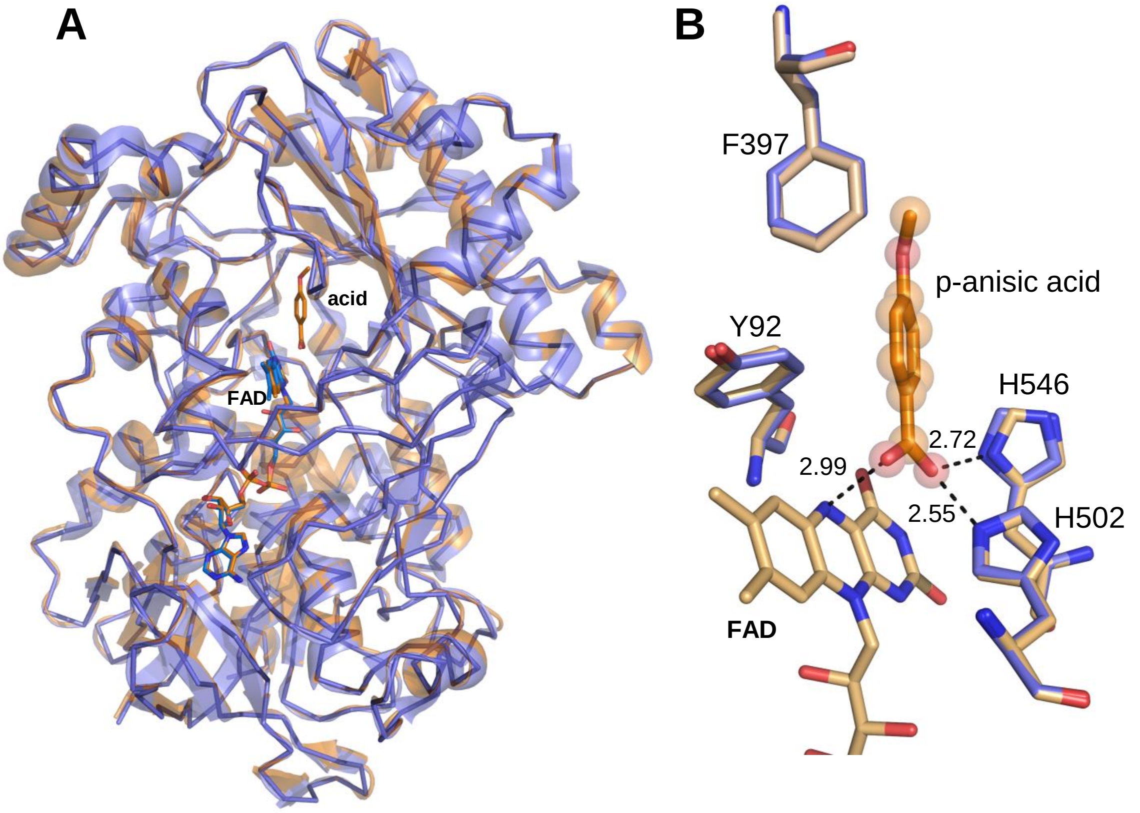

Figure 5.2. A. Cartoon superposition of the crystallographic structures of AAO:*p*-anisic acid complex (orange) and apo AAO (pdb 3FIM) (blue). **B.** Detail of the active site superimposed in AAO:*p*-anisic acid complex and in apoAAO. The H-bounds between the O carboxylic atoms of the *p*-anisic acid and the N atoms of the isoalloxazine ring and His 546 and 502 residues are drawn in black lines and distances in Å. FAD, *p*-anisic acid and residues are drawn as CPK colored sticks with Cα in wheat (complex) and blue (apoAAO).

Y92, which is mutated in this work to unveil its involvement in tunneling, is located forming a triad of residues —with F397and F501— that acts as a hydrophobic bottleneck separating the enzyme's active site from the outer environment. Moreover, it has been suggested that it establishes aromatic stacking interactions that help the substrate attain a catalytically competent position inside the active site. As depicted in **Figure 5.2B**, its position seems not to be altered upon the *p*-anisic acid binding.

5.1.2. Temperature dependence of KIEs on WT AAO catalysis

To investigate the temperature dependence of AAO catalysis, especially the HT that takes place during the reductive half reaction, bi-substrate steady-state and transient state kinetics were performed for WT AAO at different temperatures. α-Protiated and two different α-deuterated *p*-methoxybenzyl alcohols: i) the monodeuterated substrate, in which only the *pro*-R H actually abstracted by the flavin is substituted ((*R*)-[α-^{2}H]-*p*-methoxybenzyl alcohol); and ii) their dideuterated counterpart, where both H bound to the α carbon are isotopically substituted ([α-$^{2}H_{2}$]-*p*-methoxybenzyl alcohol) were employed.

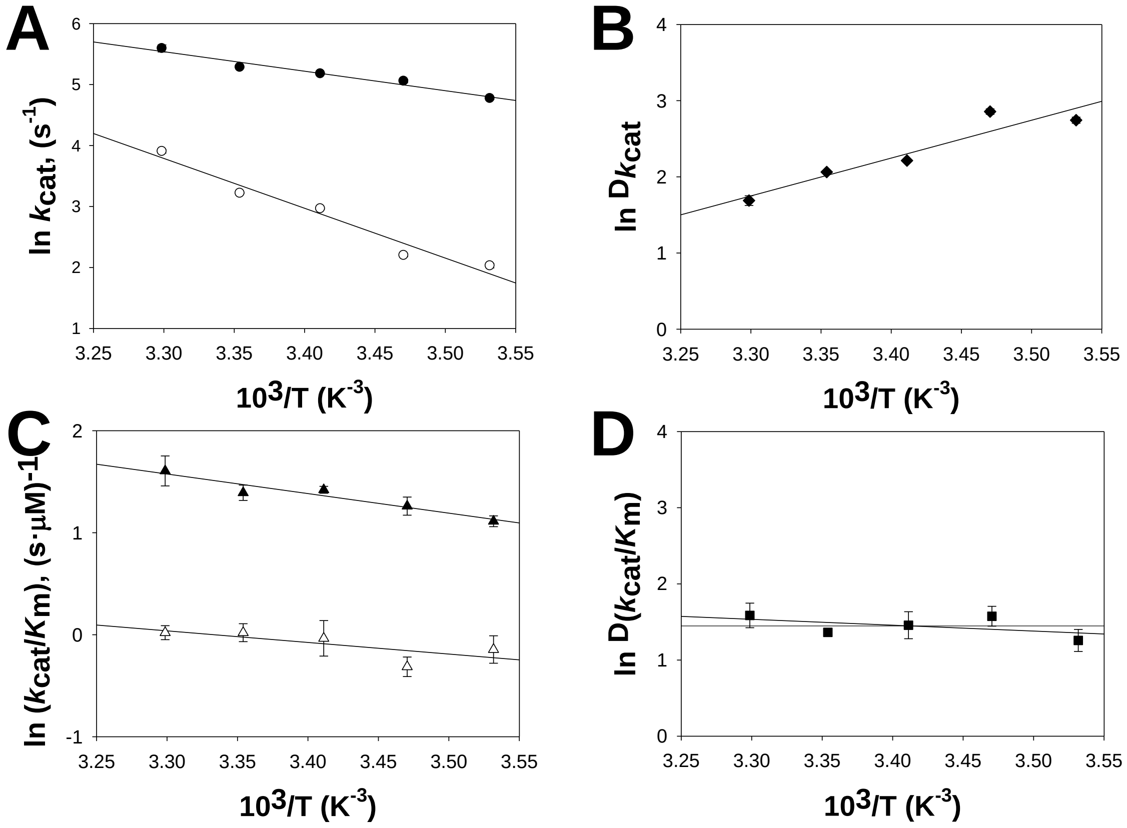

Figure 5.3. Temperature dependences of steady-state kinetic parameters for WT AAO. **A.** Arrhenius plots of k_{cat} with [α-$^{1}H_{2}$]-*p*-methoxybenzyl alcohol (filled circles) and [α-$^{2}H_{2}$]-*p*-methoxybenzyl alcohol (open circles). **B.** Temperature dependence of the KIE of k_{cat} ($^{D}k_{cat}$) with [α-$^{2}H_{2}$]-*p*-methoxybenzyl alcohol. **C.** Arrhenius plots of k_{cat}/K_m with [α-$^{1}H_{2}$]-*p*-methoxybenzyl alcohol (filled triangles) and [α-$^{2}H_{2}$]-*p*-methoxybenzyl alcohol (open triangles). **D.** Temperature dependence of the KIE of catalytic efficiency $^{D}(k_{cat}/K_m)$,. Vertical bars represent standard deviations.

On the one hand, the use of deuterated and protiated substrates will permit to calculate the primary kinetic isotope effects and, thus, elucidate if there exists a tunneling effect in the hydride transfer. On the other hand, differences in catalytic constants between monodeuterated and dideuterated substrates allow evaluating the secondary kinetic isotope effect, which is due to the presence of an isotopically labeled H whose bond is not directly involved in the reaction.

Regarding steady-state, the kinetic constants estimated every 5°C between 10°C and 30° C for the α-protiated and [α-$^2H_2$]-*p*-methoxybenzyl alcohols are shown in **Table 5.1**. The temperature dependences of k_{cat} and $k_{cat}/K_{m(al)}$values, together with the temperature dependence of the primary substrate KIE, are shown in **Figure 5.3**. The turn-over dependences were fit to Arrhenius equation to estimate Arrhenius pre-exponential factors (*A*) and activation energy (E_a), which allowed the calculations of the difference in activation energies ($\Delta E_{a(D\text{-}H)} = E_{aD} - E_{aH}$) and the ratio between pre-exponential factors (A_H/A_D) (**Table 5.2**). The E_a for turn-over with α-deuterated substrate was higher than that obtained with the α-protiated substrate, obtaining a temperature-dependent KIE ($\Delta E_{a(D\text{-}H)}$ is large) and a value for the isotope effect on the Arrhenius prefactor below unity ($A_H/A_D << 1$). In contrast, the catalytic efficiency estimated using α-deuterated substrate showed a temperature dependence pattern that is similar to that for α-protiated substrate, leading to a KIE that is temperature independent (average 4.3 ± 1.3). This $^D(k_{cat}/K_{m(al)})$ was slightly lower than the $^Dk_{cat}$ values (**Table 5.3**), indicating that substrate binding is affected by isotopic substitutions. Nevertheless, steady-state KIE values clearly indicated that the breakdown of Cα-H/D is the limiting step in flavin reduction, and hence, in the overall AAO catalysis.

Table 5.1. Estimated k_{cat}, K_m and k_{cat}/K_m constants (value ± S.D.) for the steady-state kinetics of wild-type AAO with α-protiated and α-dideuterated *p*-methoxybenzyl alcohols

T (°C)	[α-$^1H_2$]			[α-$^2H_2$]		
	k_{cat} (s^{-1})	K_m (μM)	k_{cat}/K_m ($s^{-1}\cdot\mu M^{-1}$)	k_{cat} (s^{-1})	K_m (μM)	k_{cat}/K_m ($s^{-1}\cdot\mu M^{-1}$)
10	118.3 ± 2.2	32.0 ± 1.7	3.0 ± 0.2	7.6 ± 0.3	8.8 ± 1.1	0.86 ± 0.12
15	157.2 ± 4.3	54.9 ± 3.7	3.5 ± 0.3	9.0 ± 0.2	12.4 ± 1.1	0.73 ± 0.07
20	177.3 ± 2.3	42.8 ± 1.4	4.1 ± 0.1	19.4 ± 0.2	20.1 ± 0.6	0.96 ± 0.17
25[a]	197.0 ± 2.0	49.0 ± 1.0	4.0 ± 0.3	25.0 ± 0.2	24.6 ± 2.5	1.02 ± 0.13
30	268.4 ± 15.5	53.9 ± 7.3	5.0 ± 0.7	49.6 ± 1.3	48.6 ± 3.2	1.02 ± 0.07

Bisubstrate kinetics were performed with α-protiated and α-(*R*)-*p*-methoxybenzyl alcohols

[a]Data from Hernández-Ortega *et al.* (2012)

Table 5.2. Thermodynamic parameters from the temperature dependence of the turn-over and hydride transfer reaction in WT AAO oxidation of α-protiated and α-deuterated *p*-methoxybenzyl alcohols

Parameters	Turn-over	Hydride transfer	
	[α-$^2H_2$]	[α-$^2H_2$]	(*R*)-[α-^2H]
A_H (s^{-1})	9.8×10^6	2.5×10^8	2.5×10^8
E_{aH}(kcal·mol^{-1})	6.4	8.3	8.3
A_D (s^{-1})	2.3×10^{13}	3.6×10^8	4.2×10^{10}
E_{aD} (kcal·mol^{-1})	16.2	9.8	12.2
A_H/A_D	4.3×10^7	0.7	0.006
$\Delta E_{a(D\text{-}H)}$(kcal·mol^{-1})	9.9	1.5	3.9

Table 5.3. KIEs determined from the temperature dependence of the steady-state in WT AAO

T (°C)	$^{D}\boldsymbol{k}_{\mathbf{cat}}$	$^{D}(\boldsymbol{k}_{\mathbf{cat}}/\boldsymbol{K}_{\mathbf{m}})$
10	15.6 ± 0.6	3.5 ± 0.5
15	17.4 ± 0.6	4.9 ± 0.6
20	9.1 ± 0.2	4.3 ± 0.7
25	7.9 ± 0.1	3.9 ± 0.2
30	5.4 ± 0.4	4.9 ± 0.8

KIE values are the ratio between activities from bisubstrate kinetics on α-protiated/[α-$^{2}H_{2}$]-deuterated alcohols

To reinforce the above results, the temperature dependence of HT during flavin reduction step in WT AAO was investigated by using the α-protiated and different α-deuterated —(*R*)-[α-^{2}H] and [α-$^{2}H_{2}$]— *p*-methoxybenzyl alcohols. The reduction (k_{red}) and dissociation constants (K_{d}) estimated with each substrate, every 2°C between 6 °C and 14°C, are provided in **Table 5.4**. Arrhenius plots of the estimated k_{red} for WT AAO with each substrate (**Table 5.4**) are shown in **Figure 5.4A**, and the thermodynamic parameters estimated by fitting to Arrhenius equation are provided in **Table 5.2**. The activation energy for D^{-} abstraction with (*R*)-[α-$^{2}H_{1}$]-*p*-methoxybenzyl alcohol is higher than that obtained with [α-$^{2}H_{2}$]-*p*-methoxybenzyl alcohol. As a consequence, the KIE estimated with the monodeuterated substrate is more temperature-dependent than that calculated for the dideuterated substrate (3.9 and 1.5 for $\Delta E_{a(D\text{-}H)}$, respectively). Besides, the values for A_{H}/A_{D} were very close to zero and unity for (*R*)-[α-$^{2}H_{1}$] and [α-$^{2}H_{2}$]-*p*-methoxybenzyl alcohols, respectively. The highest $^{D}k_{red}$ values obtained for [α-$^{2}H_{2}$]-*p*-methoxybenzyl alcohol with respect to those found for the *R* isomer (**Table 5.5**) indicated a secondary KIE that increases with temperature, opposite to the behavior of the primary $^{D}k_{red}$ (**Table 5.5**).

Table 5.4. Reduction rate (k_{red}) and dissociation (K_{d}) constants (value ± S.D.) for wild-type AAO with α-protiated and α-deuterated *p*-methoxybenzyl alcohols

T (°C)	**[α-$^{1}H_{2}$]**		**[(*R*)-$^{2}H_{1}$]**		**[α-$^{2}H_{2}$]**	
	$\boldsymbol{k}_{\mathbf{red}}$(s^{-1})	$\boldsymbol{K}_{\mathbf{d}}$(μM)	$\boldsymbol{k}_{\mathbf{red}}$(s^{-1})	$\boldsymbol{K}_{\mathbf{d}}$(μM)	$\boldsymbol{k}_{\mathbf{red}}$(s^{-1})	$\boldsymbol{K}_{\mathbf{d}}$(μM)
6	75.6 ± 2.4	15.7 ± 2.8	10.7 ± 0.1	15.8 ± 0.4	7.7 ± 0.1	8.4 ± 0.8
8	81.1 ± 0.8	21.4 ± 0.5	11.7 ± 0.1	18.7 ± 0.5	8.3 ± 0.1	6.7 ± 0.6
10	89.0 ± 2.0	22.6 ± 1.4	14.7 ± 0.1	18.0 ± 0.4	9.7 ± 0.1	9.3 ± 0.6
12	95.9 ± 1.8	22.0 ± 1.2	17.8 ± 0.2	20.0 ± 1.2	11.1 ± 0.1	10.0 ± 0.2
14	112.0 ± 1.6	24.4 ± 1.0	20.8 ± 0.9	25.7 ± 4.9	12.7 ± 0.1	16.6 ± 0.5

Measurements were carried out in 50 mM sodium phosphate buffer pH 6

Table 5.5. KIEs determined from the temperature dependence of hydride transfer reaction (k_{red}) in WT AAO

T (°C)	**Deuterated alcohol** **[α-$^2H_2$]**	 **(*R*)-[α-^{2}H]**
6	9.9 ± 0.3	6.7 ± 0.3
8	9.9 ± 0.1	6.9 ± 0.5
10	9.6 ± 0.2	6.0 ± 0.3
12	9.1 ± 0.2	5.7 ± 0.2
14	8.9 ± 0.3	5.8 ± 0.3

KIE values for k_{red} ($^Dk_{red}$) are the ratio between hydride transfer constants on α-protiated/α-deuterated alcohols

In relation to $K_{m(al)}$ at different temperatures (**Table 5.1**), it follows the same pattern as the K_d estimated by rapid kinetics, so it increases with temperature irrespective of the isotopic composition of the substrate (**Figure 5.4B**).

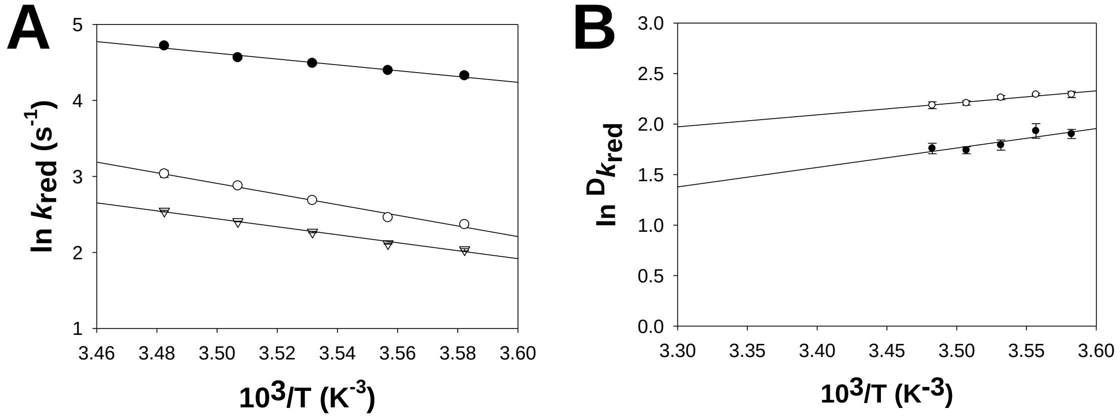

Figure 5.4. Temperature dependences of HT reaction for WT AAO **A.** Arrhenius plots of k_{red} with α-protiated *p*-methoxybenzyl alcohol (filled circles), (*R*)-[α-^{2}H]-*p*-methoxybenzyl alcohol (open circles) and [α-$^2H_2$]-*p*-methoxybenzyl alcohol (open inverted triangles). **B.** Temperature dependence of the KIE of k_{red} ($^Dk_{red}$) with (*R*)-[α-^{2}H]-*p*-methoxybenzyl alcohol (open circles) and [α-$^2H_2$]-*p*-methoxybenzyl alcohol (filled circles). Vertical bars represent standard deviations.

Regarding the K_d calculated for each of the substrates and temperatures, it is worth noting that they are dependent on temperature, and they increase with it, irrespective of the substrate employed (**Table 5.4**). Furthermore, there exists no primary ^DK_d with (*R*)-[α-$^2H_1$]-*p*-methoxybenzyl alcohol; whereas when [α-$^2H_2$]-*p*-methoxybenzyl alcohol is used, there are both primary ($^{D2}K_d$) and secondary KIEs ($^{D2}K_{dD}$) (**Table 5.6**). $^{D2}K_d$ and $^{D2}K_{dD}$ show the same values at different temperatures, indicating that the exerted effect is probably due to the presence of the second isotopic substitution in the substrate and independent of temperature).

Table 5.6. Estimated KIEs on K_d for wild-type AAO and Y92F, Y92L and Y92W

T	wild-type			Y92F	Y92L	T (°C)	Y92W
(°C)	$^{D}K_{d}$	$^{D_2}K_{d}$	$^{D_2}K_{dD}$	$^{D}K_{d}$	$^{D}K_{d}$		$^{D}K_{d}$
6	1.0 ± 0.2	1.9 ± 0.4	1.9 ± 0.2	1.8 ± 0.2	1.5 ± 0.2	12	1.1 ± 0.1
8	1.1 ± 0.0	3.2 ± 0.3	2.8 ± 0.3	1.7 ± 0.1	1.3 ± 0.0	16	0.9 ± 0.2
10	1.3 ± 0.1	2.4 ± 0.2	1.9 ± 0.1	1.6 ± 0.1	1.5 ± 0.1	20	1.1 ± 0.2
12	1.1 ± 0.1	2.2 ± 0.1	2.0 ± 0.1	1.7 ± 0.1	1.5 ± 0.1	25	1.1 ± 0.0
14	0.9 ± 0.2	1.5 ± 0.1	1.5 ± 0.3	1.7 ± 0.1	1.3 ± 0.1		

K_d constants measured with α-protiated and [α-$^2H_2$]-*p*-methoxybenzyl alcohols. (R)-[^{2}H]-*p*-methoxybenzyl alcohol was also used with the wild-type enzyme. KIE is estimated as the ratio between the constants obtained with protiated and deuterated substrate

5.1.3. Temperature dependence of the hydride transfer reaction of AAO Y92 variants

In a previous study it was demonstrated that the stacking-stabilizing interaction of aromatic substrate by Y92 active site residue is essential for concerted hydride and proton transfer in AAO alcohol oxidation (Ferreira et al. 2015b). In this chapter, we further study the role that AAO's binding pocket plays in HT modulation by kinetic characterization of the HT reaction of several Y92 variants (Y92F, Y92L and Y92W).

The reductive half-reaction of Y92F, Y92L and Y92W variants were analyzed by using α-protiated and [α-$^2H_2$]-*p*-methoxybenzyl alcohols every 2°C between 6°C and 14°C for Y92F and Y92L, and at 12, 16, 20 and 25°C for Y92W. The spectral evolutions of these Y92 variants with α-deuterated substrate were similar to those previously reported with α-protiated substrate (Ferreira et al. 2015b), indicating a full two-electron flavin reduction (**Figure 5.5**). **Tables 5.8**, **5.9** and **5.10** show the k_{red} and K_d constants estimated for Y92F, Y92L and Y92W, respectively. The Y92F and Y92L variants showed similar reduction rates and affinity to those reported for the WT AAO, while the incorporation of a bulkier residue in the Y92W variant, produced a strong decrease in HT efficiency (7-and 200-fold lower reduction rate and affinity, respectively).

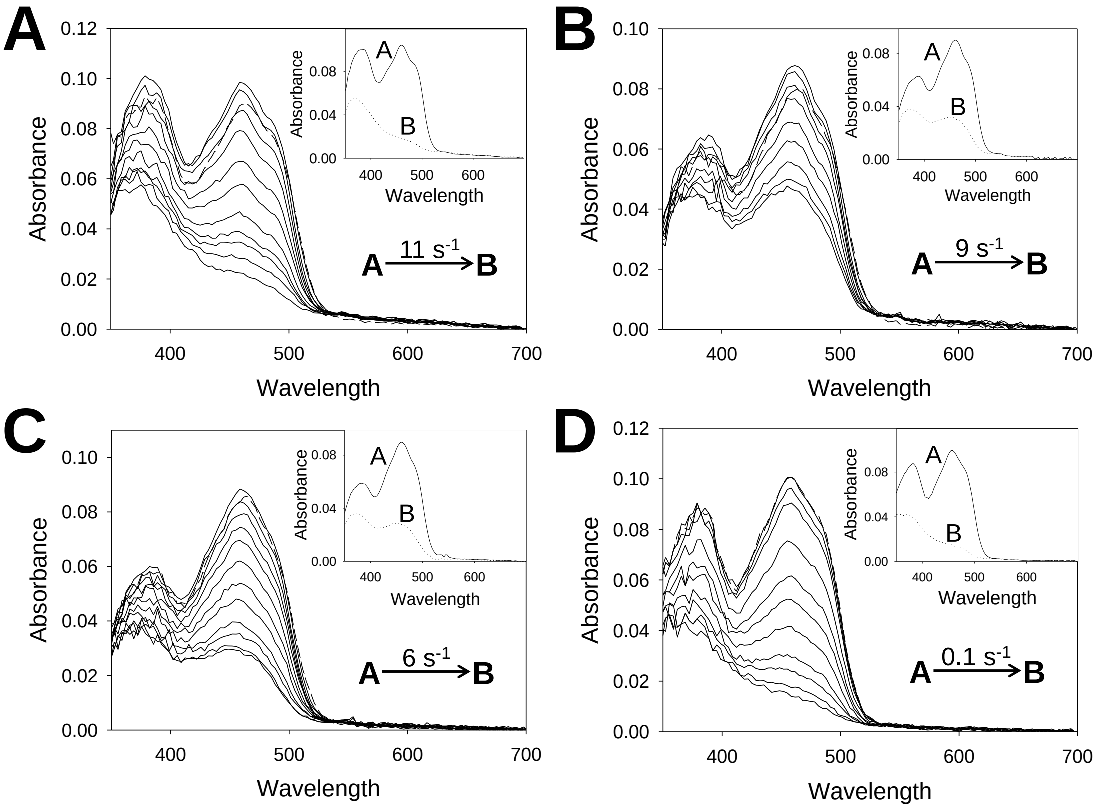

Figure 5.5. Reduction spectra of Y92 AAO variants with $[\alpha\text{-}^2H_2]$-*p*-methoxybenzyl alcohol at 12°C. **A.** WT AAO with 31 μM of substrate at times: 0.004, 0.015, 0.02, 0.03, 0.05, 0.07, 0.1, 0.13, 0.15, 0.2 and 0.3 s. **B.** Y92F with 37 μM of substrate after: 0.001, 0.01, 0.02, 0.03, 0.05, 0.07, 0.1 0.13 and 0.15 s. **C.** Y92L with 37μM of substrate at times: 0.001, 0.02, 0.03, 0.05, 0.07, 0.1 0.15, 0.2, 0.3, 0.4, 0.6 and 0.8. **D.** Y92W with 312 μM of substrate after: 0.16, 0.5, 1, 3, 5, 7, 10, 15, 20, 30 and 60 s. Dashed lines represent the unbound enzyme spectra. Insets show initial and final species determined after global fitting of the reduction spectra.

Arrhenius plots for all Y92 variants are provided in **Figure 5.6**, and their thermodynamic parameters are shown in **Table 5.7**.

Regarding the Y92F variant, its overall behavior resembles very closely that of the WT AAO, with similar activation energy for D^- versus H^- abstraction. Therefore, their thermodynamic parameters were practically identical to those calculated for the wild-type ($\Delta E_a \approx 1.5$ and $A_H/A_D \approx 0.6$). Besides, K_d values for Y92F mutant tend to increase with temperature and are, thus, dependent of it (**Table 5.8**). There is also an isotopic contribution on it, since the estimated $^{D2}K_d$ are bigger than 1, but seem not to depend on temperature (mean 1.7 ± 0.3), similarly to wild-type enzyme.

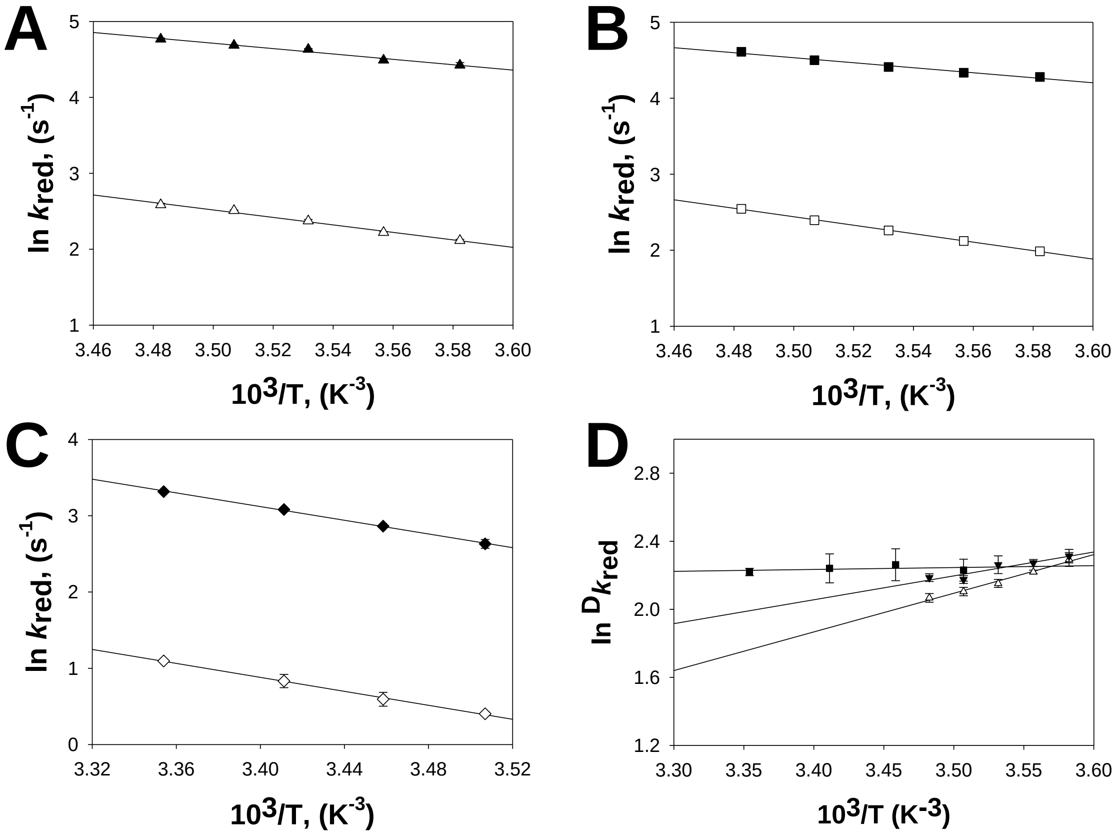

Figure 5.6. Temperature dependences of of HT reaction for AAO Y92 variants: **A.** Arrhenius plots for the reduction of Y92F with α-protiated *p*-methoxybenzyl alcohol (filled triangles) and [α-$^2H_2$]-*p*-methoxybenzyl alcohol (open triangles). **B.** Arrhenius plots for the reduction of Y92L with α-protiated *p*-methoxybenzyl alcohol (filled squares) and [α-$^2H_2$]-*p*-methoxybenzyl alcohol (open squares). C. Arrhenius plots for the reduction of Y92W with α-protiated *p*-methoxybenzyl alcohol (filled diamonds) and [α-$^2H_2$]-*p*-methoxybenzyl alcohol (open diamonds). **D.** Temperature dependence of $^{D}k_{red}$ for Y92F (filled inverted triangles), Y92L (open triangles) and Y92W (filled squares). Vertical bars represent standard deviations.

Substitution of Y92 with Leu, a non-aromatic residue that probably produces some stacking interaction with the alcohol susbstrate, led to a slightly different behaviour. This variant has a more temperature-dependent KIE than WT protein. The Y92L variant showed more temperature dependent rates for D$^-$ abstraction than for H$^-$ abstraction ($\Delta E_{a(D-H)}$ is larger than that for WT AAO). As a consequence, the Y92L variant isotope effect on the Arrhenius pre-factor is very close to zero. Regarding the K_d, although they are slightly higher than those calculated for wild-type and Y92F AAO, they follow de same pattern and are dependent on temperature as well (**Table 5.9**). In this case there is also a significant $^{D2}K_d$ (**Table 5.6**) that, analogously to the other variants analyzed so far, is independent of temperature (mean 1.4 ± 0.3).

Table 5.7. Thermodynamic parameters from the temperature dependence of the hydride transfer reaction (k_{red}) in Y92 AAO variants oxidation of α-protiated and (*R*)-[α-^{2}H]-*p*methoxybenzyl alcohols.

AAO variant	HT			DT			A_H/A_D	$\Delta E_{a(D-H)}$
	k_{red} (s^{-1})	A_H (s^{-1})	E_{aH} ($kcal \cdot mol^{-1}$)	k_{red} (s^{-1})	A_D (s^{-1})	E_{aD} ($kcal \cdot mol^{-1}$)		($kcal \cdot mol^{-1}$)
Y92F	108.4 ± 0.8	3.1×10^8	8.3	12.3 ± 0.1	4.8×10^8	9.9	0.591	1.6
Y92L	90.1 ± 0.4	9.7×10^6	6.6	11.0 ± 0.2	3.4×10^9	11.1	0.003	4.5
Y92W	13.9 ± 0.8	7.7×10^7	8.8	1.5 ± 0.1	1.5×10^7	9.1	5.260	0.3

Measurements were carried out in 50 mM phosphate buffer, pH 6, every 2°C between 6 and 14 °C for Y92F and Y92L variants and at 12, 16, 20 and 25°C for Y92W variant. k_{red} constants estimated at different temperatures for each variants were fitted to Arrhenius equation to obtain the parameters shown above.

Introduction of a bulky amino-acid in the active site seems to disrupt the behaviours analyzed so far with [α-$^1H_2$]-*p*-methoxybenzyl and [α-$^2H_2$]-*p*-methoxybenzyl alcohols. The activation energy for D^- abstraction by Y92W variant shows a temperature dependence that is similar to that for H^- abstraction ($\Delta E_{a(D-H)}$ is bellow unity), leading to a virtually temperature independent KIE and a A_H/A_D value greater than unity. With regard to the affinity for the substrate, K_d seem to be only slightly dependent on temperature (**Table 5.10**) and there is no statistically relevant $^{D2}K_d$ (**Table 5.11**), being the mean of the values 1.0 ± 0.2.

Table 5.8. Reduction rate (k_{red}) and dissociation (K_d) constants (value ± S.D.) for Y92F AAO with α-protiated and [α-$^2H_2$]-*p*-methoxybenzyl alcohol

T (°C)	[α-$^1H_2$]		[α-$^2H_2$]	
	k_{red}(s^{-1})	K_d(μM)	k_{red}(s^{-1})	K_d(μM)
6	83.4 ± 2.9	22.7 ± 2.1	8.3 ± 0.1	12.9 ± 0.7
8	89.1 ± 1.7	22.0 ± 1.1	9.2 ± 0.1	13.2 ± 0.6
10	102.7 ± 1.0	25.3 ± 0.6	10.7 ± 0.2	15.7 ± 1.0
12	108.4 ± 0.8	29.6 ± 0.6	12.3 ± 0.1	17.0 ± 0.4
14	117.6 ± 1.8	27.3 ± 0.9	13.3 ± 0.3	16.4 ± 1.0

Table 5.9. Reduction rate (k_{red}) and dissociation (K_d) constants (value ± S.D.) for Y92L AAO with α-protiated and [α-$^2H_2$]-*p*-methoxybenzyl alcohol

T (°C)	[α-$^1H_2$]		[α-$^2H_2$]	
	k_{red}(s^{-1})	K_d(μM)	k_{red}(s^{-1})	K_d(μM)
6	72.3 ± 2.8	36.8 ± 3.8	7.3 ± 0.1	25.2 ± 1.6
8	76.4 ± 0.7	42.2 ± 0.9	8.3 ± 0.1	31.4 ± 0.6
10	82.4 ± 0.9	45.0 ± 1.2	9.6 ± 0.2	29.6 ± 1.3
12	90.1 ± 0.4	47.8 ± 0.7	11.0 ± 0.2	31.1 ± 1.6
14	100.6 ± 1.4	43.7 ± 1.5	12.7 ± 0.3	33.4 ± 2.0

Table 5.10. Reduction rate (k_{red}) and dissociation (K_d) constants (value ± S.D.) for Y92W AAO with α-protiated and [α-$^2H_2$]-*p*-methoxybenzyl alcohol

T (°C)	[α-$^1H_2$]		[α-$^2H_2$]	
	k_{red}(s^{-1})	K_d(mM)	k_{red}(s^{-1})	K_d(mM)
12	13.9 ± 0.8	4.6 ± 0.5	1.5 ± 0.1	4.3 ± 0.2
16	17.5 ± 0.1	3.8 ± 0.1	1.8 ± 0.2	4.3 ± 0.9
20	21.8 ± 0.5	5.3 ± 0.4	2.3 ± 0.2	5.0 ± 0.6
25	27.6 ± 0.3	6.6 ± 0.1	3.0 ± 0.1	6.0 ± 0.2

Table 5.11. Estimated KIEs on K_d for wild-type AAO and Y92F, Y92L and Y92W

T (°C)	wild-type			Y92F	Y92L	T (°C)	Y92W
	^DK_d	$^{D2}K_d$	$^{D2}K_{dD}$	^DK_d	^DK_d		^DK_d
6	1.0 ± 0.2	1.9 ± 0.4	1.9 ± 0.2	1.8 ± 0.2	1.5 ± 0.2	12	1.1 ± 0.1
8	1.1 ± 0.0	3.2 ± 0.3	2.8 ± 0.3	1.7 ± 0.1	1.3 ± 0.0	16	0.9 ± 0.2
10	1.3 ± 0.1	2.4 ± 0.2	1.9 ± 0.1	1.6 ± 0.1	1.5 ± 0.1	20	1.1 ± 0.2
12	1.1 ± 0.1	2.2 ± 0.1	2.0 ± 0.1	1.7 ± 0.1	1.5 ± 0.1	25	1.1 ± 0.0
14	0.9 ± 0.2	1.5 ± 0.1	1.5 ± 0.3	1.7 ± 0.1	1.3 ± 0.1		

K_d constants measured with α-protiated and [α-$^2H_2$]-*p*-methoxybenzyl alcohols. (R)-[^{2}H]-*p*-methoxybenzyl alcohol was also used with the wild-type enzyme. KIE is estimated as the ratio between the constants obtained with protiated and deuterated substrate

5.2. Discussion

5.2.1. Involvement of tunneling in HT transfer for WT and Y92 AAO variants

The semiclassical model, which represents the over-the-barrier behaviour, predicts KIEs not larger than 7 and temperature-independent, that is, when the isotope effect on Arrhenius pre-exponential factors is negligible ($1.2 \geq A_H/A_D \leq 0.7$). Moreover, it postulates the difference in activation energies (ΔE_a) to be close to zero. Deviations from these premises can be better explained by a model in which the particle —H$^-$ in this very case— is transferred by a tunneling event (Knapp and Klinman 2002b).

In this regard, the obtained parameters for WT AAO reduction and steady-state kinetics suggest that tunneling plays a role in the transfer of H$^-$ from the pro-*R* position of the substrate to flavin N5 during the reductive half-reaction of AAO. Evidence for this assumption comes from the fact that $^Dk_{red}$ and $^Dk_{cat}$ values are higher than expected in a semiclassical approach when [α-$^2H_2$]-*p*-methoxybenzyl alcohol was used as a substrate, as well as deduced from A_H/A_D being much smaller than unity in steady-state kinetics and in the reduction with (*R*)-[α-$^2H_1$]-*p*-methoxybenzyl alcohol.

Surprisingly, the rapid-kinetics reactions with [α-$^2H_2$]-*p*-methoxybenzyl alcohol showed an almost negligible A_H/A_D that approaches unity, which is significantly different from the effect estimated with the monodeuterated substrate, as this revealed a substantial effect (two orders of magnitude smaller). Therefore, the temperature dependence of the primary $^{D}k_{red}$ was much higher than the combination of primary and secondary $^{D2}k_{red}$ (due to the isotopic substitution at both the pro-*R* and pro-*S* positions). In fact, the effect of the double deuteration of the substrate on the pro-*R* substitution ($^{D2}k_{redD}$) proved to be significant and to follow the opposite pattern to the $^{D}k_{red}$ (**Table 5.12**), that is, it increased with temperature. This $^{D2}k_{redD}$ values agree well with the secondary $^{D}k_{cat}$ previously reported for AAO when (*S*)-[α-$^{2}H_{1}$]-*p*-methoxybenzyl alcohol was employed as a substrate, which was 1.37 ± 0.02 (Hernández-Ortega et al. 2012c). Consequently, it can be concluded that the more independent $^{D}k_{red}$ estimated with the dideuterated substrate might be an artifact due to the presence of the second D atom bound to the Cα of the substrate, the same applying for the ΔE_a calculated for the reaction. Analogously, the estimated $^{D}k_{red}$ values are also inflated due to this secondary effect.

Table 5.12. Secondary KIE on the reduction (k_{red}) of wild-type AAO with α-deuterated *p*-methoxybenzyl alcohols

T (°C)	**KIE** (value ± S.D)
6	1.39 ± 0.02
8	1.41 ± 0.02
10	1.52 ± 0.02
12	1.60 ± 0.02
14	1.63 ± 0.08

k_{red} were calculate with (*R*)-[α-^{2}H] and [α-$^{2}H_{2}$]-*p*-methoxybenzyl alcohols. Secondary KIEs were estimated as the ratio between hydride transfer constants of monodeuterated or dideuterated substrates

Steady-state results further reinforce the above statements taking into account the values of $^{D}k_{cat}$,which reports on the HT/DT as well (Ferreira et al. 2009). Although these KIEs may be also slightly inflated by the presence of the second deuterated tag on the substrate, $^{D}k_{cat}$ values are high enough, very dependent on temperature, as deduced by the tiny A_H/A_D value; and ΔE_a is very high. This is also in agreement with the H^- tunneling below the estimated TST barrier.

5.2.2. Role of protein motions in HT and DT

The full tunneling model (Knapp et al. 2002) predicts that the protein motions play a key role in H tunneling (Nagel and Klinman 2009). Previous models failed to explain the high temperature dependence of KIEs and, thus, the full tunneling model seems suitable to explain the AAO behaviour, since it shows a highly temperature dependent KIE, as arisen from the small A_H/A_D, far from unity. As proposed by Sharma and Klinman (Sharma and Klinman 2008), the behaviour of

A_H/A_D may be indicative of the effect the environment has on tunneling efficiency in terms of approaching the donor and acceptor and, thus, reducing the transfer distance. There are two types of motions: i) passive dynamics, that help the enzyme-substrate complex attain a configuration that enables H tunneling, and ii) active dynamics, also known as "gating", which actively modulates the donor-acceptor distances for H transfer (Knapp et al. 2002).

In spite of the fact that, generally, native enzymes show almost temperature-independent KIEs due to the highly organized active sites they possess, WT AAO results point towards a H^- tunneling model in which active dynamics are critically involved in the reaction, similarly to what was found with monoamine oxidase B(Jonsson et al. 1994). This behaviour could be related to the wide range of similar compounds the enzyme is able to oxidize. Those would be able to achieve catalytically relevant positions that would further need DAD sampling for tunneling to occur. This statement comes from the fact that A_H/A_D displays a very small value, which is indicative of the higher temperature dependence of the reaction with the deuterated substrate. Since D wave function is smaller than that of H, it requires more DAD sampling for the D to attain a distance from which it can be tunneled to the acceptor. Moreover, the almost temperature independent value for ${}^{D}(k_{cat}/K_m)$ suggests that the AAO's active site has a highly pre-organized configuration that allows the substrate to position appropriately prior to H transfer, with no need of passive dynamics, as reported for choline oxidase (Fan and Gadda 2005).

The value of A_H/A_D close to unity estimated for the reduction reaction with [α-${}^{2}H_2$]-*p*-methoxybenzyl alcohol may be due to a different behaviour of the substrate to temperature. As discussed above, the ${}^{D2}k_{redD}$ effect tends to increase with increasing temperature, in contrast with the behaviour of ${}^{D}k_{red}$. This reflects the increase in stiffness of the substrate molecule as a consequence of the second isotopic substitution. Motions in the substrate molecule are also important to attain the tunneling distance between nuclei (Limbach et al. 2006). When temperature increases, so does gating contribution, thereby facilitating the D tunnel, thanks to the protein motions that reduce the DADs. It seems that temperature exerts smaller effects on the dideuterated molecule than on the monodeuterated one, due to the reduced mobility of its atoms. In this way, it is likely that tunnel contribution decreases or tends to switch from a mechanism in which active dynamics is predominant to another in which passive dynamics are more relevant.

5.2.3. Substitution of an active-site residue alters HT and DT

As discussed above, the configuration of the active site proved to be the cornerstone for HT and DT. The pre-organized structure of the cavity allows the correct positioning of the preferential substrate of the enzyme so that H can be easily tunneled to its acceptor. Therefore, disruption of this configuration could have even deleterious effects on the process. The mutated variants studied in this work correspond to substitutions of Y92. This residue was reported to be involved in establishing aromatic stacking interactions that allowed the substrate to attain a catalytically relevant position (Ferreira et al. 2015b).

Replacement of Tyr with Phe did not show any significant difference in HT and DT. It is probable, however, that these processes take place in a similar way as described for WT AAO. Since its reduction was measured only with [α-$^2H_2$]-*p*-methoxybenzyl alcohol, analogously for the results of WT AAO, it seems to transfer the particles switching from the active to the passive dynamics as predominant agents of the process. Nevertheless, it is likely that this observation be due to the abovementioned effect of the second isotopic substitution of the substrate and, thus, a mechanism in which gating is the main acting force, as proposed for WT enzyme, is involved as well.

Y92L and Y92W variants showed, in contrast, critical changes from the behaviour of the native enzyme. In this regard, although the reduction of Y92L was also measured with [α-$^2H_2$]-*p*-methoxybenzyl alcohol, it showed a very small A_H/A_D, as well as a big ΔE_a (the most significant among the four variants). Similar results were reported for soybean lipooxygenase upon reduction of the side chain of an active-site residue (Meyer et al. 2008). However, the reaction with the protiated substrate showed to be less temperature dependent than those for the other variants, as suggested by its smaller E_{aH} and A_H. This higher temperature dependence is indicative of the implications that environmentally-coupled motions have in relation to DT, since both E_{aD} and A_D increase compared to their counterparts. Substitution of the aromaticity with alkane side chain seems to promote H tunneling, but not D tunneling, probably because of the higher requirements in gating of the heavy isotope as well as the loss of proper packing of the active site. In any case, it seems that gating can compensate for this, otherwise, an increase in $^Dk_{red}$ should be significant (Kohen et al. 1999b).

Regarding the Y92W mutant, the introduction of a bulkier residue augments the rigidity of the active site, thereby impairing the gating contribution to catalysis. This assumption is a consequence of the virtually temperature independence of the measured $^Dk_{red}$, reflected by the similarity of the E_a for the reaction with protiated and deuterated buffer, as well as by the big value of A_H/A_D. These results do not indicate, however, that the mutation improves the configuration of the active site by eliminating the necessity of the gating contribution for catalysis, since k_{red} for this variant is reduced by almost 4-fold with regard to WT enzyme. Therefore, it is likely that introduction of Trp in the active site impairs the gating contribution. Consequently, the variant is forced to rely on passive dynamics to attain a tunneling relevant position for HT, which could be the reason why catalysis is impaired.

5.2.4. AAO structure fosters HT

Resolution of the crystallographic structure of AAO in complex with *p*-anisic acid (*p*-methoxybenzoic acid) has given insight into the position the substrate attains when bound at the enzyme's active site. Although it is not the actual substrate, but a product that act as a competitive inhibitor —most probably due to H bond between one of the O atoms of the carboxyl group and the Nε of His502—, its structure closely resembles that of the *p*-methoxybenzyl alcohol, and validates the computational prediction of the substrate migration and positioning into the active site previously reported (Hernández-Ortega et al. 2011a).

Comparison of the crystallographic structures of AAO alone (PDB 3FIM) and the complex shows minimal rearrangements in the residues directly involved in AAO catalysis, as well as in the whole protein. These findings reinforce the above statements of AAO active site being properly packed to offer the substrate a conformational-ready structure where it can bind for catalysis. In fact, the measured distance between the H bound to Cα in *p*-anisic acid molecule and its acceptor, FAD N5, is of 2.8 Å. However, this H is not in the same position as it is in the alcohol substrate, given that the presence of the two O atoms bound to Cα displaces H with regard to its position in the alcohol counterpart. In this way, the computational predictions, which proved to resemble the crystallographic structure of the complex, estimate a DAD of 2.4–2.5 Å. Such distances are appropriate to the HT transfer by tunneling, since motions in enzymes are said to foster even 2 Å distances transfers (Moser et al. 2010). By offering such a tight enzyme-substrate complex, AAO requires DAD sampling for HT, not necessitating passive dynamics that accommodate the substrate in a catalysis ready conformation.

6

Non-concerted hydrogen and proton transfers from AAO to dioxygen

In this chapter, *P. eryngii* AAO has been subjected to rapid kinetics experiments involving solvent, substrate and multiple kinetic isotope effect (KIE), and viscosity and pL (i.e. pH/pD) effects to unveil the nature and transfer mechanism of the said two H /H^+ during the oxidative half-reaction of the enzyme, and the possible involvement of transient species. The results obtained agree well with previous reports on the steady-state and transient-state oxidation process and, thus, shed additional light on the AAO mechanistics of O_2 reduction.

6.1. Results

6.1.1. Preparing reduced AAO

The aim of the present work is to investigate the reoxidative half-reaction of AAO by stopped-flow spectroscopic techniques using for the first time a stopped-flow spectrophotometer in a double-mixing mode and KIE studies. Reoxidation studies require that the enzyme be completely reduced by an electron-donor substrate, under anaerobic conditions that prevent turnover, before triggering reoxidation by mixing with buffer containing different O_2 concentrations. Consequently, the aim of the first experiment was to calculate the time the enzyme was meant to remain inside the so-called “ageing loop” of the stopped-flow apparatus to be reduced, after being mixed with equimolar amount of the alcohol substrate.

Four single-mixing experiments were set up, and the reaction of AAO and [α-$^1H_2$]-*p*-methoxybenzyl alcohol or [α-$^2H_2$]-*p*-methoxybenzyl alcohol, in both H_2O and D_2O buffers, was followed at 463 nm, the wavelength of the bound FAD band I (Ferreira et al. 2005). The estimated reduction times (**Table 6.1**) were, thus, the “ageing times” used throughout the experiments under each condition, unless otherwise stated. The reduction of the enzyme turned out to be a first-order reaction and showed a marked dependency on the isotopes present in the substrate, due to the reductive half-reaction being the rate-limiting step of the AAO catalytic cycle,(Hernández-Ortega et al. 2012c) and the large substrate KIE at the temperature used (12°C).

Table 6.1. Reduction times of AAO mixed protiated or dideuterated alcohol substrates **(1:1, *c:c*)** at 12 °C in H_2O or D_2O calculated by following the reaction spectrophotometrically in a stopped-flow apparatus

Alcohol substrate	Solvent	Ageing time (s)
[α-$^1H_2$]-*p*-methoxybenzyl	H_2O	1
	D_2O	1
[α-$^2H_2$]-*p*-methoxybenzyl	H2O	3
	D_2O	4

6.1.2. Reoxidation of AAO

Reoxidation was first studied at pH 6.0 with [α-$^1H_2$]-*p*-methoxybenzyl alcohol, the optimal pH for AAO catalysis and its preferential reducing substrate. Traces (at 463 nm) in **Figure 6.1** show that the AAO reoxidative half-reaction follows a biphasic pattern. As it can be seen, the first phase accounts for the main increase in absorbance and seems to be faster. This second phase becomes more evident at higher O_2 concentrations (**Figure 6.1**) since the first phase becomes faster, whereas the second one remains constant. Consequently, both phases separate due to their differential behavior towards the O_2 concentration.

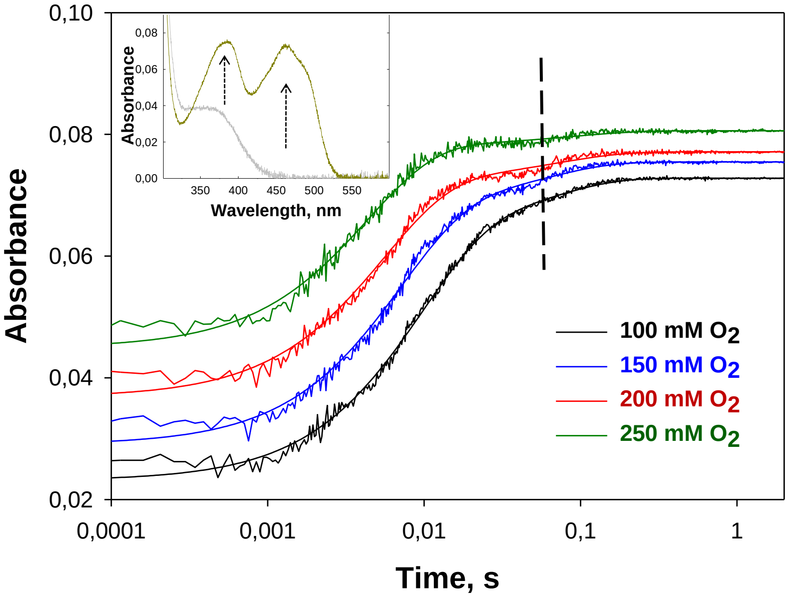

Figure 6.1. Time-resolved absorbance spectroscopy of the reoxidation of reduced AAO, which was premixed with *p*-methoxybenzyl alcohol (1:1 concentration) allowed to age for 1 s, at varying O_2 concentrations. Traces at 463 nm show the biphasic behavior of the reaction (first and second phase separation is shown by a vertical dashed line). Fits to exponential equations are shown. Inset shows spectra of the initial (reduced, black) and final (oxidized, red) flavin species.

The values of the k_{obs} for the first phase (k_{obs1}) were dependent on the O_2 concentration in a linear fashion that showed no signs of saturation. Fitting k_{obs1} to **equation 3** shows that the reoxidative half-reaction has an ${}^{app}k_{ox}$ of (7.7 ± 0.2) × 10^5 $M^{-1}\cdot s^{-1}$, as well as a k_{rev} of 27 ± 2 s^{-1} that corresponds to the intercept of the y-axis (**Figure 6.2A**). This ${}^{app}k_{ox}$value was similar to those previously reported using single-mixing assay (6.7 × 10^5 M^{-1} s^{-1}) and suggest that the presence of the aldehyde product at the active site does not affect the rate of protein reoxidation. Besides, the second phase proved to be independent of the O_2 concentration, and showed an invariable k_{obs2} of 17 ± 1 s^{-1} (**Figure 6.2B**) that is too slow to be relevant for the turnover.

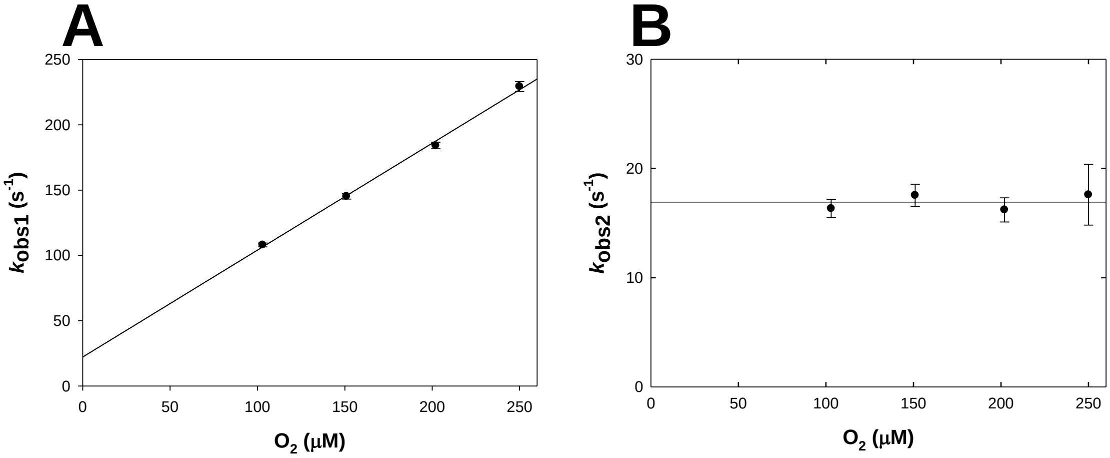

Figure 6.2. Plots of the O_2 dependency of the k_{obs} of the two phases of the reoxidation. **A.** k_{obs1} *vs* O_2 concentration showing its linear dependency. **B.** k_{obs2} *vs* O_2 concentration showing its independency. Values are shown as means and vertical lines are standard deviations. Average of the mean values in **B** is 17 ± 0.1 s^{-1}.

6.1.3. Solvent isotope and pL-related effects

Taking into account that one H atom and one H$^+$ (along with one electron) must be donated to O_2 so that it gets reduced to H_2O_2, KIEs were estimated to give insight into the mechanistics of the reoxidation of the enzyme. The first isotope experiments were carried out to determine whether there was a significant solvent isotope effect or not on the reoxidation of AAO. Reoxidation was then performed both in H_2O and D_2O buffers at pL 6.0. Surprisingly, the estimated $^{D_2O}(^{app}k_{ox})_H$, which represents the effect of the deuterated solvent on the rate constant, seemed to be close to unity (**Table 6.2**). Since effects determined when employing D_2O as a solvent may not be caused by the mass of the isotope, but by pH, as well as by the viscosity of the medium (D_2O is more viscous than H_2O), the following experiments aimed at ruling out these effects.

In order to determine whether pL 6.0 was such that the reaction proceeded in a pL-independent manner, reoxidation reactions were performed at pLs 5.0, 7.0 and 8.0, in both deuterated and protiated buffers, and the constants obtained compared to see if they met such a requirement. As shown in **Figure 6.3**, the log($^{app}k_{ox}$) at the various pH values were not statistically different. In fact, the mean of the log($^{app}k_{ox}$) was 5.8 ± 0.1.

Table 6.2. Substrate and solvent KIE at different pL values for the reoxidation of AAO at 12°C

pL	$^D(^{app}k_{ox})_{H_2O}$	$^{D_2O}(^{app}k_{ox})_H$	Viscosity effect^a
5.0	—	0.94 ± 0.13	—
6.0	1.46 ± 0.12	0.83 ± 0.05	1.02 ± 0.10
7.0	—	1.07 ± 0.13	—
8.0	1.65 ± 0.11	1.22 ± 0.11	—

^{a}Viscosity effects were calculated as the $^{app}k_{ox}$ measured at pH 6.0 in H_2O using [α-$^1H_2$]-*p*-methoxybenzyl alcohol over the $^{app}k_{ox}$ measured with the same substrate and aqueous buffer containing 7.3% glycerol.

Although no large solvent isotope effect was detected, a trend was noticeable (**Table 6.2**). At pL 5.0 and 6.0, the ${}^{D_2O}({}^{app}k_{ox})_H$ values were even smaller than 1, while there seemed to be a slight increase at higher pLs. In fact, estimated ${}^{D_2O}({}^{app}k_{ox})_H$ at pL 7.0 was of 1.1 ± 0.1 and it attained the value of 1.2 ± 0.1 at pL 8.0. Interestingly, at pH 6.0 the intersection of the y-axis, thus the k_{rev}, tended to 0 (not shown), indicating that the probable reversible reaction detected when using H_2O was negligible in the deuterated solvent. Instability of the enzyme prevented the experiments at either more acidic or more basic pLs.

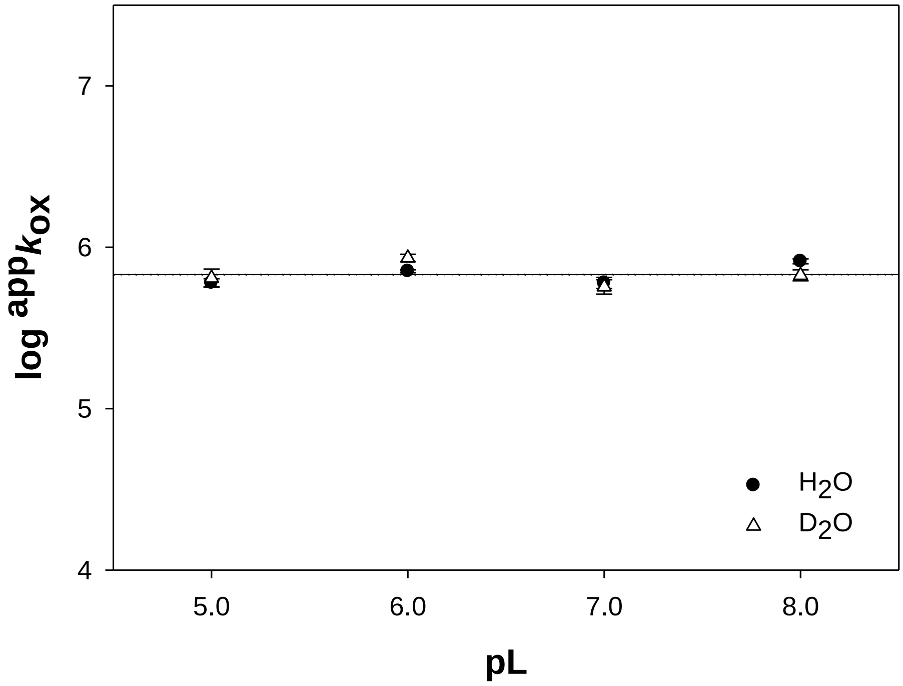

Figure 6.3. pH (filled circles) and pD (open triangles) contributions to solvent effects on ${}^{app}k_{ox}$. Values shown are means and vertical lines indicate standard deviations. Average of the log ${}^{app}k_{ox}$mean values in both H_2O and D_2O is 5.8 ± 0.1.

Moreover, it was necessary to rule out any viscosity effect in the reaction. Therefore, reactions were performed in buffer containing 7.3% glycerol (mimicking D_2O viscosity at 12°C). The viscosity effect at pH 6.0 was negligible (**Table 6.2**). Moreover, there was no effect on the y-axis intercept of the fit, showing a k_{rev} value of 22 ± 7 s^{-1}, not statistically different from the value obtained at pH 6.0.

The spectrum of the reoxidized enzyme at pH 5.0 appears to be significantly different than spectra recorded at more basic pLs, due to the protonation of one group in the active site. It displayed a shifted band I maximum (at 456 nm rather than at 463 nm) and the flavin band II peak (around 380 nm) appeared to be notably lower than that of flavin band I (**Figure 6.4**). In spite of such spectral changes, the mechanism of the reoxidation seemed to be the same at different pHs.

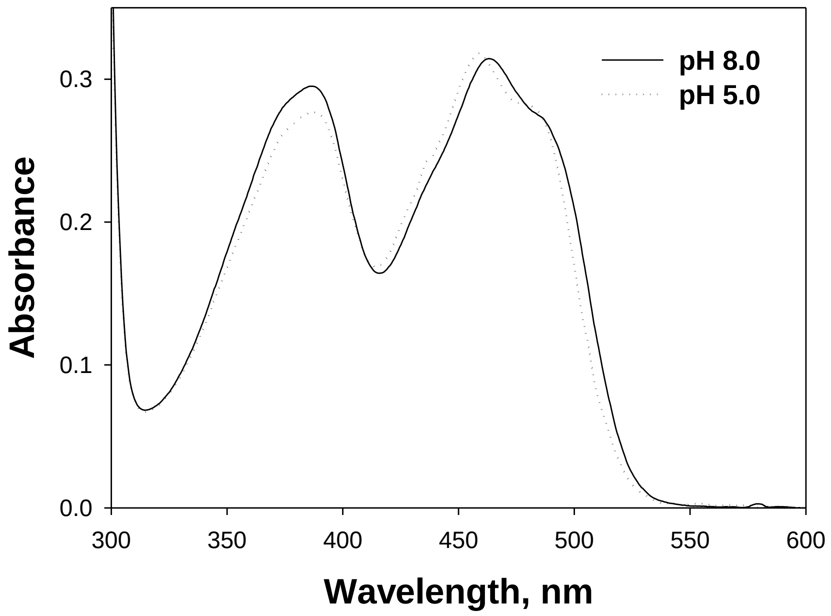

Figure 6.4. Spectra of wild-type AAO in sodium phosphate 25 mM pH 8.0 (solid line) and sodium acetate 100 mM pH 5.0 (dotted line). Differences in the shoulder around 500 nm and the ratio band I/band II are shown.

6.1.4. Substrate isotope effects

In order to determine if any of the detected phases corresponded to the breakage of the flavin N5-H bond, experiments were carried out in which the enzyme was first reduced using [α-$^2H_2$]-*p*-methoxybenzyl alcohol and then reoxidized using different O2 concentrations. It was previously described that the pro-*R* hydrogen bound to the α-carbon of the alcohol is abstracted as a hydride by the N5 of the flavin, assisted by His502, during the reductive half-reaction of the enzyme (Hernández-Ortega et al. 2012c). If this hydride remains bound to the N5 until the enzyme is reoxidized without being washed out by the buffer (i.e. it does not exchange rapidly with the solvent), a KIE should be evident. Experiments were performed both at pHs 6.0 and 8.0. For both pHs, the $^{D}(^{app}k_{ox})_{H_2O}$ effects were significantly greater than 1 (**Table 6.2**). Moreover, the similar substrate KIE observed at both pH values rule out a pH effect on the H transfer in H_2O buffers within the investigated range (pH 6.0–8.0).

6.1.5. Individual and multiple isotope effects at pL 8

Since the tendency towards the existence of a solvent $^{D_2O}(^{app}k_{ox})_H$ effect at increasing pH values was evident, individual and multiple isotope effects were estimated at pL 8.0 to establish whether or not the H and H$^+$ were transferred in the same chemical step. The $^{D}(^{app}k_{ox})_{H_2O}$ was statistically equal to that measured at pH 6.0, indicating that there existed no pH effect on the breakage of the bond between N5 of the flavin and the H or the D atoms. The $^{D_2O}(^{app}k_{ox})_H$ value at pL 8 was 1.2 ± 0.1, which is a small, but significant effect. The values of the constants for all the conditions assayed are given in **Table 6.3**.

Table 6.3. Kinetic parameters for the reoxidation of AAO with protiated (H) and deuterated (D) *p*-methoxybenzyl alcohol in protiated and deuterated solvents at different pLs and 12°C

pL	**Substrate, solvent**	$^{app}k_{ox}\times 10^5$ ($M^{-1}\cdot s^{-1}$)	k_{rev} (s^{-1})	k_2 (s^{-1})
5.0	H, H_2O	6.0 ± 0.4	16 ± 4	n.d.
	H, D_2O	6.4 ± 0.7	0	0
6.0	H, H_2O	7.7 ± 0.1	27 ± 2	17 ± 1
	H, D_2O	8.6 ± 0.5	0	0
	D, H_2O	5.3 ± 0.3	0	0
7.0	H, H_2O	6.0 ± 0.5	34 ± 5	n.d.
	H, D_2O	5.6 ± 0.5	0	0
8.0	H, H_2O	8.2 ± 0.3	22 ± 5	16 ± 3
	H, D_2O	6.7 ± 0.5	34 ± 10	17 ± 5
	D, H_2O	5.0 ± 0.3	0	0
	D, D_2O	5.4 ± 0.4	0	0
Glycerol (pL 6.0)	H, H_2O	7.3 ± 3.3	17 ± 3	17 ± 1
	H, glyc	7.1 ± 0.6	22 ± 7	16 ± 2

Interestingly, the multiple $^{D,D_2O}(^{app}k_{ox})$ value, which is the effect due to the substitution of p-methoxybenzyl alcohol with α-[$^2H_2$]-*p*-methoxybenzyl alcohol and H_2O with D_2O simultaneously, was similar to the value obtained for $^{D}(^{app}k_{ox})_{H_2O}$ and slightly lower than the product of both kinetic and solvent KIEs ($^{D}(^{app}k_{ox})_{H_2O}$ × $^{D_2O}(^{app}k_{ox})_{H}$) and suggests non-concerted H and H$^+$ transfers. Moreover, the $^{D_2O}(^{app}k_{ox})_{D}$ effect, which reflects the effect of the D_2O on the reaction with α-[$^2H_2$]-*p*-methoxybenzyl alcohol, is very close to unity. This indicates that the transfer of H from flavin to O_2 is the overall rate-limiting step of the reaction regardless of the solvent isotopic composition, meaning that substrate and solvent effects are not additive.

Table 6.4. KIE on the second-order rate constant for flavin oxidation at pL 8.0

KIE	**mean ± S.D.**
$^{D}(^{app}k_{ox})_{H_2O}$	1.65 ± 0.11
$^{D}(^{app}k_{ox})_{D_2O}$	1.24 ± 0.14
$^{D_2O}(^{app}k_{ox})_{H}$	1.22 ± 0.11
$^{D_2O}(^{app}k_{ox})_{D}$	0.92 ± 0.09
$^{D,D_2O}(^{app}k_{ox})$	1.51 ± 0.13
$^{D}(^{app}k_{ox})_{H_2O}$ × $^{D_2O}(^{app}k_{ox})_{H}$	2.01 ± 0.22

Measurements were carried out in 25 mM Na phosphate pH 8.0 at 12°C

Furthermore, $^{D}(^{app}k_{ox})_{D_2O}$, i.e. the effect of the heavy substrate on the reactions performed in D_2O,is greater than 1, but smaller than the $^{D}(^{app}k_{ox})_{H_2O}$ effect, so it points out again the fact that it is the substrate effect the one that predominates on catalysis, being larger than solvent effect (**Table 6.4**).

6.1.6. Presence of intermediate species

The stabilization of transient intermediate species involved in the catalytic mechanism of AAO oxidative half-reaction was further investigated at several wavelengths and at pH 5.0 and 8.0, fearing that different pHs could rule different mechanisms and, thus, the change could evidence intermediates. Due to the probable transient nature of such species, temperature of the experiments was lowered to 7°C.

Special attention was paid to traces at 340/540 and 370/390 nm, since they are typical of semiquinones and C4a-(hydro)peroxyflavin, respectively. However, shots every 10 nm from 300 to 540 nm did not show any intermediate, i.e. formation and disappearance of a spectroscopic species at either pH (**Figure 6.5**).These results are in agreement to those previously observed at pH 6 and using a stopped-flow spectrophotometer in a single-mixing mode. That means that, despite the existence of intermediates is obligated for the catalysis with O_2 to occur (Massey 1994), they cannot be seen under our experimental conditions.

6.1.7. Wash-out of the hydrogen bound to flavin N5

Evidence suggests that the hydride abstracted from the *pro*-R position of the alcohol substrate is transferred firstly to the N5 of the flavin and from this position to the O_2. Nonetheless, this position could be subjected to exchange with protons present in the buffer. In that case, the estimated $^{D}(^{app}k_{ox})_{H_2O}$ would tend to disappear with time due to increase in rate if exchange took place.

In order to check if the wash-out of the deuterated tag by the protiated buffer happened, an experiment was made in which AAO was reoxidized after different ageing times (3, 40, 150, 300 and 600 s) to see if the rate constants for the reoxidation increased at higher times (**Figure 6.6**). As ageing time increased, so did the k_{obs1} measured at 463 nm, most probably due to the exchange of the D with H coming from the aqueous buffer. The longest ageing time was 600 s, which corresponded to the longest ageing time the stopped-flow apparatus allowed to be set. The corresponding k_{obs1} fitted at different times were plotted *vs* time and fitted to an exponential equation (R^2 = 0.99), which showed that the k_{obs1} at t = 0 was 58 ± 1 s^{-1}, whereas the rate constant for deuterated tag loss was of 0.003 s^{-1}, which indicates the increase in k_{obs1} in time. At 600 s, the estimated k_{obs1} was half of that measured using protiated substrates under the same conditions. Therefore, it is estimated that the half life of the deuterated tag on flavin N5 at 12°C is 600 s.

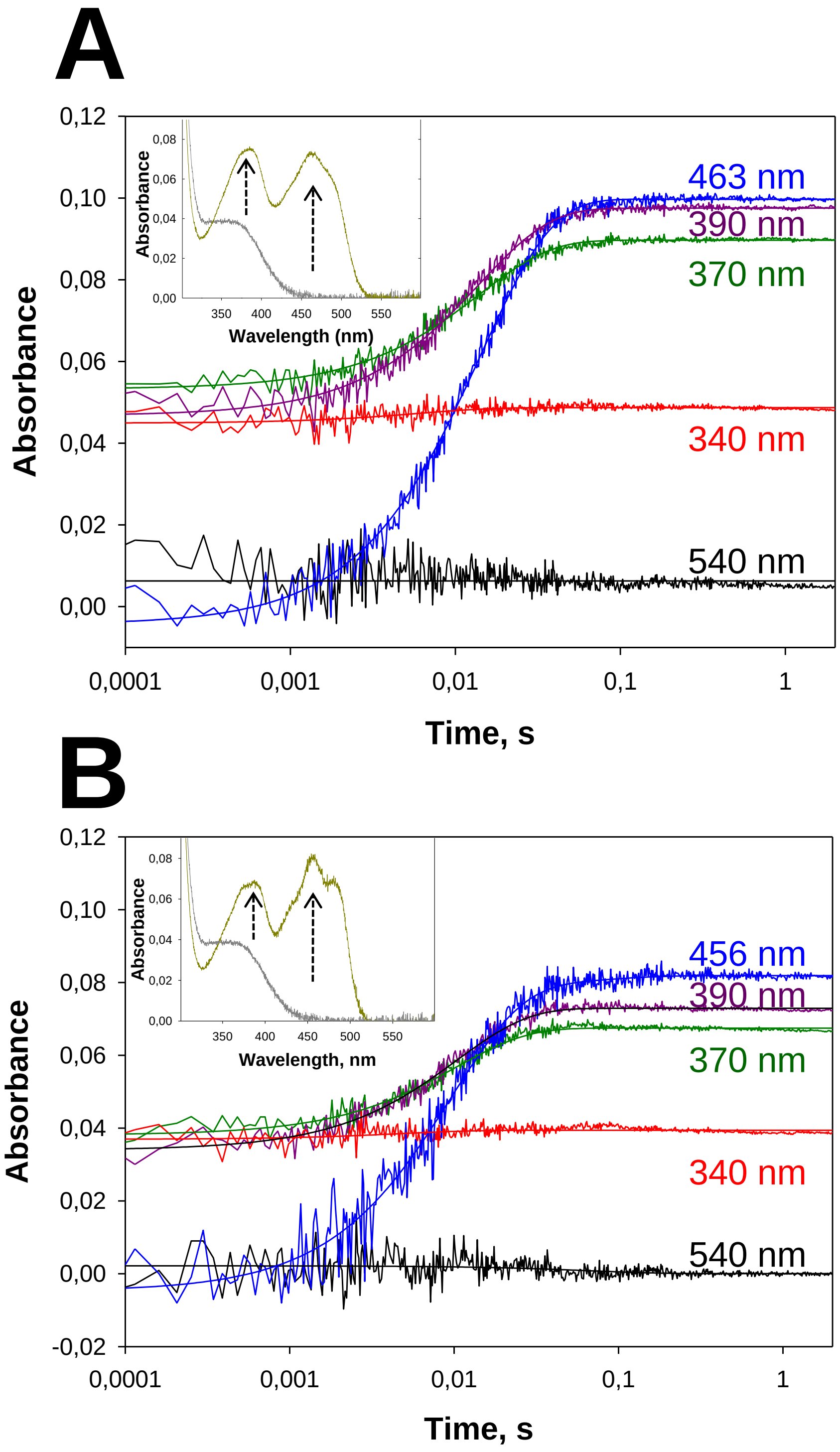

Figure 6.5. Traces showing the reoxidation of AAO (7ºC, pH 8.0 and 5.0) at different wavelengths characteristic of possible intermediates in the reaction. **A.** Reaction in 25 mM sodium phosphate, pH 8.0. **B.** Reaction in 100 mM sodium acetate, pH 5.0. Insets show the spectra of the reduced and oxidized species of the enzyme with arrows indicating the direction of the spectral changes. Lack of transient species points out the absence of any detectable intermediates. Fits to exponential equations are shown under the spectral evolution changes.

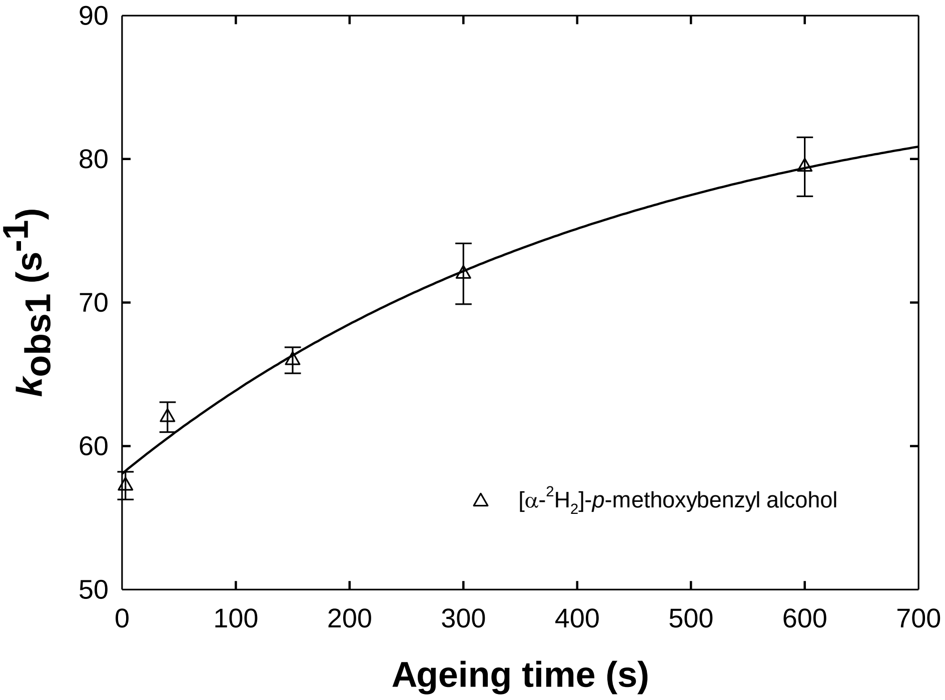

Figure 6.6. Plot of the values of k_{obs1} as a function of the time of incubation after reduction of the enzyme using [α-$^2H_2$]-*p*-methoxybenzyl alcohol in aqueous buffer, which was fitted to an exponential function yielding $y = 58 + 29 \times (1 - e^{-0.003 \times t})$ ($R^2 = 0.99$). There is an evident tendency towards the increase of the values, indicating the gradual loss of the deuterated tag on flavin N5 by exchange with the solvent. Means and standard deviations.

6.2. Discussion

6.2.1. The AAO catalytic cycle

Reoxidation of the flavin cofactor in AAO and other flavooxidases takes place concomitantly to the reduction of O_2 to H_2O_2, in a stepwise reaction that involves the transfer of a total of two electrons and two protons. In this work, KIEs, along with pL effects, have been employed to unravel the nature and relative timing of the transfer of these particles using the stopped-flow technique. Utilization of deuterated substrates gives insight into the breakage of the bond between flavin N5 and the H that has previously been abstracted from the alcohol substrate as a hydride; whereas isotopically substituted solvents shed light on the involvement of species originating from the solvent itself or a solvent exchangeable site.

The catalytic cycle of AAO is composed of two half-reactions. During the reductive half-reaction, FAD is reduced owing to the oxidation of the alcohol substrate to aldehyde. Afterwards, the reoxidative half-reaction takes place when the enzyme donates to O_2: i) one electron; ii) one H atom, supposed to originate from the hemolytic breakage of the flavin N5-H bond; and iii) one H^+ from a solvent exchangeable site, which can be the same catalytic His502 involved in the reductive half-reaction.(Hernández-Ortega et al. 2012c) It is the reductive half-reaction, in particular the H^- abstraction from the substrate, the overall rate-limiting step of the enzyme's catalysis, as deduced from the large second-order rate constants estimated for flavin oxidation (much higher than k_{cat}) as well as the coincidence between the observed k_{red} and k_{cat} (Hernández-Ortega et al. 2012c).

When the reoxidative half-reaction was investigated, the whole process turned out to be split into two distinct phases. The biphasic nature of AAO reoxidation had already been reported in literature for the native AAO and its F501Y and F501W variants (Hernández-Ortega et al. 2011b). Interestingly, non-aromatic substitutions of Phe501 showed monophasic reoxidation processes, suggesting the involvement of an aromatic residue of the *re*-side of flavin in the appearance of the two phases. Another GMC oxidase, P2O, was found to display a biphasic behavior as well (Sucharitakul et al. 2008), whereas many others —such as glucose oxidase, glycolate oxidase (Pennati and Gadda 2011) or fructosamine oxidase (Collard et al. 2011)— exhibit monophasic reoxidation.

The second-order rate constant for the first phase in AAO reoxidation is within the typical range for oxidases and around 3000-fold higher than the rate of the reaction between free flavin and O_2 (Mattevi 2006). The amplitude of the second phase accounts for a small portion (up to 15%) of the total amplitude, and its rate constant is independent of the O_2 concentration. Therefore, the species formed after the first phase must not be considered as an intermediate of the reaction, but as the reoxidized enzyme. In fact, the second phase must not be relevant for catalysis because its rate constant at 12°C (17 ± 1 s^{-1}) is much smaller than the AAO k_{cat} (129 ± 5 s^{-1}) (Ferreira et al. 2015b). This second phase could be a consequence of either the release of the product or an isomerization of the flavin. Such second phases not directly involved in catalysis have also been described in the reductive half-reaction of putrescine oxidase (Kopacz et al. 2014) or the reoxidative half-reaction of mutated variants of fructosamine oxidase (Collard et al. 2011). Therefore, all the results on AAO reoxidation discussed below correspond to the first phase.

6.2.2. H transfer limits the reoxidation reaction in AAO

In the light of the above results, the first reoxidation phase must account for both the breakage of the flavin N5-H bond, and the H and H^+ transfers. Evidence for this comes from the fact that a substrate $^{D}(^{app}k_{ox})_{H_2O}$ (due to deuterated alcohol used for AAO reduction) was evident. However, the fact that no solvent effects are noticeable at pH 5.0 and 6.0, as has been proved for glucose oxidase (Bright and Gibson 1967), indicate that H transfer is the rate-limiting step of the reoxidative half-reaction. Therefore, it is the same particle, transferred as a H^- during the reductive half-reaction and as a H during the reoxidative one, that limits the rates of both half-reactions. These rapid kinetics results agree with previous results from AAO steady-state kinetics (Hernández-Ortega et al. 2012c). Similarly, no significant solvent effect on the reoxidation efficiency —$^{D_2O}(k_{cat}/K_{mO_2})_H$ of 1.07 ± 0.05— was found at pH 6.0. Furthermore, at the same pH, a reducing substrate

KIE on the reaction with O_2 —$^{D}(k_{cat}/K_{mO_2})_{H_2O}$ of 1.57 ± 0.04— was reported, being very similar to that found here on the second-order apparent rate constant for flavin reoxidation (1.46 ± 0.12).

The existence of a significant $^{D}(^{app}k_{ox})_{H_2O}$ suggested that the D transferred from the deuterated alcohol substrate to the flavin N5 did not exchange rapidly with the solvent protons. However, in [α-$^2H_2$]-*p*-methoxybenzyl alcohol and protiated buffer experiments, the longer the ageing times were, the higher the k_{obs} became. Such increase in k_{obs} must be due to the replacement of the D bound to the N5 with H originating from the solvent. In fact, the estimated half life of this isotopically labeled flavin was around 600 s, which indicates that the exchange takes place slowly, showing a rate of exchange of around (2.5 ± 0.4) × 10^{-2} s^{-1}. The estimated rate constant for the exchange of H from N5 of free FMN was estimated of 525 s^{-1} (Macheroux et al. 2005).

This reduced exchange rate is due to the closeness of the active site of the enzyme, which is separated from the environment by: i) a loop characteristic of the AAO family that limits the access to the active site (Ferreira et al. 2015a); and ii) by a triad of aromatic residues (Tyr92, Phe397 and Trp501) that create a highly hydrophobic bottleneck isolating the active site from the outer environment, as crystallographic data reveal (Fernández et al. 2009). Another flavoenzyme, P2O, displays even smaller exchange rates (3.5 × 10^{-3} s^{-1}) due to its enclosed active site away from the solvent (Sucharitakul et al. 2011).

6.2.3. Isotope effects (at high pL) reveal non-concerted H and H^+ transfers

While investigating $^{D_2O}(^{app}k_{ox})_{H}$ at different pL values, an interesting fact came up. Although the solvent effect was negligible at pL 5.0 and 6.0, it showed an increasing trend with increasing pH. At more basic pLs, when H^+/D^+ availability is lower, there seems to be a combined effect with the isotopically substituted solvent so that the effect becomes noticeable. Therefore, investigation at more basic pLs is more informative than at more acidic ones.

Estimation of individual and multiple KIEs at pL 8.0 sheds additional light on the transfer of both H and H^+. On the one hand, at pL 8.0 there is a $^{D}(^{app}k_{ox})_{H_2O}$ significantly greater than 1 and, on the other hand, a small, yet significant, $^{D_2O}(^{app}k_{ox})_{H}$ is evident. Since $^{D}(^{app}k_{ox})_{H_2O} > {}^{D_2O}(^{app}k_{ox})_{H}$, it can be deduced that, at pL 8.0, the H (after N5-H bond breakage) and H^+ transfers are independent steps. This is in agreement with the fact that $^{D}(^{app}k_{ox})_{H_2O}$ is invariable throughout a pL range (at least 6.0 to 8.0), whereas $^{D_2O}(^{app}k_{ox})_{H}$ is only greater than 1 at higher pLs (at more acidic pL is the H transfer which limits reoxidation, as explained above).

Moreover, $^{D}(^{app}k_{ox})_{D_2O}$, which measures the contribution of the deuterated substrate on the reactions performed in heavy solvent, is greater than 1. This is indicative of the solvent effect not possessing enough limiting capacity to lower the rate constants as much as the substrate effect has. Even the estimations of $^{D_2O}(^{app}k_{ox})_D$, i.e. the effect of performing the reaction in D_2O when employing [α-$^2H_2$]-*p*-methoxybenzyl alcohol as reducing substrate, is completely negligible. The latter means that, when the heavy substrate limits the reaction, the solvent cannot slow it down any further.

Finally, the fact that the product of the isolated effects —$^{D}(^{app}k_{ox})_{H_2O}$ × $^{D_2O}(^{app}k_{ox})_H$— is higher than the $^{D,D_2O}(^{app}k_{ox})$, which represents the effect of performing the reaction in D_2O and reducing the enzyme with deuterated substrate simultaneously, indicates that both transfers occur as different chemical steps and are, thus, non-concerted. This is opposed to the transfer of H^- and H that takes place during the reductive half-reaction of the enzyme. In that case, both transfers are concerted, although asynchronous. The flavooxidase choline oxidase proved to transfer both the H and $H^+$to O_2 in a concerted manner in the same chemical step, as arisen from the studies of multiple isotope effects on k_{cat}/K_{ox} (Gannavaram and Gadda 2013).

Results exposed above demonstrate that transfers of H and H^+ to O_2 take place in separate kinetic steps and, thus, suggest that there could be intermediate species during reoxidation of AAO. However, thorough examination of traces at different wavelengths revealed that no intermediate was spectroscopically detectable at both pH 5.0 or 8.0 (at 7°C). The reason for performing the experiments at different pHs was that P2O is said to switch from one reoxidation mechanism in which the C4a-(hydro)peroxyflavin is formed to another in which the intermediate is undetectable due to pH (modifying the protonation state of a group with a pK_a of 7.6) (Prongjit et al. 2013). No differences, however, were seen on the reoxidation of AAO at different pHs. Moreover, in the case a C4a-peroxyflavin were formed, it should accumulate when the deuterated solvent and substrate were used, as well as when the pD effect could be noticeable, at pH 8.0. Nevertheless, under such conditions, examination of traces at 390 and 370 nm did not reveal stabilization of such an intermediate.

7

5-Hydroxymethylfurfural conversion by fungal aryl-alcohol oxidase and unspecific peroxygenase

In this chapter we describe that AAO is able also to oxidize some furanic compounds such as HMF and DFF to FFCA (**Figure 7.1**). This is not only an important scientific finding, given the structural differences with previously known AAO substrates, but also of biotechnological relevance due to the importance of these renewable chemicals described above. AAO was combined with an unspecific peroxygenase (UPO, EC 1.11.2.1) from *Agrocybe aegerita* (Ullrich et al. 2004) for the full oxidative conversion of HMF in an enzymatic cascade. This peroxygenase belongs to the only recently-established superfamily of heme-thiolate peroxidases and is capable of incorporating peroxide-borne oxygen into diverse substrate molecules (Hofrichter and Ullrich 2014). Among others, it catalyzes the H_2O_2-dependent stepwise hydroxylation of aliphatic and aromatic alcohols into the corresponding aldehydes (via *gem*-diol intermediates) and finally into carboxylic acids (Ullrich and Hofrichter 2005; Gutiérrez et al. 2011).

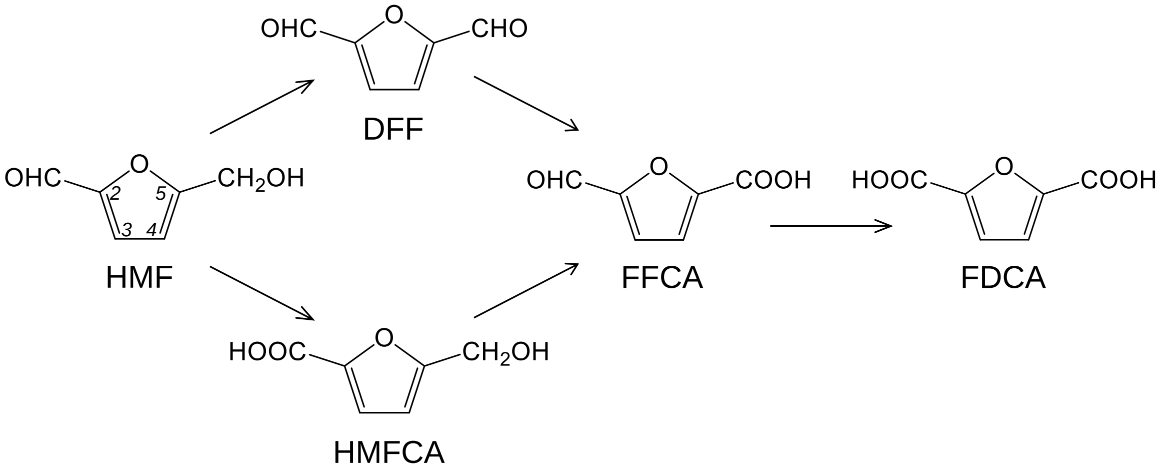

Figure 7.1. Pathway for 5-hydroxymethylfurfural (HMF) conversion into 2,5-furandicarboxylic acid (FDCA), *via* 2,5-formylfurancarboxylic acid (FFCA), including 2,5-diformylfuran (DFF) or 2,5–hydroxymethyl furancarboxylic acid (HMFCA) intermediates.

7.1. Results

7.1.1. AAO oxidation of HMF and its partially-oxidized derivatives

The ability of fungal AAO to oxidize HMF and its partially-oxidized derivatives (HMFCA, DFF and FFCA) was tested by incubating them with the enzyme, typically, in 24-h experiments. Then, all the compounds present in the reaction mixture at different times (that is, remaining substrate and products) were analyzed by GC-MS, after trimethylsilyl (TMSi) derivatization of the alcohol and carboxylic groups, and the corresponding molar percentages were estimated (MS identification of the different compounds present in these and other enzymatic reactions is described in **Annex 3**).

When AAO was incubated with HMF at pH 6 (the optimal pH for the enzyme) nearly all HMF had been converted into FFCA (98% molar percentage) after 4 h, and very little FDCA was formed (Figure 6.2A). As time passed, FFCA slowly decreased due to formation of some FDCA (6% after 24 h). Interestingly, neither DFF nor HMFCA were detected in the analyses. These results showed that AAO is able to oxidize HMF, as well as DFF and/or HMFCA considering that these two compounds are obligate intermediates in the pathway from HMF to FFCA. With the aim of revealing which pathway is more likely to be followed (**Figure 7.1A**), DFF was put together with AAO to test the ability of the enzyme to oxidize it, and the reaction compounds were analyzed (**Figure 7.2B**).

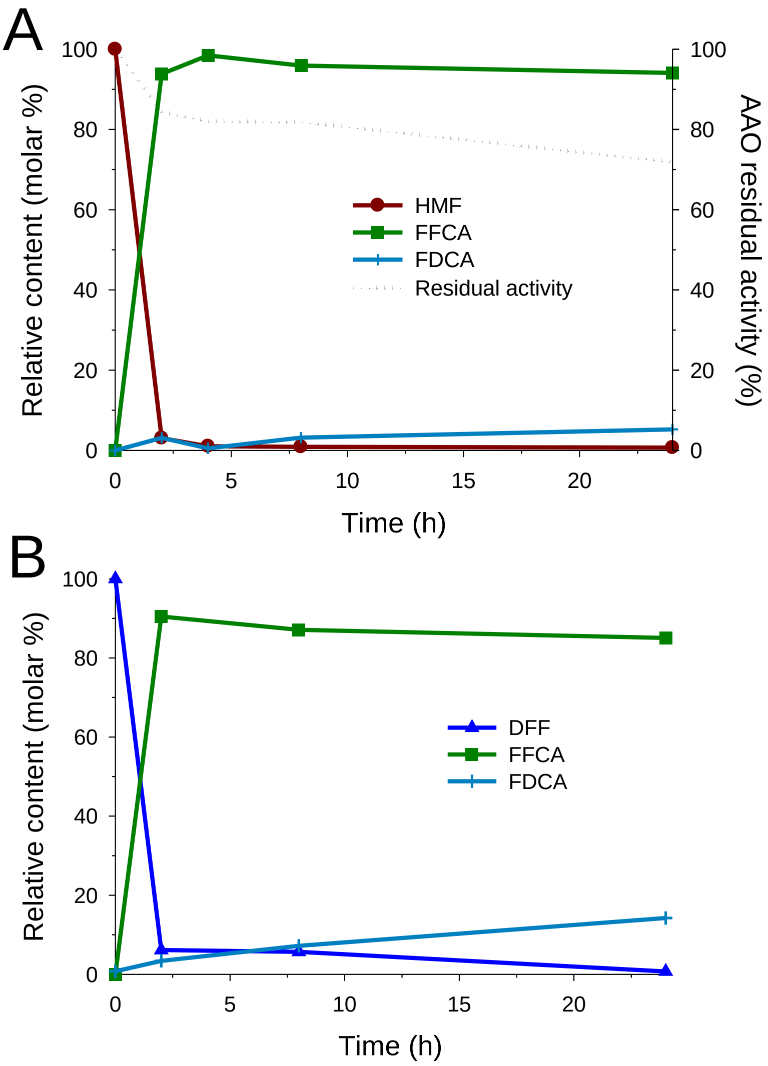

Figure 7.2. HMF and DFF transformation by *P. eryngii* AAO. (**A**, **B**) HMF and DFF (3 mM), respectively, treatment (5 mL) with AAO (5 µM, corresponding to 54 U measured with veratryl alcohol) yielding 90-98% FFCA after 4 h, which was then slowly oxidized to FDCA (6-10% after 24 h). The AAO residual activity is also shown in **A**.

Similarly to what had been seen with HMF, after 2 h of incubation almost 90% FFCA and only 3% FDCA were detected, and these percentages slightly changed during the subsequent incubation (around 10% FDCA after 24 h). On the contrary, when HMFCA was incubated with AAO, no product formation was observed. The above reactions took place during long-time incubations (24 h) at room temperature. In order to test whether or not the enzyme was active throughout the complete reaction time, its residual activity was determined. The main activity decrease during HMF conversion by AAO (**Figure 7.2A**) occurred during the first two hours, dropping from initially 100% to 84%. Between hours 2 and 24, the AAO activity slowly further decreased, but maintaining 71% of its activity in the end. These results demonstrate that the enzyme was catalytically active over the whole experiment, in spite of the loss of some activity.

7.1.2. AAO kinetic parameters for HMF and its partially-oxidized derivatives

Having seen that HMF was converted into several products by AAO, the kinetic parameters of the enzyme for the different potential substrates (HMF, DFF, HMFCA, and FFCA) were estimated in 3-min reactions by H_2O_2 release, measured in a peroxidase-coupled assay (**Table 7.1**). HMF proved to be the best AAO substrate in terms of catalytic efficiency, although the k_{cat} for DFF was higher. In contrast, HMFCA turned out to be a bad substrate of AAO. Although some AAO activity was revealed by H_2O_2 formation, it was impossible to work out the kinetic parameters since no enzyme saturation by HMFCA was observed, and only a k_{obs}/concentration value was calculated. Thus, it is likely that the reaction of HMF to FFCA proceeds *via* the formation of DFF from HMF (upon oxidation of the alcohol group) and then, one aldehyde group is further oxidized to a carboxylic group, which is in agreement with the GC-MS results (see below). Regarding FFCA, no activity could be detected in the kinetic study.

Table 7.1. Kinetic parameters for HMF, DFF, FFCA and HMFCA oxidation by AAO (estimated from H_2O_2 formed)

Substrate	Structure	K_m (mM)	k_{cat} (min^{-1})	k_{cat}/K_m (min^{-1}·mM^{-1})
HMF	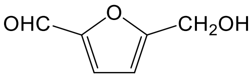	1.6 ± 0.2	20.1 ± 0.6[a]	12.9 ± 1.2[a]
DFF	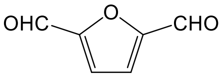	3.3 ± 0.2	31.4 ± 0.7	9.4 ± 0.5
HMFCA	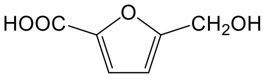	-	-	1.0 ± 0.1[b]
FFCA	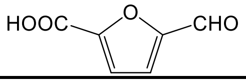	0	0	-

[a] Values corrected taking into account that two H_2O_2 equivalents are formed in two successive oxidations to convert HMF into FFCA (as shown by GC-MS). [b]AAO was not saturated at increasing HMFCA concentrations and only a k_{obs}/concentration value could be obtained

In order to confirm which products were formed in the above kinetic studies, the reaction mixtures were analyzed by GC-MS. It turned out that, during 3-min of HMF incubation with AAO, FFCA is formed with the concomitant decrease of HMF. As in the case of the 24-h reactions, no DFF and only traces of HMFCA were detectable (after 30 s, 1 min and 3 min reaction). Therefore, the H_2O_2 estimated in the HMF reactions corresponds to two subsequent oxidations steps performed by AAO (from an alcohol group to a carboxylic group); and the corresponding correction was introduced for k_{cat} estimation in **Table 7.1**. In the case of DFF, the product formed during the 3-min incubation was FFCA, as expected, accompanied by a decrease of DFF.

In the light of all the above results, we propose that the oxidative pathway leading from HMF to FFCA may proceed *via* the formation of DFF that is rapidly oxidized to FFCA. AAO shows very low activity towards HMFCA and, if formed, it should have accumulated and then been detectable by GC-MS.

7.1.3. Oxidation of FFCA's aldehyde group by H_2O_2

Since no activity of AAO on FFCA was observed and low but significant amounts of FDCA were detected in the reaction mixtures with HMF and DFF, its formation remained unclear. H_2O_2 is a strong oxidant, and hence its possible involvement in (chemical) FFCA oxidation was taken into consideration (H_2O_2 is formed by AAO in stoichiometric amounts *via* O_2 reduction). To prove this possibility, FFCA (3 mM) was incubated with 6 mM H_2O_2, the maximal concentration that could have been produced by AAO during HMF oxidation to FFCA, for 24 h and the reaction was analyzed by GC-MS. The amount of FDCA formed (11%) was in fact in the same range as that obtained in the reactions of HMF and DFF with AAO (6-10%) and strongly supports the above made assumption of a chemical oxidation of FFCA into FDCA by AAO-derived H_2O_2. This was additionally confirmed by the fact that a higher H_2O_2 concentration (200 mM) resulted in a higher amount of formed FDCA (84%).

7.1.4. Fungal peroxygenase for HMF conversion

Because AAO was seemingly not able to oxidize FFCA into FDCA, we tested the ability of a second fungal enzyme, *A. aegerita* UPO, to catalyze the reaction. UPO needs H_2O_2 as co-substrate to carry out the desired oxidation and AAO produces it by reducing O_2, so the former enzyme may benefit from the activity of the latter.

First, we followed by GC-MS the oxidation of HMF by UPO, in the presence of exogenous H_2O_2, to get an idea of how the conversion proceeds with this enzyme. Opposite to that observed for AAO, the UPO reaction was found to start with the oxidation of the HMF carbonyl group yielding HMFCA (72% after 8 h, enabling to estimate a turnover rate of 7 min^{-1}, and 97% in 24 h). Then, HMFCA was converted into FFCA (up to 50%) and some FDCA (up to 10%). The latter conversion was confirmed by FFCA treatment with UPO forming FDCA (**Figure 7.3**), although the reaction was much slower than observed with HMF, and 96 h were required to attain 90% conversion (~80% conversion in 72 h, enabling to estimate a turnover rate of 0.9 min^{-1}).

The oxidation of FFCA was catalyzed by UPO, and was not the result of the H_2O_2 added, since only 10% FDCA was obtained in the controls without enzyme (in agreement with previous results). As in the case of AAO, UPO maintained most activity (over 90%) during the 24-h reaction, and more than 50% activity after 120 h.

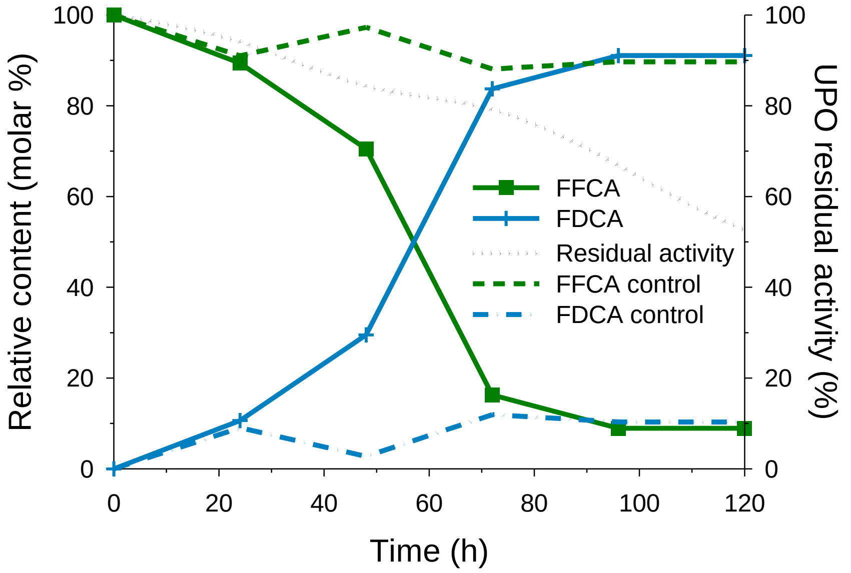

Figure 7.3. FFCA transformation by *A. aegerita* UPO. FFCA (3 mM, 5 mL reaction) was slowly oxidized by UPO (20 U measured with veratryl alcohol) and H_2O_2 (4 mM) to FDCA (~90% after 120 h). The UPO residual activity is also shown, as well as the comparison with the blank reactions (controls without enzyme).

7.1.5. Complete HMF conversion by an AAO-UPO reaction cascade

Considering the above results, we designed a one-pot reaction system using HMF as substrate and AAO and UPO as biocatalysts. First, both enzymes were added together from the beginning of the reaction and were left to react for 24 h. UPO catalyzed oxidation at expenses of the H_2O_2 released by AAO. After 24 h no HMF was left and almost equal amounts of FFCA and HMFCA (46-47%) had been produced, together with some FDCA. This result suggests that, while AAO catalyzes the oxidation of the hydroxyl group of HMF, UPO performs the oxidation of the carbonyl group (as shown in the short incubation-time reactions) at the expense of the H_2O_2 simultaneously produced by AAO. Then, the reaction stops due to AAO's inability to oxidize further the HMFCA produced by UPO.

Finally, a sequential reaction system (cascade) with AAO plus later added UPO was intended. The aim was to enable AAO to oxidize HMF to FFCA releasing two H_2O_2 equivalents, and then add UPO, which would use the H_2O_2 in a way that a higher overall amount of FDCA will be obtained. While all previous reactions were performed at pH 6, this reaction was performed at pH 7 (the optimal pH for UPO reactions and still a good pH for AAO). After a 4-h incubation of HMF with AAO, UPO was added and left up till HMF to FDCA conversion was completed (**Figure 7.4**). During these first 4 h, almost all HMF had been converted by AAO to FFCA (98%) and a small amount of FDCA, at the same time that atmospheric O_2 was reduced to H_2O_2. After adding UPO, the levels of FFCA progressively decreased, accompanied by increasing amounts of FDCA. At hour 120, only some FFCA remained (9%), and the rest was almost completely converted into FDCA (91%).

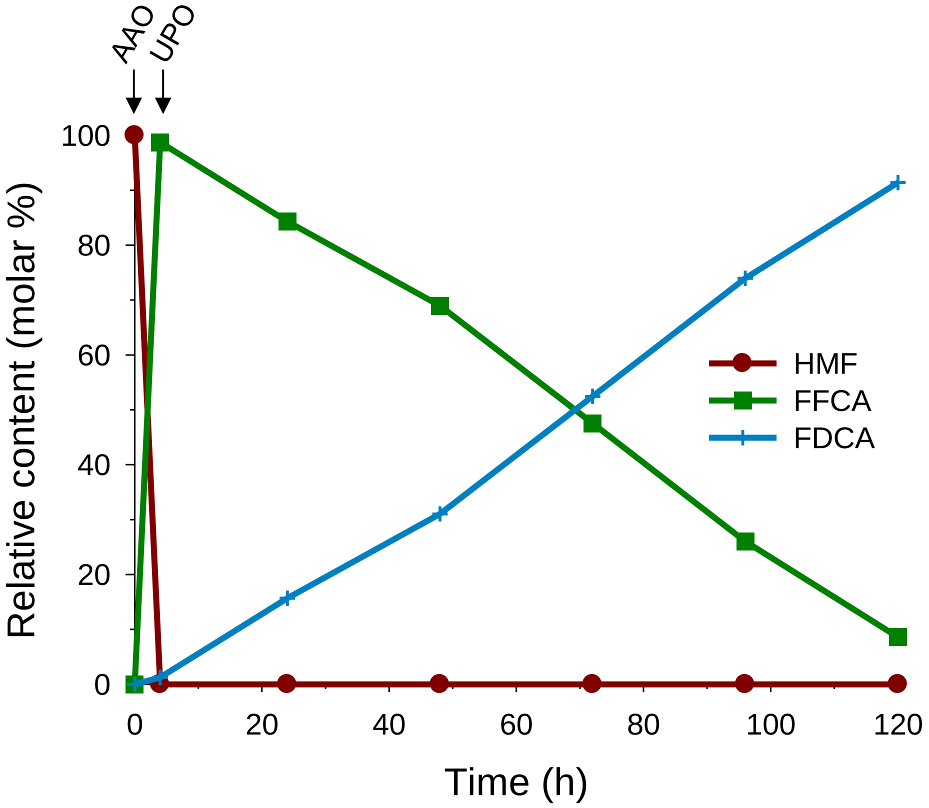

Figure 7.4. HMF transformation by P. eryngii AAO plus A. aegerita UPO (successive addition). After 4 h treatment of HMF with AAO almost all HMF was converted into FFCA, and UPO was added to complete the HMF transformation into FDCA.

A final comparison of the results of the different conversions described above (24-h reactions unless otherwise stated) is provided in **Table 7.2**, including the oxidation of: i) HMF by AAO, UPO, and AAO+UPO added simultaneously or successively (the latter in 24-h and 120-h reactions); ii) DFF by AAO; and iii) FFCA by 6 mM and 200 mM H2O2.

Table 7.2. Molar percentages (from 5-mL reactions) after 24-h treatment of HMF (3 mM) with AAO alone (5 µM, corresponding to 54 U measured with veratryl alcohol), UPO alone (0.65 µM, corresponding to 20 U measured with veratryl alcohol), and with AAO (5 µM, 54 U) and UPO (0.65 µM, 20 U) added simultaneously (sim) or successively (suc); as well as after 24-h treatment of DFF (3 mM) with AAO (5 µM, 54 U), and FFCA (3 mM) with 6 and 200 mM H_2O_2

	HMF					DFF	FFCA + H_2O_2	
	AAO (24 h)	UPO (24 h)	AAO+UPO			AAO (24 h)	6 mM (24 h)	0.2 M (24 h)
			sim (24 h)	suc (24 h)	suc (120 h)			
HMF	0	3	0	0	0	-	-	-
HMFCA	0	97	46	0	0	0	-	-
DFF	0	0	0	0	0	0	-	-
FFCA	94	0	47	84	9	86	89	16
FDCA	6	0	7	16	91	14	11	84

7.1.6. NMR analysis of carbonyl hydration in HMF-derived furanaldehydes

The ^{1}H-NMR spectrum of HMF in deuterated dimethylsulfoxide (DMSO-d_6) shows five signals corresponding to the aldehyde proton (H_1, 9.5 ppm), the two protons of the furanic ring (H_2 and H_3, 7.6 and 6.7 ppm, respectively), the two benzylic protons (4.5 ppm) and the hydroxyl proton (5.6 ppm) (the two latter not shown in Figure **7.5A**). The spectrum of HMF in ^2H_2O buffer (pH 6) displayed four signals, since the proton from the hydroxyl group interchanges with ^2H_2O, that were the same found in DMSO-d_6: H_2 (7.6 ppm), H_3 (6.7 ppm), H_1 (9.5 ppm) and H_4 (4.5 ppm) (the latter not shown in **Figure 7.6A**). In the light of these results, it seems that HMF does not produce any *geminal* diol (*gem*-diol) form. This reinforces the hypothesis that AAO oxidation of HMF to FFCA occurs *via* DFF, since the absence of hydration rules out the oxidation of the aldehyde group yielding HMFCA.

The DFF spectrum in DMSO-d_6 (**Figure 7.5B**) gives only two signals owing to the symmetry of the molecule. These correspond to the protons of the aldehyde (H_{1+4}) and the ones from the furanic ring (H_{2+3}). On the contrary, the spectrum in ^2H_2O (**Figure 7.6B**) is more complex, displaying six signals: H_{1+4} (9.8 ppm), H_{2+3} (7.7 ppm) coinciding with those of DFF in DMSO; and H_{1^*} (6.1 ppm), H_{2^*}, (6.8 ppm), H_{3^*} (7.6 ppm) and H_{4^*} (9.5 ppm) corresponding to the hydrated forms. The similar intensities of the H_{1^*}, H_{2^*}, H_{3^*} and H_{4^*} signals indicate that only one of the DFF carbonyl groups gets (partially) hydrated. The DFF hydration degree, estimated from the integration of H_{1+4}, H_{4^*}, and H_{1^*}, is of 53%, and corresponds to *gem*-diol formation at one of the carbonyl groups.

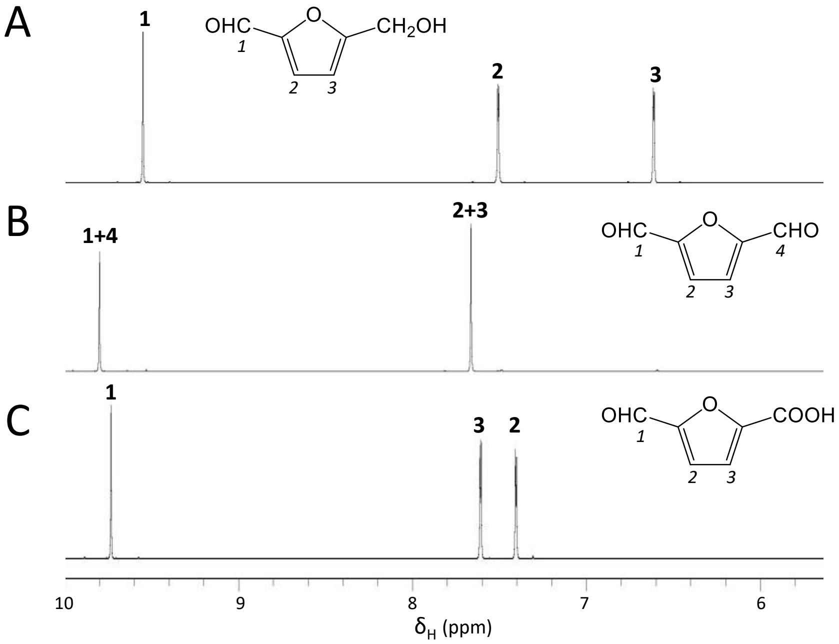

Figure 7.5. ^{1}H-NMR spectra (5.6-10.0 ppm) of HMF (A), DFF (B) and FFCA (C) in DMSO-d_6.

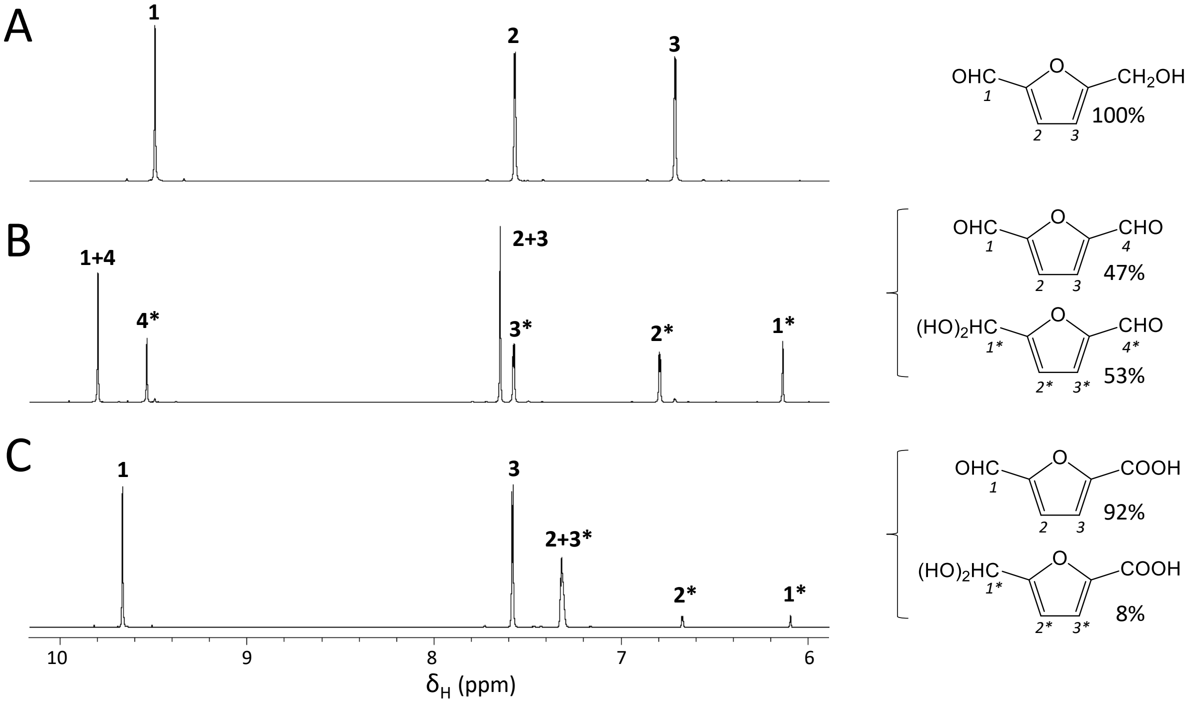

Figure 7.6. ^{1}H-NMR analyses revealing different hydration degrees. The ^{1}H-NMR spectra (5.8-10.2 ppm) of 10 mM HMF (A), DFF (B) and FFCA (C) in ^2H_2O show the H_1 to H_4 signals in the aldehyde and *gem*-diol (asterisks) forms, enabling calculation of their hydration degrees.

The FFCA spectrum in DMSO-d_6 includes four signals: H_1 bound to the carbonyl carbon, H_2 and H_3 in the furanic ring, and that of the proton of the carboxylic group (the latter not shown in **Figure 7.5C**). The spectrum in ^2H_2O (**Figure 7.6C**) has five signals: H_1 (9.7 ppm) and H_3 (7.6 ppm) correspond to those found in DMSO-*d*$_6$; while H_{1*} (6.1 ppm) and H_{2*} (6.7 ppm) correspond to the hydrated form; and H_{2+3*} (7.3 ppm) results from overlapping of the above aldehyde H_2 signal and the *gem*-diol H_{3*} signal (the carboxylic proton is exchanged in ^2H_2O). By integrating the areas of H_1 and H_{1*}, an 8% hydration degree was calculated at pH 6. FFCA hydration was also estimated in pH 3 and pH 9 ^2H_2O buffer, and ~3% and ~6% degrees were obtained, respectively. In agreement with this low hydration degree, no significant FFCA oxidation by AAO was found (in the pH 3-9 range).

7.2. Discussion

7.2.1. Substrate specificity of a fungal model flavooxidase (AAO)

AAO belongs to the superfamily of GMC oxidoreductases, whose name derives from three of its first and best characterized members: glucose oxidase (EC 1.1.3.4), methanol oxidase (EC 1.1.3.13) and choline oxidase (EC 1.1.3.17) (Cavener 1992). Recently, AAO structure-function and mechanistic aspects have been studied in-depth (Ferreira et al. 2009; Fernández et al. 2009; 2011a; Hernández-Ortega et al. 2011b; 2012b; 2012c) and its ability to oxidize aromatic (and some aliphatic polyunsaturated) primary alcohols, as well as related aldehydes has been shown (Ferreira et al. 2005; 2010). Comparison of AAO activities oxidizing these substrates reveals much lower catalytic efficiency oxidizing aldehydes than alcohols, due to both lower k_{cat} and higher K_m values. Moreover, the effect of the same ring substituents on AAO activity was opposite for substituted benzyl alcohols and aldehydes, a fact already noticed by Guillén et al. (1992b) when the AAO aldehyde oxidase activity was recognized for the first time, that is related to the required aldehyde hydration discussed below.

7.2.2. HMF and DFF: Two new AAO substrates

The enzyme kinetics and product GC-MS analyses showed that AAO is able to carry out two subsequent oxidations using HMF and O_2 as substrates, yielding FFCA and two equivalents of H_2O_2. In the first step, AAO oxidizes the hydroxyl group of HMF to a carbonyl giving DFF and, in the second step, it oxidizes one of the aldehyde groups of DFF to the corresponding carboxylic acid (FFCA). The fact that DFF was not detected as a reaction product is in agreement with the higher AAO turnover number on this compound compared to HMF, making that all the DFF formed rapidly turns into FFCA.

In the light of the above results, the possibility that four-electron oxidation of HMF to FFCA by AAO takes place with DFF acting as a transient intermediate remaining at the active site during the whole reaction must be considered. Simultaneous alcohol and aldehyde oxidase activities have been already reported in the reaction of AAO with other substrates (such as 3-chloro-*p*-methoxybenzyl and *m*- and *p*-fluorobenzyl alcohols) (Ferreira et al. 2010) and oxidation of the aldehyde intermediate without leaving the enzyme active site is supported by the ternary-complex mechanism described in AAO (Ferreira et al. 2009). The latter means that the aldehyde product is still at the active site when the enzyme is reoxidized by O_2 and, if it is an AAO substrate as DFF is, it will be hydrated and immediately oxidized without leaving the active site. In this scenario, the active site histidine (His502) that acts as a catalytic base accepting the proton from the C-5 hydroxyl of HMF for subsequent hydride transfer to the flavin, will accept the proton from the C-5 hydroxyl of the DFF *gem*-diol that will remain at the same position at the active site. Rapid HMF conversion into FFCA by AAO contrasts with results reported for some galactose oxidase (EC 1.1.3.9) variants (Kalum et al. 2014) that predominantly yielded DFF from HMF oxidation. Oxidation of aryl-alcohols by galactose oxidase variants had been previously reported (Escalettes and Turner 2008), and the different HMF products compared with AAO are most probably the result of the different catalytic mechanisms of both enzymes, since galactose oxidase belongs to the group of copper-radical oxidases (Whittaker 2002) while AAO is a flavoenzyme.

AAO has in general terms much lower activities on aldehydes than on their alcohol counterparts (**Table 7.2**) but this is not the case for HMF and DFF. It had been described by Ferreira et al. (2010) that hydration of aldehydes forming the *gem*-diol forms is required for their reactivity with AAO (which in fact always acts as an alcohol oxidase). The results from ^{1}H-NMR estimation of the carbonyl hydration degree in HMF derivatives agree with this reactivity. DFF showed a 53% hydration degree, which means that the *gem*-diol form is more abundant than the aldehyde one. Hydration of one of the carbonyls is promoted by the electron withdrawing effect of the second one and, therefore, no double hydration of DFF was detected. This means that there exists a dynamic equilibrium between the two aldehydes and the one-aldehyde plus the *gem*-diol forms, the latter being constantly formed while transformed into FFCA by AAO. On the other hand, the carbonyl substituent in HMF acts as electron withdrawer, lowering the reactivity of the alcohol group for hydride transfer to the AAO cofactor, as shown for aryl alcohols with other electron withdrawing substituents (such as F and Cl atoms in **Table 7.2**). The opposite consequences of these electron withdrawing effects (i) reducing oxidation of the HMF hydroxyl group due to the simultaneous carbonyl presence, and (ii) promoting hydration of one of the DFF carbonyls due to the presence of the second carbonyl group, resulted in the unexpected similar activity of AAO on the alcohol and aldehyde groups of these two furanic compounds.

Nevertheless, the enzyme is seemingly not able to catalyze the next step, which is the oxidation of the remaining aldehyde functionality present in FFCA. The carboxyl group in FFCA could also act as an electron withdrawer promoting the carbonyl reaction with water. However, GC-MS analyses did not show products of the reaction of FFCA with AAO, in agreement with the lack of H_2O_2 release when the reaction was followed using the peroxidase-coupled assay. Both the comparatively low hydration degree, 8% estimated by ^{1}H-NMR, and the deactivating effect of the carboxyl group in hydride transfer to flavin could be responsible for the lack of AAO activity on FFCA. In the case of DFF, oxidation to FFCA can take place at the C-5 carbonyl formed during AAO oxidation of HMF without substrate reaccommodation or exit from the active site, as discussed above. However, FFCA oxidation to FDCA must be produced at the C-2 position, and most probably requires exit and new entrance of the substrate to adopt the catalytically relevant position, a process that will be complicated by the bulky nature of the carbonyl group, making more difficult the third oxidation step by AAO.

However, some FDCA was always detected by GC-MS when HMF, or even DFF, were incubated with AAO. Since AAO releases H_2O_2, we hypothesized that it might chemically oxidize the aldehyde group of FFCA to some extent (Hanke 2012), which was in fact proven by an appropriate experiment with FFCA and a higher amount of H_2O_2. In conclusion, it is possible to state that AAO catalytically oxidizes HMF to FFCA and, indirectly, may oxidize some FFCA yielding FDCA.

7.2.3. Oxidase/peroxygenase cascade for HMF conversion into FDCA

Even though the oxidative biotransformation of HMF into FFCA by AAO (*via* DFF) has been a good achievement, we were interested in the biocatalytic synthesis of FDCA because of its potential as precursor of renewable polyesters (Bozell and Petersen 2010). That was the reason why we introduced a second enzyme, the UPO from the basidiomycete *A. aegerita* (Ullrich et al. 2004) to complete the enzymatic conversion of HMF. Owing to the wide range of reactions catalyzed by UPO, we started by elucidating the oxidative pathway the enzyme was using in HMF oxidation. We observed that it preferentially catalyzed the oxidation of the aldehyde group of HMF producing HMFCA, which was opposite to what AAO was doing when oxidizing the hydroxyl group to yield DFF. Then, the reaction proceeded up to FDCA, although the conversion was rather inefficient, since UPO activity towards FFCA was much lower compared to HMF. Although oxidation of HMF and related compounds was not previously described for a basidiomycete UPO, similar reactions were reported for another member of the heme-thiolate peroxidase superfamily, chloroperoxidase (CPO, EC 1.11.1.10) of the ascomycete *Caldariomyces fumago*, albeit in the presence of high enzyme doses (van Deurzen et al. 1997).

The simultaneous action of AAO and UPO on HMF did not result in its substantial conversion into FDCA, most probably because the H_2O_2 generated by the AAO oxidation of HMF to DFF was immediately used by UPO to oxidize the same compound (HMF) to HMFCA. According to the reactions described above, this proceeded in such a way that a mixture of HMFCA and FFCA was finally obtained. However, the addition of UPO when most HMF had already been transformed into FFCA resulted in the almost complete conversion of HMF into

FDCA due to FFCA oxidation by UPO (in a long-term reaction) using the H_2O_2 excess provided by AAO. This enzymatic cascade, whose two initial steps are the AAO-catalyzed oxidation of HMF and DFF (*gem*-diol form) with the concomitant reduction of two O_2 to two H_2O_2, followed by a third step catalyzed by UPO, which resulted in the oxidation of predominantly unhydrated FFCA at expenses of the previously formed H_2O_2, is illustrated in **Figure** 7.7.

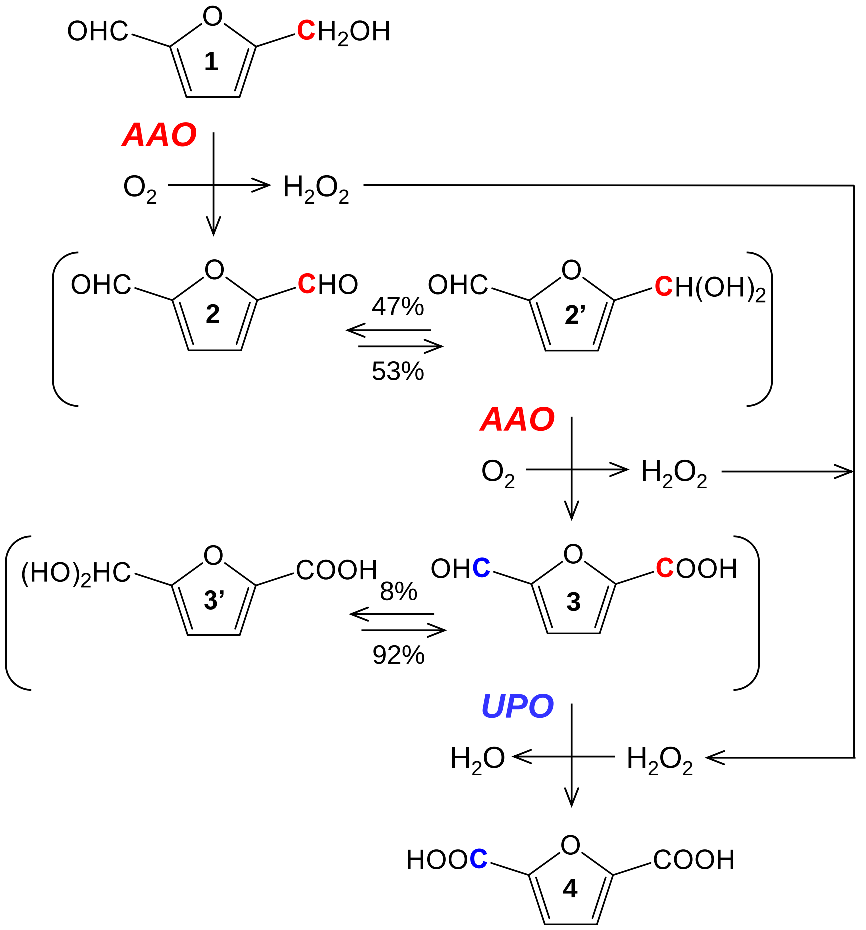

Figure 7.7. Scheme for enzymatic conversion of HMF into FDCA in a cofactor-free reaction cascade involving *P. eryngii* AAO and *A. aegerita* UPO. 1, HMF; 2, DFF; 3, FFCA; 4, FDCA. Symbols by numbers indicate hydrated, *gem*-diol forms of the carbonyl groups. Percentages on the reactions indicate the abundance of each of the species at equilibrium.

The results presented in this chapter have been redrafted from the publication: 5-Hydroxymethylfurfural conversion by fungal aryl-alcohol oxidase and unspecific peroxygenase. Carro J, Ferreira P, Rodríguez L, Prieto A, Serrano A, Balcells B, Ardá A, Jiménez-Barbero J, Gutiérrez A, Ullrich R, Hofrichter M, Martínez AT. FEBS J 282:3218–3229, 2015

8

Discussion

The present Thesis contains several studies on different aspects of GMC oxidoreductases, focusing on AAO from *P. eryngii* as a representative of the superfamily:

Firstly, a genomic screening was conducted in search for gene sequences encoding for members of six families belonging to the GMC oxidoreductase superfamily that, besides, are related to lignocellulose decay (**Chapter 2**). Ten genomes were selected from basidiomycetous fungi from the order Polyporales, which are known for being the only organisms capable of completely mineralizing lignin. The importance of these enzymes was evidenced by the high numbers of sequences (95) present in the genomes of these fungi. These studies allowed outlining the possible roles of these enzymes in the different modalities of lignocellulose decay and to relate the co-evolution of the GMC oxidoreductases —as auxiliary enzymes— and the agents of this process.

Secondly, several studies were carried out to gain insight into the catalytic mechanism and the structure-function relationships in the GMC enzymes. One relevant representative of the superfamily was chosen as a model, AAO from the basidiomycetous fungus *Pleurotus eryngii*, which had already been extensively characterized. Nonetheless, the results present in this work shed light on different aspects that had not been studied in previous works.

That is the case of the temperature dependence of the hydride transfer from the substrate to the enzyme's cofactor during the reduction of AAO and its involvement in the quantum-mechanical effect known as tunneling (**Chapter 5**). This effect, nowadays considered to be involved in all hydrogen (hydride or proton) transfer reactions, allows the particle to be transferred under the theoretical energy barrier for the reaction. Kinetic data confirmed the involvement of tunneling in the hydride transfer that takes place during the reductive half-reaction of the enzyme from the α carbon of the substrate to flavin N5. Moreover, kinetics revealed that the enzyme-substrate complex was formed in such an organized configuration that permitted the hydride transfer with the only assistance of thermally-activated motions of the side chains of active-site residues known as gating. The resolution of a crystallographic structure of AAO in complex with an enzyme's inhibitor, *p*-anisic acid, reinforced this hypothesis as very little differences between the structures of the enzyme alone and complexed were found. Furthermore, the distances measured from the inhibitor's α carbon to flavin N5 are such that allow tunneling to occur.

The role of Phe397, a residue located in a loop unique to the AAO family and which forms, along with other aromatic residues, a bottleneck that separates the catalytic pocket from the outer environment, was elucidated (**Chapter 4**). Kinetic results suggested that, in contrast to what happens to wild-type enzyme, neither the reductive half-reaction nor the reoxidative one is the rate-limiting step in several Phe397-mutated variants. Additional studies on the formation and dissociation of the enzyme-inhibitor complex suggested that Phe397 is involved in the product release from the catalytic pocket. Besides, the reoxidation pattern is altered if Phe397 is substituted by a non-aromatic residue, pointing towards the role of aromaticity in facilitating reactivity with O_2.

The knowledge on the mechanism of AAO's reoxidation and the concomitant O_2 reduction to H_2O_2 was complemented by kinetic isotope effects estimated by stopped-flow spectroscopy. These allowed the elucidation of the origin of the particles transferred to O_2 —one electron, one hydrogen atom and one proton— (**Chapter 6**). Studies revealed that, apart from the initial and obligate one-electron transfer from flavin N5 to O_2, the other two particles were transferred in a non-concerted manner, that is, in two separate chemical steps, required for the reduction of O_2 by AAO. Moreover, the combined effect of high pH and use of deuterated solvents revealed the solvent isotope effect that permitted to conclude that the proton transferred originates from a solvent exchangeable site. The exchange of the particle bound to the reduced flavin N5 locus was also unveiled and the exchange rate estimated.

Finally, the applicability of GMC oxidoreductases in biotechnological processes was tested for the laboratory-scale production of FDCA from the renewable, plant-biomass-derived, chemical HMF (**Chapter 7**). In this case, AAO proved to be a good catalyst involved in the chemical pathway of interest that, in addition to oxidizing the substrate and some partially oxidized derivatives, produced H_2O_2. This latter feature was exploited for the catalysis of reactions that AAO was not able to carry out by the addition of an UPO able to catalyze them at expenses of the H_2O_2 previously formed by AAO.

8.1. Wealth of GMC genes and their biotechnological potential.

The identification of 95 putative GMC oxidoreductases belonging to 5 different families in the 10 Polyporales genomes described in **Chapter 3** (Ferreira et al. 2015a) gives a hint about the enormous number of different GMC enzymes involved in lignocelluloses degradation that may exist in nature. Taking these results into account, it can be deduced that ligninolytic fungi possess a great number of genes whose proteins might be exploited for biotechnological purposes, similarly to the results obtained from the applications of AAO presented in **Chapter 7**.

In general, ligninolytic enzymes share features that make them suitable for biotechnological applications: i) the wide range of substrates they can act on, and ii) the possibility of creating enzymatic cascades taking advantage of their synergistic natural roles.

On the one hand, given the amorphous and variable chemical structure of lignocellulose, fungi have developed an immense repertoire of different enzymes capable of mineralizing or, at least, modify it (Gupta et al. 2016). On the other, the chemical characteristics of lignocelluloses have forced the enzymatic extracellular oxidative systems of these fungi to be unspecific and, thus, very promiscuous (Kersten and Cullen 2007).

In **Chapter 1**, a plethora of several different AAO substrates is listed. They act as electron donors for AAO to reduce O_2 for the production of H_2O_2 for ligninolytic peroxidases and can originate from the fungal secondary metabolism, as the *p*-methoxybenzyl alcohol, or be products of the lignocellulose degradation, like the veratryl alcohol (Ruiz-Dueñas and Martínez 2009). In this work, the biotechnological applicability of one GMC oxidase, AAO, as well as its ever-growing substrate range, are made evident by the discovery of several new AAO substrates —HMF and DFF— that derive from the hydrolysis of the hydrocarbons forming the secondary cell wall (**Chapter 7**).

The physiological roles of the GMC oxidoreductases involved in lignocellulose degradation are, in general, and as explained in **Chapter 3**, related to the H_2O_2 production for peroxidases or Fenton reaction (Ferreira et al. 2015a). Taking AAO as an example, its role is to establish a redox recycling in which intracellular NAPD-dependent dehydrogenases are involved, to generate a continuous supply of H_2O_2 at the expenses of the fungus that is feeding on the carbohydrates released from the lignocelullose degradation (Guillén and Evans 1994; Guillén et al. 1994). The produced H_2O_2 fuels high redox potential peroxidases that oxidize lignin.

In the present work, advantage was taken of this ability to create two different enzymatic cascades that are based on the production of H_2O_2 concomitantly to the obtention of chemicals of interest. **Chapter 7** is an example of this, since AAO was used, along with a H_2O_2-dependent enzyme, UPO, to carry out reactions of industrial interest. As explained, not only were their activities on the different intermediates of the chemical pathway complementary, but also the ability of UPO to consume the by-product generated by AAO. In this way, self-sufficient enzymatic cascades were developed, thanks to the *in situ* H_2O_2 generation.

Even if the appropriate biocatalysts are selected from the pool of different sequences nowadays at our disposal, additional tools do exist that permit the improvement of their abilities to act on specific substrates. Protein engineering is an ever-growing field that allows us to either mutate specific residues in the enzyme to obtain variants or to artificially evolve our enzymes towards a given activity.

Rational design of enzymes is a biotechnological approach that has had good results in ligninolytic enzymes, such as the improvement of the stability of versatile peroxidase (VP) towards H_2O_2 (Sáez-Jiménez et al. 2015) or the engineering of the heme pocket to improve the asymmetric sulfoxidations by a dye-decolorizing peroxidase (DyP) (Linde et al. 2016). Regarding the GMC oxidoreductases, they have also been engineered to create better variants for specific purposes. That is the case of AAO from *P. eryngii*, which was mutated in order to make more room available for secondary alcohols to fit in its active site and, thus, improve their oxidation (Hernández-Ortega et al. 2012b). **Chapters 4** and **5** demonstrate the ease of these techniques, although the mutants created in this work aimed at unveil the catalytic properties of the enzymes. The use of computational methods for this purpose may act as guide, as it was shown by the collaborations to create mutated variants of AAO, in which these studies complemented the experimental findings (2011a; Hernández-Ortega et al. 2011b; 2012c).

There exists also the possibility of mutating a given enzyme towards a specific task. This is known as directed evolution and is based on creating variability in a sequence and screening for a determined activity. AAO has been subjected to these approaches for its improved expression in a determined heterologous host (Viña-González et al. 2015a; 2015b). Apart from these findings with AAO, other ligninolytic enzymes, such as laccases (Pardo and Camarero 2015; Pardo et al. 2016) or the unspecific peroxygenase employed in **Chapter 7** (Molina-Espeja et al. 2014; Alcalde et al. 2015; 2015) have been evolved towards different activities.

Therefore, with all the above tools at our disposal, the current availability of sequences thanks to the modern sequencing techniques is a great starting point for the selection of biocatalysts for industry.

8.2. Elucidation of the catalytic mechanisms to obtain better biocatalysts.

A significant part of this thesis is devoted to unveiling the catalytic mechanism and its relation to the structure of AAO from *P. eryngii* as a model enzyme of the GMC superfamily. The structure-function studies as those described in **Chapters 4**, **5** and **6** are crucial for the understanding of the biocatalysts' mode of action and may help the development of more robust and efficient ones.

The catalytic mechanism of AAO had been extensively investigated (Ferreira et al. 2009; Hernández-Ortega et al. 2011a; 2011b; 2012b; 2012c; 2015b) and reviewed (Hernández-Ortega et al. 2012a; Carro et al. 2016). However, the three above-mentioned chapters shed additional light into the mechanistics of AAO reduction and reoxidation.

Identification of the specific residues responsible for the catalysis of the enzyme is of great importance because they can be mutated in order to obtain a better activity for a purpose, as already discussed in the precedent section. **Chapter 4** deals with the role of F397 in AAO catalysis. Its involvement may be important, for instance, to overcome the inability to access the AAO active site that FFCA displays. This kind of studies may help determine which changes must be introduced in a protein to make it a better biocatalyst, or to gain a specific activity.

Other kinetic studies shed light on the involvement of the O_2 concentration in AAO catalysis. As revealed by the bi-substrate kinetics carried out in **Chapters 4** and **5**, AAO is not saturated at an atmospheric O_2 pressure. Therefore, improvement of the aeration of enzymatic reactions might lead to increase in the efficiency of the reactions of these GMC enzymes as biocatalysts.

8.3. Reoxidation of wild-type AAO and mutated variants

For the first time, the estimation of kinetic isotope effects in transient-state kinetics permitted the elucidation of the mechanism of the reoxidative half-reaction of AAO. The use of a double-mixing stopped-flow system turned out to be essential for their estimation, since, as detailed in **Chapter 6**, the tag (deuterated or protiated) on flavin N5 is washed out by the atoms present in the solvent relatively quickly. Therefore, the use of single mixing techniques, which require the enzyme to be reduced prior to the actual experiment, may mask the contributions of the deuterated solvent or substrate.

Therefore, the double-mixing experiments established that the origin of the hydrogen atom transferred to superoxide radical after the formation of the so-called caged radical pair by the transfer of the initial electron from FAD to O_2, was the N5 of the flavin itself. Moreover, the solvent isotope effect that was made evident at high pHs permitted to conclude that the origin of the proton transferred was a solvent exchangeable site, most probably, the proton abstracted by the catalytic His502 during the reduction of the enzyme. Besides, the fact that these two effects are independent and, thus, the multiple effect is similar to the substrate isotope effect, revealed that these transfers are not concerted.

In spite of their independence, they cannot be separated spectroscopically, as they proved to be detected as the same phase in the stopped-flow apparatus. However, transient-state studies of the reoxidation of two Phe397-mutated variants, F397A and F397L, revealed the existence of two separate, and relevant, phases, both linearly dependent on O_2 concentration (**Chapter 4**). This was in opposed to the second phases reported for other variants, wild-type included, which seemed not to be catalytically relevant. Although their origin has not yet been elucidated, they could represent the two transfers (hydrogen and proton) that take place during O_2 reduction. Future transient-state experiments of these variants' reoxidation using the double mixing mode will shed light on this aspect.

8.4. Rate-limiting steps in AAO catalysis

As already explained, the reaction of AAO is stereoselective, which would allow the use of the enzyme to create enantiomerically pure compounds from racemic mixtures (**Chapter 1**). AAO, in fact, abstracts the pro-*R* hydrogen bound to the α carbon of the alcohol substrate to be transferred to the flavin N5 in the form of a hydride (Hernández-Ortega et al. 2012b). The stereoselectivity of the enzyme has not been inverted through any of the mutations introduced in its active site. Other flavoenzymes as the vanillyl alcohol oxidase, had their stereoselectivity altered due to changes in the active site that disrupted the whole configuration of the active site (van den Heuvel et al. 2000).

The importance of this atom in AAO catalysis is great since it limits the reactions of both the half-reactions of the native enzyme. As explained in **Chapter 5**, the transfer of the pro-*R* hydrogen as a hydride to reduce flavin with the involvement of the mechano-quantical effect known as tunneling constitutes the main bottleneck of the catalytic cycle. This is reflected in the same values found for k_{cat} and k_{red} in most of the variants. Moreover, the kinetic isotope effects on the ${}^{app}k_{ox}$ for the native enzyme demonstrated that the transfer of the hydrogen atom bound to flavin N5 (which originated from the substrate) is the rate-limiting step of the reoxidation (**Chapter 6**).

Nevertheless, two mutated variants, F397Y and F397W, did not follow the same pattern as the wild-type enzyme and showed that, in their catalytic cycles, the hydride transfer was not the rate-limiting step (**Chapter 4**). k_{cat} and k_{red} values were not of the same range, being k_{cat} lower than k_{red}, indicating that another step limited the reaction. In the same manner, the estimated ${}^{app}k_{ox}$ for these mutants were similar to that of the native enzyme, ruling out the contribution of this process to limiting the catalysis. Therefore, it was concluded that the product release, a step that is englobed in the k_{cat} value, was the rate-limiting step.

8.5. New AAO substrates

In the light of the results described in **Chapter 7**, several new AAO substrates have been found: HMF and DFF. The molecules that have proved to be substrates of the enzyme, as it can be seen in **Chapter 1**, were mainly aromatic conjugated alcohols or aldehydes, or aliphatic unsaturated alcohols, such as hexadienol (Ferreira et al. 2005). In general terms, AAO proved to have more activity on alcohols than on their aldehyde counterparts (Ferreira et al. 2010). However, this was not the case for HMF and DFF, since AAO demonstrated to have the same activity on both of them. This is due to the fact that AAO has activity on the *gem*-diol forms of aldehydes that arise as a consequence of the hydration of the carbonyl group. Such reactions are promoted by the presence of electron withdrawing substituents on the ring. The carbonyl group in HMF acts as an electron withdrawing group and, thus, fosters the hydration of DFF molecule to produce a diol as the more abundant form of the carbonyl-diol pair (**Chapter 7**). In contrast, the presence of such substituents impairs the AAO reactivity with alcohols. This is the reason why AAO shows a similar activity on HMF and DFF.

All in all, these new aromatic compounds, although they exhibit a furanic ring instead of the benzenic ring found for the majority of AAO substrates, are benzylic alcohols whose oxidation is catalyzed by AAO.

C

Conclusions

1. In wood-rotting Polyporales GMC oxidases constitute a source of H_2O_2 that contributes: i) to white-rot decay as the oxidizing substrate of ligninolytic peroxidases, and ii) to brown-rot decay oxidizing ferrous iron with generation of hydroxyl free radical involved in cellulose degradation.

2. The most numerous genes of GMC oxidases in the Polyporales genomes are AAO and MOX, but they are differently represented: AAO is virtually absent from brown-rot fungi, while MOX is more abundant using as substrate the product from lignin demethoxylation characterizing brown-rot decay.

3. The catalytic mechanism of AAO, as a model oxidase in white-rot decay, is based on the transfer of a H^- from the alcohol pro-*R* position to the flavin N5 through a *tunneling* mechanism that characterizes the reductive half-reaction of the enzyme.

4. The active site of AAO has evolved in such a way that it can accommodate the substrate in a tunneling-ready position enabling the H^- transfer thanks to the temperature-dependent active dynamics, as revealed by kinetic and crystallographic data.

5. Phe397, located in a loop at the entrance of AAO’s active site, plays a role in helping the product of the reaction exit the cavity, at the same time that it affects FAD reoxidation by compressing the enzyme’s catalytic pocket.

6. Reduction of O_2 to H_2O_2 during AAO reoxidation implies the transfers of one H atom from the flavin N5 of the enzyme and one H^+ originating from the solvent or a solvent exchangeable site in two separate chemical steps, besides to an obligate initial electron transfer.

7. In addition to its contribution to natural degradation of lignin, enabling carbon recycling in land ecosystems, AAO is also an enzyme of biotechnological interest.

8. Almost full conversion of the renewable platform chemical HMF into the bioplastic precursor FDCA can be attained thanks to an enzymatic cascade established between AAO and UPO, which relies on their concerted action on the intermediates of the reaction and their synergistic production/consumption of H_2O_2.

A

Annexes

Annex 1. JGI (www.jgi.doe.gov) references (protein ID #) for the 95 GMC genes (plus 5 alleles) identified in the genomes of ten wood-rotting Polyporales (for species abbreviations see **Table 3.1**; the existence of alleles and recognized signal peptides is indicated, see notes below)

-- *White-rot* ------------------- ------------- *Brown-rot* -----

	BJEAD	PHLBR	PHACH	DICSQ	GANSP	TRAVE	GELSU	FOMPI	RHOPL	WOLCO
AAO	52991[#] 66377 71431 114902 114954 156054 171002 171059 183896 245049 245297	22550 131358 164178	6199 37188 135972	96414 102587 103879 86071 160139 160546 171752 182736	67648 67654 85135 117498 124428 130042 138009	40237 176148 133945	84544 117387 118493 137959	40728	44654* 54008 55496 58266*	
MOX	34705 45314 143000 227734 241975	27956 29466 128210 128980 157963 157964	5574 6010 126879	149587 157363 173648 181599	114505 116436 116439 130292	144610 167157 170473 43286	80773	90445 127556 129478 156775	55972 56055* 106935 118723 126217* 129158 129841*	24953 25722 121505 132654
GOX			131961						108849 128830	
CDH	45135	160653	11098	153749	86428	73596	84792			
P2O	34622	123747	137275			174721				

* RHOPL_129841, RHOPL_126217 and RHOPL_56055 are allelic variants of MOX RHOPL_118723, RHOPL_129158 and RHOPL_55972, respectively; while RHOPL_44654 and RHOPL_58266 were considered as variants of AAO RHOPL_55496. [#] The protein models including a recognized signal peptide are underlined.

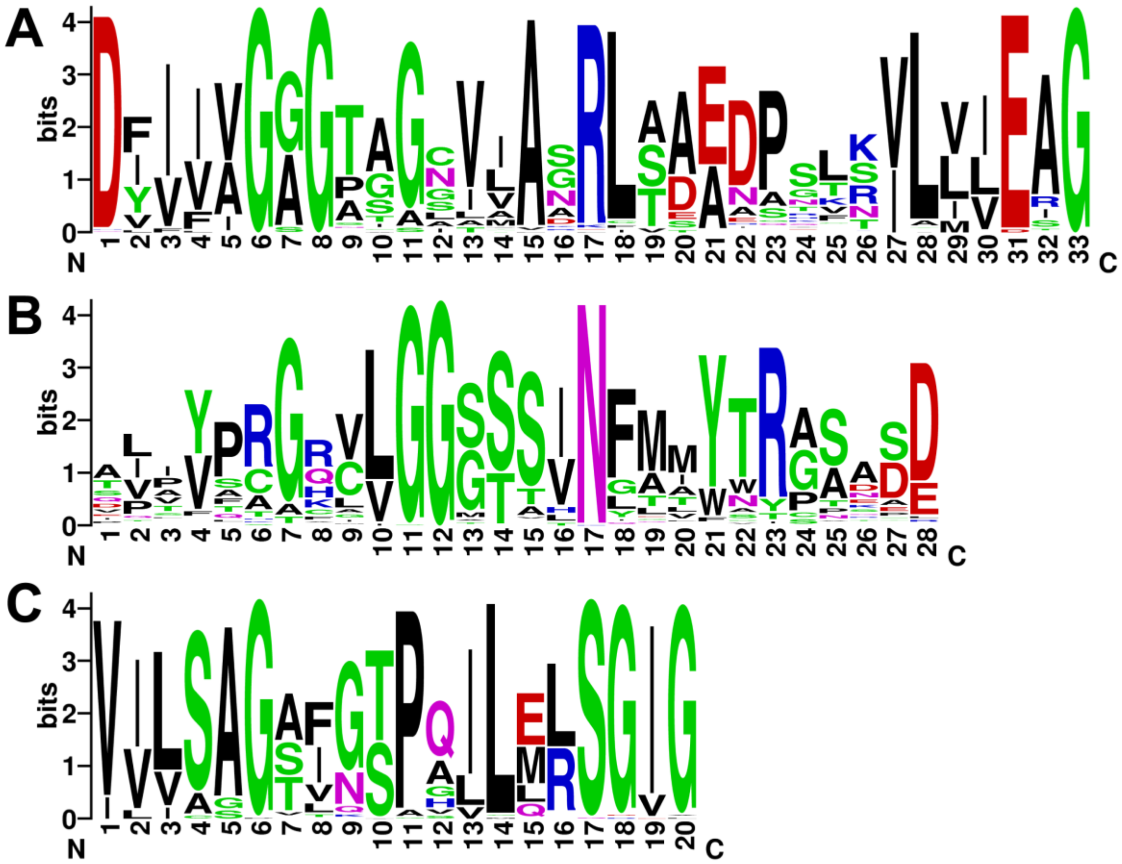

Annex 2. Sequence logo of the ADP-binding motif (**A**), with consensus sequence [DP]-x-[VIL]-[VI]-x-G-x-G-x(2)-[GA]-x(3)-A-X-[RKT]-L-x(7)-[VT]-x(2)-[LIV]-E-x-G, and GMC signatures 1 (**B**) and 2 (**C**), with consensus sequences [GA]-[RKNC]-x-[LIVW]-G(2)-[GST](2)-x-[LIVM]-[NH]-x(3)-[FYWA]-x(2)-[PAG]-x(5)-[DNESHQA] and [GS]-[PSTA]-x(2)-[ST]-[PS]-x-[LIVM](2)-x(2)-S-G-[LIVM]-G respectively, in 95 GMC sequences (TABLE SI) from 10 Polyporales genomes. The overall height of each stack represents the sequence conservation at that position, and the height of each letter reflects the relative frequency of the corresponding amino acid. Residues in **A**, **B** and **C** correspond to positions 2-33, 73-100 and 264-283, respectively in *B. adusta* AAO (JGI protein ID 245059), and equivalent positions in the other GMCs.

Annex 3. Supplemental results describing MS identification of products from HMF conversion into FDCA

All identified compounds in the AAO and UPO reactions with HMF and its partially-oxidized derivatives co-eluted and shared their mass spectra with standards. They include FFCA and FDCA from HMF conversion by successive addition of AAO and UPO, as well as DFF detected as traces in AAO reactions with HMF, and HMFCA resulting from UPO conversion of HMF. All of them showed several ions characteristic of the fragmentation patterns that these molecules undergo upon ionization, as detailed below.

The spectrum of TMSi-HMF showed a small molecular peak (*m/z* 198), as it normally occurs when ionizing TMSi cyclic alcohols. Its base peak (*m/z* 183) corresponds to the ion $[M\text{-}CH_3]^+$, *m/z* 169 to $[M\text{-}COH]^+$, and *m/z* 109 is the ion $[M\text{-}OTMSi]^+$, which rises from the loss of 89 units characteristic of silylated compounds. The ion *m/z* 73 corresponds to the TMSi group. The spectrum of TMSi-FFCA has a small molecular peak (*m/z* 212), the ion *m/z* 197 corresponds to $[M\text{-}CH_3]^+$, and *m/z* 123 to $[M\text{-}OTMSi]^+$. The spectrum of TMSi-FDCA shows the small molecular peak (*m/z* 300), the ion $[M\text{-}CH_3]^+$ at *m/z* 285 and ions *m/z* 73 and 147 that suggest that it is silylated at both carboxylic groups.

The spectrum of DFF is simpler since the molecule cannot be silylated. It shows a small molecular peak at *m/z* 124, *m/z* 95 corresponds to the ion $[M\text{-}CH_3]^+$, and *m/z* 67 is $[M\text{-}2CHO]^+$. Finally, the spectrum of TMSi-HMFCA is more complex due to the fact that it gets silylated at two positions (hydroxyl and carboxyl groups). As in the former compounds, the molecular peak (*m/z* 286) is small. It possesses other ions, such as $[M\text{-}CH_3]^+$ at *m/z* 271, $[M\text{-}OTMSi]^+$ at *m/z* 197, and $[M\text{-}COOTMSi]^+$ at *m/z* 169. Both peaks at *m/z* 73 and 147 indicate that this compound bears at least two TMSi groups.

B

Bibliography

Akhtar M, Attridge MC, Myers GC, Blanchette RA (1993) Biomechanical pulping of loblolly pine chips with selected white-rot fungi. Holzforschung 47:36-40

Akhtar M, Blanchette RA,Kirk TK (1997) Fungal delignification and biomechanical pulping of wood. In: Scheper T (ed) Advances in biochemical engineering/biotechnology. Springer-Verlag Berlin, Heidelberg, pp 160-195

Alcalde M, Molina-Espeja P, García-Ruiz E, González-Pérez D, Ullrich R, Hofrichter M (2015) Unspecific peroxygenase with high monooxygenase activity. Patent (Spain) P201430595-1:

Allemann RK, Evans RM, Tey LH, Maglia G, Pang J, Rodriguez R, Shrimpton PJ, Swanwick RS (2006) Protein motions during catalysis by dihydrofolate reductases. Philos Trans R Soc Lond B Biol Sci 361:1317

Antal MJ, Mok WSL, Richards GN (1990) Kinetic-studies of the reactions of ketoses and aldoses in water at high-temperature.1. Mechanism of formation of 5-(hydroxymethyl)-2-furaldehyde from D-fructose and sucrose. Carbohyd Res 199:91-109

Arantes V, Jellison J, Goodell B (2012) Peculiarities of brown-rot fungi and biochemical Fenton reaction with regard to their potential as a model for bioprocessing biomass. Appl Microbiol Biotechnol 94:323-338

Artolozaga MJ, Kubátová E, Volc J, Kalisz HM (1997) Pyranose 2-oxidase from *Phanerochaete chrysosporium* - Further biochemical characterisation. Appl Microbiol Biotechnol 47:508-514

Asada Y, Watanabe A, Ohtsu Y, Kuwahara M (1995) Purification and characterization of an aryl-alcohol oxidase from the lignin-degrading basidiomycete *Phanerochaete chrysosporium*. Biosci Biotechnol Biochem 59:1339-1341

Ayers AR, Ayers SB, Eriksson K-E (1978) Cellobiose oxidase, purification and partial characterization of a hemoprotein from *Sporotrichum pulverulentum*. Eur J Biochem 90:171-181

Baldrian P, Valaskova V (2008) Degradation of cellulose by basidiomycetous fungi. FEMS Microbiol Rev 32:501-521

Ballance DJ (1986) Sequences important for gene expression in filamentous fungi. Yeast 2:229-236

Bankar SB, Bule MV, Singhal RS, Ananthanarayan L (2009) Glucose oxidase - An overview. Biotechnol Adv 27:489-501

Bao WJ, Usha SN, Renganathan V (1993) Purification and characterization of cellobiose dehydrogenase, a novel extracellular hemoflavoenzyme from the white-rot fungus *Phanerochaete chrysosporium*. Arch Biochem Biophys 300:705-713

Bao WL, Fukushima Y, Jensen KA, Moen MA, Hammel KE (1994) Oxidative degradation of non-phenolic lignin during lipid peroxidation by fungal manganese peroxidase. FEBS Lett 354:297-300

Barrasa JM, Gutiérrez A, Escaso V, Guillén F, Martínez MJ, Martínez AT (1998) Electron and fluorescence microscopy of extracellular glucan and aryl-alcohol oxidase during wheat-straw degradation by *Pleurotus eryngii*. Appl Environ Microbiol 64:325-332

Basran J, Masgrau L, Sutcliffe MJ,Scrutton NS (2006) Solution and computational studies of kinetic isotope effects in flavoprotein and quinoprotein catalyzed substrate oxidations as probes of enzymatic hydrogen tunneling and mechanism. In: Kohen A, Limbach H-H (eds) Isotope effects in chemistry and biology. CRC Press, Boca Raton, pp 671-689

Bell RP (1980) The tunnel effect in chemistry. Springer US, New York.

Bes B, Ranjeva R, Boudet AM (1983) Evidence for the involvement of activated oxygen in fungal degradation of lignocellulose. Biochimie 65:283-289

Binder M, Hibbett DS, Larsson KH, Larsson E, Langer E, Langer G (2005) The phylogenetic distribution of resupinate forms across the major clades of mushroom-forming fungi (Homobasidiomycetes). Syst Biodivers 3:113-157

Binder M, Justo A, Riley R, Salamov A, Lopez-Giraldez F, Sjokvist E, Copeland A, Foster B, Sun H, Larsson E, Larsson KH, Townsend J, Grigoriev IV, Hibbett DS (2013) Phylogenetic and phylogenomic overview of the Polyporales. Mycologia 105:1350-1373

Blanchette RA, Burnes TA, Eerdmans MM, Akhtar M (1992) Evaluating isolates of *Phanerochaete chrysosporium* and *Ceriporiopsis subvermispora* for use in biological pulping processes. Holzforschung 46:109-115

Bordoli L, Kiefer F, Arnold K, Benkert P, Battey J, Schwede T (2009) Protein structure homology modeling using SWISS-MODEL workspace. Nat Protoc 4:1-13

Borrelli KW, Vitalis A, Alcantara R, Guallar V (2005) PELE: Protein energy landscape exploration. A novel Monte Carlo based technique. J Chem Theory Comput 1:1304-1311

Bourbonnais R, Paice MG (1988) Veratryl alcohol oxidases from the lignin degrading basidiomycete *Pleurotus sajor-caju*. Biochem J 255:445-450

Bozell JJ, Petersen GR (2010) Technology development for the production of biobased products from biorefinery carbohydrates-the US Department of Energy's "Top 10" revisited. Green Chem 12:539-554

Breen A, Singleton FL (1999) Fungi in lignocellulose breakdown and biopulping. Curr Opin Biotechnol 10:252-258

Bright HJ, Gibson QH (1967) The oxidation of 1-deuterated glucose by glucose oxidase. J Biol Chem 242:994-1003

Camarero S, Barrasa JM, Pelayo M, Martínez AT (1998) Evaluation of *Pleurotus* species for wheat-straw biopulping. J Pulp Paper Sci 24:197-203

Camarero S, Böckle B, Martínez MJ, Martínez AT (1996) Manganese-mediated lignin degradation by *Pleurotus pulmonarius*. Appl Environ Microbiol 62:1070-1072

Carey JS, Laffan D, Thomson C, Williams MT (2006) Analysis of the reactions used for the preparation of drug candidate molecules. Org Biomol Chem 4:2337-2347

Carro J, Ferreira P, Rodríguez L, Prieto A, Serrano A, Balcells B, Ardá A, Jiménez-Barbero J, Gutiérrez A, Ullrich R, Hofrichter M, Martínez AT (2015) 5-Hydroxymethylfurfural conversion by fungal aryl-alcohol oxidase and unspecific peroxygenase. FEBS J 282:3218-3229

Carro J, Matínez-Júlvez M, Medina M, Martínez AT, Ferreira P (2017) Protein motions promote hydride tunneling in the reduction of AAO. (in preparation)

Carro J, Serrano A, Ferreira P,Martínez AT (2016) Fungal aryl-alcohol oxidase in lignocellulose degradation and bioconversion. In: Gupta VK, Tuohy MG (eds) Microbial Enzymes in Bioconversions of Biomass. Springer, Berlin, Germany, pp 301-322

Cavener DR (1992) GMC oxidoreductases. A newly defined family of homologous proteins with diverse catalytic activities. J Mol Biol 223:811-814

Chen VB, Arendall WB, Headd JJ, Keedy DA, Immormino RM, Kapral GJ, Murray LW, Richardson JS, Richardson DC (2010) MolProbity: all-atom structure validation for macromolecular crystallography. Acta Crystallogr D Biol Crystallogr 66:12-21

Cheng NS (2008) Formula for the viscosity of a glycerol-water mixture. Ind Eng Chem Res 47:3285-3288

Collard F, Fagan RL, Zhang J, Nemet I, Palfey BA, Monnier VM (2011) The Cation-pi Interaction between Lys53 and the Flavin of Fructosamine Oxidase (FAOX-II) Is Critical for Activity. Biochemistry 50:7977-7986

Crooks GE, Hon G, Chandonia JM, Brenner SE (2004) WebLogo: A sequence logo generator. Genome Research 14:1188-1190

Daniel G, Volc J, Filonova L, Plihal O, Kubátová E, Halada P (2007) Characteristics of *Gloeophyllum trabeum* alcohol oxidase, an extracellular source of H2O2 in brown rot decay of wood. Appl Environ Microbiol 73:6241-6253

Daniel G, Volc J, Kubátová E (1994) Pyranose oxidase, a major source of H_2O_2 during wood degradation by *Phanerochaete chrysosporium, Trametes versicolor*, and *Oudemansiella mucida*. Appl Environ Microbiol 60:2524-2532

Danneel HJ, Reichert A, Giffhorn F (1994) Production, purification and characterization of an alcohol oxidase of the ligninolytic fungus *Peniophora gigantea*. J Biotechnol 33:33-41

Danneel HJ, Rossner E, Zeeck A, Giffhorn F (1993) Purification and characterization of a pyranose oxidase from the basidiomycete *Peniophora gigantea* and chemical analyses of its reaction products. Eur J Biochem 214:795-802

de Albuquerque NCP, de Gaitani CM, de Oliveira ARM (2015) A new and fast DLLME-CE method for the enantioselective analysis of zopiclone and its active metabolite after fungal biotransformation. J Pharm Biomed Anal 109:192-201

de Jong E, Cazemier AE, Field JA, de Bont JAM (1994) Physiological role of chlorinated aryl alcohols biosynthesized de novo by the white rot fungus *Bjerkandera* sp strain BOS55. Appl Environ Microbiol 60:271-277

de Jong E, Field JA (1997) Sulfur tuft and turkey tail: Biosynthesis and biodegradation of organohalogens by basidiomycetes. Annu Rev Microbiol 51:375-414:375-414

de Jong E, Field JA, Dings JAFM, Wijnberg JBPA, de Bont JAM (1992) De novo biosynthesis of chlorinated aromatics by the white-rot fungus *Bjerkandera* sp BOS55. Formation of 3-chloro-anisaldehyde from glucose. FEBS Lett 305:220-224

de Koker TH, Mozuch MD, Cullen D, Gaskell J, Kersten PJ (2004) Isolation and purification of pyranose 2-oxidase from *Phanerochaete chrysosporium* and characterization of gene structure and regulation. Appl Environ Microbiol 70:5794-5800

Dijkman WP, Fraaije MW (2014) Discovery and characterization of a 5-hydroxymethylfurfural oxidase from *Methylovorus* sp strain MP688. Appl Environ Microbiol 80:1082-1090

Dijkman WP, Groothuis DE, Fraaije MW (2014) Enzyme-catalyzed oxidation of 5-hydroxymethylfurfural to furan-2,5-dicarboxylic acid. Angewandte Chemie 126:6633-6636

Dijkman WP, Binda C, Fraaije MW, Mattevi A (2015) Structure-based enzyme tailoring of 5-hydroxymethylfurfural oxidase. ACS Catal 5:1833-1839

Dreveny I, Gruber K, Glieder A, Thompson A, Krastky C (2001) The hydroxynitrile lyase from almond: A lyase that looks like a oxidoreductase. Structure 9:803-815

Dumonceaux TJ, Bartholomew KA, Charles TC, Moukha SM, Archibald FS (1998) Cloning and sequencing of a gene encoding cellobiose dehydrogenase from *Trametes versicolor*. Gene 210:211-219

Durand D, Halldorsson BV, Vernot B (2006) A hybrid micro-macroevolutionary approach to gene tree reconstruction. J Comput Biol 13:320-335

Edgar RC (2004) MUSCLE: multiple sequence alignment with high accuracy and high throughput. Nucleic Acids Res 32:1792-1797

Emanuelsson O, Nielsen H, Brunak S, von Heijne G (2000) Predicting subcellular localization of proteins based on their N-terminal amino acid sequence. Journal of Molecular Biology 300:1005-1016

Emsley P, Lohkamp B, Scott WG, Cowtan K (2010) Features and development of Coot. Acta Crystallogr D Biol Crystallogr 66:486-501

Eriksson K-E, Pettersson B, Volc J, Musílek V (1986) Formation and partial characterization of glucose-2-oxidase, a H_2O_2 producing enzyme in *Phanerochaete chrysosporium*. Appl Microbiol Biotechnol 23:257-262

Escalettes F, Turner NJ (2008) Directed evolution of galactose oxidase: Generation of enantioselective secondary alcohol oxidases. ChemBioChem 9:857-860

Evans CS, Dutton MV, Guillén F, Veness RG (1994) Enzymes and small molecular mass agents involved with lignocellulose degradation. FEMS Microbiol Rev 13:235-240

Faison BD, Kirk TK (1983) Relationship between lignin degradation and production of reduced oxygen species by *Phanerochaete chrysosporium*. Appl Environ Microbiol 46:1140-1145

Fan F, Gadda G (2005) Oxygen- and temperature-dependent kinetic isotope effects in choline oxidase: correlating reversible hydride transfer with environmentally enhanced tunneling. J Am Chem Soc 127:17954-17961

Farmer VC, Henderson MEK, Russell JD (1960) Aromatic-alcohol-oxidase activity in the growth medium of *Polystictus versicolor*. Biochem J 74:257-262

Fernández IS, Ruiz-Dueñas FJ, Santillana E, Ferreira P, Martínez MJ, Martínez AT, Romero A (2009) Novel structural features in the GMC family of oxidoreductases revealed by the crystal structure of fungal aryl-alcohol oxidase. Acta Crystallogr D Biol Crystallogr 65:1196-1205

Fernández-Fueyo E, Ruiz-Dueñas FJ, Ferreira P, Floudas D, Hibbett DS, Canessa P, Larrondo L, James TY, Seelenfreund D, Lobos S, Polanco R, Tello M, Honda Y, Watanabe T, Watanabe T, Ryu JS, Kubicek CP, Schmoll M, Gaskell J, Hammel KE, St.John FJ, Vanden Wymelenberg A, Sabat G, Bondurant SS, Syed K, Yadav J, Doddapaneni H, Subramanian V, Lavín JL, Oguiza JA, Perez G, Pisabarro AG, Ramírez L, Santoyo F, Master E, Coutinho PM, Henrissat B, Lombard V, Magnuson JK, Kües U, Hori C, Igarashi K, Samejima M, Held BW, Barry K, LaButti K, Lapidus A, Lindquist E, Lucas S, Riley R, Salamov A, Hoffmeister D, Schwenk D, Hadar Y, Yarden O, de Vries RP, Wiebenga A, Stenlid J, Eastwood DC, Grigoriev IV, Berka R, Blanchette RA, Kersten P, Martínez AT, Vicuña R, Cullen D (2012) Comparative genomics of *Ceriporiopisis subvermispora* and *Phanerochaete chrysosporium* provide insight into selective ligninolysis. Proc Natl Acad Sci USA 109:5458-5463

Ferraz A, Guerra A, Mendonça R, Masarin F, Vicentim MP, Aguiar A, Pavan PC (2008) Technological advances and mechanistic basis for fungal biopulping. Enzyme Microb Technol 43:178-185

Ferreira P, Carro J, Serrano A, Martínez AT (2015a) A survey of genes encoding H2O2-producing GMC oxidoreductases in 10 Polyporales genomes. Mycologia 107:1105-1119

Ferreira P, Hernández-Ortega A, Borrelli K, Carro J, Lucas F, Herguedas B, Guallar V, Martínez AT, Medina M (2015b) Aromatic stacking interactions govern catalysis in aryl-alcohol oxidase. FEBS J 282:3091-3106

Ferreira P, Hernández-Ortega A, Herguedas B, Martínez AT, Medina M (2009) Aryl-alcohol oxidase involved in lignin degradation: A mechanistic study based on steady and pre-steady state kinetics and primary and solvent isotope effects with two different alcohol substrates. J Biol Chem 284:24840-24847

Ferreira P, Hernández-Ortega A, Herguedas B, Rencoret J, Gutiérrez A, Martínez MJ, Jiménez-Barbero J, Medina M, Martínez AT (2010) Kinetic and chemical characterization of aldehyde oxidation by fungal aryl-alcohol oxidase. Biochem J 425:585-593

Ferreira P, Medina M, Guillén F, Martínez MJ, van Berkel WJH, Martínez AT (2005) Spectral and catalytic properties of aryl-alcohol oxidase, a fungal flavoenzyme acting on polyunsaturated alcohols. Biochem J 389:731-738

Ferreira P, Ruiz-Dueñas FJ, Martínez MJ, van Berkel WJH, Martínez AT (2006) Site-directed mutagenesis of selected residues at the active site of aryl-alcohol oxidase, an H2O2-producing enzyme. FEBS J 273:4878-4888

Fishelovitch D, Shaik S, Wolfson HJ, Nussinov R (2009) Theoretical characterization of substrate access/exit channels in the human cytochrome P450 3A4 enzyme: Involvement of phenylalanine residues in the gating mechanism. J Phys Chem B 113:13018-13025

Floudas D, Binder M, Riley R, Barry K, Blanchette RA, Henrissat B, Martínez AT, Otillar R, Spatafora JW, Yadav JS, Aerts A, Benoit I, Boyd A, Carlson A, Copeland A, Coutinho PM, de Vries RP, Ferreira P, Findley K, Foster B, Gaskell J, Glotzer D, Górecki P, Heitman J, Hesse C, Hori C, Igarashi K, Jurgens JA, Kallen N, Kersten P, Kohler A, Kües U, Kumar TKA, Kuo A, LaButti K, Larrondo LF, Lindquist E, Ling A, Lombard V, Lucas S, Lundell T, Martin R, McLaughlin DJ, Morgenstern I, Morin E, Murat C, Nolan M, Ohm RA, Patyshakuliyeva A, Rokas A, Ruiz-Dueñas FJ, Sabat G, Salamov A, Samejima M, Schmutz J, Slot JC, St.John F, Stenlid J, Sun H, Sun S, Syed K, Tsang A, Wiebenga A, Young D, Pisabarro A, Eastwood DC, Martin F, Cullen D, Grigoriev IV, Hibbett DS (2012) The Paleozoic origin of enzymatic lignin decomposition reconstructed from 31 fungal genomes. Science 336:1715-1719

Fonseca MI, Farina JI, Castrillo ML, Rodriguez MD, Nunes CE, Villalba LL, Zapata PD (2014) Biopulping of wood chips with *Phlebia brevispora* BAFC 633 reduces lignin content and improves pulp quality. International Biodeterioration & Biodegradation 90:29-35

Forney LJ, Reddy CA, Tien M, Aust SD (1982) The involvement of hydroxyl radical derived from hydrogen peroxide in lignin degradation by the white rot fungus *Phanerochaete chrysosporium*. J Biol Chem 257:11455-11462

Fraatz MA, Zorn H (2011) Fungal flavours. In: Hofrichter M (ed) The Mycota. X Industrial applications. Springer, Berlin, pp 249-268

Frederick KR, Tung J, Emerick RS, Masiarz F, Chamberlain SH, Vasavada A, Rosenberg S, Chakraborty S, Schopter LM, Massey V (1990) Glucose oxidase from *Aspergillus niger*. Cloning, sequence, secretion from *Saccharomyces cerevisiae* and kinetic analysis of a yeast-derived enzyme. J Biol Chem 265:3793-3802

Gadda G (2008) Hydride transfer made easy in the reaction of alcohol oxidation catalyzed by flavin-dependent oxidases. Biochemistry 47:13745-13753

Gadda G (2012) Oxygen activation in flavoprotein oxidases: The importance of being positive. Biochemistry 51:2662-2669

Gallagher IM, Fraser MA, Evans CS,Atkey PT (1989) Ultrastructural localization of lignocellulose-degrading enzymes. In: Lewis NG, Paice MG (eds) ACS Symposium "Plant Cell-Wall Polymers: Biogenesis and Biodegradation", Vol 399. Amer.Chem.Soc., pp 426-442

Gallezot P (2012) Conversion of biomass to selected chemical products. Chem Soc Rev 41:1538-1558

Gannavaram S, Gadda G (2013) Relative timing of hydrogen and proton transfers in the reaction of Ffavin oxidation catalyzed by choline oxidase. Biochemistry 52:1221-1226

Gellerstedt G, Henriksson G (2008) Lignins: Major sources, structure and properties. In: Belgacem M, Gandini A (eds) Monomers, polymers and composites from renewable resources. Elsevier, Amsterdam, pp 201-224

Ghisla S, Massey V (1989) Mechanisms of flavoprotein-catalyzed reactions. Eur J Biochem 181:1-17

Giles RL, Galloway ER, Zackeru JC, Naithani V, Parrow MW (2014) Two stage fungal biopulping solubilizes lignocellulosic carbohydrates without supplemental enzymatic hydrolysis. International Biodeterioration & Biodegradation 86:265-271

Goetghebeur M, Brun S, Galzy P, Nicolas M (1993) Benzyl alcohol oxidase and laccase synthesis in *Botrytis cinerea*. Biosci Biotechnol Biochem 57:1380-1381

Goetghebeur M, Nicolas M, Brun S, Galzy P (1992) Production and excretion of benzyl alcohol oxidase in *Botrytis cinerea*. Phytochemistry 31:413-416

Gómez-Toribio V, García-Martín AB, Martínez MJ, Martínez AT, Guillén F (2009) Induction of extracellular hydroxyl radical production by white-rot fungi through quinone redox cycling. Appl Environ Microbiol 75:3944-3953

González A, Grinbergs J, Griva E (1986) Biologische Umwandlung von Holz in Rinderfutter-'Palo podrido'. Zentralbl Mikrobiol 141:181-186

Goodell B, Jellison J, Liu J, Daniel G, Paszczynski A, Fekete F, Krishnamurthy S, Jun L, Xu G (1997) Low molecular weight chelators and phenolic compounds isolated from wood decay fungi and their role in the fungal biodegradation of wood. J Biotechnol 53:133-162

Green III F, Clausen CA, Larsen MJ, Highley TL (1992) Immuno-scanning electron microscopic localization of extracellular wood-degrading enzymes within the fibrillar sheath of the brown-rot fungus *Postia placenta*. Can J Microbiol 38:898-904

Grigoriev IV, Nordberg H, Shabalov I, Aerts A, Cantor M, Goodstein D, Kuo A, Minovitsky S, Nikitin R, Ohm RA, Otillar R, Poliakov A, Ratnere I, Riley R, Smirnova T, Rokhsar D, Dubchak I (2012) The genome portal of the Department of Energy Joint Genome Institute. Nucleic Acids Res 40:D26-D32

Guillén F, Evans CS (1994) Anisaldehyde and veratraldehyde acting as redox cycling agents for H_2O_2 production by *Pleurotus eryngii*. Appl Environ Microbiol 60:2811-2817

Guillén F, Martínez AT, Martínez MJ (1990a) Characterization and purification of an aryl-alcohol oxidase from *Pleurotus eryngii*. Abs 4th Intern Mycol Congr ,Regensburg232

Guillén F, Martínez AT, Martínez MJ (1990b) Production of hydrogen peroxide by aryl-alcohol oxidase from the ligninolytic fungus *Pleurotus eryngii*. Appl Microbiol Biotechnol 32:465-469

Guillén F, Martínez AT,Martínez MJ (1992a) Aryl-alcohol oxidase from *Pleurotus eryngii*: substrate specificity and H_2O_2-producing system. In: Kuwahara M, Shimada

M (eds) Biotechnology in pulp and paper industry. UNI Pub. Co., Ltd., Tokyo, pp 371-376

Guillén F, Martínez AT, Martínez MJ (1992b) Substrate specificity and properties of the aryl-alcohol oxidase from the ligninolytic fungus *Pleurotus eryngii*. Eur J Biochem 209:603-611

Guillén F, Martínez AT, Martínez MJ, Evans CS (1994) Hydrogen peroxide-producing system of *Pleurotus eryngii* involving the extracellular enzyme aryl-alcohol oxidase. Appl Microbiol Biotechnol 41:465-470

Gupta VK, Kubicek CP, Berrin JG, Wilson DW, Couturier M, Berlin A, Filho EXF, Ezeji T (2016) Fungal enzymes for bio-products from sustainable and waste biomass. Trends in Biochemical Sciences 41:633-645

Gutiérrez A, Babot ED, Ullrich R, Hofrichter M, Martínez AT, del Río JC (2011) Regioselective oxygenation of fatty acids, fatty alcohols and other aliphatic compounds by a basidiomycete heme-thiolate peroxidase. Arch Biochem Biophys 514:33-43

Gutiérrez A, Caramelo L, Prieto A, Martínez MJ, Martínez AT (1994) Anisaldehyde production and aryl-alcohol oxidase and dehydrogenase activities in ligninolytic fungi from the genus *Pleurotus*. Appl Environ Microbiol 60:1783-1788

Hallberg BM, Henriksson G, Pettersson G, Divne C (2002) Crystal structure of the flavoprotein domain of the extracellular flavocytochrome cellobiose dehydrogenase. J Mol Biol 315:421-434

Hallberg BM, Leitner C, Haltrich D, Divne C (2004) Crystal structure of the 270 kDa homotetrameric lignin-degrading enzyme pyranose 2-oxidase. J Mol Biol 341:781-796

Halliwell G (1965) Catalytic decomposition of cellulose under biological conditions. Biochem J 95:35-40

Hanke PD (2012) Enzymatic oxidation of hydroxymethylfurfural. Patent (USA) 8,183,020 B2

Hecht HJ, Kalisz HM, Hendle J, Schmid RD, Schomburg D (1993) Crystal structure of glucose oxidase from *Aspergillus niger* refined at 2.3 Å resolution. J Mol Biol 229:153-172

Heinfling A, Martínez MJ, Martínez AT, Bergbauer M, Szewzyk U (1998) Purification and characterization of peroxidases from the dye-decolorizing fungus *Bjerkandera adusta*. FEMS Microbiol Lett 165:43-50

Henriksson G, Johansson G, Pettersson G (2000) A critical review of cellobiose dehydrogenases. J Biotechnol 78:93-113

Hernández-Ortega A, Borrelli K, Ferreira P, Medina M, Martínez AT, Guallar V (2011a) Substrate diffusion and oxidation in GMC oxidoreductases: An experimental and computational study on fungal aryl-alcohol oxidase. Biochem J 436:341-350

Hernández-Ortega A, Ferreira P, Martínez AT (2012a) Fungal aryl-alcohol oxidase: A peroxide-producing flavoenzyme involved in lignin degradation. Appl Microbiol Biotechnol 93:1395-1410

Hernández-Ortega A, Ferreira P, Merino P, Medina M, Guallar V, Martínez AT (2012b) Stereoselective hydride transfer by aryl-alcohol oxidase, a member of the GMC superfamily. ChemBioChem 13:427-435

Hernández-Ortega A, Lucas F, Ferreira P, Medina M, Guallar V, Martínez AT (2011b) Modulating O2 reactivity in a fungal flavoenzyme: Involvement of aryl-alcohol oxidase Phe-501 contiguous to catalytic histidine. J Biol Chem 286:41105-41114

Hernández-Ortega A, Lucas F, Ferreira P, Medina M, Guallar V, Martínez AT (2012c) Role of active site histidines in the two half-reactions of the aryl-alcohol oxidase catalytic cycle. Biochemistry 51:6595-6608

Hibbett DS, Stajich J, Spatafora JW (2013) Toward genome-enabled mycology. Mycologia online:

Higuchi T (1997) Biochemistry and molecular biology of wood. Springer Verlag, London.

Hofrichter M, Ullrich R (2014) Oxidations catalyzed by fungal peroxygenases. Curr Opin Chem Biol 19:116-125

Hori C, Gaskell J, Igarashi K, Samejima M, Hibbett DS, Henrissat B, Cullen D (2013) Genomewide analysis of polysaccharides degrading enzymes in 11 white- and brown-rot Polyporales provides insight into mechanisms of wood decay. Mycologia 105:1412-1427

Horton P, Park KJ, Obayashi T, Fujita N, Harada H, Adams-Collier CJ, Nakai K (2007) WoLF PSORT: protein localization predictor. Nucleic Acids Res 35:W585-W587

Iida K, Cox-Foster DL, Yang XL, Ko WY, Cavener DR (2007) Expansion and evolution of insect GMC oxidoreductases. BMC Evolutionary Biology 7:75

Iwahara S, Nishihira T, Jomori T, Kuwahara M, Higuchi T (1980) Enzymic oxidation of a,b-unsaturated alcohols in the side chains of lignin-related aromatic compounds. J Ferment Technol 58:183-188

Jensen KAJr, Evans KMC, Kirk TK, Hammel KE (1994) Biosynthetic pathway for veratryl alcohol in the ligninolytic fungus *Phanerochaete chrysosporium*. Appl Environ Microbiol 60:709-714

Jonsson T, Edmondson DE, Klinman JP (1994) Hydrogen tunneling in the flavoenzyme monoamine oxidase B. Biochemistry 33:14871-14878

Kabsch W (1988) Evaluation of single-crystal X-ray diffraction data from a position-sensitive detector. Journal of Applied Crystallography916-924

Kabsch W (2010) XDS. Acta Crystallogr D Biol Crystallogr 66:125-132

Kalum L, Morant MD, Lund H, Jensen J, Lapainaite I, Soerensen NH, Pedersen S, Østergaard L, Xu F (2014) Enzymatic oxidation of 5-hydroxymethylfurfural and derivatives thereof. Patent (International) WO2014-015256A2

Kersten P, Cullen D (2007) Extracellular oxidative systems of the lignin-degrading basidiomycete *Phanerochaete chrysosporium*. Fungal Genet Biol 44:77-87

Kersten P, Cullen D (2014) Copper radical oxidases and related extracellular oxidoreductases of wood-decay Agaricomycetes. Fungal Genet Biol 72:124-130

Kersten PJ, Kirk TK (1987) Involvement of a new enzyme, glyoxal oxidase, in extracellular H_2O_2 production by *Phanerochaete chrysosporium*. J Bacteriol 169:2195-2201

Kiess M, Hecht HJ, Kalisz HM (1998) Glucose oxidase from *Penicillium amagasakiense*. Primary structure and comparison with other glucose-methanol-choline (GMC) oxidoreductases. Eur J Biochem 252:90-99

Kimura Y, Asada Y, Kuwahara M (1990) Screening of basidiomycetes for lignin peroxidase genes using a DNA probe. Appl Microbiol Biotechnol 32:436-442

Kimura Y, Asada Y, Oka T, Kuwahara M (1991) Molecular analysis of a *Bjerkandera adusta* lignin peroxidase gene. Appl Microbiol Biotechnol 35:510-514

Kirk TK (1975) Effects of brown-rot fungus *Lenzites trabea* on lignin of spruce wood. Holzforschung 29:99-107

Kirk TK, Farrell RL (1987) Enzymatic "combustion": The microbial degradation of lignin. Annu Rev Microbiol 41:465-505

Kittl R, Sygmund C, Halada P, Volc J, Divne C, Haltrich D, Peterbauer CK (2008) Molecular cloning of three pyranose dehydrogenase-encoding genes from *Agaricus meleagris* and analysis of their expression by real-time RT-PCR. Curr Genetics 53:117-127

Klinman JP (2007) How do enzymes activate oxygen without inactivating themselves? Account Chem Res 40:325-333

Klinman JP (2015) Dynamically achieved active site precision in enzyme catalysis. Acc Chem Res 48:449-456

Klinman JP, Kohen A (2013) Hydrogen tunneling links protein dynamics to enzyme catalysis. Annu Rev Biochem 82:471-496

Knapp MJ, Klinman JP (2002a) Environmentally coupled hydrogen tunneling. Eur J Biochem 269:3113-3121

Knapp MJ, Klinman JP (2002b) Environmentally coupled hydrogen tunneling. Eur J Biochem 269:3113-3121

Knapp MJ, Rickert K, Klinman JP (2002) Temperature dependent isotope effects in soybean lipoxygenase-1: Correlating hydrogen tunneling with protein dynamics. J Am Chem Soc 124:3865-3874

Kohen A, Cannio R, Bartolucci S, Klinman JP (1999b) Enzyme dynamics and hydrogen tunnelling in a thermophilic alcohol dehydrogenase. Nature 399:496-499

Kohen A, Cannio R, Bartolucci S, Klinman JP (1999a) Enzyme dynamics and hydrogen tunnelling in a thermophilic alcohol dehydrogenase. Nature 399:496-499

Kohen A, Klinman JP (1999) Hydrogen tunneling in biology. Chem Biol 6:R191-R198

Koopman F, Wierckx N, de Winde JH, Ruijssenaars HJ (2010) Efficient whole-cell biotransformation of 5-(hydroxymethyl)furfural into FDCA, 2,5-furandicarboxylic acid. Bioresource Technol 101:6291-6296

Kopacz MM, Heuts DP, Fraaije MW (2014) Kinetic mechanism of putrescine oxidase from Rhodococcus erythropolis. FEBS J 281:4384-4393

Kovalchuk A, Lee YH, Asiegbu FO (2013) Diversity and evolution of ABC proteins in basidiomycetes. Mycologia 105:1456-1470

Kraut J (1988) How do enzymes work? Science 242:533

Kremer SM, Wood PM (1992) Production of Fenton's reagent by cellobiose oxidase from cellulolytic cultures of *Phanerochaete chrysosporium*. Eur J Biochem 208:807-814

Krings U, Berger RG (1998) Biotechnological production of flavours and fragrances. Appl Microbiol Biotechnol 49:1-8

Krissinel E, Henrick K (2007) Inference of macromolecular assemblies from crystalline state. Journal of Molecular Biology 372:774-797

Krondorfer I, Brugger D, Paukner R, Scheiblbrandner S, Pirker KF, Hofbauer S, Furtmüller PG, Obinger C, Haltrich D, Peterbauer CK (2014a) *Agaricus meleagris* pyranose dehydrogenase: Influence of covalent FAD linkage on catalysis and stability. Arch Biochem Biophys 558:111-119

Krondorfer I, Lipp K, Brugger D, Staudigl P, Sygmund C, Haltrich D, Peterbauer CK (2014b) Engineering of pyranose dehydrogenase for increased oxygen reactivity. PLoS ONE 9(3): e91145. doi:10.1371/journal.pone.0091145:

Kujawa M, Volc J, Halada P, Sedmera P, Divne C, Sygmund C, Leitner C, Peterbauer C, Haltrich D (2007) Properties of pyranose dehydrogenase purified from the litter-degrading fungus *Agaricus xanthoderma*. FEBS J 274:879-894

Langston JA, Shaghasi T, Abbate E, Xu F, Vlasenko E, Sweeney MD (2011) Oxidoreductive cellulose depolymerization by the enzymes cellobiose dehydrogenase and glycoside hydrolase 61. Appl Environ Microbiol 77:7007-7015

Lapadatescu C, Bonnarme P (1999) Production of aryl metabolites in solid-state fermentations of the white-rot fungus *Bjerkandera adusta*. Biotechnol Lett 21:763-769

Lapadatescu C, Giniès C, Le Quéré J-L, Bonnarme P (2000) Novel scheme for biosynthesis of aryl metabolites from L-phenylalanine in the fungus *Bjerkandera adusta*. Appl Environ Microbiol 66:1517-1522

Laskowski RA, MacArthur MW, Moss DS, Thornton JM (1993) PROCHECK - a program to check the stereochemical quality of protein structures. Journal of Applied Crystallography 26:283-291

Laskowski RA, Swindells MB (2011) LigPlot+: Multiple ligand-protein interaction diagrams for drug discovery. J Chem Inf Model 51:2778-2786

Leferink NGH, Heuts DPHM, Fraaije MW, van Berkel WJH (2008) The growing VAO flavoprotein family. Arch Biochem Biophys 474:292-301

Leitner C, Haltrich D, Nidetzky B, Prillinger H, Kulbe KD (1998) Production of a novel pyranose 2-oxidase by basidiomycete *Trametes multicolor*. Appl Biochem Biotechnol 70:237-248

Leitner C, Volc J, Haltrich D (2001) Purification and characterization of pyranose oxidase from the white rot fungus *Trametes multicolor*. Appl Environ Microbiol 67:3636-3644

Leskovac V, Trivic S, Wohlfahrt G, Kandrac J, Pericin D (2005) Glucose oxidase from *Aspergillus niger*: The mechanism of action with molecular oxygen, quinones, and one-electron acceptors. Int J Biochem Cell Biol 37:731-750

Limbach HH, Lopez JM, Kohen A (2006) Arrhenius curves of hydrogen transfers: tunnel effects, isotope effects and effects of pre-equilibria. Philos Trans R Soc Lond B Biol Sci 361:1399-1415

Linde D, Canellas M, Coscolín C, Davó-Siguero I, Romero A, Lucas F, Ruiz-Dueñas FJ, Guallar V, Martínez AT (2016) Asymmetric sulfoxidation by engineering the heme pocket of a dye-decolorizing peroxidase. Catal Sci Technol 6:6277-6285

Lomascolo A, Uzan-Boukhris E, Herpoel-Gimbert I, Sigoillot JC, Lesage-Meessen L (2011) Peculiarities of *Pycnoporus* species for applications in biotechnology. Appl Microbiol Biotechnol 92:1129-1149

Luk LYP, Loveridge EJ, Allemann RK (2015) Protein motions and dynamic effects in enzyme catalysis. Phys Chem Chem Phys 17:30817-30827

Macheroux P, Ghisla S, Sanner C, Ruterjans H, Muller F (2005) Reduced flavin: NMR investigation of N5-H exchange mechanism, estimation of ionisation constants and assessment of properties as biological catalyst. BMC Biochem 6:26

Malmstrom BG (1982) Enzymology of oxygen. Annu Rev Biochem 51:21-59

Martínez AT, Barrasa JM, Martínez MJ, Almendros G, Blanco M,González AE (1995) *Ganoderma australe*: A fungus responsible for extensive delignification of some Austral hardwoods. In: Buchanan PK, Hseu RS, Moncalvo JM (eds) *Ganoderma*.

Systematics, phytopathology and pharmacology. National Taiwan University, Taipei, pp 67-77

Martínez AT, Rencoret J, Nieto L, Jiménez-Barbero J, Gutiérrez A, del Río JC (2011) Selective lignin and polysaccharide removal in natural fungal decay of wood as evidenced by *in situ* structural analyses. Environ Microbiol 13:96-107

Martínez AT, Speranza M, Ruiz-Dueñas FJ, Ferreira P, Camarero S, Guillén F, Martínez MJ, Gutiérrez A, del Río JC (2005) Biodegradation of lignocellulosics: Microbiological, chemical and enzymatic aspects of fungal attack to lignin. Int Microbiol 8:195-204

Martinez D, Challacombe J, Morgenstern I, Hibbett DS, Schmoll M, Kubicek CP, Ferreira P, Ruiz-Dueñas FJ, Martínez AT, Kersten P, Hammel KE, Vanden Wymelenberg A, Gaskell J, Lindquist E, Sabat G, Bondurant SS, Larrondo LF, Canessa P, Vicuña R, Yadav J, Doddapaneni H, Subramanian V, Pisabarro AG, Lavín JL, Oguiza JA, Master E, Henrissat B, Coutinho PM, Harris P, Magnuson JK, Baker SE, Bruno K, Kenealy W, Hoegger PJ, Kües U, Ramaiya P, Lucas S, Salamov A, Shapiro H, Tu H, Chee CL, Misra M, Xie G, Teter S, Yaver D, James T, Mokrejs M, Pospisek M, Grigoriev IV, Brettin T, Rokhsar D, Berka R, Cullen D (2009) Genome, transcriptome, and secretome analysis of wood decay fungus *Postia placenta* supports unique mechanisms of lignocellulose conversion. Proc Natl Acad Sci USA 106:1954-1959

Martinez D, Larrondo LF, Putnam N, Gelpke MD, Huang K, Chapman J, Helfenbein KG, Ramaiya P, Detter JC, Larimer F, Coutinho PM, Henrissat B, Berka R, Cullen D, Rokhsar D (2004) Genome sequence of the lignocellulose degrading fungus *Phanerochaete chrysosporium* strain RP78. Nat Biotechnol 22:695-700

Masarin F, Pavan PC, Vicentim MP, Souza-Cruz PB, Loguercio-Leite C, Ferraz A (2009) Laboratory and mill scale evaluation of biopulping of *Eucalyptus grandis* Hill ex Maiden with *Phanerochaete chrysosporium* RP-78 under non-aseptic conditions. Holzforschung 63:259-263

Massey V (1994) Activation of molecular oxygen by flavins and flavoproteins. J Biol Chem 269:22459-22462

Mathieu Y, Piumi F, Valli R, Aramburu JC, Ferreira P, Faulds CB, Record E (2016) Activities of secreted aryl alcohol quinone oxidoreductases from *Pycnoporus cinnabarinus* provide insights into fungal degradation of plant biomass. Appl Environ Microbiol 82:2411-2423

Matsuda T, Yamanaka R, Nakamura K (2009) Recent progress in biocatalysis for asymmetric oxidation and reduction. Tetrahedron-Asymmetry 20:513-557

Mattevi A (1998) The PHBH fold: not only flavoenzymes. Biophys Chem 70:217-222

Mattevi A (2006) To be or not to be an oxidase: challenging the oxygen reactivity of flavoenzymes. Trends Biochem Sci 31:276-283

Melander L,Saunders WH (1987) Reaction rates of isotopic molecules.

Meyer MP, Tomchick DR, Klinman JP (2008) Enzyme structure and dynamics affect hydrogen tunneling: The impact of a remote side chain (I553) in soybean lipoxygenase-1. Proceedings of the National Academy of Sciences 105:1146-1151

Mgbeahuruike AC, Kovalchuk A, Asiegbu FO (2013) Comparative genomics and evolutionary analysis of hydrophobins from three species of wood-degrading fungi. Mycologia online:

Molina-Espeja P, Garcia-Ruiz E, Gonzalez-Perez D, Ullrich R, Hofrichter M, Alcalde M (2014) Directed evolution of unspecific peroxygenase from *Agrocybe aegerita*. Appl Environ Microbiol 80:3496-3507

Molina-Espeja P, Plou F, Alcalde M (2015) Unspecific peroxygenase mutants with high monooxygenase activity and their applications. Patent (Spain) P201531641:

Moreau C, Belgacem MN, Gandini A (2004) Recent catalytic advances in the chemistry of substituted furans from carbohydrates and in the ensuing polymers. Top Catal 27:11-30

Moser CC, Anderson JLR, Dutton PL (2010) Guidelines for tunneling in enzymes. Biochimica et Biophysica Acta (BBA) - Bioenergetics 1797:1573-1586

Moukha SM, Dumonceaux TJ, Record E, Archibald FS (1999) Cloning and analysis of *Pycnoporus cinnabarinus* cellobiose dehydrogenase. Gene 234:23-33

Muheim A, Leisola MSA, Schoemaker HE (1990a) Aryl-alcohol oxidase and lignin peroxidase from the white-rot fungus *Bjerkandera adusta*. J Biotechnol 13:159-167

Muheim A, Waldner R, Leisola MSA, Fiechter A (1990b) An extracellular aryl-alcohol oxidase from the white-rot fungus *Bjerkandera adusta*. Enzyme Microb Technol 12:204-209

Murshudov GN, Vagin A, Dodson EJ (1997) Refinement of macromolecular structures by the maximum-likelihood method. Acta Crystallogr D Biol Crystallogr240-255

Nagel ZD, Klinman JP (2009) A 21(st) century revisionist's view at a turning point in enzymology. Nat Chem Biol 5:543-550

Niemenmaa O, Uusi-Rauva A, Hatakka A (2008) Demethoxylation of [O14CH3]-labelled lignin model compounds by the brown-rot fungi *Gloeophyllum trabeum* and *Poria* (*Postia*) *placenta*. Biodegradation 19:555-565

Nishida A, Eriksson K-E (1987) Formation, purification, and partial characterization of methanol oxidase, a H_2O_2-producing enzyme in *Phanerochaete chrysosporium*. Biotechnol Appl Biochem 9:325-338

Nyanhongo GS, Gubitz G, Sukyai P, Leitner C, Haltrich D, Ludwig R (2007) Oxidoreductases from *Trametes* spp. in biotechnology: A wealth of catalytic activity. Food Technol Biotechnol 45:250-268

Okamoto K, Narayama S, Katsuo A, Shigematsu I, Yanase H (2002) Biosynthesis of *p*-anisaldehyde by the white-rot basidiomycete *Pleurotus ostreatus*. J Biosci Bioeng 93:207-210

Otjen L, Blanchette RA (1986) A discussion of microstructural changes in wood during decomposition by white rot basidiomycetes. Can J Bot 64:905-911

Overhage J, Steinbüchel A, Priefert H (2003) Highly efficient biotransformation of eugenol to ferulic acid and further conversion to vanillin in recombinant strains of Escherichia coli. Appl Environ Microbiol 69:6569-6576

Ozimek P, Veenhuis M, van der Klei IJ (2005) Alcohol oxidase: A complex peroxisomal, oligomeric flavoprotein. FEMS Yeast Res 5:975-983

Papageorgiou GZ, Tsanaktsis V, Bikiaris DN (2014) Synthesis of poly(ethylene furandicarboxylate) polyester using monomers derived from renewable resources: thermal behavior comparison with PET and PEN. Phys Chem Chem Phys 16:7946-7958

Pardo I, Camarero S (2015) Exploring the oxidation of lignin-derived phenols by a library of laccase mutants. Molecules 20:15929-15943

Pardo I, Gerard S, Gentili P, Lucas F, Monza E, Medrano FJ, Romero A, Galli C, Martínez AT, Guallar V, Camarero S (2016) Re-designing the substrate binding pocket of laccase for enhanced oxidation of sinapic acid. Catal Sci Technol doi 10.1039/C5CY01725D:

Patel RN (2013) Biocatalytic synthesis of chiral alcohols and amino acids for development of pharmaceuticals. Biomolecules 3:741-777

Peláez F, Martínez MJ, Martínez AT (1995) Screening of 68 species of basidiomycetes for enzymes involved in lignin degradation. Mycol Res 99:37-42

Pennati A, Gadda G (2011) Stabilization of an intermediate in the oxidative half-reaction of human liver glycolate oxidase. Biochemistry 50:1-3

Petersen TN, Brunak S, von Heijne G, Nielsen H (2011) SignalP 4.0: discriminating signal peptides from transmembrane regions. Nature Methods 8:785-786

Pitsawong W, Sucharitakul J, Prongjit M, Tan TC, Spadiut O, Haltrich D, Divne C, Chaiyen P (2010) A conserved active-site threonine is important for both sugar and flavin oxidations of pyranose 2-oxidase. J Biol Chem 285:9697-9705

Priefert H, Rabenhorst J, Steinbüchel A (2001) Biotechnological production of vanillin. Appl Microbiol Biotechnol 56:296-314

Prongjit M, Sucharitakul J, Palfey BA, Chaiyen P (2013) Oxidation mode of pyranose 2-oxidase is controlled by pH. Biochemistry 52:1437-1445

Prongjit M, Sucharitakul J, Wongnate T, Haltrich D, Chaiyen P (2009) Kinetic mechanism of pyranose 2-oxidase from *Trametes multicolor*. Biochemistry 48:4170-4180

Quaye O, Lountos GT, Fan F, Orville AM, Gadda G (2008) Role of Glu312 in binding and positioning of the substrate for the hydride transfer reaction in choline oxidase. Biochemistry 47:243-256

Raices M, Montesino R, Cremata J, Garcia B, Perdomo W, Szabo I, Henriksson G, Hallberg BM, Pettersson G, Johansson G (2002) Cellobiose quinone oxidoreductase from the white rot fungus *Phanerochaete chrysosporium* is produced by intracellular proteolysis of cellobiose dehydrogenase. BBA Gene Struct Express 1576:15-22

Raices M, Paifer E, Cremata J, Montesino R, Stahlberg J, Divne C, Szabo IJ, Henriksson G, Johansson G, Pettersson G (1995) Cloning and characterization of a cDNA encoding a cellobiose dehydrogenase from the white rot fungus *Phanerochaete chrysosporium*. FEBS Lett 369:233-238

Ralph JP, Graham LA, Catcheside DEA (1996) Extracellular oxidases and the transformation of solubilised low rank coal by wood-rot fungi. Appl Microbiol Biotechnol 46:226-232

Rasmussen ML, Shrestha P, Khanal SK, Pometto AL, van Leeuwen J (2010) Sequential saccharification of corn fiber and ethanol production by the brown rot fungus *Gloeophyllum trabeum*. Bioresource Technol 101:3526-3533

Romero E, Ferreira P, Martínez AT, Martínez MJ (2009) New oxidase from *Bjerkandera* arthroconidial anamorph that oxidizes both phenolic and nonphenolic benzyl alcohols. Biochim Biophys Acta 1794:689-697

Romero E, Gadda G (2014) Alcohol oxidation by flavoenzymes. Biomolecular concepts 5:299-318

Romero E, Martínez AT, Martínez MJ (2010a) Manganese peroxidase and aryl-alcohol oxidase: A ligninolytic tandem in *Bjerkandera* arthroconidial anamorph. Proc OxiZymes in Leipzig, 14-16 June

Romero E, Martínez AT, Martínez MJ (2010b) Molecular characterization of a new flavooxidase from a *Bjerkandera adusta* anamorph. Proc OESIB, Santiago de Compostela, 14-15 September(Eds, G. Feijoo and M.T. Moreira; ISBN-13: 978-84-614-2824-3) pp 86-91

Rosatella AA, Simeonov SP, Frade RFM, Afonso CAM (2011) 5-Hydroxymethylfurfural (HMF) as a building block platform: Biological properties, synthesis and synthetic applications. Green Chem 13:754-793

Roth JP, Klinman JP (2003) Catalysis of electron transfer during activation of O_2 by the flavoprotein glucose oxidase. Proc Natl Acad Sci USA 100:62-67

Roth JP, Wincek R, Nodet G, Edmondson DE, McIntire WS, Klinman JP (2004) Oxygen isotope effects on electron transfer to O2 probed using chemically modified flavins bound to glucose oxidase. J Am Chem Soc 126:15120-15131

Ruiz-Dueñas FJ, Ferreira P, Martínez MJ, Martínez AT (2006) In vitro activation, purification, and characterization of *Escherichia coli* expressed aryl-alcohol oxidase, a unique H2O2-producing enzyme. Protein Express Purif 45:191-199

Ruiz-Dueñas FJ, Lundell T, Floudas D, Nagy LG, Barrasa JM, Hibbett DS, Martínez AT (2013) Lignin-degrading peroxidases in Polyporales: An evolutionary survey based on ten sequenced genomes. Mycologia 105:1428-1444

Ruiz-Dueñas FJ, Martínez AT (2009) Microbial degradation of lignin: How a bulky recalcitrant polymer is efficiently recycled in nature and how we can take advantage of this. Microbial Biotechnol 2:164-177

Sáez-Jiménez V, Acebes S, Guallar V, Martínez AT, Ruiz-Dueñas FJ (2015) Improving the oxidative stability of a high redox potential fungal peroxidase by rational design. PLoS ONE10(4):e0124750. doi:10.1371/journal.pone.0124750

Sannia G, Limongi P, Cocca E, Buonocore F, Nitti G, Giardina P (1991) Purification and characterization of a veratryl alcohol oxidase enzyme from the lignin degrading basidiomycete *Pleurotus ostreatus*. Biochim Biophys Acta 1073:114-119

Sawyer DT (1988) The redox thermodynamics for dioxygen species (O2, O2-., HOO., HOOH, HOO-) an monooxygen species (O, O-., .OH, and -OH) in water and aprotic solvents. Basic Life Sci 49:11-20

Schmidhalter DR, Canevascini G (1993) Isolation and characterization of the cellobiose dehydrogenase from the brown-rot fungus *Coniophora puteana* (Schum ex Fr.) Karst. Arch Biochem Biophys 300:559-563

Schwarze FWMR, Baum S, Fink S (2000) Dual modes of degradation by *Fistulina hepatica* in xylem cell walls of *Quercus robur*. Mycol Res 104:846-852

Scott GM, Swaney R (1998) New technologies for papermaking: biopulping economics. Tappi J 81:153-157

Serra S, Fuganti C, Brenna E (2005) Biocatalytic preparation of natural flavours and fragrances. Trends Biotechnol 23:193-198

Setoyama C, Nishina Y, Tamaoki H, Mizutani H, Miyahara I, Hirotsu K, Shiga K, Miura R (2002) Effects of hydrogen bonds in association with flavin and substrate in flavoenzyme D-amino acid oxidase. The catalytic and structural roles of Gly313 and Thr317. Journal of Biochemistry 131:59-69

Sharma SC, Klinman JP (2008) Experimental evidence for hydrogen tunneling when the isotopic Arrhenius prefactor (AH/AD) is unity. J Am Chem Soc 130:17632-17633

Sheng D, Ballou DP, Massey V (2001) Mechanistic studies of cyclohexanone monooxygenase: Chemical properties of intermediates involved in catalysis. Biochemistry 40:11156-11167

Shimada M, Higuchi T (1991) Microbial, enzymatic and biomimetic degradation of lignin. In: Hon DNS, Shiraishi N (eds) Wood and cellulosic chemistry. Marcel Dekker, N.Y., pp 557-619

Sigoillot C, Camarero S, Vidal T, Record E, Asther M, Pérez-Boada M, Martínez MJ, Sigoillot J-C, Asther M, Colom J, Martínez AT (2005) Comparison of different fungal enzymes for bleaching high-quality paper pulps. J Biotechnol 115:333-343

Singh P, Francis K, Kohen A (2015) Network of remote and local protein dynamics in dihydrofolate reductase catalysis. ACS Catal 5:3067-3073

Stamatakis A, Hoover P, Rougemont J (2008) A rapid bootstrap algorithm for the RAxML web servers. Syst Biol 57:758-771

Sucharitakul J, Prongjit M, Haltrich D, Chaiyen P (2008) Detection of a C4a-hydroperoxyflavin intermediate in the reaction of a flavoprotein oxidase. Biochemistry 47:8485-8490

Sucharitakul J, Wongnate T, Chaiyen P (2011) Hydrogen peroxide elimination from C4a-hydroperoxyflavin in a flavoprotein oxidase occurs through a single proton transfer from flavin N5 to a peroxide leaving group. J Biol Chem 286:16900-16909

Sulej J, Janusz G, Osinska-Jaroszuk M, Malek P, Mazur A, Komaniecka I, Choma A, Rogalski J (2013) Characterization of cellobiose dehydrogenase and its FAD-domain from the ligninolytic basidiomycete Pycnoporus sanguineus. Enzyme Microb Technol 53:427-437

Sun W, Shen YH, Yang WJ, Cao YF, Xiang ZH, Zhang Z (2012) Expansion of the silkworm GMC oxidoreductase genes is associated with immunity. Insect Biochemistry and Molecular Biology 42:935-945

Syed K, Nelson DR, Riley R, Yadav JS (2013) Genome-wide annotation and comparative genomics of cytochrome P450 monooxygenases (P450s) in the Polyporale species *Bjerkandera adusta, Ganoderma* sp. and *Phlebia brevispora*. Mycologia 105:1445-1455

Tamura K, Peterson D, Peterson N, Stecher G, Nei M, Kumar S (2011) MEGA5: Molecular evolutionary genetics analysis using maximum likelihood, evolutionary distance, and maximum parsimony methods. Mol Biol Evol 28:2731-2739

Tan TC, Spadiut O, Wongnate T, Sucharitakul J, Krondorfer I, Sygmund C, Haltrich D, Chaiyen P, Peterbauer CK, Divne C (2013) The 1.6 angstrom crystal structure of pyranose dehydrogenase from *Agaricus meleagris* rationalizes substrate specificity and reveals a flavin intermediate. PLoS ONE 8(1): e53567. doi:10.1371/journal.pone.0053567:

Teixidó E, Santos FJ, Puignou L, Galceran MT (2006) Analysis of 5-hydroxymethylfurfural in foods by gas chromatography-mass spectrometry. J Chromatogr A 1135:85-90

Turner WB,Aldridge DC (1983) Fungal metabolites II. Academic Press, London.

Ullrich R, Hofrichter M (2005) The haloperoxidase of the agaric fungus *Agrocybe aegerita* hydroxylates toluene and naphthalene. FEBS Lett 579:6247-6250

Ullrich R, Nuske J, Scheibner K, Spantzel J, Hofrichter M (2004) Novel haloperoxidase from the agaric basidiomycete *Agrocybe aegerita* oxidizes aryl alcohols and aldehydes. Appl Environ Microbiol 70:4575-4581

Vagin A, Teplyakov A (1997) MOLREP: An automated program for molecular replacement. Journal of Applied Crystallography 30:1022-1025

Valley MP, Fenny NS, Ali SR, Fitzpatrick PF (2010) Characterization of active site residues of nitroalkane oxidase. Bioorganic Chemistry 38:115-119

van den Heuvel RH, Fraaije MW, Ferrer M, Mattevi A, van Berkel WJ (2000) Inversion of stereospecificity of vanillyl-alcohol oxidase. Proc Natl Acad Sci USA 97:9455-9460 van Deurzen MPJ, van Rantwijk F, Sheldon RA (1997) Chloroperoxidase-catalyzed oxidation of 5-hydroxymethylfurfural. J Carbohyd Chem 16:299-309

Vanden Wymelenberg A, Gaskell J, Mozuch M, Sabat G, Ralph J, Skyba O, Mansfield SD, Blanchette RA, Martinez D, Grigoriev I, Kersten PJ, Cullen D (2010) Comparative transcriptome and secretome analysis of wood decay fungi *Postia placenta* and *Phanerochaete chrysosporium*. Appl Environ Microbiol 76:3599-3610

Varela E, Guillén F, Martínez AT, Martínez MJ (2001) Expression of *Pleurotus eryngii* aryl-alcohol oxidase in *Aspergillus nidulans*: purification and characterization of the recombinant enzyme. Biochim Biophys Acta 1546:107-113

Varela E, Martínez AT, Martínez MJ (1999) Molecular cloning of aryl-alcohol oxidase from *Pleurotus eryngii*, an enzyme involved in lignin degradation. Biochem J 341:113-117

Varela E, Martínez AT, Martínez MJ (2000) Southern blot screening for lignin peroxidase and aryl-alcohol oxidase genes in 30 fungal species. J Biotechnol 83:245-251

Vecerek B, Maresova H, Kocanova M, Kyslik P (2004) Molecular cloning and expression of the pyranose 2-oxidase cDNA from *Trametes ochracea* MB49 in *Escherichia coli*. Appl Microbiol Biotechnol 64:525-530

Vicentim MP, Faria RD, Ferraz A (2009) High-yield kraft pulping of *Eucalyptus grandis* Hill ex Maiden biotreated by *Ceriporiopsis subvermispora* under two different culture conditions. Holzforschung 63:408-413

Viña-González J, González-Pérez D, Alcalde M (2015a) Directed evolution method in *Saccharomyces cerevisiae*: Mutant library creation and screening. J Vis Exp (in press):

Viña-González J, González-Pérez D, Ferreira P, Martínez AT, Alcalde M (2015b) Focused directed evolution of aryl-alcohol oxidase in *Saccharomyces cerevisiae* by using chimeric signal peptides. Appl Environ Microbiol 81:6451-6462

Volc J, Kubátová E, Daniel G, Prikrylova V (1996) Only C-2 specific glucose oxidase activity is expressed in ligninolytic cultures of the white rot fungus *Phanerochaete chrysosporium*. Arch Microbiol 165:421-424

Volc J, Kubátová E, Daniel G, Sedmera P, Haltrich D (2001) Screening of basidiomycete fungi for the quinone-dependent sugar C-2/C-3 oxidoreductase, pyranose dehydrogenase, and properties of the enzyme from *Macrolepiota rhacodes*. Arch Microbiol 176:178-186

Volc J, Kubátová E, Wood DA, Daniel G (1997) Pyranose 2-dehydrogenase, a novel sugar oxidoreductase from the basidiomycete fungus *Agaricus bisporus*. Arch Microbiol 167:119-125

Vrielink A, Ghisla S (2009) Cholesterol oxidase: biochemistry and structural features. FEBS J 276:6826-6843

Vrielink A, Lloyd LF, Blow DM (1991) Crystal structure of cholesterol oxidase from *Brevibacterium sterolicum* refined at 1.8 Å resolution. J Mol Biol 219:533-554

Waldner R, Leisola MSA, Fiechter A (1988) Comparison of ligninolytic activities of selected white-rot fungi. Appl Microbiol Biotechnol 29:400-407

Westermark U, Eriksson KE (1974) Carbohydrate-dependent enzymic quinone reduction during lignin degradation. Acta Chem Scand B 28:204-208

Whittaker JW (2002) Galactose oxidase. Adv Protein Chem (Copper-Containing Proteins) 60:1-49

Wierenga RK, Drenth J, Schulz GE (1983) Comparison of the three-dimensional protein and nucleotide structure of the FAD-binding domain of *p*-hydroxybenzoate hydroxylase with the FAD - as well as NADPH-binding domains of glutathione reductase. J Mol Biol 167:725-739

Witt S, Wohlfahrt G, Schomburg D, Hecht HJ, Kalisz HM (2000) Conserved arginine-516 of *Penicillium amagasakiense* glucose oxidase is essential for the efficient binding of b-D-glucose. Biochem J 347:553-559

Wohlfahrt G, Witt S, Hendle J, Schomburg D, Kalisz HM, Hecht H-J (1999) 1.8 and 1.9 Å resolution structures of the *Penicillium amagasakiense* and *Aspergillus niger* glucose oxidase as a basis for modelling substrate complexes. Acta Crystallogr D Biol Crystallogr 55:969-977

Wongnate T, Chaiyen P (2013) The substrate oxidation mechanism of pyranose 2-oxidase and other related enzymes in the glucose-methanol-choline superfamily. FEBS J 280:3009-3027

Wongnate T, Sucharitakul J, Chaiyen P (2011) Identification of a catalytic base for sugar oxidation in the pyranose-2 oxidation reaction. ChemBioChem 12:2577-2586

Wongnate T, Surawatanawong P, Visitsatthawong S, Sucharitakul J, Scrutton NS, Chaiyen P (2014) Proton-coupled electron transfer and adduct configuration are important for C4a-hydroperoxyflavin formation and stabilization in a flavoenzyme. J Am Chem Soc 136:241-253

Wood JD, Wood PM (1992) Evidence that cellobiose-quinone oxidoreductase from *Phanerochaete chrysosporium* is a breakdown product of cellobiose oxidase. Biochim Biophys Acta 1119:90-96

Wu X, Palfey BA, Mossine VV, Monnier VM (2001) Kinetic studies, mechanism, and substrate specificity of amadoriase I from Aspergillus sp. Biochemistry 40:12886-12895

Xin Y, Gadda G, Hamelberg D (2009) The cluster of hydrophobic residues controls the entrance to the active site of choline oxidase. Biochemistry 48:9599-9605

Yelle DJ, Ralph J, Lu F, Hammel KE (2008) Evidence for cleavage of lignin by a brown rot basidiomycete. Environ Microbiol 10:1844-1849

Yelle DJ, Wei DS, Ralph J, Hammel KE (2011) Multidimensional NMR analysis reveals truncated lignin structures in wood decayed by the brown rot basidiomycete . Environ Microbiol 13:1091-1100

Zabel R,Morrell J (1992) Wood microbiology: Decay and its prevention. Academic Press, London.

Zámocký M, Hallberg M, Ludwig R, Divne C, Haltrich D (2004) Ancestral gene fusion in cellobiose dehydrogenases reflects a specific evolution of GMC oxidoreductases in fungi. Gene 338:1-14

Zámocký M, Ludwig R, Peterbauer C, Hallberg BM, Divne C, Nicholls P, Haltrich D (2006) Cellobiose dehydrogenase - A flavocytochrome from wood-degrading, phytopathogenic and saprotropic fungi. Curr Protein Pept Sci 7:255-280

Zhao H, Holladay JE, Brown H, Zhang ZC (2007) Metal chlorides in ionic liquid solvents convert sugars to 5-hydroxymethylfurfural. Science 316:1597-1600